DOCTOR OF PHILOSOPHY

Synthesis, characterization and computational studies of Boron-Oxygen compounds

Jones, Charlotte Louise

Award date:
2016

Awarding institution:
Bangor University

SYNTHESIS, CHARACTERIZATION AND COMPUTATIONAL STUDIES OF BORON-OXYGEN COMPOUNDS

A thesis submitted for the degree of

Doctor of Philosophy

Prifysgol Bangor • Bangor University

by

Charlotte Louise Jones

Declaration and Consent

Details of the Work

I hereby agree to deposit the following item in the digital repository maintained by Bangor University and/or in any other repository authorized for use by Bangor University.

Author Name: ……..……

Title: ……..……

……

Supervisor/Department: ……...

Funding body (if any): .....

Qualification/Degree obtained: ……...

This item is a product of my own research endeavours and is covered by the agreement below in which the item is referred to as “the Work”. It is identical in content to that deposited in the Library, subject to point 4 below.

Non-exclusive Rights

Rights granted to the digital repository through this agreement are entirely non-exclusive. I am free to publish the Work in its present version or future versions elsewhere.

I agree that Bangor University may electronically store, copy or translate the Work to any approved medium or format for the purpose of future preservation and accessibility. Bangor University is not under any obligation to reproduce or display the Work in the same formats or resolutions in which it was originally deposited.

Bangor University Digital Repository

I understand that work deposited in the digital repository will be accessible to a wide variety of people and institutions, including automated agents and search engines via the World Wide Web.

I understand that once the Work is deposited, the item and its metadata may be incorporated into public access catalogues or services, national databases of electronic theses and dissertations such as the British Library’s EThOS or any service provided by the National Library of Wales.

I understand that the Work may be made available via the National Library of Wales Online Electronic Theses Service under the declared terms and conditions of use

(http://www.llgc.org.uk/index.php?id=4676). I agree that as part of this service the National Library of Wales may electronically store, copy or convert the Work to any approved medium or format for the purpose of future preservation and accessibility. The National Library of Wales is not under any obligation to reproduce or display the Work in the same formats or resolutions in which it was originally deposited.

Statement 1:

This work has not previously been accepted in substance for any degree and is not being concurrently submitted in candidature for any degree unless as agreed by the University for approved dual awards.

Signed …….. (candidate)

Date ……..

Statement 2:

This thesis is the result of my own investigations, except where otherwise stated. Where correction services have been used, the extent and nature of the correction is clearly marked in a footnote(s).

All other sources are acknowledged by footnotes and/or a bibliography.

Signed ……. (candidate)

Date …….

Statement 3:

I hereby give consent for my thesis, if accepted, to be available for photocopying, for inter-library loan and for electronic storage (subject to any constraints as defined in statement 4), and for the title and summary to be made available to outside organisations.

Signed ……. (candidate)

Date …….

NB: Candidates on whose behalf a bar on access has been approved by the Academic Registry should use the following version of **Statement 3:**

Statement 3 (bar):

I hereby give consent for my thesis, if accepted, to be available for photocopying, for inter-library loans and for electronic storage (subject to any constraints as defined in statement 4), after expiry of a bar on access.

Signed …… (candidate)

Date ……

Statement 4:

Choose **one** of the following options

a) I agree to deposit an electronic copy of my thesis (the Work) in the Bangor University (BU) Institutional Digital Repository, the British Library ETHOS system, and/or in any other repository authorized for use by Bangor University and where necessary have gained the required permissions for the use of third party material.	
b) I agree to deposit an electronic copy of my thesis (the Work) in the Bangor University (BU) Institutional Digital Repository, the British Library ETHOS system, and/or in any other repository authorized for use by Bangor University when the approved **bar on access** has been lifted.	
c) I agree to submit my thesis (the Work) electronically via Bangor University's e-submission system, however I **opt-out** of the electronic deposit to the Bangor University (BU) Institutional Digital Repository, the British Library ETHOS system, and/or in any other repository authorized for use by Bangor University, due to lack of permissions for use of third party material.	

Options B should only be used if a bar on access has been approved by the University.

In addition to the above I also agree to the following:

1. That I am the author or have the authority of the author(s) to make this agreement and do hereby give Bangor University the right to make available the Work in the way described above.

2. That the electronic copy of the Work deposited in the digital repository and covered by this agreement, is identical in content to the paper copy of the Work deposited in the Bangor University Library, subject to point 4 below.

3. That I have exercised reasonable care to ensure that the Work is original and, to the best of my knowledge, does not breach any laws – including those relating to defamation, libel and copyright.

4. That I have, in instances where the intellectual property of other authors or copyright holders is included in the Work, and where appropriate, gained explicit permission for the inclusion of that material in the Work, and in the electronic form of the Work as accessed through the open access digital repository, *or* that I have identified and removed that material for which adequate and appropriate permission has not been obtained and which will be inaccessible via the digital repository.

5. That Bangor University does not hold any obligation to take legal action on behalf of the Depositor, or other rights holders, in the event of a breach of intellectual property rights, or any other right, in the material deposited.

6. That I will indemnify and keep indemnified Bangor University and the National Library of Wales from and against any loss, liability, claim or damage, including without limitation any related legal fees and court costs (on a full indemnity bases), related to any breach by myself of any term of this agreement.

Signature: ……

Date : …….

Abstract

This thesis describes the synthesis and characterization of a number compounds containing B-O bonds; most of these compounds contain 6-membered B_3O_3 boroxole rings within their structures.

A total of twenty-one new non-metal cation polyborate salts are reported; nineteen of these contain the pentaborate anion, $[B_5O_6(OH)_4]^-$, one contains the triborate monoanion, $[B_3O_3(OH)_4]^-$, and one contains the heptaborate dianion, $[B_7O_9(OH)_5]^{2-}$. The crystal structures of ten salts containing these polyborate anions are reported: pyrrolidinium pentaborate (**1**), *N*-methylpyrrolidinium pentaborate·½ acetone (**2**·½CH_3COCH_3), *N,N*-dimethylpyrrolidinium pentaborate (**3**), 2-hydroxymethylpyrrolidinium pentaborate hemihydrate (**4**·½H_2O), (2-hydroxyethyl)-*N*-methylpyrrolidinium pentaborate·0.3 hydrate (**5**·0.3H_2O), 4-aminobenzylammonium pentaborate hemihydrate (**9**·½H_2O), *N,N*-dimethyl-1-adamantylammonium pentaborate sesquihydrate (**14**·1.5H_2O), *N,N,N*-trimethyl-1-adamantylammonium pentaborate trihydrate (**15**·3H_2O), *N,N,N*-trimethyl-2-adamantylammonium pentaborate trihydrate (**17**·3H_2O) and 4,4'-bipiperidinium heptaborate dihydrate (**20**·2H_2O). The crystal structure of an additional amine-boric acid co-crystallized species is also reported. All of the synthesized compounds reported in Chapter 3 were characterized using spectroscopic (IR, multi-element NMR) and analytical (melting point, elemental analysis, thermal analysis, powder X-ray diffraction) techniques.

The solid-state structures of the polyborate salts form giant H-bonded anionic lattices, with the 'brickwall' structure found to be sufficiently flexible to accommodate larger cations (within limits). When these limits are approached, they may be stretched further to accommodate the size of the cations by using 'spacer' molecules which increase the size of the lattice. It is only once the lattice cannot be stretched any further and/or when there are sufficient cation-anion interactions to dominate the energetics that polyborates other than pentaborates may be observed. The strength of the H-bonds found within polyborate salts were calculated using DFT theory; the results show that the α-reciprocal $R_2^2(8)$ H-bond interaction is the most energetically favoured (-21 kJ mol^{-1}), which is also the most commonly observed interaction within the solid-state structures of pentaborate salts.

The synthesis and characterization of Lewis base adducts of triorganoboroxines is also described within this thesis. Eight new adducts are reported, including the crystal structures of the triorganoboroxine·amine adducts of tri(4-chlorophenyl)boroxine·morpholine (**30**) and tri(4-chlorophenyl)boroxine·benzylamine (**33**). The Lewis acidity of the triorganoboroxines were also investigated and it was discovered that strongly electron-withdrawing pentafluorophenyl substituents greatly increase the Lewis acidity of the B atoms, resulting in a higher acceptor number.

Acknowledgements

First and foremost, I wish to offer my sincerest gratitude to my PhD supervisor, Professor Mike Beckett for his continued support, guidance and encouragement throughout the project. I could not have wished for a better supervisor, Mike, and I am extremely grateful for everything that you have done for me and helped me to achieve.

I would also like to thank my research committee, Dr Lorrie Murphy and Dr Keith Hughes, for their constructive feedback and guidance over the duration of my project. Thanks must also be given to Dr Andrew Davies for his assistance with the computational aspect of the project. Mr Thomas Perry, Ms Melanie Hughes and Ms Ashleigh Hayward must also be acknowledged for their assistance within the project.

I would like to give a big thank you to all of the technical staff at the School of Chemistry for their assistance and friendship throughout the project, in particular to Mr Nick Welsby and Dr David Hughes for training me to use the NMR in order to obtain the variable temperature data. Thanks must also be extended to Dr Peter Horton (National Crystallographic Service, Southampton) for obtaining and solving the crystallographic data; Dr Simon Curling (Bangor University) for obtaining the BET analysis data and to Professor Das (Indian Institute of Science, Bangalore) for obtaining the non-linear optical activity data.

Thank you also to all of the administrative staff within the School of Chemistry for all that they have done for me over the duration of my time at Bangor University.

Thanks to Dr Mohammed Alqhatani, Mr Mohammed Altahan, Dr Anna Tochwin and Dr Srikanth Kommanaboyina for their support, friendship and constructive discussion.

Last, but not least, I would like to thank my loved ones for their continued love, support and encouragement, in particular to Sean for putting up with me. Thank you for believing in me and for always being there for me. Caru chi gymaint.

Contents

List of Figures

List of Tables

Chapter 1:

Introduction

1.1 General introduction

This thesis consists of an investigation into the synthesis and characterization of some novel boron-oxygen compounds. Some of these are organic boron derivatives and others which are inorganic derivatives. Theoretical investigations into how the inorganic boron derivatives interact with each other through hydrogen bonding is also described.

The first chapter reviews the basic chemistry of boron and introduces the relevant inorganic and organic boron derivatives, which are studied experimentally within this thesis. A detailed description of their chemical and physical properties and their commercial uses is also outlined in this chapter.

The second chapter describes all the experimental work undertaken in this research project and provides the numbering scheme used for all the compounds throughout the thesis.

The third chapter describes the synthesis and characterization of a number of new non-metal cation polyborate salts. These compounds have been characterized using spectroscopic (IR, multi-element NMR) and analytical techniques (elemental analysis, thermogravimetric analysis, powder X-ray diffraction), with some also studied in the solid-state through single-crystal X-ray diffraction. Porosity measurements were also undertaken on a few samples, and these are also described within this chapter.

The fourth chapter concentrates on the computational (theoretical) studies of polyborate anions. Optimized geometries for polyborate anions were calculated, anion-anion interactions were investigated and the results of these calculations are described in detail within this chapter.

The fifth chapter describes the synthesis and characterization of a series of previously unreported amine adducts of triorganoboroxines. These adducts were characterized using spectroscopic (multi-element NMR, IR) and analytical (elemental analysis, powder X-ray diffraction) techniques. The solid-state crystal structures of two of these adducts are described within this chapter, as well as variable-temperature NMR studies and measurements of the Lewis acidity of the triorganoboroxines.

The sixth chapter is a succinct summary of all of the work described in this thesis.

1.2 Elemental boron

The chemistry of boron and its compounds is well documented in many undergraduate textbooks[1,2] and a generalized account of this literature is outlined below.

Elemental boron was first isolated in a very impure form in 1808 independently by Humphry Davy (England), and Joseph Louis Gay-Lussac and Louis Jacques Thénard (France). Towards the end of the 19th century, Henri Moissan had obtained higher purity (95 – 98 %) samples of boron through the reduction of boron oxide (B_2O_3) with magnesium. Samples of elemental boron with higher purity (>99 %) have been obtained from the reduction of volatile boron trihalides using hydrogen in the presence of a glowing filament.[3] The name *boron* was coined by Davy, to indicate the source of the element and its similarity to carbon, i.e. *bor*(ax + carb)*on*.

Boron is found in relatively low abundances in the solar system and within the Earth's crust, and is naturally found as mineral deposits, bound primarily to oxygen (borates), or oxygen and silicon (borosilicates), as opposed to its pure elemental form. Commercially viable mineral deposits are rare but do occur in places such as Boron in California and in some areas of Turkey.

Boron is the only non-metal element in group 13 of the periodic table and shows many similarities to its neighbour, carbon, and its diagonal relative, silicon. Boron is similar to silicon in that they both form acidic oxides, polymeric oxide structures and flammable gaseous hydrides. Like carbon and silicon, boron has a tendency to form covalent bonds in its compounds, but differs in that it has one less valence electron than the number of valence orbitals (electronic configuration $1s^2 2s^2 2p^1$). This electronic configuration renders boron(III) as a stable oxidation state with only 6 electrons in its valence shell, leaving the boron centre 'electron deficient'. This electron deficiency results in the boron centre behaving as a Lewis

acid, and so readily forms adducts with electron-pair donors. Boron shows a high affinity for electronegative atoms such as oxygen.

Numerous allotropes of boron exist, with all of the crystalline forms containing the icosahedral B_{12} building block, as shown in Figure 1.1. This icosahedral motif is also found in the structures of metal borides and boron hydrides.

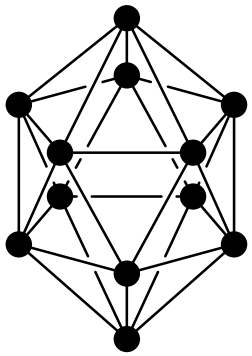

Figure 1.1: The B_{12} icosahedral unit.

There are two naturally occurring stable isotopes of boron: ^{10}B (19.9% abundance) and ^{11}B (80.1% abundance). Both of these are NMR active isotopes, with spin numbers of I = 3 and I = 3/2, respectively. ^{10}B also has a high neutron absorption cross-section which has led to many uses, such as neutron absorbers in nuclear reactor coolant rods[4] and pressurized water reactors,[5] and in boron neutron capture therapy – a type of cancer therapy used to treat brain tumours.[6,7]

1.3 Boron-oxygen chemistry

1.3.1 Inorganic derivatives: Polyborates

Boron is always found in nature in the form of boron-oxygen compounds such as anhydrous mixed metal oxides or as hydrated metal borates,[8] where boron is bound directly to oxygen and not to any other element. Anions that contain boron which is directly bound to oxygen are generally referred to as borates, and will continue to be referred to as borates within this thesis, although the preferred IUPAC

name is oxidoborates.[9] The strength of B-O bonds are relatively high, in the region of 540 kJ mol^{-1}, with only the B-F bond in BF_3 challenging this at ~640 kJ mol^{-1}.[10]

The principal oxide of boron is boron(III) oxide (B_2O_3), which can be obtained from the combustion of boron in air, or more commonly from the dehydration of boric acid, $B(OH)_3$, which is the primary source of many boron-oxygen compounds.[11]

In aqueous solutions, $B(OH)_3$ does not behave as a Brønsted acid by formation of the conjugate base $[BO(OH)_2]^-$, but instead behaves as a Lewis acid, by accepting a hydroxyl ion to form the tetrahedral anion $[B(OH)_4]^-$,[11,12] as shown in Equation 1.1.

$$B(OH)_3 + 2H_2O \rightarrow [B(OH)_4]^- + H_3O^+ \qquad (1.1)$$

In dilute aqueous solutions, this weakly monobasic acid exists almost exclusively as an equilibrated mixture of the undissociated molecule $B(OH)_3$ and the tetrahydroxyborate anion $[B(OH)_4]^-$.[13] The $[BO(OH)_2]^-$ anion is unknown in solution, however, there are crystalline structures in which this anion type has been found to exist, with one example being: $Cu_2[BO(OH)_2](OH)_3$.[14] At higher concentration and pH values, secondary equilibria involving condensation reactions of the two dominant monomeric species results in polymerisation.[11,12]

Polyborate species have been studied by ^{11}B NMR, but the spectra obtained depend upon the stability of the polyborate ion in solution, and the exchange rate of boron atoms between different chemical sites.[13] The most common polyborate species that exist in rapid equilibrium in relatively concentrated borate solutions are: the pentaborate anion $[B_5O_6(OH)_4]^-$, the triborate monoanion $[B_3O_3(OH)_4]^-$, the tetraborate anion $[B_4O_5(OH)_4]^{2-}$, and the triborate dianion $[B_3O_3(OH)_5]^{2-}$.[11,15,16]

It is interesting to note, that should a pentaborate salt enter an aqueous solution in the solid-state form, then over 90% dissociates by hydrolysis to give the triborate, tetraborate and monoborate species.[16]

1.3.1.1 Solid-state studies

There are over 200 minerals, and many more synthetic crystalline borate compounds, where boron is bound only to oxygen, that have been considered to have industrial importance.[17,18] Although the name generally refers to the octahydrate salt, the term *borax* is also given to the closely related sodium tetraborate minerals, *tincalconite*, $[Na]_2[B_4O_5(OH)_4]\cdot 3H_2O$ and *tincal*, $[Na]_2[B_4O_5(OH)_4]\cdot 8H_2O$, both of which contain the tetraborate anion and differ only by the number of waters of crystallization found in the unit cell; they both have uses in fire retardants, buffers, detergents and food additives.[2,19] *Sborgite*, $[Na][B_5O_6(OH)_4]\cdot 3H_2O$, and *stantite*, $[K][B_5O_6(OH)_4]\cdot 2H_2O$, are examples of naturally occurring minerals which contain the pentaborate anion, $[B_5O_6(OH)_4]^-$, which is the main focus of the synthetic work presented in Chapter 3. These borates contain anionic structural units composed of both trigonal, BO_3, and tetrahedral, BO_4, groups. These groups can link together *via* common oxygen atoms to form isolated rings and cages, or further condense into infinite chains, sheets and networks.[20-25]

Becker found there were over 800 reported borate structures on the Inorganic Crystal Structure Database (ICSD) in 2001, including many anhydrous synthetic borates, with the majority of them containing metal cations.[26] Grice *et al*. reviewed the borate minerals and also found the majority contained metal cations.[27] Recent access to the ICSD shows there are now over 1400 reported borate structures, with the majority of these still containing metal counter-cations.[28]

The borate structures can be categorised into 'isolated' and (infinite) polymeric borates, as well as containing metal or non-metal counter-cations. 'Isolated' borates can be hydrated or anhydrous, and may condense into infinite complex polyborates, as described earlier. In general, the polyborates contain boroxole rings (B_3O_3) as reoccurring units, with the Lewis acidity of the (often metal) counter ions influencing the observed structures.[8] Christ and Clark[29,30] developed a number of rules in order to classify the hydrated borate compounds, as detailed below:

1. Boron will link with three oxygen atoms in a trigonal plane, Δ, or with four oxygens to form a tetrahedron, T.

2. Polyborate anions are formed by corner sharing only of boron-oxygen triangles and tetrahedra in such a manner that a compact insular group results.
3. In the hydrated polyborates, protonatable oxygen atoms will be protonated in the following sequence: available protons are first assigned to free O^{2-} ions to convert these to free OH^- ions, additional protons are assigned to tetrahedral oxygens in the borate ion, protons are next assigned to triangular oxygens in the borate ion, and finally any remaining protons are assigned to free OH^- ions to form H_2O molecules.
4. The hydrated insular groups may polymerize in various ways by splitting out water; this process may be accompanied by the breaking of boron-oxygen bonds within the polyanion framework.
5. Complex polyborate anions may be modified by attachment of an individual side group, such as (but not limited to) an extra borate tetrahedron, an extra borate triangle, two linked triangles, and so on.
6. Isolated $B(OH)_3$ groups, or polymers of these, may exist in the presence of other anions.

This classification is based upon the numerous combinations of Fundamental Building Blocks (FBBs) with *n* boron atoms. For example, $[Na][B_5O_6(OH)_4]\cdot 3H_2O$ (FBB = 5) with four trigonal boron centres and one tetrahedral boron centre is represented as 5:4Δ+T. Polymeric borate anions are differentiated by the addition of ∞_y for chains (y = 1), sheets (y = 2) or networks (y = 3). Burns *et al*.[27,31,32] expanded upon their set of rules to incorporate into the classification descriptor a way of differentiating between different topological FBBs, with focus on the reoccurring boroxole (B_3O_3) units and how they are linked together. Taking this in to consideration, the Burns' descriptor for $[Na][B_5O_6(OH)_4]\cdot 3H_2O$ can therefore be described as 4Δ1□:<2Δ□>-<2Δ□>, where '-' indicates a spiro boron centre shared by two boroxole rings.

Borate materials with various alkali metal, alkaline earth metal, rare earth and transition metal cations have been widely studied;[22,23] with many of these synthesized under solvothermal conditions.[22,24,33-37] Borate materials containing non-metal cations have received much less attention, and only two borate minerals exist in nature that do not contain metal cations: *ammonioborite*,

$[NH_4][B_{15}O_{20}(OH)_8]\cdot 4H_2O$,[38] and *larderellite*, $[NH_4][B_5O_7(OH)_2]\cdot H_2O$,[39] both of which contain the ammonium cation. Non-metal cations differ from metal cations in their potential for interactions with borate anions: metal cations are spherical and primarily accept electron density from oxygen donors, whilst non-metal cations may be non-spherical and may have H-bond donor sites.[8,17] Properties such as these may lead to previously unobserved borate structural moieties, and further offers the opportunity to explore structure directing H-bond relationships.[8]

Many isolated polyborates, natural and synthetic, have been found to contain between one and six borons,[20,22] such as: orthoborates $[B(OH)_4]^-$; diborates $[B_2O(OH)_6]^{2-}$; triborates $[B_3O_3(OH)_4]^-$; tetraborates $[B_4O_5(OH)_4]^{2-}$; pentaborates $[B_5O_6(OH)_4]^-$; and hexaborates $[B_6O_7(OH)_6]^{2-}$.[20,27] Isolated polyborates containing more than six borons are much rarer, with only a few examples, *e.g*. heptaborates $[B_7O_9(OH)_{15}]^{2-}$, templated using both a metal cation[22,40] and a non-metal cation;[41-43] nonaborates $[B_9O_{12}(OH)_6]^{3-}$;[44] tetradecaborate $[B_{14}O_{20}(OH)_6]^{4-}$;[20] and pentadecaborate $[B_{15}O_{20}(OH)_8]^{3-}$, which has so far been found only in the mineral *ammonioborite*.[38] It is interesting to note that the larger isolated borate anions have been templated by organic cations; the nonaborate anion is only seen in species with organic (non-metal) cations.[44]

The first in-depth study of synthetic non-metal borates containing amines as cations was published in 1939.[45] Quaternary ammonium cations were first used in pentaborate synthesis in 1959,[46] but since this initial work,[46-48] the area remained relatively dormant until the 1990s.[12,49] Other amines have also been used as cations to synthesise borates with varying number of boron atoms within the anion,[11,17,20,21,23,42-44,47,48,50-55] although the majority of these contain the pentaborate anion.[15,37,42,49,56-69] Exploring how various amine cations structurally direct borate units is fundamental to the rational design of novel borates having potentially useful properties.[23] At the time of writing this thesis, isolated cation polyborate salts containing between one and fifteen boron atoms have been reported and Figures 1.2, 1.3 and 1.4 illustrate these anion types; a more detailed account of each borate anion type is outlined below, with the main focus on those which form salts with non-metal cations.

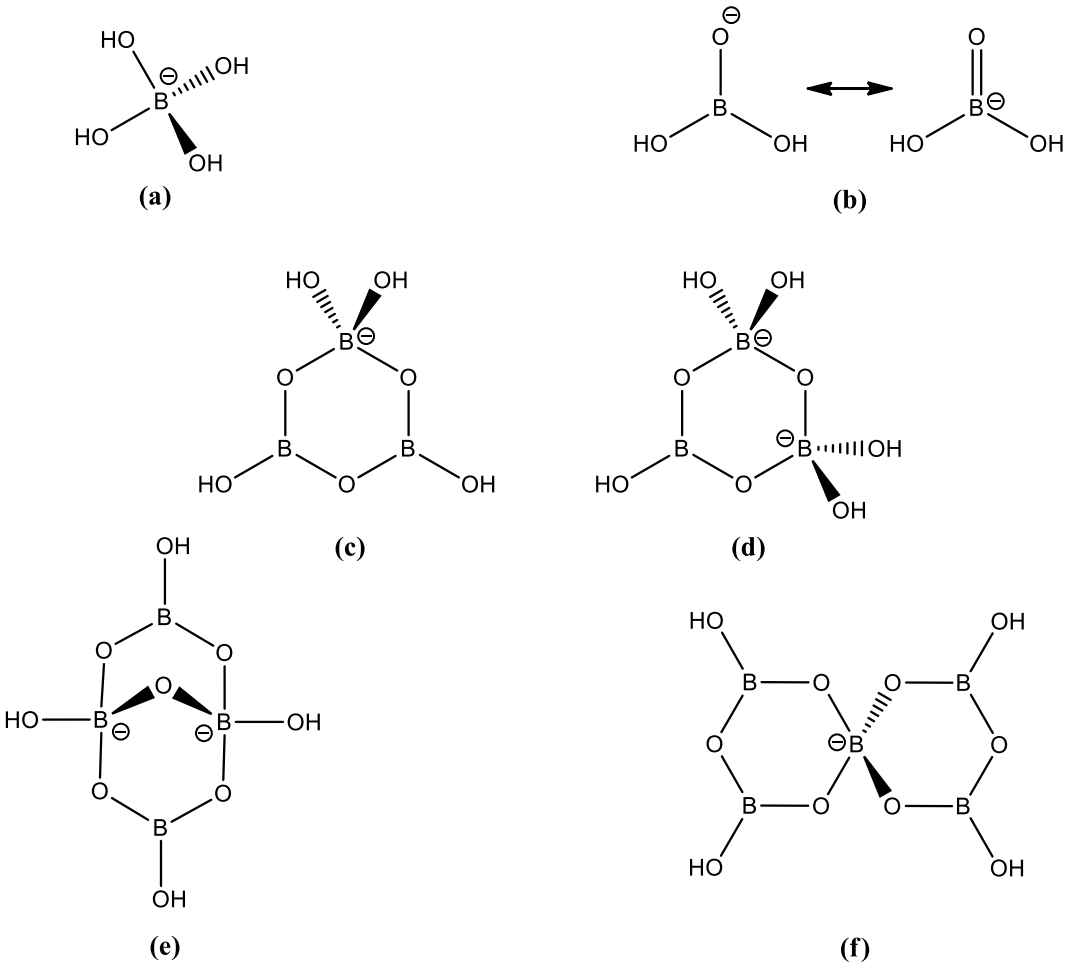

Figure 1.2: The isolated borate anion types containing fewer than six borons at the time of writing this thesis: (a) the orthoborate anion, $[B(OH)_4]^-$, as found in $NaB(OH)_4$;[70] (b) the monoborate anion, $[BO(OH)_2]^-$, as found in an urea inclusion complex;[11] (c) the triborate anion, $[B_3O_3(OH)_4]^-$, as found in $[HOCH_2C(CH_3)_2NH_3][B_3O_3(OH)_4]$;[21] (d) the triborate dianion, $[B_3O_3(OH)_5]^{2-}$, as found in the mineral inderite;[71] (e) the tetraborate anion, $[B_4O_5(OH)_4]^{2-}$, as found in borax;[72] (f) the pentaborate anion, $[B_5O_6(OH)_4]^-$, as found in a number of substituted imidazolium pentaborates.[73]

1.3.1.2 Monoborates

$B(OH)_3$ behaves as a Lewis acid in aqueous solution to form the tetrahedral monoborate anion, $[B(OH)_4]^-$ (Figure 1.2a). Although this anion has been found to occur in the solid-state in the compound $NaB(OH)_4$[70] it is not known, at the time of writing this thesis, to exist with any non-metal cations. There are, however, two reports of an elusive monoborate anion, $[BO(OH)_2]^-$ (Figure 1.2b), existing in non-metal borate structures; these were reported to have been found in an urea inclusion

complex $[(CH_3)_4N][BO(OH)_2]\cdot 2(NH_2)_2CO\cdot H_2O$,[11] and in the crystal structure $(NEt_4)_2[BO(OH)_2]_2\cdot B(OH)_3\cdot 5H_2O$. The former exists as a zig zag H-bonded ribbon of monoborate anions, with a water molecule H-bonded to the unique oxygen atom of the anion. The latter co-exists with $B(OH)_3$ in the solid-state, and the two form an infinite H-bonded ribbon of alternating species.

1.3.1.3 Triborates

The existence of the isolated triborate monoanion, $[B_3O_3(OH)_4]^-$ (Figure 1.2c), is rare, although there are a few reports of structures containing this isolated polyborate anion type. There are two reports of salts containing non-metal cations: $[H_2N(CH_2CH_2)_2NH_2][B_3O_3(OH)_4]$[54] and $[HOCH_2C(CH_3)_2NH_3][B_3O_3(OH)_4]$,[21] where in both cases the B_3O_3 boroxole ring deviates from planarity and exhibits the half-chair conformation. There are also reports of the triborate monoanion existing in structures containing metal cations: $K[B_3O_3(OH)_4]\cdot H_2O$,[74] $Na[B_3O_3(OH)_4]$[75] and, more recently, $[Co(diNOsar)]_2[B_3O_3(OH)_4]5Cl\cdot 4.75H_2O$ (diNOsar = 1,8-dinitro-3,6,10,13,16,19-hexaazabicyclo-(6.6.6)icosane).[76]

The isolated triborate dianion, $[B_3O_3(OH)_5]^{2-}$ (Figure 1.2d), has also been reported to exist in the non-metal cation salt $[C(NH_2)_3]_2[B_3O_3(OH)_5]$[48] (although not structurally characterized), as well as in the minerals *inderite* and *kurnakovite*, $Mg[B_3O_3(OH)_5]\cdot 5H_2O$,[71,77] *meyerhofferite*, $Ca[B_3O_3(OH)_5]\cdot H_2O$,[78] *inyoite*, $Ca[B_3O_3(OH)_5]\cdot 4H_2O$,[79,80] and *inderborite*, $CaMg[B_3O_3(OH)_5]_2\cdot 6H_2O$.[81]

1.3.1.4 Tetraborates

The isolated tetraborate dianion, $[B_4O_5(OH)_4]^{2-}$ (Figure 1.2e), has been reported in two structures, both partnered with non-metal cations: $[C_6H_{10}(NH_3)_2][B_4O_5(OH)_4]\cdot 2.5H_2O$,[82,83] which contains the cyclohexane-1,4-diammonium cation, and in $[H_2en]_2[B_4O_5(OH)_4][B_7O_9(OH)_5]\cdot 3H_2O$,[55] which contains the 1,2-ethylenediammonium cation. The latter of the two salts is a unique example of a non-metal cation double salt containing two different isolated polyborate anion types.

The tetraborate dianion also exists in structures containing alkaline metal cations, such as in *borax*, $Na_2[B_4O_5(OH)_4]\cdot 8H_2O$,[72] as well as transition metal cations, such as $[Cu(en)_2\{B(OH)_3\}][B_4O_5(OH)_4]\cdot B(OH)_3$,[84] and $[Co(en)_3][B_4O_5(OH)_4]Cl\cdot H_2O$.[85] The former transition metal cation salt's structure is octahedral, having a monodentate $B(OH)_3$ ligand coordinated *trans* to a coordinated tetraborate anion about the square planar $Cu(en)_2$ core. In addition to this, there is a $B(OH)_3$ 'spacer' molecule H-bonded to the tetraborate anion. The descriptor given for this molecule is 4:[2Δ+2T]+Δ, where the '+Δ' arises from the $B(OH)_3$ spacer molecule.

1.3.1.5 Pentaborates

The isolated pentaborate monoanion, $[B_5O_6(OH)_4]^-$ (Figure 1.2f), is the most commonly observed polyborate anion type and is comprised of two planar B_3O_3 boroxole rings which share a common boron atom. This tetrahedral boron atom is a spiro boron centre, resulting in the two boroxole rings being perpendicular to one another. The remaining boron atoms are trigonal and each have a hydroxyl group attached. The structural descriptor given for this molecule is 5:4Δ+T, or 4Δ1□:<2Δ□>-<2Δ□>.

This anion type is found in the majority of structurally characterized polyborates since the turn of the 21st century and is, perhaps, the easiest polyborate anion to prepare. Since 2000, the $[B_5O_6(OH)_4]^-$ anion has been reported in the structures of salts which contain non-metal (organic base) cations,[8,15,21,37,42,56,59,63-67,69,73,86-95] transition metal complex cations[24,25,33-35,85,89,96-104] and *s*-block element cations.[56,105,106]

The solid-state structures of all isolated pentaborate anion salts contain extensive anion-anion H-bond interactions. A three-dimensional H-bonded anionic lattice is formed, which is facilitated by the spiro boron centre of the pentaborate anion; the perpendicular boroxole rings allow the structure to become a three-dimensional lattice, rather than a layered, two-dimensional lattice. Each pentaborate anion forms H-bonds with four neighbouring anions, with a number of possible configurations. Schubert labelled the H-bond acceptor sites in the pentaborate anion as α, β or γ, depending on their position relative to the tetrahedral boron centre, with

the α position being the closest.[15] Four commonly observed H-bonding motifs have been observed in pentaborate anion-anion interactions and can be differentiated by using this labelling system, along with Etter nomenclature.[107]

The Etter nomenclature describes various intermolecular H-bond interactions, with these being denoted by 'C' for chain, 'R' for ring and 'D' for dimer or other finite set; intramolecular H-bond interactions are denoted by 'S' but are generally not observed in pentaborate anions. The number of H-bond donors (d) and acceptors (a) associated with each H-bond interaction are assigned as subscripts and superscripts, respectively, and the number of atoms partaking in the repetitive motif is indicated in parentheses, as shown in Equation 1.2.

$$\mathrm{X}_{\mathrm{d}}^{\mathrm{a}}(n) \qquad \text{(where X = R, C, D or S)} \quad (1.2)$$

To give an example of the use of the Etter notation for polyborate anion interactions, one of the four commonly observed H-bond motifs is the $\mathrm{R}_2^2(8)$, which is an eight-membered ring formed between two anions which are H-bonded together *via* two H-bond donor sites and two H-bond acceptor sites. To combine this Etter notation with the Schubert labelling system, these $\mathrm{R}_2^2(8)$ motifs can occur at reciprocal-α and -γ H-bond acceptor sites, whereas the ring formed between two β-acceptor sites is a twelve-membered ring, and is given the notation $\mathrm{R}_2^2(12)$. In addition to the H-bonded ring formations, repeating units are also observed as chains which run through the pentaborate anionic framework and are often observed as a C(8) β-chain – an eight atom chain which repeats *via* H-bonding at a β-acceptor site. These are the four most commonly observed H-bond interactions and the strength of these H-bonds are discussed in Chapter 4.

As previously mentioned, the pentaborate anions can H-bond to four neighbouring anions; this can happen in a variety of combinations – some of which are unique to particular compounds – however, the α,α,α,β acceptor site configuration is very common. Two variants of this configuration – both also including C(8) β-chains – are observed, and are referred to as having either a 'brickwall'[8,42,66,69,108] or 'herringbone'[15,37,42,63,65,66,73,87,93] structure. Another variant to

the α,α,α,β configuration exists, in which the β-interaction is a reciprocal-β $R_2^2(12)$.[24,33,54,73,103] There are two reported structures in which the α,α,α,γ configuration is observed, where the γ-interaction is a reciprocal-γ $R_2^2(8)$,[42,95] and one reported structure containing the α,α,α,α configuration: the salt [1,2,3-$(CH_3)_3C_3H_2N_2$][$B_5O_6(OH)_4$].[73] This anion-anion interactions leave little space for the cation, but the boroxole rings adopt a boat conformation in order to overcome this.

The ability of pentaborates to form such strong anionic lattices is an important driving force in their facile synthesis from aqueous solutions.[9] The anionic lattices of 'brickwall' structures – and presumably other lattice structures – have sufficient flexibility in that they may, within limits, accommodate cations of varying sizes.[69] Many pentaborate salts contain interstitial molecules which are present to simply fill space within the lattice[69] or they may be present and are H-bonded to, and/or bridge, pentaborate anions, leading to unique structures.[8,15,56,58,67,73,88,95,96,98,109] Polyborates other than pentaborates are probably only formed when there is insufficient space within the lattice, when cations are highly charged or when there are sufficient cation-cation H-bonds to outweigh the pentaborate anion-anion interactions.[9,40,76,110]

There are two reported structures in which π···π stacking interactions have been observed between cations: [PPh_4][$B_5O_6(OH)_4$]·1.5H_2O[109] and [$Cu(C_{12}H_8N_2)_2(CH_3CO_2)$][$B_5O_6(OH)_4$]·$C_4H_9NO$.[102] In both of these structures, the presence of the π···π stacking interactions between cations as well as the anion-anion H-bond interactions were found to further stabilize the structures.

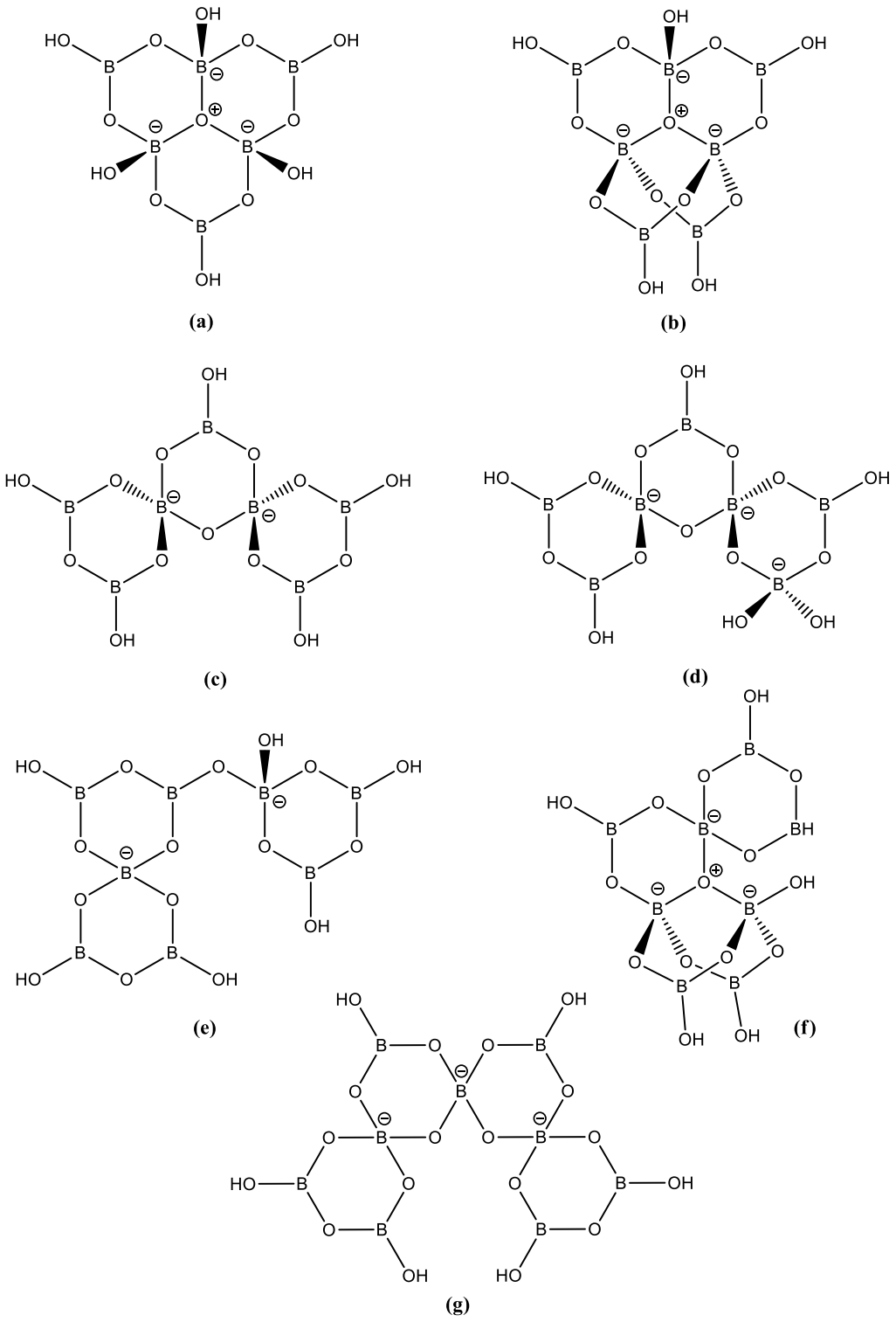

Figure 1.3: The rarer isolated polyborate anion types: (a) the hexaborate anion, $[B_6O_7(OH)_6]^{2-}$, as found in $[C_5H_{11}N_3][Co\{B_6O_7(OH)_6\}_2]\ 4H_2O$;[111] (b-d) the heptaborate anions, $[B_7O_9(OH)_5]^{2-}$, $[B_7O_9(OH)_5]^{2-}$ and $[B_7O_9(OH)_6]^{3-}$, as found in $[cyclo\text{-}C_6H_{11}NH_3]_2[B_7O_9(OH)_5]\cdot 3H_2O\cdot B(OH)_3$,[42] $[H_2dab][B_7O_9(OH)_5]\cdot H_2O$,[23] and $[Co(dien)_2][B_7O_9(OH)_6]\cdot 9H_2O$,[40] respectively; (e) and (f) the octaborate anions, $[B_8O_{10}(OH)_6]^{2-}$ as found in $[H_3N(CH_2)_7NH_3][B_8O_{10}(OH)_6]\cdot 2B(OH)_3$[15] and $[Co(en)_3][B_5O_6(OH)_4][B_8O_{10}(OH)_6]\cdot 5H_2O$,[98] respectively; (g) the nonaborate anion, $[B_9O_{12}(OH)_6]^{3-}$, as found in $[C(NH_2)_3]_3[B_9O_{12}(OH)_6]$.[44]

1.3.1.6 Hexaborates

There are three reports in the literature of the hexaborate dianion, $[B_6O_7(OH)_6]^{2-}$ (Figure 1.3a), where it is found coordinated to metal cations; apart from this coordination to the cations, the hexaborate dianions remain unchanged. The first report of the hexaborate dianion synthesized in the presence of an organic amine was in 2003, where it was found that the hexaborate dianion was coordinated to a Zn(II) centre in the salt $[(Me)_2NH(CH_2)_2NH(Me)_2][Zn\{B_6O_7(OH)_6\}_2]\cdot 2H_2O$.[112] The hexaborate dianions and water molecules are connected through extensive H-bonding, which build up a 3D structure of the anionic framework in a herringbone pattern; the amine molecules sit within the cavities of the anionic framework. A similar hexaborate salt is observed in $[C_5H_6N][Al\{B_6O_7(OH)_6\}_2]$[113] in which two tridentate hexaborate dianions are coordinated to an Al atom. The hexaborates are interconnected through H-bonding and form a large 3D supramolecular framework with cavities occupied by the $[C_5H_6N]^+$ cations.

Two further hexaborate structures are reported where they have been synthesized in the presence of an organic amine: the salt $[C_4N_2H_{12}][Co\{B_6O_7(OH)_6\}_2]\cdot 6H_2O$,[114] which contains the 1,4-piperazinium dication, and the salt $[C_5H_{11}N_3][Co\{B_6O_7(OH)_6\}_2]$ $4H_2O$,[111] which contains the 1-cyanopiperazinium cation. Both structures consist of two tridentate hexaborate anions which are coordinated to a Co(III) centre, adopting an octahedral geometry. The hexaborate anions and the water molecules in both structures also form large supramolecular frameworks containing ‘cavities’ in which the amine molecules are able to occupy. The hexaborate dianions found in all of these structures are found to be not dissimilar to the hexaborate dianion found in the mineral *aksaite*, $Mg[B_6O_7(OH)_6]\cdot 2H_2O$.[115] It is interesting to note that, at the time of writing this thesis, there have been no reports of the hexaborate dianion existing in salts containing exclusively non-metal cations.

1.3.1.7 Heptaborates

The heptaborate dianion is known to exist in two different isomers with the formula $[B_7O_9(OH)_5]^{2-}$ (Figure 1.3b and c). The ‘O^+’ isomer (Figure 1.3b) is based on the

hexaborate structure (Figure 1.3a) with an additional $B(OH)_3$ unit condensed with hydroxyl groups on two of the four-coordinate boron centres, thus forming a fourth boroxole ring. This type of heptaborate dianion isomer is found in the structures [*cyclo*-$C_6H_{11}NH_3]_2[B_7O_9(OH)_5]\cdot 3H_2O\cdot B(OH)_3$,[42] [*cyclo*-$C_7H_{13}NH_3][B_7O_9(OH)_5]\cdot 2H_2O\cdot 2B(OH)_3$,[42] and $[H_3N(CH_2)_7NH_3][B_7O_9(OH)_5]\cdot H_2O$,[43] which all consist of the heptaborate 'O^{+}' dianion partnered with non-metal cations.

The alternative $[B_7O_9(OH)_5]^{2-}$ isomer is referred to as the 'chain' isomer, (Figure 1.3c) consisting of two spiro four-coordinate boron centres and can be considered as an 'extended' pentaborate system.[9] This heptaborate isomer is observed in the structures of the non-metal cation salts $[H_2en]_2[B_4O_5(OH)_4][B_7O_9(OH)_5]\cdot 3H_2O$,[55] and $[H_2dab][B_7O_9(OH)_5]\cdot H_2O$ (dab = 1,4-diaminobutane),[23] as well as in the metal cation salts of $Rb_2[B_7O_9(OH)_5]$[20] and $Cs_2[B_7O_9(OH)_5]$[22] and in the mixed metal/non-metal cation salt $Na_2[H_2tmed][B_7O_9(OH)_5]\cdot H_2O$ (tmed = *N,N,N',N'*-tetramethylethylenediamine).[87] The commercial salt, commonly referred to as ammonium octaborate, has recently been characterized by XRD studies to reveal it has the 'chain' heptaborate anion with a boric acid of crystallization.[116]

The third heptaborate anion type is the $[B_7O_9(OH)_6]^{3-}$ trianion (Figure 1.3d), which is structurally similar to the chain isomer above, but differing in that there is an additional hydroxyl group on one of the outer boroxole rings. This anion type is found in the transition-metal complex cation salt $[Co(dien)_2][B_7O_9(OH)_6]\cdot 9H_2O$.[40]

1.3.1.8 Octaborates

The isolated octaborate dianion, $[B_8O_{10}(OH)_6]^{2-}$, has been reported to exist as two different isomers (Figure 1.3e and f). The first isomer (Figure 1.3e) can be described as a pentaborate anion condensed with a triborate monoanion; there are three linked boroxole rings, each containing one tetrahedral and two trigonal boron atoms. Two of the rings share a four-coordinate boron atom in the same way a pentaborate anion does, whereas the third ring shares an oxygen atom with a tetrahedral boron of the third ring with a trigonal boron atom of one of the first two rings. This anion type has been reported in the structure $[H_3N(CH_2)_7NH_3][B_8O_{10}(OH)_6]\cdot 2B(OH)_3$.[15]

The only other report of an isolated octaborate dianion can be found as the alternative octaborate dianion isomer (Figure 1.3f) in the transition-metal complex cation salt $[Co(en)_3][B_5O_6(OH)_4][B_8O_{10}(OH)_6]\cdot 5H_2O$ (en = 1,2-diaminoethane),[98] and is a unique example of a transition-metal complex cation salt which contains more than one isolated polyborate anion type. This octaborate dianion isomer can be described as a fusion of a tetraborate dianion with a pentaborate monoanion in which they have two oxygen atoms and a boron atom in common.[98] This anion contains four linked boroxole rings, compared with three in the other octaborate isomer, and contains a formally positively charged O atom which is shared by three of these rings.

1.3.1.9 Nonaborates

The nonaborate trianion, $[B_9O_{12}(OH)_6]^{3-}$ (Figure 1.3g), is rare and, at the time of writing this thesis, is limited to only two reported salt structures, both of which contain non-metal cations: $[C(NH_2)_3]_3[B_9O_{12}(OH)_6]$,[44] which contains the guanidinium cation, and $[C_3H_5N_2]_3[B_9O_{12}(OH)_6]$, which contains the imidazolium cation.

The nonaborate anion is made up of four boroxole rings which share three tetrahedral boron centres in a chain-like arrangement. The remaining boron atoms are trigonal, each with one hydroxyl group attached. The two ‘inner’ boroxole rings contain two tetrahedral and one trigonal boron atoms, whereas the ‘outer’ boroxole rings contain two trigonal and one tetrahedral boron atoms.

1.3.1.10 Larger polyborate anions

Isolated polyborate anions containing more than nine boron atoms are rare, however there have been a few reports of larger polyborate anions.

One of these larger anion types is the dodecaborate anion, which exists as both the tetraanion, $[B_{12}O_{16}(OH)_8]^{4-}$ (Figure 1.4a), and as the hexaanion, $[B_{12}O_{18}(OH)_6]^{6-}$ (Figure 1.4b). Both of these structures can be viewed as polymeric triborate moieties; the tetraanion, $[B_{12}O_{16}(OH)_8]^{4-}$, is comprised of four boroxole rings, with each ring sharing an oxygen atom between a tetrahedral boron and a

trigonal boron atom. This type of dodecaborate anion exists in the metal cation salt of $K_4[B_{12}O_{16}(OH)_8]$.[117]

The dodecaborate hexaanion, $[B_{12}O_{18}(OH)_6]^{6-}$, is comprised of six interconnected boroxole rings which are connected *via* common tetrahedral boron centres, resulting in each boroxole ring containing two tetrahedral boron centres and one trigonal boron centre, which has a hydroxyl group connected. This dodecaborate anion type has been observed in the structures of $K_7[(BO_3)Mn\{B_{12}O_{18}(OH)_6]\cdot H_2O$[118] and $Na_8[B_{12}O_{20}(OH)_4]$.[119] In the former, the dodecaborate anion is coordinated to the Mn^{2+} ion in a tridentate manner, through three of the six bridging oxygen atoms between the tetrahedral boron centres (the coordinated oxygen atoms are alternate). This anion type has not yet been observed in salts containing non-metal cations.

Another isolated polyborate anion type is the tetradecaborate tetraanion, $[B_{14}O_{20}(OH)_6]^{4-}$ (Figure 1.4c), which has been reported in the following non-metal cation salts: $[H_3N(CH_2)_2NH_3]_2[B_{14}O_{20}(OH)_6]$,[88] $[H_3N(CH_2)_3NH_3]_2[B_{14}O_{20}(OH)_6]$,[120] $[H_3N(CH_2)_4NH_3]_2[B_{14}O_{20}(OH)_6]$,[23] $[H_3N(CH_2)_6NH_3]_2[B_{14}O_{20}(OH)_6]$[120] and $[H_2dien]_2[B_{14}O_{20}(OH)_6]$ (dien = diethylenetriamine).[20] This polyborate anion can be described as two fused ‘chain’ isomer heptaborates which are connected *via* two bridging oxygen atoms after condensation and loss of two water molecules.

Finally, the largest known isolated polyborate anion to date is the pentadecaborate trianion, which is found exclusively in the structure of the mineral *ammonioborite*, $[NH_4][B_{15}O_{20}(OH)_8]\cdot 4H_2O$.[38] This polyborate anion can be described as three pentaborates which are connected *via* two bridging oxygen atoms, arising from the condensation and elimination of two water molecules. It is interesting to note that, at the time of writing this thesis, this polyborate anion type is only found in this mineral and has not been synthesized in a laboratory and it does not coexist partnered by a metal cation.

These larger, rarer polyborate anion types have been found to exist in structures containing non-metal cations – some exclusively with non-metal cations – and therefore raises the possibility of synthesising further non-metal polyborate salts containing larger and unusual polyborate anion types.

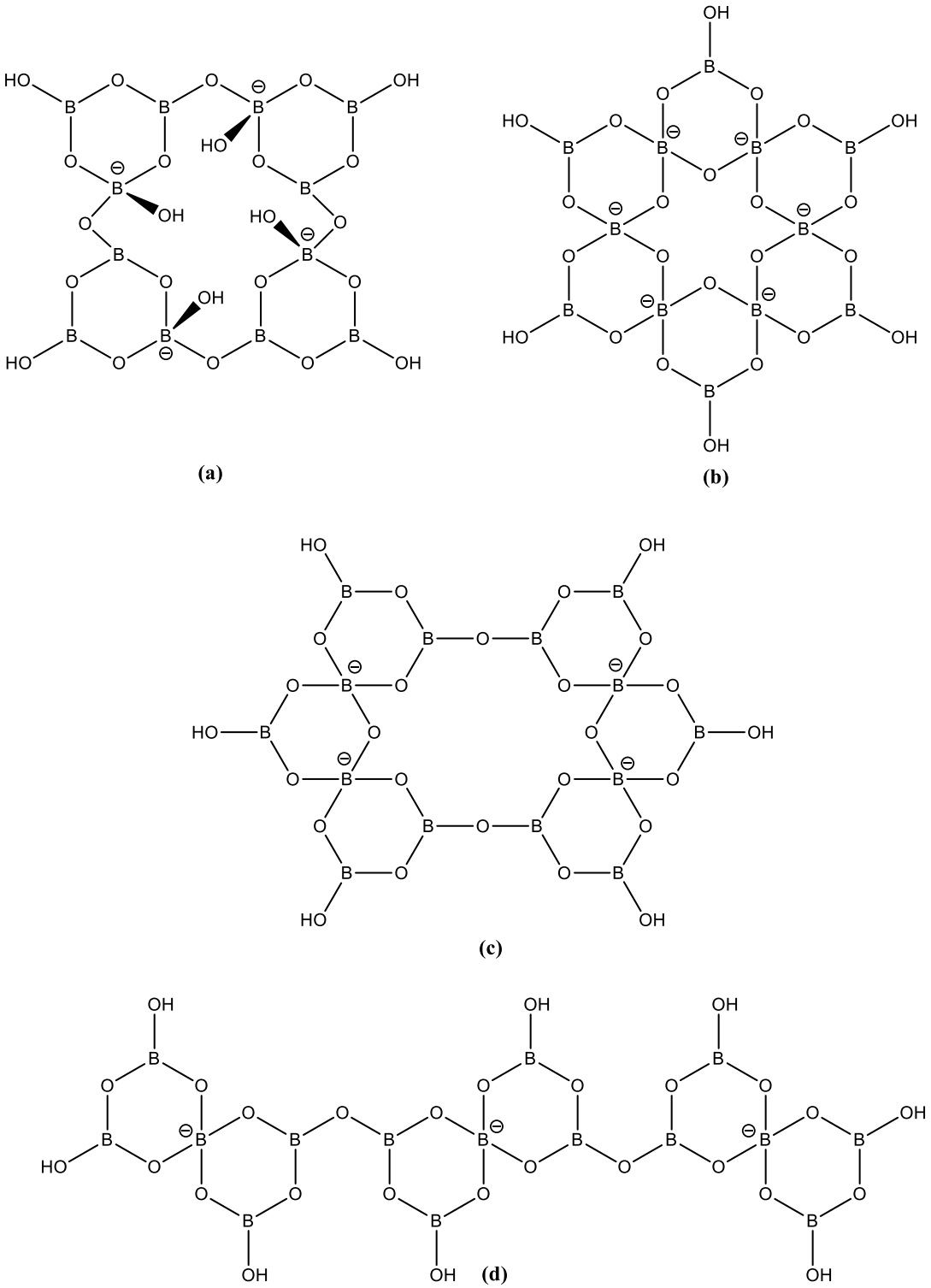

Figure 1.4: The rarer isolated polyborate anion types: (a) and (b) the dodecaborate anions, $[B_{12}O_{16}(OH)_8]^{4-}$, and $[B_{12}O_{18}(OH)_6]^{6-}$, as found in $K_4[B_{12}O_{16}(OH)_8]$[117] and $K_7[(BO_3)Mn\{B_{12}O_{18}(OH)_6]\cdot H_2O$,[118] respectively; (c) the tetradecaborate anion, $[B_{14}O_{20}(OH)_6]^{4-}$, as found in $[H_3N(CH_2)_3NH_3]_2[B_{14}O_{20}(OH)_6]$;[120] (d) the pentadecaborate anion, $[B_{15}O_{20}(OH)_8]^{3-}$, as found in the mineral ammonioborite.[38]

1.3.1.11 Synthetic methods

Salts containing the pentaborate anion, are easily prepared in aqueous solutions by mixing reagents in a 5:1 ratio, and awaiting crystallization. The majority of the polyborate salts discussed in Chapter 3 were prepared in this way. The planned synthesis of salts containing other polyborate anions are generally rare and synthetic reactions often lead to unexpected borate stoichiometries. The reason for this is that in aqueous solutions, borates exist as a 'Dynamic Combinatorial Library' (DCL)[121] of various polyborate anions, which exist in concentrations determined by total boron concentration, temperature and pH.[9,16,122].

Apart from stoichiometric reactions in aqueous solutions, reported polyborate salts have also been prepared under solvothermal conditions. Solvothermal reactions are usually carried out in a sealed vessel below 200 °C, where the contents can reach autogenous pressure. The reaction solvents in *solvothermal* reactions are usually organic solvents, but they may also be water, and in this case are usually referred to as *hydrothermal* reactions although the term solvothermal appears to be interchangeable for both types of solvent.[9] Figure 1.5 illustrates what a typical solvothermal reaction vessel looks like.

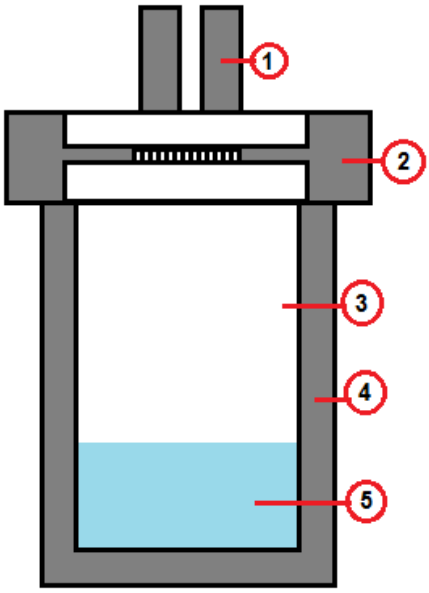

Figure 1.5: Schematic of a solvothermal reaction vessel where 1 is the pressure release valve, 2 is the stainless steel lid, 3 is the Teflon liner, 4 is the stainless steel reaction vessel and 5 is the reaction mixture.

The use of a solvothermal synthetic method can be beneficial as the method enables the use of amines as the reactants, which decompose at elevated temperatures. In addition to this, the solvent viscosity is reduced under these conditions, thus enhancing the solubility of the reactants and promoting the growth of good quality single crystals.[123]

1.3.1.12 Industrial uses

Polyborate salts have been shown to have a wide variety of industrial applications including buffers,[124] flame retardants,[125,126] foodstuffs,[127] detergents,[128] fluorescence and UV laser materials.[53,129]

Polyborates, due to their porous nature, have also shown applications as molecular sieves and as potential hydrogen stores.[123] Recent years have seen a recognition of the future need for a hydrogen based economy.[130] Using hydrogen as a fuel would be beneficial both strategically and environmentally, arising from a decreased reliance on oil, and a major reduction in air pollution.[130] There are, however, major challenges to overcome before the technology necessary to change from petroleum to hydrogen as an energy carrier can be implemented.[130,131] One such problem is the hydrogen store. The US Department of Energy (DoE) requires that a potential hydrogen store must be capable of storing 6% wt. H_2.[132] Amongst others, porous sorbents have been proposed as a candidate type for hydrogen storage;[133] boron oxide has been proposed as a porous sorbent which meets the US DoE's requirements.[134,135] Many polyborate salts can be thermally decomposed to boron oxide[15] and, for this reason, these polyborate salts could be perceived as thermal precursors to porous boron oxide, and therefore potential hydrogen stores themselves.

Polyborate salts have also found application in optical devices and are under increasing investigation due to their non-linear optical (NLO) properties.[22,37,56,61,136] They are one of the large resources of NLO materials and are comprised of mainly inorganic (metal) cation polyborate salts. These NLO materials may be second order and show an additional property referred to as *second harmonic generation* (SHG) in which photons with the same frequency interact with a non-linear material and 'combine', forming new photons which have twice the frequency and half the

wavelength of the initial photons. This type of NLO property was first reported in 1961 by Franken *et al*.[137] and is sometimes referred to as *frequency doubling*. SHG properties only appears in solid-state materials that do not contain inversion symmetry. There have, recently, been a few reports of pentaborate salts showing NLO properties: $[C_6H_{13}N_2][B_5O_6(OH)_4]$,[94] $[C_2H_{10}N_2][B_5O_8(OH)]$,[61] $[NH_4][B_5O_6(OH)_4]\cdot 2H_2O$,[56] $Rb[B_5O_6(OH)_4]\cdot 2H_2O$[56] and $[Zn(B_5O_7)(OH)_3(C_{10}H_{24}N_4)]$.[138] All of these compounds display second-order NLO behaviour, with $[C_2H_{10}N_2][B_5O_8(OH)]$[61] and $[C_6H_{13}N_2][B_5O_6(OH)_4]$[94] having a second harmonic generation (SHG) efficiency of 1.2- and 0.9-times, of that of KH_2PO_4, respectively. NLO materials such as non-metal polyborate salts show potential for finding new materials which could replace heavy metals in optical devices.

1.3.2 Organic derivatives

The following sub-sections describe a small number of the organoboron derivative compound classes which are relevant to the work undertaken during this research project.

1.3.2.1 Orthoborate esters

Orthoborate esters, which have the general formula $(RO)_3B$, are the simplest organoboron derivatives and are the esters of boric acid. They have a 3:1 ratio of organooxy groups to the boron atom, which is found in a trigonal planar geometry (Figure 1.6) and contain B-O-C bonds within its structure. Other synonyms of orthoborate esters include triorganoborates or triorganooxyboranes.

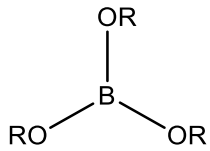

Figure 1.6: The general structure of orthoborate esters, where R is an organic group.

The most common method for the preparation of orthoborate esters is through the esterification of boric acid (Equation 1.3) or boron oxide using a stoichiometric reaction with an alcohol or phenol.

$$B(OH)_3 + 3ROH \rightarrow (RO)_3B + 3H_2O \quad (1.3)$$

The equilibrium for this reaction lies far to the left and in order for the reaction to take place, the water produced must be removed.[139] This can be achieved by formation on an azeotrope using benzene or toluene[140] which is then collected and removed through means of a Dean-Stark apparatus. The orthoborate esters are generally moisture and air sensitive and readily undergo complete hydrolysis to the boric acid and alcohol starting materials.

Orthoborate esters may also be prepared by transesterification. This method allows the conversion of low molecular weight orthoborate esters into higher molecular weight orthoborate esters. The method involves treating the low molecular weight orthoborate ester with an alcohol, which simply displaces the alkoxy substituents on boron, as shown in Equation 1.4.[141]

$$B(OR)_3 + 3R'OH \rightarrow B(OR')_3 + 3ROH \quad (1.4)$$

The alcohol liberated in this reaction must have a lower boiling point than that of the orthoborate ester, in order for it to be conveniently removed by distillation.

Boron trichloride may also be converted in to an orthoborate ester by reacting with an alcohol or phenol (Equation 1.5).[142] No heating is required for the reaction to proceed, with trimethoxy- and triethoxy- orthoborate esters having been prepared below -60 °C.[143,144]

$$BCl_3 + 3ROH \rightarrow B(OR)_3 + 3HCl \quad (1.5)$$

Orthoborate esters will react with amines to form either 1:1 complexes,[145] or will undergo a displacement of one of the alkoxy groups by an alkylamino group[146] (Equations 1.6 and 1.7). This latter formation can be reacted with additional amine until all alkoxy groups have been displaced by the alkylamino groups.

$$(RO)_3B + R'NH_2 \rightarrow (RO)_3B{:}NH_2R' \quad (1.6)$$

$$(RO)_3B + R'NH_2 \rightarrow ROH + (RO)_2BNHR' \quad (1.7)$$

Orthoborate esters will also react with a variety of different acids,[147-150] halogenated compounds,[151] metals,[152] sulfur compounds[153] and boron-carbon compounds.[154]

Several industrial uses of orthoborate esters can be found in the literature, including, but not limited to: plasticisers for resins,[155] antioxidants in PVC and rubbers,[156] as additives in lubricants,[157] purification of alcohols in the perfume industry,[158] and gas fluxes for welding.[159]

1.3.2.2 Metaborate esters

Metaboric acid esters are generally referred to as triorganooxyboroxines or metaborate esters. They have the general formula $(RO)_3B_3O_3$ and differ from orthoborate esters in that they have a 1:1 stoichiometric ratio of organooxy groups to boron, and also contain a 6-membered cyclic B_3O_3 boroxole ring as shown in Figure 1.7. Like orthoborate esters, metaborate esters also contain B-O-C bonds within their structure.

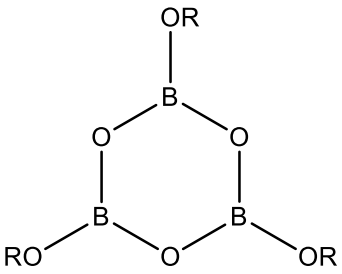

Figure 1.7: The general structure for a metaborate ester, which contains the 6-membered B_3O_3 boroxole ring.

These metaborate esters were first reported in 1865 by Schiff and Bechi[160] and were prepared by reacting analogous orthoborate esters with boron oxide as shown in Equation 1.8. This equimolar reaction always yields the metaborate ester as the sole product and is a preferred method as no further purification is required. Boric acid may be converted into a metaborate ester through the reaction with primary or secondary alcohol. The reaction takes place by simply heating,[161] evacuating the mixture,[162] or by removing water by formation of an azeotrope with toluene or benzene (Equation 1.9).[163]

$$(RO)_3B + B_2O_3 \rightarrow (RO)_3B_3O_3 \quad (1.8)$$

$$3ROH + 3B(OH)_3 \rightarrow (ROBO)_3 + 6H_2O \quad (1.9)$$

Metaborate esters partake in a number of reactions. The most common reaction is hydrolysis; the metaborate esters are readily hydrolysed to boric acid and the alcohol starting materials.[164] They will also react with halogens; the reaction of trimethoxyboroxine with excess chlorine at room temperature has been shown to produce boron trichloride (Equation 1.10).[151]

$$(MeOBO)_3 + 9Cl_2 \rightarrow BCl_3 + 3COCl_2 + 9HCl + B_2O_3 \quad (1.10)$$

Metaborate esters will also react with hydrogen halides, although they are less reactive than those with halogens, and therefore require heating for the reaction to proceed. For example, heating a metaborate ester in the presence of hydrogen bromide in a sealed tube results in dealkylation,[164] as shown in Equation 1.11.

$$(ROBO)_3 + HBr \rightarrow B(OH)_3 + 3RBr + B_2O_3 \qquad (1.11)$$

Metaborate esters have found applications as epoxide polymerisation initiators,[165,166] antioxidants in plastics and rubber,[167] and as additives in jet fuels[168] and greases.[169] Due to their high thermal stability, metaborate esters also have uses as additives in heat resistant inks[170] and as welding fluxes.[171]

1.3.2.3 Boronic acids

Boronic acids are similar in structure to boric acids, but have one hydroxy group replaced with an alkyl or aryl group, as illustrated in Figure 1.8 below. They contain two B-O and one B-C bonds.

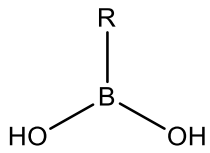

Figure 1.8: The general structure of boronic acids.

Boronic acids may be prepared from the reaction of a Grignard reagent with boron trihalides or borate esters (Equation 1.12),[2] where the Grignard supplies the hydrocarbon R group and the boron trihalide or borate esters supply the boron.[172] Many compounds have been used successfully as the boron source, including boron trifluoride,[173] triisobutyl borate,[174] tri-*n*-butyl borate[175] and trimethyl borate.[176] Cowie *et al*.[177] successfully modified the Grignard reagent method by heating a mixture of

a bromobenzene, tri-*n*-butyl borate and magnesium for 2-3 hours at 230°C to obtain phenylboronic acid in moderate yield (~40%).

$$B(OR)_3 + ArMgX \rightarrow ArB(OR)_2 \xrightarrow{2H_2O} ArB(OH)_2 \qquad (1.12)$$

Organolithium reagents may also be used during the synthesis of boronic acids,[178,179] and other routes include reacting organozinc, tin, mercury or aluminium compounds with borate esters and boron trihalides.[180] This latter method was one of the first synthetic methods discovered for the synthesis of boronic acids, with most of the initial work carried out by Michaelis and Becker,[181,182] who investigated the reaction of boron trichloride and with diphenylmercury (Equation 1.13).

$$BCl_3 + Ph_2Hg \rightarrow PhHgCl + PhBCl_2 \xrightarrow{2H_2O} PhB(OH)_2 \qquad (1.13)$$

Burch *et al*.[183] investigated the reaction of tetraphenyltin with boron trichloride, with the resulting boron halides easily hydrolysed to the corresponding boronic acid (Equation 1.14).

$$Ph_4Sn + 4BCl_3 \rightarrow 4PhBCl_2 + SnCl_4 \qquad (1.14)$$

Boronic acids can react in a number of ways, with one of the most frequently reported reactions being dehydration to form the anhydrides. These anhydrides are generally trimeric and are easily prepared through dehydration of the boronic acids and are generally referred to as triorganoboroxines (Section 1.3.2.5).[184] Some sterically hindered boronic acids (such as mesitylene boronic acid) dehydrate to form dimeric anhydrides which contain a 4-membered B_2O_2 cyclic ring,[185] as shown in Figure 1.9, rather than the 6-membered B_3O_3 cyclic boroxole ring more commonly observed.

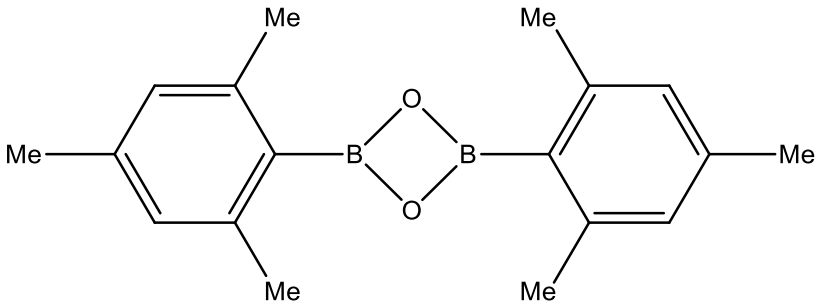

Figure 1.9: Mesitylene boronic anhydride; an example of a sterically hindered boronic acid anhydride containing a 4-membered cyclic ring.

The reaction of boronic acids with alcohols and azeotropic removal of water using benzene of toluene yield esters (Equation 1.15).[186]

$$RB(OH)_2 + 2R'OH \rightarrow RB(OR')_2 + 2H_2O \qquad (1.15)$$

There are many uses for boronic acids reported in the literature, including alkylboronic acids being used as oxidation inhibitors in oils,[187] gasoline[188] and petroleum spirit. Boronic acids are used extensively in organic chemistry as chemical building blocks and intermediates.[189] One example is the Suzuki coupling reaction, first published in 1979,[190] which is a cross-coupling reaction between organoboronic acids and halides, in the presence of a palladium catalyst (Equation 1.16), and is one of the better known applications of boronic acids to date.

$$R_1\text{-}BY_2 + R_2\text{-}X \xrightarrow[\text{Base}]{\text{Pd catalyst}} R_1\text{-}R_2 \qquad (1.16)$$

Akira Suzuki, Richard F. Heck and Ei-ichi Negishi were awarded the 2010 Nobel Prize in chemistry for their work on developing palladium catalysed cross coupling reactions.

Other uses of boronic acids are in chemotherapy. The compound Bortezomib (Figure 1.10) contains a boronic acid group and is used as a protease inhibitor.[191] It is the first therapeutic protease inhibitor to be tested in humans and has been approved in the US for treating relapsed multiple myeloma.[192,193]

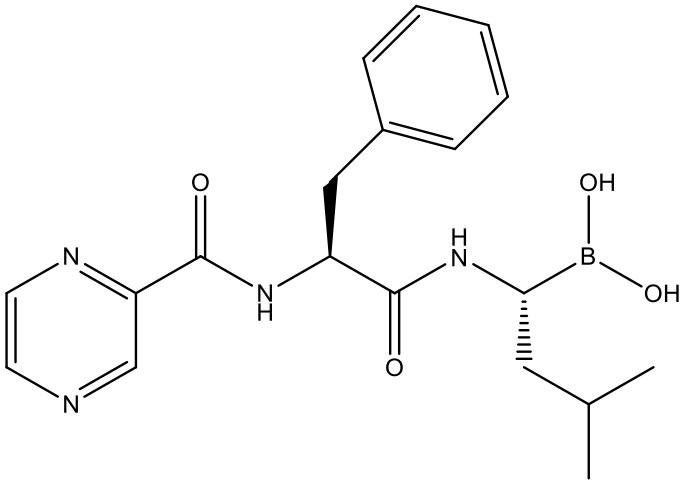

Figure 1.10: The structure of Bortezomib, an anti-cancer drug containing a boronic acid group.

Proteasomes break down proteins and in some cancers, the proteins that normally kill cancerous cells are broken down too quickly. Bortezomib interrupts this process through specific binding of the boron atom to the catalytic site of one of the proteasomes, allowing the proteins to kill the cancer cells.[194] Boronophenylalanine (BPA, Figure 1.11) is also an effective boronic acid which has been used as a ^{10}B source in boron neutron capture therapy (BNCT) to treat melanoma tumours.[195,196]

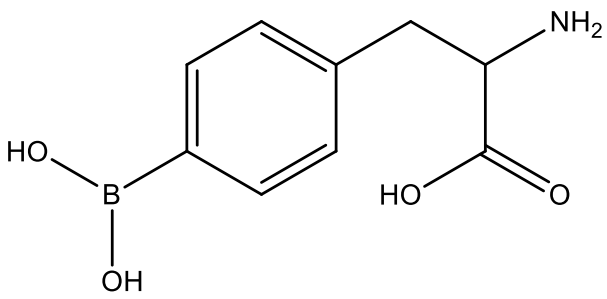

Figure 1.11: The structure of boronophenylalanine (BPA) which is used as a ^{10}B source in BNCT therapy.

1.3.2.4 Borinic acids

Borinic acids differ from boronic acids in that they have two alkyl or aryl substituents in place of the hydroxy groups, resulting in two B-C bonds and one B-O bond, as illustrated in Figure 1.12.

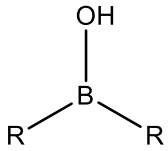

Figure 1.12: The general structure of borinic acids.

Borinic acids can generally be prepared by reacting alkyl borates with two moles of a Grignard reagent followed by hydrolysis.[197,198] Oxidative cleavage of trialkyl- or triarylboranes, followed by hydrolysis also yields borinic acids, as shown in Equation 1.17.[199]

$$R_3B \xrightarrow{O_2} R_2BOR \xrightarrow{H_2O} R_2BOH \qquad (1.17)$$

Boron trihalides can be reacted with borinic anhydrides to form dialkyl or diarylboron halides which can then be hydrolysed to give the borinic acids.[200] Borinic acids can also be prepared by reacting trialkylboranes with ammonia or amines under pressure and high temperature. The dialkyl(amino)boranes can be hydrolysed to obtain the borinic acids.[201]

The borinic acids are less stable than the boronic acids towards air-oxidation; when the borinic acids are stored for long periods of time, they decompose to the corresponding boronic acid and hydrocarbon.[202] This can be overcome by converting into the corresponding aminoethylborinate by reacting the borinic acid with 2-aminoethanol (Equation 1.18).[203] This protects the borinic acid from hydrolysis and oxidation for long periods of time and is easily returned to the deprotected borinic acid by hydrolysis using dilute acid.[204]

$$Ph_2BOH + NH_2(CH_2)_2OH \rightarrow Ph_2BO(CH_2)_2NH_2 \qquad (1.18)$$

Borinic acids are used as antioxidants in rubber, which slows the cracking and discolouration processes;[205] the borinic acids also have found use as additives in jet fuels to prevent ice-formation.[206]

1.3.2.5 Triorganoboroxines

Triorganoboroxines (Figure 1.13) can be considered to fall under the same category as boronic and borinic acids as they also contain both B-O and B-C bonds. The difference with triorganoboroxines, though, is that these are cyclic compounds, containing a 6-membered B_3O_3 boroxole ring, similar to those observed in the inorganic polyborate anion salts mentioned in Section 1.3.1. They differ from metaborate esters (Section 1.3.2.2) in that although they contain boroxole rings, the alkyl or aryl groups are attached directly to the boron atom, rather than *via* an oxygen bridging atom.

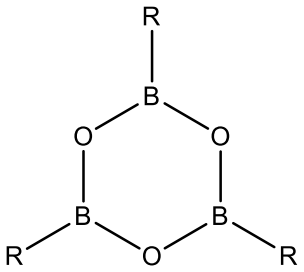

Figure 1.13: The structure of triorganoboroxines, which contain a B_3O_3 6-membered cyclic ring.

Triorganoboroxines are generally prepared through dehydration of the corresponding boronic acid, which can be carried out either in by heating at atmospheric pressure or in a vacuum oven,[207] or by desiccation at room temperature over drying agents such as phosphorus pentoxide, sulfuric acid or anhydrous calcium chloride.[208] Other methods of preparing triorganoboroxines include

azeotropic removal of water by use an appropriate solvent such as toluene or benzene.[209]

The triorganoboroxines are susceptible to ring cleavage through simple hydrolysis (Equation 1.19), yielding the corresponding boronic acid. Ring cleavage can also occur through the addition of boron trihalides to the triorganoboroxines, which yields the organoboron dihalide as a product,[210] which can be hydrolysed to the boronic acid. It is interesting to note that the mesitylene boronic anhydride, mentioned in Section 1.3.2.3, is stable in water at room temperature for months and ring cleavage of the 4-membered ring only occurs after heating in boiling water, converting the anhydride back to the boronic acid.[185]

$$(RBO)_3 + 3H_2O \rightarrow 3RB(OH)_2 \qquad (1.19)$$

Triorganoboroxines will react with alcohols to prepare boronic acid esters. Removal of the water as an azeotrope increases the yield of these reactions.[211]

Triorganoboroxines will also react with amines and other Lewis bases to give 1:1, and in some cases 2:1 or 1:2, coordination complexes; these reactions are the main focus of the synthetic work presented in Chapter 5 and more information on these complexes can be found there.

Triorganoboroxines have found a number of industrial applications, such as uses as herbicides and bacteriocides,[212] as well as lubricant aids in grease,[213] and as stabilizers and additives in polymers.[214] In 2005, Yaghi *et al*.[215] were the first to report the synthesis and characterization of the first crystalline arylboroxine-based porous materials - covalent organic framework (COF). Since then, a number of COFs have been reported and this area is expanding rapidly.[216-223]

Triorganoboroxines have also found use as additives in batteries, where is is blended with poly(ethylene oxide),[224,225] PEO; PEO is a solid polymer electrolyte. The Lewis acidic boroxine rings are designed to coordinate the anion of the dissolved electrolytic salt leading to improved single ion conduction.

As with the inorganic polyborate salts (Section 1.3.1.12), triorganoboroxines have also been investigated as potential NLO materials. Blanchard-Desce *et al*.[226] have extensively studied the NLO response from a number or trisubstituted arylboroxines. Theoretical studies showed little to no second order NLO property, however upon the addition of electron-donating groups to the *para* position of the phenyl rings, the NLO response was dramatically increased. Experimental work by Alcaraz *et al*.[226] confirmed these findings. Blanchard-Desce and co-workers followed this up with another computational study[227] which showed that increasing the conjugation length by introduction of an alkyne or an olefin between the electron-donating substituents and electron-accepting boroxine ring, further increases the hyperpolarisability (β) value compared to compounds lacking spacers.

Chapter 2:

Experimental

2.1 General

All chemicals and reagents were purchased from Sigma Aldrich (UK), Fisher Scientific (UK) or Lancaster Synthesis (UK) and used as supplied, without further purification, unless otherwise stated.

NMR spectra were recorded at room temperature (298K) on a Bruker Ultrashield™ Plus 400, operating at: 400 MHz for ^{1}H and 101 MHz for ^{13}C, with $CDCl_3$, D_2O or CD_3OD used as an internal standard; 162 MHz for ^{31}P, using H_3PO_4 as an external standard; and 128 MHz for ^{11}B, using $BF_3{\cdot}OEt_2$ as an external standard. Variable temperature NMR spectra were recorded on a Bruker Ultrashield™ Plus 500, operating at 500 MHz for ^{1}H, using $CDCl_3$ as an internal standard, and at 160 MHz for ^{11}B, using $BF_3{\cdot}OEt_2$ as an external standard. All NMR spectra were recorded using TopSpin™ 3.2 software package and were further analysed using MestReNova v6.0.2.

Infrared (FTIR) spectra were obtained as KBr disks on a Perkin-Elmer 100 FTIR spectrometer over 450-4000 cm^{-1}.

Thermogravimetric analyses (TGA) and differential scanning calorimetry (DSC) were performed between 25-800 °C (in air) on an SDT Q600 V4.1 Build 59 instrument, using alumina crucibles, at a ramp rate of 5 °C min^{-1}.

Powder X-ray diffraction (p-XRD) was carried out on a Phillips X-Pert 3040/60 XRD diffractometer using a Cu K_α source; spectra were obtained using the Phillips X'Pert Data Collector software package.

C, H and N elemental analyses were carried out at external laboratories; OEA Laboratories Ltd., Callington, Cornwall, and Elemtex Ltd., Launceston, Cornwall. %Boron determination was carried out using the barium borotartarate method (Section 2.2).

Single-crystal X-ray crystallography was carried out at the EPSRC National Crystallographic Service at the University of Southampton. Full details are given in the supplementary information.

Brunnauer-Emmett-Teller (BET) analyses were carried out by Dr S Curling (Biocomposites, Bangor University) on a Gemini 2375 analyser, using N_2 gas as the adsorbent.

2.2 Gravimetric determination of boron content

Boron determination (%) was carried out using an adaptation of a gravimetric literature procedure,[228] as described below.

A stock solution was prepared from the following: ammonium chloride (240 g), D-tartaric acid (14 g) and barium chloride dihydrate (13 g), made up to 1 L with deionised water.

A known amount of borate salt was dissolved in deionised water (10 mL) and transferred to a 100 mL volumetric flask. Concentrated ammonium hydroxide solution (10 mL) was added and the solution made up to the mark with the barium-containing stock. The solution was mixed by inversion and allowed to stand for 24 hr. The insoluble barium tartarate complex was collected by suction filtration and then washed with concentrated ammonium hydroxide solution (2 x 25 mL), 1:1 concentrated ammonium hydroxide:acetone (2 x 25 mL) and industrial methylated spirits (2 x 25 mL). The remaining solid was oven-dried at 110 °C and weighed as $4BaC_4H_4O_6{\cdot}Ba(BO_2)_2{\cdot}4H_2O$.

2.3 Activation of Dowex™ anion exchange resin

Dowex™ anion exchange resin (Cl^- form) was stirred in NaOH (8 M) for 24 hr, then washed thoroughly with deionised water until the washings were at ~pH 7. 30 g of activated Dowex™ (OH^- form) enabled the complete anion exchange of 8 mmol of base.

2.4 Preparation of free amines and quaternary ammonium salts

2.4.1 Synthesis of *N*,*N*-dimethylpyrrolidinium iodide[229]

N,*N*-Dimethylpyrrolidinium iodide was synthesized according to the method of MacFarlane *et al*.[229] *N*-methylpyrrolidine (6.30 g, 69.0 mmol) was mixed with anhydrous CH_3CN (15.0 g, 19.2 mL), under N_2 atmosphere; MeI (12.08 g, 5.3 mL, 85.0 mmol) was added dropwise into the *N*-methylpyrrolidine solution, and the mixture stirred overnight at room temperature. The solvent was removed by distillation, and the resulting solid washed with petrol ether (3 x 10 mL). The solid

was dried under vacuum, at room temperature, for more than 48 hr (14.9 g, 95% yield).

NMR (400 MHz, D_2O) δ_H (ppm): 2.22 - 2.24 (m, 4H, CH_2), 3.13 (s, 6H, CH_3), 3.49 - 3.53 (m, 4H, CH_2N). (101 MHz, D_2O) δ_C (ppm): 21.57 (CH_2), 51.61 (CH_3), 65.77 (CH_2).

2.4.2 Obtaining 2-adamantylamine from its hydrochloride salt

NaOH (0.22 g, 5.4 mmol) was slowly added to an aqueous solution of 2-adamantylamine hydrochloride (1.00 g, 5.3 mmol). The mixture was extracted with CH_3Cl (3 x 20 mL). The organic layer was dried using $MgSO_4$, then the solvent removed under vacuum to yield the product as a white solid which was oven dried at 60 °C (0.78 g, 97% yield).

NMR (400 MHz, D_2O) δ_H (ppm):1.44 (br,s, 2H, NH_2), 1.53 – 1.56 (d, 2H, CH_2, ^3J = 12.0 Hz), 1.74 – 1.76 (m, 6H, 2CH and $2CH_2$), 1.81 – 1.89 (m, 4H, $2CH_2$), 1.98 – 2.02 (d, 2H, 2CH, ^3J = 12.8 Hz), 3.01 (s, 1H, CH). (101 MHz, D_2O) δ_C (ppm): 30.92 (CH_2), 35.32 (CH), 37.90 (CH_2), 38.13 (CH_2), 55.65 (CH).

2.4.3 Synthesis of *N*,*N*-dimethyl-1-adamantylamine[230]

N,N-Dimethyl-1-adamantylamine was prepared according to a method of Vashkevich *et al*.[230] A solution of 1-adamantylamine (1.98 g, 13.2 mmol) in propan-2-ol (14 mL) was heated to 50 – 53 ^oC and 85% aqueous HCOOH (2.8 mL, 76.4 mmol) was added drop-wise over 10 minutes. 37 wt% H_2CO solution (6 mL, 162.7 mmol) was then added drop-wise over 30 minutes and maintained at 80 ^oC for 20 hrs. The cooled solution was alkalised with 25% aqueous NaOH, until universal indicator paper indicated a pH of 10. Using a dropping funnel, the top layer was isolated and washed with deionised water, before drying over $MgSO_4$. The solvent was removed under reduced pressure, yielding a yellow liquid (1.65 g, 70% yield).

NMR (400 MHz, $CDCl_3$) δ_H (ppm): 1.58 – 1.69 (m, 12H, $6CH_2$, ^3J = 12.0 Hz), 2.09 (s, 3H, 3CH), 2.27 (s, 6H, $2CH_3$). (101 MHz, $CDCl_3$) δ_C (ppm): 29.71 (3CH), 37.01 ($3CH_2$), 37.22 ($2CH_3$), 38.12 ($3CH_2$), 53.81 (C).

2.4.4 Synthesis of *N*,*N*,*N*-trimethyl-1-adamantylammonium hydroxide[230]

N,*N*,*N*-Trimethyl-1-adamantylammonium hydroxide was prepared by adaptation of a method of Vashkevich *et al*.[230] A solution of *N,N* dimethyl-1-adamantylamine (1.11 g, 6.1 mmol) in propan-2-ol (7 mL) was heated to 45 ^{o}C. MeI (0.40 mL, 6.4 mmol) was added drop-wise over 10 minutes. The mixture was heated to *ca*.75 ^{o}C, with constant stirring, and maintained at this temperature for 4 hrs. The solution was allowed to cool, the solvent removed under reduced pressure and the product (as an iodide salt[230]) oven-dried at 70 ^{o}C overnight (1.92 g, 98% yield).

NMR (400 MHz, $CDCl_3$) δ_H (ppm): 1.57 – 1.76 (m, 12H, $6CH_2$, ^3J = 12.0 Hz), 2.33 (3H, 3CH), 3.32 (s, 9H, $3CH_3$). (101 MHz, $CDCl_3$) δ_C (ppm): 30.00 (CH), 35.11 (CH_2), 36.80 (CH_2), 48.50 (CH_3), 73.06 (C).

The iodide salt was converted to the OH^- form by stirring with activated DOWEX™ ion exchange resin for 24 hr in aqueous solution prior to reacting with $B(OH)_3$, as described in Section 2.5.15. A negative silver nitrate test indicated all of the Cl^- ions had been exchanged for OH^- ions.

2.4.5 Synthesis of *N*,*N*-dimethyl-2-adamantylamine

N,*N*-Dimethyl-2-adamantylamine was obtained using a method of Borch *et al*.[231, 232] $NaCNBH_3$ (1.02 g, 16.2 mmol) was cautiously added to a stirred solution of 2-adamantylamine (0.87 g, 5.4 mmol) and 37% H_2CO solution (5.0 mL, 54.0 mmol), in CH_3CN (20 mL). Glacial CH_3CO_2H (0.5 mL) was added over a period of 10 mins, and the reaction was stirred at room temperature for 2 hr. A further 0.5 mL glacial CH_3CO_2H was added, and the solution stirred for a further 30 mins. The reaction mixture was poured in to Et_2O (75 mL) and washed with KOH solution (1M, 3 x 20 mL) and brine solution (20 mL). The solvent was removed under vacuum to yield the product as a white solid (0.44 g, 46% yield).

NMR (400 MHz, $CDCl_3$) δ_H (ppm): 1.46-1.49 (d, 2H, CH_2, ^3J = 12.0 Hz), 1.66 – 1.72 (m, 4H, $2CH_2$), 1.83 – 1.89 (m, 4H, $2CH_2$), 2.05 – 2.09 (m, 5H, CH and $2CH_2$), 2.32 (s, 6H, $2CH_3$). (101 MHz, $CDCl_3$) δ_C (ppm): 27.21 (CH), 27.39 (CH), 29.68 (2CH), 31.36 ($2CH_2$), 37.51 ($2CH_2$), 37.86 (CH_2), 43.29 (2CH).

2.4.6 Synthesis of *N*,*N*,*N*-trimethyl-2-adamantylammonium hydroxide

N,*N*,*N*-Trimethyl-2-adamantylammonium hydroxide was prepared using the same method as for *N*,*N*,*N*-trimethyl-1-adamantylammonium iodide[230] and then converted to the hydroxide, as in Section 2.4.4 (0.47 g from 0.33 g *N*,*N*-dimethyl-2-adamantylamine, 82% yield).

NMR (400 MHz, $CDCl_3$) δ_H (ppm): 1.77 – 1.80 (m, 2H, 2CH), 1.85 – 1.88 (d, 2H, CH_2, ^3J = 12.0 Hz), 2.04 – 2.08 (m, 8H, $4CH_2$), 2.59 (s, 2H, 2CH), 3.49 (s, 9H, $2CH_3$), 3.82 (s, 1H, CH). (101 MHz, D_2O) δ_C (ppm): 25.87 (CH), 26.87 (CH), 28.63 (2CH), 30.2 (CH), 30.73 (CH_2), 36.84 ($2CH_2$), 39.49 ($2CH_2$), 53.42 ($3CH_3$), 79.68 (CH).

2.4.7 Synthesis of *arachno*-6,9-bis(acetonitrile)-decaborane(12)[233]

$B_{10}H_{14}$ (5.00 g, 40.90 mmol) was refluxed (80 °C, N_2 atmosphere) in anhydrous CH_3CN (6.00 g, 7.60 mL, 146.10 mmol) for 4 hr. The excess solvent was removed under reduced pressure to yield an off-white solid (8.22 g, 99% yield).

NMR (128 MHz, CH_3CN) δ_B (ppm) $^{11}B\{^1H\}$: -41.3 (1B), -30.5 (1B), -19.1 (2B), -4.9 (1B).

2.4.8 Synthesis of 1-(phthalimidomethyl)-1,2-dicarba-*closo*-dodecaborane[234]

1-(Phthalimidomethyl)-1,2-dicarba-*closo*-dodecaborane was synthesized according to the method of Wilson *et al*.[234] $B_{10}H_{12}(CH_3CN)_2$ (5.40 g, 27.0 mmol) and propargylphthalimide (5.0 g, 27.0 mmol) were refluxed in toluene (110 mL) for 2 hr. The cooled solution was filtered from a fine insoluble precipitate, then evaporated to dryness under reduced pressure. The residue was stirred with EtOH (24 mL) for 3 hr, until gas evolution had ceased. The resulting solid was collected and washed with a small amount of cold EtOH, before being recrystallized from toluene (4.02 g, 50% yield).

NMR (400 MHz, $CDCl_3$) δ_H (ppm): 1.57 – 2.93 (b, 10H, BHs), 3.99 (bs, 1H, CH), 4.38 (s, 2H, CH_2), 7.79 – 7.92 (sym. m, 4H, arom.). (101 MHz, $CDCl_3$) δ_C (ppm): 42.61, 60.12, 73.28, 124.27, 133.32, 135.02, 167.28. (128 MHz, $CDCl_3$) δ_B (ppm) $^{11}B\{^1H\}$: -12.6 (4B), -11.3 (2B), -9.7 (2B), -4.8 (1B), -1.0 (1B).
m.p. 201-203 °C (lit. 200-202 °C).

2.4.9 Synthesis of (((2-hydroxymethyl)benzoyl)amino)methyl-*o*-carborane[234]

(((2-Hydroxymethyl)benzoyl)amino)methyl-*o*-carborane was prepared according to the method of Wilson *et al*.[234] A stirred suspension of 1-(phthalimidomethyl)1,2-dicarba-*closo*-dodecaborane (4.45 g, 14.7 mmol) in 2-propanol (133 mL) and H_2O (22.2 mL) was treated with $NaBH_4$ (2.78 g, 73.5 mmol). The solid dissolved after *ca*. 1 hr and stirring was continued for a further 22 hr. The separated crystals were collected and combined with the residue from evaporation of the solvent, then vigorously extracted with hot H_2O (2 x 20 mL) and the dried product was recrystallized from 9:1 EtOH:H_2O (3.27 g, 81% yield).

NMR (400 MHz, $CDCl_3$) δ_H (ppm): 1.43 – 3.11 (b, 10H, BHs), 3.53 (bs, 1H, NH), 4.08 (s, 1H, CH), 4.13 (d, 2H, CH_2), 4.65 (s, 2H, CH_2), 7.41 – 7.65 (m, 5H, arom. and OH overlap). (128 MHz, $CDCl_3$) δ_B (ppm) $^{11}B\{^1H\}$: -12.7 (4B), -11.6 (2B), -9.6 (2B), -4.9 (1B), -1.6 (1B).

2.4.10 Synthesis of (aminomethyl)-*o*-carborane hydrochloride[234]

(Aminomethyl)-*o*-carborane hydrochloride was synthesized according to the method by Wilson *et al*.[234] (((2-Hydroxymethyl)benzoyl)amino)methyl-*o*-carborane (3.42 g, 11.1 mmol), glacial CH_3CO_2H (41 mL), H_2O (10.3 mL) and concentrated HCl (10.3 mL) were combined and heated on a steam bath for 2 hr. The clear, colourless solution was evaporated under reduced pressure to dryness and the residue stirred with CH_3Cl (68.5 mL) for 2 hr to remove the phthalide. The remaining solid was taken up in CH_3COCH_3 (300 mL), filtered and concentrated to half its volume. The product separated on cooling as fine colourless crystals (1.79 g, 77% yield).

NMR (400 MHz, D_2O) δ_H (ppm): 1.46 – 3.04 (b, 10H, BHs), 3.92 (s, 2H, CH_2), 4.59 (s, 1H, CH), 4.79 (s, NH, DOH rapidly exchanging in D_2O). (101 MHz, D_2O) δ_C (ppm): 43.65 (CH_2), 62.41 (C), 76.68 (CH). (128 MHz, D_2O) δ_B (ppm) $^{11}B\{^1H\}$: -12.6 (4B), -9.1 (2B), -4.5 (2B), -2.5 (2B).

M.p: sublimes to cooler part of melting tube outside the block above 220 °C (lit. sublimes to cooler part of melting tube outside the block 220-280 °C).

2.4.11 Synthesis of (aminomethyl)-*o*-carborane

A solution of (aminomethyl)-*o*-carborane·HCl (0.42 g, 2 mmol) in H_2O (15 mL) was neutralised with 2.2 mmol NaOH (22 mL, 0.1 M) and the free amine which was released was recovered in CH_3Cl. The organic layer was separated, washed with water and dried over $MgSO_4$. The solvent was removed under reduced pressure to yield the product as a white solid (0.33 g, 95% yield).

NMR (400 MHz, $CDCl_3$) δ_H (ppm): 1.46 (s, 2H, NH_2), 1.58 – 2.88 (b, 10H, BHs), 3.31 (s, 2H, CH_2), 4.04 (s, 1H, CH). (101 MHz, $CDCl_3$) δ_C (ppm): 47.08 (CH_2), 58.09 (C), 76.64 (CH). (128 MHz, $CDCl_3$) δ_B (ppm) $^{11}B\{^1H\}$: -13.2 (4B), -11.7 (2B), -9.2 (2B), -5.8 (1B), -3.2 (1B).

2.4.12 Synthesis of 1-(*N*,*N*-dimethylaminomethyl)-*o*-carborane[235]

(*N,N*-Dimethylamino)methyl-*o*-carborane was synthesized through adaptation of a method of Heying *et al*.[235] *N,N*-Dimethylamino-2-propyne (5.0 g, 60 mmol) and decarborane (5.5 g, 45 mmol) were refluxed in C_6H_6 (45 mL) for 7.5 hrs. After cooling, the mixture was filtered and the filtrate was extracted with dilute HCl. The acid was neutralised and the amine was recovered in Et_2O, then the solvent removed under reduced pressure to yield a yellow viscous liquid (3.8 g, 43% yield).

NMR (400 MHz, CD_3OD) δ_H (ppm): 1.55 – 2.80 (b, 10H, BHs), 2.33 (s, 6H, $2CH_3$), 3.06 (s, 2H, CH_2), 4.50 (bs, 1H, C*H*$CB_{10}H_{10}$). (101 MHz, CD_3OD) δ_C (ppm): 47.32 ($2CH_3$), 61.46 (CH), 64.92 (CH_2), 68.76 (C). (128 MHz, CD_3OD) δ_B (ppm) $^{11}B\{^1H\}$:-12.4 (6B), -8.8 (2B), -3.4 (1B), -2.0 (1B).

R_f = 0.70 by silica gel TLC (5:1 Et_2O:petrol ether).

2.5 Preparation of polyborate salts

Polyborate salts **1** – **19** and **21** were all prepared using a general procedure, as detailed for **1**, below.

2.5.1 Preparation of pyrrolidinium pentaborate $[C_4H_8NH_2][B_5O_6(OH)_4]$ (**1**)

$B(OH)_3$, (5.01 g, 81.0 mmol), was dissolved in 1:1 MeOH:H_2O (100 mL). Pyrrolidine (1.15 g, 16.2 mmol) was added with stirring. The solvent was removed under pressure after 1 hr, resulting in the formation of the product as a white solid, which was oven-dried at 60 °C for 24 hr (4.68 g, 99% yield). Recrystallization from H_2O yielded a few colourless crystals of **1**, which were suitable for single-crystal XRD (see appendix, with NCS number 2012NCS0162).

NMR (400 MHz, D_2O) δ_H (ppm): 1.95 - 1.99 (m, 4H, $2CH_2$, ^3J = 6.8 Hz), 3.24 - 3.27 (m, 4H, $2CH_2$, ^3J = 6.8 Hz), 4.79 (HOD, OH and NH rapidly exchanging in the D_2O). (101 MHz, D_2O) δ_C (ppm): 23.58 (CH_2), 45.44 (CH_2N). (128 MHz, D_2O) δ_B (ppm): 1.1, 13.0, 18.1.

IR (KBr) (ν_{max}/cm^{-1}): 3378 (br, s), 2360 (m), 1425 (br, s), 1320 (br, s), 1185 (m), 1120 (m), 1017 (m), 923 (vs), 777 (s), 697 (s), 485 (m).

Elemental Anal. Calc. (%) for **1**, $C_4H_{14}NO_{10}B_5$; C, 16.6; H, 4.9; N, 4.8. Found (%): C, 16.8; H, 4.9; N, 4.9.

p-XRD: d-spacing/Å (% rel. int.): 5.66 (100.00), 4.39 (80.35), 6.78 (72.38), 3.39 (68.51), 4.33 (49.10), 9.38 (46.36).

TGA: Loss of H_2O (200 – 225 °C): 12.3% (12.4% calc.); residual B_2O_3 (>700 °C): 60.5% (60.0% calc.).

M.p: >300 °C.

2.5.2 Preparation of *N*-methylpyrrolidinium pentaborate·1.5 hydrate $[C_4H_8NMeH][B_5O_6(OH)_4]\cdot 1.5H_2O$ (**2**·1.5H_2O) and *N*-methylpyrrolidinium pentaborate·½ acetone $[C_4H_8NMeH][B_5O_6(OH)_4]\cdot ½CH_3COCH_3$ (**2**·½CH_3COCH_3)

Yield 4.85 g from 5.01 g $B(OH)_3$, (98% yield).

NMR: (400 MHz, D_2O) δ_H (ppm): 2.08 (4H, s, $2CH_2$), 2.90 (3H, s, CH_3), 3.05 (s, 2H, 2CH), 3.61 (2H, s, 2CH), 4.79 (s, HOD, OH and NH rapidly exchanging in the D_2O).

(101 MHz, D_2O) δ_C (ppm): 22.80 (CH_2), 40.55 (CH_3), 55.72 (CH_2N). (128 MHz, D_2O) δ_B (ppm): 1.2, 13.2, 18.8.

IR (KBr) (ν_{max}/cm^{-1}): 3434 (br, m), 3309 (br, m), 3236 (br, m), 3057 (m), 2777 (m), 2552, 2386, 2343, 1394 (br, s), 1311 (s), 1182 (m), 1140 (m), 1080 (m), 1018 (m), 921 (vs), 820 (m), 775 (s), 706 (s), 478 (s).

Elemental Anal. Calc. (%) for **2**·1.5H_2O, $C_5H_{19}NB_5O_{11.5}$; C, 18.1; H, 5.8; N, 4.2. Found (%): C, 18.4; H, 5.2; N, 4.3.

p-XRD: d-spacing/Å (% rel. int.): 3.54 (101.00), 5.09 (97.66), 6.32 (82.79), 4.05 (56.23), 6.00 (47.83), 8.36 (36.23).

TGA: Loss of interstitial H_2O (100 – 120 °C): 8.2% (8.2% calc.); loss of H_2O (200 – 225 °C): 18.6% (19.0% calc.); residual B_2O_3 (>750 °C): 56.7% (52.5% calc.).

Recrystallization of **2**·1.5H_2O from H_2O/CH_3COCH_3 yielded a few colourless crystals of $[C_5H_{12}N][B_5O_6(OH)_4]\cdot½CH_3COCH_3$ (**2**·½CH_3COCH_3), suitable for single-crystal XRD (see appendix, with NCS number 2012NCS0960).

Elemental Anal. Calc. (%) for **2**·½CH_3COCH_3, $C_{6.5}H_{19}NB_5O_{10.5}$; C, 23.4; H, 5.8; N, 4.2. Found (%): C, 23.4; H, 5.8; N, 4.2.

M.p: >300 ^oC.

2.5.3 Preparation of *N,N*-dimethylpyrrolidinium pentaborate hemihydrate $[C_6H_{14}N][B_5O_6(OH)_4]\cdot½H_2O$ (**3**·½H_2O) and *N,N*-dimethylpyrrolidinium pentaborate $[C_6H_{14}N][B_5O_6(OH)_4]$ (**3**)

N,*N*-Dimethylpyrrolidinium iodide (3.68 g, 16.2 mmol) was dissolved in H_2O (50 mL), to which an excess of Dowex™ Monosphere™ 550A ion exchange resin (OH^- form) was added. The solution was stirred for 24 hr, the resin removed by filtration, and MeOH (50 mL) was added to the filtrate. $B(OH)_3$, (5.01 g, 81.0 mmol), was added, with stirring, and the solution warmed gently. The solvent was removed under pressure after 45 mins, resulting in the formation of a cream solid, **3**·½H_2O which was oven-dried at 60 °C for 24 hr (5.07 g, 99% yield).

NMR: (400 MHz, D_2O) δ_H (ppm): 2.22–2.23 (4H, m, $2CH_2$), 3.13 (6H, s, $2CH_3$), 3.49–3.52 (4H, m, $2CH_2$), 4.79 (HOD, s, OH and NH rapidly exchanging in the D_2O). (101

MHz, D_2O) δ_C (ppm): 21.58 (CH_2), 51.61 (CH_3), 65.77 (CH_2N). (128 MHz, D_2O) δ_B (ppm): 1.1, 13.2, 18.4.
IR (KBr) (ν_{max}/cm^{-1}): 3419 (br, m), 3254 (br, s), 2352 (w), 1415 (br, m), 1309 (br, m), 1148 (m), 1093 (m), 1018 (m), 913 (vs), 772 (s), 724 (m), 708 (s), 478 (m), 464.
Elemental Anal. Calc. (%) for **3**·½H_2O, $C_6H_{19}NB_5O_{10.5}$; C, 22.0; H, 5.9; N, 4.3. Found (%): C, 22.4; H, 5.7; N, 4.3.
p-XRD: d-spacing/Å (% rel. int.): 3.60 (100.00), 4.77 (91.42), 5.34 (90.14), 7.20 (67.08), 3.66 (55.14), 3.81 (47.33).
TGA: Loss of interstitial H_2O (100 – 120 °C): 2.7% (2.7% calc.); loss of H_2O (200 – 255 °C): 13.8% (13.8% calc.); residual B_2O_3 (>750 °C): 53.3% (53.2% calc.).

Recrystallization of **3**·½H_2O from H_2O/CH_3COCH_3 yielded a few single-crystal XRD quality colourless crystals of $[C_6H_{14}N][B_5O_6(OH)_4]$, **3** (see appendix, with NCS number 2013NCS0027).

Elemental Anal. Calc. (%) for **3**, $C_6H_{18}NB_5O_{10}$; C, 22.6; H, 5.7; N, 4.4. Found (%): C, 22.6; H, 5.7; N, 4.2.
M.p: >300 ^oC.

2.5.4 Preparation of 2-hydroxymethylpyrrolidinium pentaborate hemihydrate [(2-CH_2OH)-$C_4H_7NH_2$][$B_5O_6(OH)_4$]·½H_2O (**4**·½H_2O)
Yield 3.19 g from 3.09 g $B(OH)_3$, (98% yield). Recrystallization from H_2O/EtOH yielded a few single-crystal XRD quality colourless crystals of **4**·½H_2O (see appendix, with NCS number 2014NCS0729).

NMR: (400 MHz, D_2O) δ_H (ppm): 1.73–1.78 (1H, m, CH), 1.99–2.19 (3H, m, CH & CH_2), 3.32–3.36 (2H, t, CH_2N, ^3J = 7.2 Hz), 3.67–3.78 (1H, m, CH), 3.67–3.80 (2H, m, CH_2OH), 3.86–3.90 (1H, dd, CHN, J = 3.6 Hz & 12 Hz), 4.79 (DOH, NH and OH rapidly exchanging in D_2O). (101 MHz, D_2O) δ_C (ppm): 23.28 (CH_2), 25.72 (CH_2N), 45.44 (CH_2OH), 60.24 (CH_2), 61.15 (CHN). (128 MHz, D_2O) δ_B (ppm): 1.1, 13.1, 18.0.
IR (KBr) (ν_{max}/cm^{-1}): 3308 (br), 1621 (m), 1423 (br, s), 1313 (s) 1183 (m), 1149 (m), 1027 (m), 923 (vs), 827 (m), 774 (s), 704 (s), 481 (s).

Elemental Anal. Calc (%) for **4**·½H_2O, $C_5H_{17}NB_5O_{10.5}$: C, 18.2; H, 5.2; N, 4.3. Found (%): C, 18.1; H, 5.2; N, 4.1.

p-XRD: d spacing/Å (% rel. int.): 4.77 (100.00); 3.54 (96.43); 3.71 (85.64); 5.17 (67.94); 3.66 (67.63); 4.40 (55.49).

TGA: Loss of interstitial H_2O (100 – 150 °C): 2.8% (2.7% calc.); loss of H_2O (200 – 225 °C): 11.9% (10.9% calc.); residual B_2O_3 (>700 °C): 53.8% (52.9% calc.).

M.p: >300 ^oC.

2.5.5 Preparation of (2-hydroxyethyl)-*N*-methylpyrrolidinium pentaborate·0.3 hydrate [(2-CH_2CH_2OH)C_4H_7NMeH][$B_5O_6(OH)_4$]·0.3H_2O (**5**·0.3H_2O)

Yield 2.71 g from 2.47 g $B(OH)_3$, (97% yield). Recrystallization from H_2O/EtOH yielded a few single-crystal XRD quality colourless crystals of **5**·0.3H_2O (see appendix, with NCS number 2014NCS0787).

NMR (400 MHz, D_2O) δ_H (ppm): 1.76 – 1.86 (2H, m), 2.01 – 2.19 (3H, m), 2.32 – 2.41 (1H, m), 2.90 (3H, s), 3.12 – 3.18 (1H, q, ^3J = 8 Hz), 3.38 – 3.46 (1H, m), 3.61 – 3.72 (2H, m), 3.76 – 3.82 (1H, m), 4.79 (DOH, NH and OH rapidly exchanging in D_2O). (101 MHz, D_2O) δ_C (ppm): 66.8 (CH), 58.2 (CH_2), 55.9 (CH_2), 38.9 (CH_3), 32.0 (CH_2), 28.8 (CH_2), 21.1 (CH_2). (128 MHz, D_2O) δ_B (ppm): 1.2, 13.2, 16.8.

IR (KBr) (ν_{max}/cm^{-1}): 3399 (br,s), 2973 (m), 2893, 2753, 2382, 1639, 1432 (s), 1362 (m), 1315(s), 1137, 1100 (s), 1027 (s), 923 (vs), 776 (s) 723 (m), 707 (s).

Elemental Anal. Calc (%) for **5**·0.3H_2O, $C_7H_{20.60}B_5NO_{11.30}$: C, 23.8; H 5.9; N, 4.0. Found (%): C, 23.8; H 5.7; N, 3.9.

p-XRD: d spacing/Å (% rel. int.): 3.73 (100), 4.64 (99.89), 3.71 (78.07), 5.75 (75.59), 3.35 (43.60), 6.70 (42.60).

TGA: Loss of interstitial H_2O (60 – 70 °C): 1.6% (1.5% calc.); loss of OH from cation (120 – 145 °C): 5.3% (4.1% calc.); loss of H_2O (200 – 240 °C): 14.5% (14.3% calc.); residual B_2O_3 (>750 °C): 49.5% (49.2% calc.).

M.p: >300 ^oC.

2.5.6 Preparation of 1-(2-aminoethyl)-pyrrolidinium pentaborate [$C_6H_{15}N_2$][$B_5O_6(OH)_4$] (**6**)

Yield 5.33 g from 5.01 g $B(OH)_3$, (99% yield).

NMR (400 MHz, D_2O) δ_H (ppm): 1.97 (4H, brs), 3.07 – 3.11 (8H, brs), 4.79 (s, HOD, OH and NH rapidly exchanging in the D_2O). (101 MHz, D_2O) δ_C (ppm): 22.55 ($2CH_2$), 36.86 (CH_2), 53.89 ($2CH_2$), 54.50 (CH_2). (128 MHz, D_2O) δ_B (ppm): 1.2, 13.1, 17.3.
IR (KBr) (ν_{max}/cm^{-1}): 3293 (br, s), 3056, 2881, 2760 (m), 2528, 2385, 1397 (br, s), 1314 (s), 1147 (s), 1073 (br, s), 1031 (br, s), 925 (vs), 821 (m), 774 (vs), 706 (vs), 584 (w), 525 (w), 472 (s).
Elemental Anal. Calc (%) for **6**, $C_6H_{19}N_2B_5O_{10}$: C, 21.6; H, 5.8; N, 8.4. Found (%): C, 21.9; H, 5.9; N, 8.3.
p-XRD: d-spacing/Å (% rel. int.): 3.71 (100.00), 4.12 (78.86), 3.73 (61.49), 5.74 (49.30), 8.75 (29.51), 3.15 (19.21).
TGA: Loss of H_2O (180 – 200 °C): 10.4% (10.8% calc.); residual B_2O_3 (>750 °C): 52.2% (52.2% calc.).

2.5.7 Preparation of 2-aminobenzylammonium pentaborate $[C_7H_{11}N][B_5O_6(OH)_4]$ (**7**)
Yield 5.46 g from 5.01 g $B(OH)_3$, (99% yield).

NMR (400 MHz, D_2O) δ_H (ppm): 4.13 (s, 2H, CH_2), 4.79 (s, HOD, OH and NH rapidly exchanging in the D_2O), 6.93 (m, 2H, arom.), 7.28 (m, 2H, arom.). (101 MHz, D_2O) δ_C (ppm): 39.19 (CH_2), 117.74 (CH), 119.11 (C), 119.93 (CH), 130.09 (CH), 130.34 (CH), 144.68 (C). (128 MHz, D_2O) δ_B (ppm): 1.5, 13.2, 17.5.
IR (KBr) (ν_{max}/cm^{-1}): 3379 (br, s), 1639 (m), 1432 (br, m), 1362 (br, m), 1099 (m), 1025 (m), 924 (s), 858 (m), 815 (s), 781 (m), 697 (s).
Elemental Anal. Calc. (%) for **7**, $C_7H_{15}N_2B_5O_{10}$; C, 24.6; H, 4.4; N, 8.2. Found (%): C, 24.5; H, 4.7; N, 8.0.
p-XRD: d-spacing/Å (% rel. int.): amorphous solid.
TGA: Loss of H_2O (180 – 210 °C): 12.0% (10.6% calc.); residual B_2O_3 (>750 °C): 52.7% (51.0% calc.).
M.p: >300 °C.

2.5.8 Preparation of 3-aminobenzylammonium pentaborate $[C_7H_{11}N][B_5O_6(OH)_4]$ (**8**)

Yield 5.45 g from 5.01 g $B(OH)_3$, (98% yield).

NMR (400 MHz, D_2O) δ_H (ppm): 4.07 (s, 2H, CH_2), 4.79 (s, HOD, OH and NH rapidly exchanging in the D_2O), 6.87 (m, 3H, arom.), 7.28 (t, 1H, arom, ^3J = 7.4 Hz). (101 MHz, D_2O) δ_C (ppm): 43.09 (CH_2), 116.11 (CH), 116.71 (CH), 119.28 (CH), 130.15 (CH), 134.36 (C), 166.81 (C). (128 MHz, D_2O) δ_B (ppm): 13.4, 17.0.

IR (KBr) (ν_{max}/cm^{-1}): 3385 (br, m), 3227 (br, m), 2692, 2604, 2532, 2419, 1620 (m), 1537, 1421 (br, s), 1387 (m), 1311 (s), 1154 (m), 1111 (m), 1081 (m), 1010 (m), 917 (vs), 773 (s), 695 (s), 467 (s).

Elemental Anal. Calc. (%) for **8**, $C_7H_{15}N_2B_5O_{10}$; C, 24.6; H, 4.4; N, 8.2. Found (%): C, 24.9; H, 4.5; N, 8.0.

p-XRD: d-spacing/Å (% rel. int.): amorphous solid.

TGA: Loss of H_2O (180 – 210 °C): 8.1% (10.6% calc.); residual B_2O_3 (>750 °C): 59.1% (51.0% calc.).

M.p: >300 °C.

2.5.9 Preparation of 4-aminobenzylammonium pentaborate $[C_7H_{11}N][B_5O_6(OH)_4]$ (**9**) and 4-aminobenzylammonium pentaborate hemihydrate $[C_7H_{11}N][B_5O_6(OH)_4]\cdot\frac{1}{2}H_2O$ (**9**$\cdot\frac{1}{2}H_2O$)

5.46 g from 5.01 g $B(OH)_3$, (99% yield).

NMR (400 MHz, D_2O) δ_H (ppm): 4.05 (s, 2H, CH_2), 4.79 (s, HOD, OH and NH rapidly exchanging in the D_2O), 6.86 (d, 2H, arom, ^3J = 8.0 Hz), 7.26 (d, 2H, arom, ^3J = 8.0 Hz). (101 MHz, D_2O) δ_C (ppm): 42.80 (CH_2), 116.47 (2CH), 123.32 (C), 130.18 (2CH), 147.06 (C). (128 MHz, D_2O) δ_B (ppm): 1.3, 12.9, 16.9.

IR (KBr) (ν_{max}/cm^{-1}): 3487 (m), 3171 (br, s), 2404 (w), 1621 (m), 1526 (m), 1428 (br, m), 1377, 1327 (s), 1190 (s), 1059 (s), 1029 (s), 1018 (s), 919 (vs), 842 (s), 775 (s), 699 (s), 552 (m), 472 (m).

Elemental Anal. Calc. (%) for **9**, $C_7H_{15}N_2B_5O_{10}$; C, 24.6; H, 4.4; N, 8.2. Found (%): C, 24.5; H, 4.7; N, 8.0.

p-XRD: d-spacing/Å (% rel. int.): 3.88 (100.00), 3.80 (97.26), 3.70 (70.77), 3.43 (69.50), 4.37 (57.40), 4.24 (48.01).

TGA: Loss of H_2O (180 – 200 °C): 11.2% (10.6% calc.); residual B_2O_3 (>750 °C): 53.3% (51.0% calc.).
M.p: >300 °C.

The product was recrystallized from H_2O to yield a few single-crystal XRD quality colourless crystals of $[C_7H_{11}N_2][B_5O_6(OH)_4].½H_2O$ (**9**·½H_2O) (see appendix, with NCS number 2014NCS0055).

Elemental Anal. Calc. (%) for **9**·½H_2O, $C_7H_{16}N_2B_5O_{10.5}$; C, 24.0; H, 4.6; N, 8.0. Found (%): C, 24.0; H, 4.6; N, 7.7.
TGA: Loss of interstitial H_2O (110 – 120 °C): 2.6% (2.6% calc.); loss of H_2O (180 – 200 °C): 12.2% (12.9% calc.) residual B_2O_3 (>800 °C): 51.3% (49.7% calc.).
M.p. >300 °C.

2.5.10 Preparation of 2-(3-indolyl)ethylammonium pentaborate hemihydrate $[C_{10}H_{13}N_2][B_5O_6(OH)_4]·½H_2O$ (**10**·½H_2O)

2.34 g from 1.93 g $B(OH)_3$, (99% yield).

NMR (400 MHz, D_2O) δ_H (ppm): 3.15 – 3.18 (t, 2H, CH_2, ^3J = 6.8 Hz), 3.31 – 3.34 (t, 2H, CH_2, ^3J = 7.2 Hz), 4.79 (HOD, NH and OH rapidly exchanging with D_2O), 7.18 – 7.22 (t, 1H, CH arom, ^3J = 7.6 Hz), 7.27 – 7.30 (t, 1H, CH arom, ^3J = 8.0 Hz), 7.31 (s, 1H, CH arom), 7.53 – 7.55 (d, 1H, CH arom, ^3J = 8.4 Hz), 7.68 – 7.70 (d, 1H, CH arom, ^3J = 8.0 Hz). (101 MHz, D_2O) δ_C (ppm): 22.63 (CH_2), 39.68 (CH_2), 109.02 (C), 111.98 (CH), 119.34 (CH), 122.10 (CH), 124.24 (CH), 126.34 (C), 136.36 (C). (128 MHz, D_2O) δ_B (ppm): 1.2, 13.3, 16.9.
IR (KBr) (ν_{max}/cm^{-1}): 3408 (br, m), 3237 (br, m), 2263, 1626 (w), 1421 (m), 1338 (m), 1160 (m), 1072 (m), 919 (m), 862 (m), 813 (m), 781 (m), 744 (m), 548, 467, 425 (m).
Elemental Anal. Calc. (%) for **10**·½H_2O, $C_{10}H_{18}N_2B_5O_{10.5}$; C, 30.9; H, 4.7; N, 7.2. Found (%): C, 30.7; H, 5.1; N, 7.3.
p-XRD: d-spacing/Å (% rel. int.): amorphous solid.
TGA: Loss of H_2O (140 – 150 °C): 11.5% (11.6% calc.); residual B_2O_3 (>750 °C): 44.6% (44.8% calc.).
Mp >300 °C.

2.5.11 Preparation of 1,2,3,4-tetrahydroisoquinoline pentaborate $[C_9H_{12}N][B_5O_6(OH)_4]$ (**11**) and 1,2,3,4-tetrahydroisoquinoline pentaborate·1.5 boric acid·monohydrate $[C_9H_{12}N][B_5O_6(OH)_4]\cdot 1.5B(OH)_3\cdot H_2O$ (**11**·1.5$B(OH)_3\cdot H_2O$)

5.59 g from 5.01 g $B(OH)_3$, (98% yield).

NMR (400 MHz, D_2O) δ_H (ppm): 3.10 – 3.14 (t, 2H, CH_2, ^3J = 8.0 Hz), 3.49 – 3.52 (t, 2H CH_2, ^3J = 8.0 Hz), 4.36 (s, 2H, CH_2), 7.23 – 7.37 (m, 4H, arom.). (101 MHz, D_2O) δ_C (ppm): 24.56 (CH_2), 41.59 (CH_2), 44.48 (CH_2), 126.62 (CH), 126.84 (CH), 127.88 (CH), 128.90 (CH). (128 MHz, D_2O) δ_B (ppm): 13.0, 16.6.

IR (KBr) (ν_{max}/cm^{-1}): 3379 (s), 3225 (br, m), 3068, 2918, 2825, 2691, 2599, 2548, 2486, 1606 (m), 1427 (br, m), 1295 (m), 1124 (s), 1021 (s), 916 (vs), 774 (s), 748 (s), 701 (s), 475 (s), 455 (s).

Elemental Anal. Calc. (%) for **11**, $C_9H_{16}NB_5O_{10}$; C, 30.7; H, 4.6; N, 4.0. Found (%): C, 30.0; H, 4.7; N, 4.0.

p-XRD: d-spacing/Å (% rel. int.): 3.56 (100), 3.90 (74.30), 5.15 (62.27), 4.94 (55.27), 4.30 (39.70).

TGA: Loss of H_2O (140 – 180 °C): 10.4% (10.2% calc.); residual B_2O_3 (>750 °C): 53.3% (49.4% calc.).

Recrystallization of **11** from H_2O yielded a few single-crystal XRD quality colourless crystals of **11**·1.5$B(OH)_3\cdot H_2O$.

Elemental Anal. Calc. (%) for **11**·1.5$B(OH)_3\cdot H_2O$, $C_9H_{22.5}B_6NO_{15.5}$; C, 23.6; H, 5.0; N, 3.1. Found (%): C, 23.4; H, 5.2; N, 3.0.

TGA: Loss of interstitial H_2O (70 – 100 °C): 11.4% (11.8% calc.); loss of H_2O (130 – 160 °C): 21.6% (19.7% calc.); residual B_2O_3 (>750 °C): 50.8% (49.4% calc.).

Mp >300 °C.

2.5.12 Preparation of 1,2,3,4-tetrahydro-1-naphthylammonium pentaborate hemihydrate $[C_{10}H_{14}N][B_5O_6(OH)_4]\cdot ½H_2O$ (**12**·½H_2O)

6.00 g, from 5.22 g $B(OH)_3$, (97% yield).

NMR (400 MHz, D_2O) δ_H (ppm): 1.82 – 1.89 (m, 2H, CH_2), 1.96 – 2.03 (m, 1H), 2.09 – 2.18 (m, 1H), 2.71 – 2.89 (m, 2H, CH_2), 4.54 (t, 1H, CH, ^3J = 5.2 Hz), 4.79 (s,

HOD, NH and OH rapidly exchanging in D_2O), 7.22 – 7.36 (m, 4H, arom). (101 MHz, D_2O) δ_C (ppm): 17.74 (CH_2), 27.20 (CH_2), 27.92 (CH_2), 48.94 (CH), 126.45 (CH), 128.23 (CH), 128.88 (CH), 129.77 (CH), 131.16 (C), 138.15 (C). (128 MHz, D_2O) δ_B (ppm): 1.1, 13.0, 18.5.

IR (KBr) (ν_{max}/cm^{-1}): 3354 (br, s), 3253 (br, s), 3080 (br), 2969 (s), 1638 (m), 1597 (m), 1418 (br, s), 1300 (br, s), 1089 (m), 1021 (m), 919 (vs), 776 (s), 731 (s), 705 (s), 528 (m), 481 (s), 468 (s).

Elemental Anal. Calc. (%) for **12**·½H_2O, $C_{10}H_{19}NB_5O_{10.5}$; C, 32.0; H, 5.1; N, 3.7. Found (%): C, 32.0; H, 5.1; N, 3.7.

p-XRD: d-spacing/Å (% rel. int.): 3.85 (100.00), 3.85 (90.54), 5.40 (86.66), 3.62 (66.77), 3.79 (59.69), 5.45 (44.48).

TGA: Loss of interstitial H_2O (150 – 190 °C): 2.4% (2.4% calc.); loss of H_2O (240 – 270 °C): 12.1% (11.3% calc.); residual B_2O_3 (>750 °C): 49.5% (43.8%).

Recrystallization of **12**·½H_2O was attempted from H_2O, but crystals suitable for single-crystal XRD were not obtained.

2.5.13 Preparation of 1-adamantylammonium pentaborate $[C_{10}H_{18}N][B_5O_6(OH)_4]$ (**13**)

2.44 g from 2.04 g $B(OH)_3$, (99% yield).

NMR (400 MHz, D_2O) δ_H (ppm): 1.60 – 1.72 (m, 6H), 1.83 (s, 6H), 2.12 (br s, 3H, 3CH), 4.79 (DOH, NH and OH rapidly exchanging in D_2O). (101 MHz, D_2O) δ_C (ppm): 28.63 (CH), 34.71 (CH_2), 39.87 (CH_2), 52.16 (C). (128 MHz, D_2O) δ_B (ppm): 1.2, 13.3, 17.5.

IR (KBr) (ν_{max}/cm^{-1}): 3393 (br, m), 3248 (br, m), 2916 (s), 2856 (m), 1633 (m), 1422 (br, s), 1381 (m), 1314 (br, m), 1163 (m), 1086 (br), 918 (s), 861 (m), 821 (m), 781 (m), 706 (m), 670, 547, 459, 424.

Elemental Anal. Calc. (%) for **13**, $C_{10}H_{22}NB_5O_{10}$: C, 32.5; H, 6.0; N, 3.8. Found (%): C, 32.7; H, 6.1; N 3.6.

p-XRD: d spacing /Å (% rel. int.): amorphous solid.

TGA: Loss of H_2O (210 – 250 °C): 9.7% (9.7% calc.); residual B_2O_3 (>750 °C): 46.6% (47.0% calc.).

2.5.14 Preparation of *N*,*N*-dimethyl-1-adamantylammonium pentaborate·1.5 hydrate $[C_{12}H_{22}N][B_5O_6(OH)_4]$ (**14**·$1.5H_2O$) and *N*,*N*-dimethyl-1-adamantylammonium pentaborate·boric acid monohydrate $[C_{12}H_{22}N][B_5O_6(OH)_4]\cdot B(OH)_3\cdot H_2O$ (**14**·$B(OH)_3\cdot H_2O$)

4.46 g from 3.61 g $B(OH)_3$, (96% yield).

NMR (400 MHz, D_2O) δ_H (ppm): 1.63 – 1.74 (m, 6H), 1.91 (s, 6H), 2.23 (s, 3H, 3CH), 2.76 (s, 6H, $2CH_3$), 4.79 (DOH, NH and OH rapidly exchanging in D_2O). (101 MHz, D_2O) δ_C (ppm): 29.13 (CH), 34.77 (CH_2), 35.75 (CH_2), 35.87 (CH_3), 63.20 (C). (128 MHz, D_2O): δ_B (ppm) 1.2, 13.1, 17.1.

IR (KBr) (ν_{max}/cm^{-1}) 3403 (br, m), 2916 (s), 2853 (m), 1635 (w), 1421 (br, m), 1316 (m), 1159 (m), 1075 (m), 1054 (m), 912 (s), 865 (m), 842 (m), 809 (s), 778 (s), 707 (s), 672, 561, 527, 485, 463.

Elemental Anal. Calc. (%) for **14**·$1.5H_2O$, $C_{12}H_{29}NB_5O_{11.5}$: C, 33.9; H, 6.9; N, 3.3. Found (%): C, 34.0; H, 7.0; N, 3.0.

p-XRD: d spacing/Å (% rel. int.): 4.51 (100.00), 12.57 (71.74), 4.97 (67.33), 4.87 (50.12), 4.47 (50.09), 7.79 (44.49).

Recrystallization of **14**·$1.5H_2O$ from H_2O yielded very few single-crystal XRD quality colourless crystals of $[C_{12}H_{22}N][B_5O_6(OH)_4]\cdot B(OH)_3\cdot H_2O$, **14**·$B(OH)_3\cdot H_2O$ (see appendix, with NCS number 2014NCS0278).

TGA: Loss of interstitial H_2O (110 – 130 °C): 5.4% (5.7% calc.); loss of further interstitial H_2O (140 – 150 °C): 12.1% (9.4% calc.); loss of H_2O (180 – 210 °C): 18.1% (17.0% calc.); residual B_2O_3 (>800 °C): 45.8% (43.7% calc.).

2.5.15 Preparation of *N*,*N*,*N*-trimethyl-1-adamantylammonium pentaborate trihydrate $[C_{13}H_{24}N][B_5O_6(OH)_4]\cdot 3H_2O$ (**15**·$3H_2O$)

2.11 g from 1.86 g $B(OH)_3$, (85% yield). Recrystallization from H_2O yielded a few single-crystal XRD quality colourless crystals of **15**·$3H_2O$ (see appendix, with NCS number 2014NCS0730).

NMR (400 MHz, D_2O) δ_H (ppm): 1.64 – 1.75 (m, 6H, $3CH_2$), 2.07 (s, 6H, $3CH_2$), 2.31 (brs, 3H, 3CH), 2.99 (s, 9H, $3CH_3$), 4.79 (DOH and OH rapidly exchanging in D_2O).

(101 MHz, D_2O) δ_C (ppm): 29.95 (CH), 34.13 (CH_2), 34.47 (CH_2), 47.48 – 47.56 ($3CH_3$). (128 MHz, D_2O) δ_B (ppm): 1.2, 13.1, 17.1.

IR (KBr) (ν_{max}/cm^{-1}): 3437 (br, m), 3261 (br, m) 2922 (s), 2860 (m), 1656 (w), 1422 (br, m), 1409 (m), 1306 (m), 1152 (s), 1072 (m), 1025 (m), 1008 (s), 916 (s), 841 (m), 771 (s), 708 (s), 573, 462 (m).

Elemental Anal. Calc. (%) for **15**·$3H_2O$, $C_{13}H_{34}NB_5O_{13}$: C, 33.5; H, 7.4; N, 3.0. Found (%); C, 33.2; H, 6.9; N, 3.0.

p-XRD: d spacing/Å (% rel. int.): 3.18 (100.00), 5.20 (33.86), 4.56 (30.00), 4.52 (17.46), 7.79 (17.16); 3.87 (16.86).

TGA: Loss of interstitial H_2O (100 – 150 °C): 12.4% (12.6% calc.); loss of H_2O (250 – 270 °C): 18.8% (18.9% calc.) residual B_2O_3 (>750 °C): 49.2% (42.6% calc.).

2.5.16 Preparation of 2-adamantylammonium pentaborate dihydrate [$C_{10}H_{18}N$][$B_5O_6(OH)_4$]·$2H_2O$ (**16**·$2H_2O$)

1.80 g from 1.60 g $B(OH)_3$, (94%).

NMR (400 MHz, D_2O) δ_H (ppm): 1.73 – 1.97 (m, 12H, 2CH and $5CH_2$), 2.05 (s, 2H, 2CH), 3.53 (s, 1H, CH), 4.79 (HOD, NH and OH rapidly exchanging in D_2O). (101 MHz, D_2O) δ_C (ppm): 26.32 (CH), 26.47 (CH), 29.58 ($2CH_2$), 30.40 (2CH), 36.15 ($2CH_2$), 36.49 (CH_2), 55.91 (CH). (128 MHz, D_2O) δ_B (ppm): 13.1, 16.8.

IR (KBr) (ν_{max}/cm^{-1}): 3381 (br, s), 3223 (br, s), 2916 (m), 1619, 1427 (br, m), 1361 (br, m), 1101 (m), 1028 (m), 923 (s), 783 (s), 702 (s).

Elemental Anal. Calc. (%) for **16**·$2H_2O$, $C_{10}H_{26}NB_5O_{12}$: C, 29.6; H, 6.4; N, 3.5. Found (%); C, 29.7; H, 6.2; N, 3.3.

p-XRD: d spacing/Å (% rel. int.): amorphous solid.

TGA: Loss of interstitial H_2O (90 – 110 °C): 9.0 % (8.9% calc.); loss of H_2O (260 – 290 °C): 18.8 % (17.7% calc.); residual B_2O_3 (>750 °C): 42.9% (42.8% calc.).

2.5.17 Preparation of *N*,*N*,*N*-trimethyl-2-adamantylammonium pentaborate trihydrate [$C_{13}H_{24}N$][$B_5O_6(OH)_4$]·$3H_2O$ (**17**·$3H_2O$)

0.59 g from 0.48 g $B(OH)_3$ (92% yield). Recrystallization from H_2O yielded a few single-crystal XRD quality colourless crystals of **17**·$3H_2O$ (see appendix, with NCS number 2015NCS0474).

NMR (400 MHz, D_2O) δ_H (ppm): 1.78 – 2.12 (m, 12H), 2.61 (s, 2H), 3.19 (s, 9H, $3CH_3$), 3.53 (s, 1H, CH), 4.79 (HOD, NH and OH rapidly exchanging in D_2O). (101 MHz, D_2O) δ_C (ppm): 25.87 (CH), 26.87 (CH), 28.67 (2CH), 30.20 (CH), 30.73 ($2CH_2$), 36.84 (CH_2), 39.49 (CH_2), 53.46 ($3CH_3$), 79.68 (CH). (128 MHz, D_2O) δ_B (ppm): 13.3, 17.6.

IR (KBr) (ν_{max}/cm^{-1}): 3436 (m), 3378 (m), 3220 (br, s), 2909 (m), 2496, 2385. 2260 (m), 1649, 1439 (br, m), 1361 (br, m), 1252 (s), 1197 (m), 1102 (s), 1026 (s), 926 (s), 782 (m), 696 (m), 650 (m).

Elemental Anal. Calc. (%) for **17**·$3H_2O$, $C_{13}H_{34}B_5NO_{13}$: C, 33.5; H, 7.4; N, 3.0. Found (%); C, 33.6; H, 7.4; N, 2.9

p-XRD: d spacing/Å (% rel. int.): 4.59 (100), 4.43 (37.33), 4.24 (32.34), 3.05 (27.14), 5.42 (27.02), 8.86 (21.13).

TGA: Loss of interstitial H_2O (100 – 140 °C): 12.0% (11.6% calc.); loss of H_2O (220 – 260 °C): 19.0% (19.3% calc.) residual B_2O_3: 40.7% (37.3% calc.).

M.p. >300 °C.

2.5.18 Preparation of bis(triphenylphosphine)iminium pentaborate sesquihydrate $[C_{36}H_{30}NP_2][B_5O_6(OH)_4]\cdot 1.5H_2O$ (**18**·$1.5H_2O$)

1.26 g from 0.54 g $B(OH)_3$ (95 % yield). Several attempts were made to recrystallize the product, in numerous solvents, but single-crystals suitable for X-ray diffraction studies were not obtained. The product was also prepared under solvothermal conditions, as described in Section 2.6.12.

NMR (400 MHz, D_2O) δ_H (ppm): 4.79 (HOD and OH rapidly exchanging in D_2O), 7.31 – 7.35 (m, 12H), 7.47 – 7.57 (m, 18H). (101 MHz, D_2O) δ_C (ppm): 126.83 (dd, $^1J_{PC}$ = 108.1 Hz, $^3J_{PC}$ = 2.0 Hz, *ipso*, 6C, arom.), 129.14 (m, *meta*, 12C, CH arom.), 132.13 (m, *ortho*, 12C, CH arom), 133.49 (brs, *para*, 6C, CH arom.). (128 MHz, D_2O) δ_B (ppm): 16.4. (162 MHz, D_2O) δ_P (ppm): 21.2.

IR (KBr) (ν_{max}/cm^{-1}): 3372 (br, m), 3227 (br, m), 3058 (w), 2261, 1976, 1909, 1827, 1630 (w), 1589 (w), 1437 (s), 1303 (br, m), 1265 (m), 1184 (w), 1159 (w), 1115 (vs), 1026 (m), 922 (s), 781 (m), 748 (m), 723 (vs), 692 (vs), 534 (s), 500 (s).

Elemental Anal. Calc. (%) for **18**·$1.5H_2O$, $C_{36}H_{37}B_5NO_{11.5}P_2$: C, 55.2; H, 4.8; N, 1.8. Found (%); C, 55.4; H, 4.7; N, 1.9.

p-XRD: d spacing/Å (% rel. int.): 3.89 (100.00), 3.74 (95.30), 7.38 (91.18), 3.71 (68.47), 7.85 (66.72), 10.65 (62.54).
TGA: Loss of H_2O (120 – 150 °C): 7.1% (8.0% calc.); residual B_2O_3 (>650 °C): 22.9% (22.3% calc.).

2.5.19 Preparation of bis(triphenylphosphine)iminium triborate·2.5 hydrate $[C_{36}H_{30}NP_2][B_3O_3(OH)_4]\cdot 2.5H_2O$ (**19**·2.5H_2O)

1.25 g from 0.33 g $B(OH)_3$ (94 % yield). The product was also prepared under solvothermal conditions, as described in Section 2.6.13.

NMR (400 MHz, D_2O) δ_H (ppm): 4.79 (HOD and OH rapidly exchanging in D_2O), 7.26 – 7.29 (m, 12H), 7.42 – 7.52 (m, 18H). (101 MHz, D_2O) δ_C (ppm): 126.78 (dd, $^1J_{PC}$ = 108.7 Hz, $^3J_{PC}$ = 2.0 Hz, *ipso*, 6C), 129.15 (m, *meta*, 12H, CH arom.), 132.08 (m, *ortho*, 12C, CH arom.), 133.52 (brs, *para*, 6C, CH arom.). (128 MHz, D_2O) δ_B (ppm): 13.7. (162 MHz, D_2O) δ_P (ppm): 21.1.
IR (KBr) (ν_{max}/cm^{-1}): 3286 (br, m), 3058 (m), 1975, 1907, 1827, 1643 (w), 1589 (m), 1482 (w), 1437 (s), 1296 (m), 1261 (m), 1185 (w), 1159 (w), 1115 (vs), 1025 (m), 997 (m), 918 (m), 855 (m), 801 (m), 779 (m), 747 (s), 723 (vs), 691 (vs), 532 (s), 500 (s).
Elemental Anal. Calc. (%) for **19**·2.5H_2O, $C_{36}H_{39}B_3NO_{9.5}P_2$: C, 59.1; H, 5.4; N, 1.9. Found (%); C, 58.8; H, 5.1; N, 1.9.
p-XRD: d spacing/Å (% rel. int.): 4.41 (100.00), 3.68 (56.47), 4.17 (42.50), 3.56 (34.14), 6.62 (34.02), 8.95 (30.33).
TGA: Loss of interstitial H_2O (90 – 100 °C): 6.0% (6.2% calc.); loss of H_2O 190 – 220 °C): 10.5% (11.1% calc.); residual B_2O_3 (>750 °C): 17.8% (14.3% calc.).

Recrystallization of **19**·2.5H_2O from toluene yielded very few crystals suitable for single-crystal X-ray diffraction studies. These crystals are currently under investigation by the National Crystallographic Service, Southampton (NCS number 2016NCS0211).

NMR (400 MHz, D_2O) δ_H (ppm): 4.79 (HOD and OH rapidly exchanging in D_2O), 7.28 – 7.31 (m, 12H), 7.44 – 7.53 (m, 18H). (101 MHz, D_2O) δ_C (ppm): 126.84 (dd, $^1J_{PC}$ = 108.1 Hz, $^3J_{PC}$ = 2.0 Hz, *ipso*, 6C), 129.14 (m, *meta*, 12H, CH arom.), 132.13

(m, *ortho*, 12C, CH arom.), 133.48 (brs, *para*, 6C, CH arom.). (128 MHz, D_2O) δ_B (ppm): 15.7. (162 MHz, D_2O) δ_P (ppm): 21.2.

2.5.20 Preparation of 4,4'-bipiperidinium heptaborate dihydrate $[C_{10}H_{22}N_2][B_7O_9(OH)_5]\cdot 2H_2O$ (**20**$\cdot 2H_2O$)

An aqueous solution of 4,4'-bipiperidinyl hydrochloride (1.0 g, in 50 mL H_2O) was stirred for 24 hr with DOWEX (OH^- form). The filtrate was collected and methanol (50 mL) was added, together with 1.01 g $B(OH)_3$. The mixture was stirred for a further 1 hr followed by removal of the solvent under reduced pressure, yielding the crude product as an off-white solid (1.57 g, 74% yield). The solid was recrystallized from H_2O to yield a few single-crystal XRD quality crystals of **20**$\cdot 2H_2O$ (see appendix, with NCS number 2015NCS0560).

NMR (400 MHz, D_2O) δ_H (ppm): 1.39 – 1.54 (m, 6H, $2CH_2$ and 2CH), 2.0 (d, 4H, ^3J = 12.0 Hz, $2CH_2$), 2.97 (t, 4H, ^3J = 12.0 Hz, $2CH_2$), 3.45 (d, 4H, ^3J = 12.0 Hz, $2CH_2$), 4.79 (HOD and OH rapidly exchanging in D_2O). (101 MHz, D_2O) δ_C (ppm): 25.37 ($4CH_2$), 37.33 (2CH), 44.09 ($4CH_2$). (128 MHz, D_2O) δ_B (ppm): 14.7.

IR (KBr) (ν_{max}/cm^{-1}): 3602 (w), 3436 (br, m), 3265 (m), 3022 (br, m), 2921 (m), 2863 (m), 2822 (m), 2761 (m), 2551 (s), 1650 (m), 1636 (m), 1448 (m), 1437 (m), 1419 (m), 1356 (s), 1165 (br, m), 1078 (m), 1044 (m), 986 (m), 919 (w), 909 (w), 855 (m), 810 (s), 719 (w), 689 (w), 670 (w), 622 (w), 489, 469, 440, 420.

Elemental Anal. Calc. (%) for **20**$\cdot 2H_2O$, $C_{10}H_{31}B_7N_2O_{16}$: C, 23.5; H, 6.1; N, 5.5. Found (%); C, 23.5; H, 6.3; N, 5.8.

TGA: Loss of H_2O (160 – 220 °C): 15.7% (15.9% calc.); residual B_2O_3 (>750 °C): 47.9% (47.7% calc.).

M.p: >300 °C.

2.5.21 Preparation of dibenzylammonium pentaborate sesquihydrate $[C_{14}H_{16}N][B_5O_6(OH)_4]\cdot 1.5H_2O$ (**21**$\cdot 1.5H_2O$)

6.63 g from 5.02 g $B(OH)_3$, (98% yield).

NMR (400 MHz, D_2O) δ_H (ppm): 4.24 (s, 4H, $2CH_2$), 4.79 (HOD and OH rapidly exchanging in D_2O), (7.45 – 7.50 (m, 10H, arom.). (101 MHz, D_2O) δ_C (ppm): 50.57

(2CH_2), 129.21 (4CH), 129.52 (2CH), 129.73 (4CH), 131.02 (2C). (128 MHz, D_2O) δ_B (ppm): 1.2, 13.1, 19.0.
IR (KBr) (ν_{max}/cm^{-1}): 3552 (s), 3271 (br, s), 3062 (br, m), 2818 (m), 2632 (w), 2472 (w), 1995, 1929, 1602 (w), 1447 (m), 1423 (m), 1305 (s), 1154 (m), 1093 (m), 1055 (m), 1024 (m), 1009 (m), 916 (vs), 834 (m), 781 (s), 764 (m), 700 (s), 571 (w), 531 (m), 486 (m).
Elemental Anal. Calc. (%) for **21**·1.5H_2O, $C_{14}H_{23}NB_5O_{11.5}$: C, 37.9; H, 5.2; N, 3.2. Found (%); C, 37.7; H, 5.0; N, 3.0.
p-XRD: d spacing/Å (% rel. int.): 3.67 (100), 4.56 (93.70), 4.26 (92.36), 4.79 (64.50), 4.46 (46.10), 4.04 (35.57).
TGA: Loss of interstitial H_2O (150 – 160 °C): 5.0 % (6.1 % calc.); loss of H_2O (220 – 250 °C): 14.4 % (14.2 % calc.) residual B_2O_3 (>750 °C): 43.4 % (39.3 % calc.)

Recrystallization of **21**·1.5H_2O from H_2O/EtOH yielded a few single-crystal XRD quality crystals of **21**.

Elemental Anal. Calc. (%) for **21**, $C_{14}H_{20}NB_5O_{11.5}$: C, 40.4; H, 4.8; N, 3.4. Found (%); C, 40.6; H, 4.9; N, 3.4.
TGA: Loss of H_2O (220 – 250 °C): 8.2% (8.7% calc.); residual B_2O_3 (>750 °C): 45.0% (41.8% calc.).

2.5.22 Preparation of 4,4'-trimethylene*bis*(*N*-methylpiperidine)·boric acid complex [$C_{15}H_{30}N_2$]·[$B(OH)_3$] (**22**)

Prepared as attempted synthesis of a triborate dianion salt (see Section 2.7.11), 1.48 g from 3.71 g $B(OH)_3$ (24% yield).

Crystallization of the crude product led to **22** (see appendix, with NCS number 2014NCS0908).

NMR (400 MHz, D_2O) δ_H (ppm): 1.26 – 1.35 (m, 10H), 1.47 (brs, 2H), 1.87 (d, 4H, ^3J = 12.0 Hz), 2.60 (brs, 10H), 3.22 (d, 4H, ^3J = 12.0 Hz), 4.79 (HOD and OH rapidly exchanging in D_2O). (101 MHz, D_2O) δ_C (ppm): 22.66 (CH_2), 29.98 (4CH_2), 32.75 (2CH), 35.10 (2CH_2), 43.54 (2CH_3), 54.68 (4CH_2). (128 MHz, D_2O) δ_B (ppm): 4.7.

IR (KBr) (v_{max}/cm^{-1}): 3345 (br, m), 2925 (s), 2853 (s), 2804 (s), 2384, 1880, 1629, 1457 (s), 1429 (s), 1412 (s), 1379 (m), 1281 (s), 1217 (br, m), 1143 (s), 1113 (w), 1099 (w), 1072 (m), 1042 (w), 988, 976, 960 (m), 869 (m), 832 (m), 798 (br, m), 766 (s), 706 (w), 680 (s), 530 (m), 506 (m), 444 (m).

Elemental Anal. Calc. (%) for **22**, $C_{15}H_{33}N_2BO_3$: C, 60.0; H, 11.1; N, 9.3. Found (%): C, 59.6; H, 11.0; N, 9.3.

Gravimetric determination of %B: 0.229 g precipitate from 0.101 g of **22**, 3.4% (3.6% Calc.).

p-XRD: d spacing/Å (% rel. int.): 5.28 (100.00), 5.27 (62.85), 5.53 (50.22), 4.46 (31.53), 5.51 (30.05), 3.59 (25.41).

TGA: Loss of H_2O (60 – 70 °C): 6.1% (9.0% calc.); residual B_2O_3 (>600 °C): 11.7% (11.6% calc.).

M.p: 72 – 74 °C.

2.5.23 Preparation of samples for Brunauer-Emmett-Teller (BET) surface area analysis

Polyborate salt samples of **1** were ground into fine powders and placed in to alumina crucibles which were then heated separately in a furnace for 24 hr at 250 °C, 500 °C or 750 °C, respectively. After allowing to cool, the samples were collected and ground again in to fine powders before being submitted for BET analysis. Similar analyses were performed on **2**·1.5H_2O and **3**·½H_2O.

2.6 Solvothermal syntheses of polyborate salts

2.6.1 Solvothermal synthesis of pyrrolidinium pentaborate, $[C_4H_{10}N][B_5O_6(OH)_4]$ (**1**)

$B(OH)_3$ (10.02 g, 162 mmol), pyrrolidine (2.30 g, 32.4 mmol) and H_2O (5 mL) were combined and sealed in a Teflon-lined stainless steel autoclave, which was heated to 145 °C, at autogenous pressure, for 24 hr. The autoclave was allowed to cool to room temperature before opening to reveal the product as colourless crystals (3.80 g, 40% yield). The spectroscopic data was identical to that of compound **1**, which can be found in Section 2.5.1.

2.6.2 Solvothermal synthesis of *N*-methylpyrrolidinium pentaborate sesquihydrate, $[C_5H_{12}N][B_5O_6(OH)_4]$ (**2**·1.5H_2O)

$B(OH)_3$ (10.02 g, 162 mmol), *N*-methylpyrrolidine (2.76 g, 3.4 mL, 32.4 mmol) and H_2O (5 mL) were combined and sealed in a Teflon-lined stainless steel autoclave, which was heated to 145 °C, at autogenous pressure, for 24 hr. The autoclave was allowed to cool to room temperature before opening to reveal the product as colourless crystals (2.81 g, 29% yield). Spectroscopic data was found to be identical to that of compound **2**·1.5H_2O, which can be found in Section 2.5.2.

2.6.3 Solvothermal synthesis of *N,N*-dimethylpyrrolidinium pentaborate hemihydrate, $[C_6H_{14}N][B_5O_6(OH)_4]$ (**3**·½H_2O)

N,*N*-Dimethylpyrrolidinium iodide (3.68 g, 16.2 mmol) was dissolved in H_2O (50 mL), to which an excess of Dowex™ Monosphere™ 550A ion exchange resin (OH^- form) was added. The solution was stirred for 24 hr, the resin removed by filtration, and the solvent removed under pressure to a final volume of ~5 mL. $B(OH)_3$ (5.01 g, 81.0 mmol) was added, and the mixture was sealed in a Teflon-lined stainless steel autoclave which was heated to 145 °C, at autogenous pressure, for 24 hr. The autoclave was allowed to cool to room temperature before opening to reveal the product as colourless crystals (5.93 g, 58% yield). The spectroscopic data was identical to that of **3**·1.5H_2O, which can be found in Section 2.5.3.

2.6.4 Attempted solvothermal synthesis of pyrrolidinium triborate, $[C_4H_{10}N][B_3O_3(OH)_4]$

$B(OH)_3$ (3.00 g, 48.6 mmol), pyrrolidine (1.11 g, 1.3 mL, 16.2 mmol) and H_2O (5 mL) were combined in a Teflon-lined, stainless steel autoclave, which was heated to 145 °C, at autogenous pressure, for 24 hr. The autoclave was allowed to cool to room temperature before opening to reveal colourless crystals (1.83 g). Spectroscopic analysis showed the resulting solid to be identical to compound **1**, which can be found in Section 2.5.1.

2.6.5 Attempted solvothermal synthesis of *N*-methylpyrrolidinium triborate, $[C_5H_{12}N][B_3O_3(OH)_4]$

$B(OH)_3$ (3.00 g, 48.6 mmol), pyrrolidine (1.39 g, 1.7 mL, 16.2 mmol) and H_2O (5 mL) were combined in a Teflon-lined, stainless steel autoclave, which was heated to 145

°C, at autogenous pressure, for 24 hr. The autoclave was allowed to cool to room temperature before opening to reveal colourless crystals (1.36 g). Spectroscopic analysis showed the resulting solid to be identical to compound **2**·1.5H_2O, which can be found in Section 2.5.2.

2.6.6 Attempted solvothermal synthesis of *N,N*-dimethylpyrroldinium triborate, [$C_6H_{14}N$][$B_3O_3(OH)_4$]

N,*N*-Dimethylpyrrolidinium iodide (3.68 g, 16.2 mmol) was dissolved in H_2O (50 mL), to which an excess of Dowex™ Monosphere™ 550A ion exchange resin (OH^- form) was added. The solution was stirred for 24 hr, the resin removed by filtration, and the solvent removed under pressure to a final volume of ~3 mL. $B(OH)_3$ (3.01 g, 48.6 mmol) and C_5H_5N (5 mL) were combined with the *N*,*N*-dimethylpyrrolidinium hydroxide solution (16.2 mmol, ~3 mL), and sealed in a Teflon lined stainless steel autoclave. The autoclave was heated to 160 °C, at autogenous pressure, for 4 days. The autoclave was then allowed to cool to room temperature, before opening revealed a large number of X-ray analytical quality colourless crystals (1.48 g). The crystals were collected by filtration and washed with minimal H_2O, to remove residual C_5H_5N. NMR and FTIR analysis determined the crystals were that of **3**·½H_2O (48% yield) (full characterisation data of **3**·½H_2O is given in Section 2.5.3).

2.6.7 Attempted solvothermal synthesis of choline triborate, [$(CH_3)_3NCH_2CH_2OH$][$B_3O_3(OH)_4$]

$B(OH)_3$ (3.71 g, 60 mmol), choline hydroxide (5.27 g, 4.91 mL of a 46% w/w solution, 20 mmol) and C_5H_5N (2 mL) were combined and sealed in a Teflon lined autoclave. The autoclave was heated to 160 °C, at autogenous pressure, for 4 days. The autoclave was allowed to cool to room temperature before opening to reveal a charred paper-like, insoluble solid.

2.6.8 Attempted solvothermal synthesis of carboranylmethylammonium pentaborate, [$C_2B_{10}H_{11}(CH_2NH_3)$][$B_5O_6(OH)_4$]

Aminomethyl-*o*-carborane, $C_2B_{10}H_{11}(CH_2NH_2)$ (0.37 g, 1.9 mmol), $B(OH)_3$ (0.60 g, 9.6 mmol) and C_5H_5N (2 mL) were combined and sealed in a Teflon-lined stainless steel autoclave. The autoclave was heated to 145 °C, at autogenous pressure, and

was maintained at this temperature for 72 hr. The autoclave was allowed to cool to room temperature before opening to reveal an off-white solid. NMR analyses showed the resulting solid to be a mixture of starting materials only.

2.6.9 Attempted solvothermal synthesis of carboranylmethyl(dimethyl)ammonium pentaborate, $[C_2B_{10}H_{11}(CH_2NH(CH_3)_2)][B_5O_6(OH)_4]$

(Dimethylamino)methyl-*o*-carborane, $C_2B_{10}H_{11}(CH_2N(CH_3)_2)$ (1.01 g, 5.0 mmol), $B(OH)_3$ (1.5 g, 25.0 mmol) EtOH (1 mL) and H_2O (1 mL) were combined and sealed in a Teflon-lined stainless steel autoclave. The autoclave was heated to 145 °C, at autogenous pressure, and maintained at this temperature for 72 hr. The autoclave was allowed to cool to room temperature before opening to reveal an off-white solid. NMR analyses showed the resulting solid to be a mixture of starting materials only.

2.6.10 Attempted solvothermal synthesis of pyrrolidinium tetraborate, $[C_4H_{10}N]_2[B_4O_5(OH)_4]$

Ammonium tetraborate (5.3 g, 20 mmol), pyrrolidine (2.8 g, 3.4 mL, 40 mmol) and C_5H_5N (5 mL) were combined and sealed in a Teflon-lined stainless steel autoclave. The autoclave was heated to 145 °C, at autogenous pressure, and maintained for 7 days before cooling to room temperature. The resulting white powder was shown, by NMR analyses, to be pyrrolidinium pentaborate (**1**) (full characterisation of compound **1** is given in Section 2.5.1).

2.6.11 Attempted solvothermal synthesis of hexadecylammonium pentaborate, $[C_{16}H_{36}N][B_5O_6(OH)_4]$

Hexadecylamine (1.5 g, 6.2 mmol) and $B(OH)_3$ (1.92 g, 31.1 mmol) were combined with H_2O (5 mL) and C_5H_5N (5 mL) in a Teflon-lined stainless steel autoclave. The autoclave was heated to 145 °C, at autogenous pressure, for 24 hr, before allowing the autoclave to cool slowly to room temperature. The resulting solid was found, by NMR analyses, to be a mixture of starting materials only.

2.6.12 Solvothermal synthesis of bis(triphenylphosphine)iminium pentaborate $[C_{36}H_{30}NP_2][B_5O_6(OH)_4]$ (**18**·$1.5H_2O$)

Bis(triphenylphosphine)iminium chloride (1.02 g, 1.76 mmol) was dissolved in H_2O (~50 mL) and was stirred for 24 hr with activated DOWEX anion exchange resin

(OH^- form). The resin was filtered off, and the filtrate concentrated to a volume of ~3 mL. $B(OH)_3$ (0.54 g, 8.8 mmol) was added and the mixture was sealed in a Telfon-lined stainless steel autoclave, which was then heated to 145 °C, at autogenous pressure, for 24 hr. The autoclave was allowed to cool to room temperature before opening to reveal the product as glistening, fragile needle-like crystals (1.10 g, 83% yield). The spectroscopic data was found to be identical to that of compound **18**·1.5H_2O, which can be found in Section 2.5.18.

2.6.13 Solvothermal synthesis of bis(triphenylphosphine)iminium pentaborate [$C_{36}H_{30}NP_2$][$B_5O_6(OH)_4$] (**19**·2.5H_2O)

Bis(triphenylphosphine)iminium chloride (1.09 g, 1.9 mmol) was dissolved in H_2O (~50 mL) and was stirred for 24 hr with activated DOWEX anion exchange resin (OH^- form). The resin was filtered off, and the filtrate concentrated to a volume of ~3 mL. $B(OH)_3$ (0.24 g, 3.8 mmol) was added and the mixture was sealed in a Telfon-lined stainless steel autoclave, which was then heated to 145 °C, at autogenous pressure, for 24 hr. The autoclave was allowed to cool to room temperature before opening to reveal the product as fragile crystals which were collected by suction filtration and washed with minimal H_2O (0.40 g, 31% yield). The spectroscopic data was found to be identical to that of compound **19**·2.5H_2O, which can be found in Section 2.5.19.

2.7 Attempted syntheses of polyborate salts

2.7.1 Attempted synthesis of 1-(1-cyclopenten-1-yl)pyrrolidinium pentaborate [$C_9H_{16}N$][$B_5O_6(OH)_4$]

1-Pyrrolidino-cyclopentene (2.22 g, 2.4 mL, 16.2 mmol) was added to a stirred solution of $B(OH)_3$ (5.01 g, 81.0 mmol) in 1:1 H_2O:MeOH (100 mL). The solution was stirred for 1 hr, before removal of the solvent under reduced pressure, yielding an off-white solid which was oven – dried at 60 °C for 24 hr (3.99 g).

NMR (400 MHz, D_2O) δ_H (ppm): 1.14 (t, ^3J = 7.2 Hz, 2H), 1.93 – 1.96 (m, 4H), 3.21 – 3.25 (m, 4H), 3.61 (q, ^3J = 7.2 Hz, 2H), 4.79 (HOD and OH rapidly exchanging in

D_2O). (101 MHz, D_2O) δ_C (ppm): 16.71, 23.56, 45.40, 57.55. (128 MHz, D_2O) δ_B (ppm):1.1, 13.2, 16.1.

2.7.2 Attempted synthesis of 1-(1-cyclohexen-1-yl)pyrrolidinium pentaborate $[C_{10}H_{18}N][B_5O_6(OH)_4]$

1-Pyrrolidino-cyclohexene (2.45 g, 2.6 mL, 16.2 mmol) was added to a stirred solution of $B(OH)_3$ (5.01 g, 81.0 mmol) in 1:1 H_2O:MeOH (100 mL). The solution was stirred for 1 hr, before removal of the solvent under reduced pressure, yielding an off-white solid was oven-dried at 60 °C for 24 hr (3.95 g).

NMR (400 MHz, D_2O) δ_H (ppm): 1.04 (t, ^3J = 7.2 Hz, 2H), 1.83 – 1.87 (m, 4H), 3.12 – 3.15 (m, 4H), 3.51 (q, ^3J = 7.2 Hz, 2H), 4.79 (HOD and OH rapidly exchanging in D_2O). (101 MHz, D_2O) δ_C (ppm): 16.71, 23.56, 45.40, 57.35. (128 MHz, D_2O) δ_B (ppm):1.2, 13.1, 16.0.

2.7.3 Attempted synthesis of pyrrolidinium triborate $[C_4H_{10}N][B_3O_3(OH)_4]$

$B(OH)_3$, (3.01 g, 48.6 mmol), was dissolved in 1:1 MeOH:H_2O (100 mL) and pyrrolidine (1.15 g, 16.2 mmol) was added with stirring. The solvent was removed under pressure after 30 minutes, resulting in the formation of a white solid, which was oven-dried at 60 °C for 24 hours. NMR analysis of the solid was consistent with the data for compound **1** (3.53 g, yield 75%), which can be found in Section 2.5.1.

NMR (400 MHz, D_2O) δ_H (ppm): 1.92 – 1.95 (m, 4H, $2CH_2$), 3.20 – 3.24 (m, 4H, $2CH_2$), 4.79 (HOD and OH rapidly exchanging in D_2O). (128 MHz, D_2O) δ_B (ppm): 1.1, 13.2, 17.9.

2.7.4 Attempted synthesis of *N*-methylpyrrolidinium triborate $[C_5H_{12}N][B_3O_3(OH)_4]$

$B(OH)_3$, (3.01 g, 48.6 mmol), was dissolved in 1:1 MeOH:H_2O (100 mL) and *N*-methylpyrrolidine (1.38 g, 16.2 mmol) was added with stirring. The solvent was removed under pressure after 30 minutes, resulting in the formation of a white solid, which was oven-dried at 60 °C for 24 hours. NMR analysis of the solid was consistent with the data for compound **2**·$1.5H_2O$ (3.73 g, yield 76%), which can be found in Section 2.5.2.

NMR (400 MHz, D_2O) δ_H (ppm): 2.05 (s, 4H, $2CH_2$), 2.87 (s, 3H, CH_3), 3.05 (s, 2H, CH_2), 3.56 (s, 2H, CH_2), 4.79 (HOD and OH rapidly exchanging in D_2O). (128 MHz, D_2O) δ_B (ppm): 1.2, 13.5, 18.2.

2.7.5 Attempted synthesis of *N,N*-dimethylpyrrolidinium triborate, $[C_6H_{14}N][B_3O_3(OH)_4]$

N,*N*-Dimethylpyrrolidinium iodide (3.68 g, 16.2 mmol) was dissolved in H_2O (50 mL), to which an excess of Dowex™ Monosphere™ 550A ion exchange resin (OH^- form) was added. The solution was stirred for 24 hr, the resin removed by filtration, and MeOH (50 mL) was added to the filtrate. $B(OH)_3$ (3.01 g, 48.6 mmol) was added, with stirring, and the solution warmed gently. The solvent was removed under pressure after 1 hour, to yield a cream solid, which was then oven-dried at 60 °C for 24 hours (3.75 g).

NMR (400 MHz, D_2O) δ_H (ppm): 2.24 (m, 4H, CH_2), 3.15 (s, 6H, CH_3), 3.50 - 3.54 (m, 4H, CH_2), 4.79 (s, HOD, OH and NH rapidly exchanging in the D_2O). (100 MHz, D_2O) δ_C (ppm): 21.59 (CH_2), 51.57 (CH_3), 65.77 (CH_2N). (128 MHz, D_2O) δ_B (ppm): 14.28.

IR (KBr) (ν_{max}/cm^{-1}): 3422, 3266, 2997, 2349, 1654, 1415, 1311 (m), 1148, 1075 (m), 1017 (m), 915 (vs), 816, 772 (s), 724 (m), 708 (s), 478 (m), 464.

Elemental Anal. Calc. (%), $C_6H_{18}NB_3O_7$; C, 29.0; H, 7.3; N, 5.6. Found (%): C, 29.6; H, 6.8; N, 5.6.

p-XRD: d-spacing/Å (% rel. int.): 7.77 (100.00), 4.41 (86.76), 3.86 (82.61), 4.92 (74.14), 4.36 (69.70), 3.80 (64.75).

TGA: loss of H_2O: 15.7% (14.5% calc.); residual B_2O_3: 43.3% (42.0% calc.).

Recrystallization of the crude product from H_2O/CH_3COCH_3 yielded a few colourless crystals of compound **3** (full characterisation data can be found in Section 2.5.3).

2.7.6 Attempted synthesis of carboranyl-methylammonium pentaborate $[C_3B_{10}H_{16}][B_5O_6(OH)_4]$

To a solution of aminomethyl-*o*-carborane (0.3 g, 1.9 mmol) in MeOH (90 mL) was added $B(OH)_3$ (0.6 g, 9.5 mmol) in H_2O (10 mL) with stirring, at room temperature. After 3 hrs, the solvent was removed under reduced pressure to yield a white solid

which was oven-dried overnight at 70 °C. NMR analyses showed the resulting solid was a mixture of starting materials only.

2.7.7 Attempted synthesis of carboranylmethyl(dimethyl)ammonium pentaborate, $[C_5B_{10}H_{19}][B_5O_6(OH)_4]$

(Dimethylamino)methyl-*o*-carborane (1.01 g, 5.0 mmol) was added to a solution of $B(OH)_3$ (1.50 g, 25 mmol) in MeOH:H_2O (1:1, 100 mL), with stirring at room temperature. After 2 hrs the solvent was removed under reduced pressure to yield an off-white solid. NMR analyses showed this solid to be a mixture of starting materials only.

2.7.8 Attempted synthesis of *N*,*N*-dimethyl-2-adamantylammonium pentaborate $[C_{12}H_{22}N][B_5O_6(OH)_4]$

N,*N*-Dimethyl-2-adamantylamine (0.36 g, 2.0 mmol), was added to a stirred solution of $B(OH)_3$ (0.62 g, 10.0 mmol) in 1:1 H_2O:MeOH (100 mL). The solution was stirred for 1 hr, before removal of the solvent under reduced pressure to yield the product as an off-white solid which was oven-dried at 60 °C overnight (0.71 g).

NMR (400 MHz, D_2O) δ_H (ppm): 1.74 – 1.76 (m, 8H), 1.88 (m, 2H), 1.97 – 2.00 (m, 2H), 2.37 (s, 2H, 2CH), 2.88 (s, 6H, $2CH_3$), 3.24 (s, 1H, CH), 4.79 (HOD, NH and OH rapidly exchanging in D_2O). (101 MHz, D_2O) δ_C (ppm): 25.76 (CH), 25.88 (CH), 27.69 ($2CH_2$), 29.63 (2CH), 36.02 (CH_2), 36.09 ($2CH_2$), 41.10 ($2CH_3$), 71.59 (CH). (128 MHz, D_2O) δ_B (ppm): 18.2.

IR (KBr) (ν_{max}/cm^{-1}): 3653, 3218 (br, s), 2925 (m), 2868, 2509, 2387, 2262 (m), 1637, 1440 (br, s), 1312 (m), 1195 (s), 1037 (m), 931 (s), 813 (m), 777 (s), 705 (m), 671 (m), 646 (m), 548 (s).

Elemental Anal. Calc. (%) for $C_{12}H_{26}NB_5O_{10}$: C, 36.2; H, 6.6; N, 3.5. Found (%); C, 18.3; H, 6.4; N, 1.8.

p-XRD: d spacing/Å (% rel. int.): 3.22 (100), 3.18 (95.97), 4.70 (63.39), 5.60 (53.75), 4.73 (45.58).

Recrystallization from H_2O was attempted, but crystals suitable for single-crystal XRD were not obtained.

2.7.9 Attempted synthesis of hexadecylammonium pentaborate, $[C_{16}H_{36}N][B_5O_6(OH)_4]$

To a solution of $B(OH)_3$ (1.92 g, 31.0 mmol) in 1:1 MeOH:H_2O (100 mL), was added hexadecylamine (1.50 g, 6.2 mmol), with stirring. The solvent was removed under reduced pressure after 1 hr to yield a white solid. NMR analyses showed this solid to be a mixture of the starting materials only.

2.7.10 Attempted synthesis of 4,4'-trimethylenedipiperidinium triborate, $[C_{13}H_{28}N_2][B_3O_3(OH)_5]$

4,4'-Trimethylenedipiperidine (4.21 g, 20.0 mmol) and $B(OH)_3$ (2.47 g, 40.0 mmol) were dissolved in a 1:1 MeOH:H_2O mixture (100 mL) with gentle warming. The solution was allowed to stir for 1 hr before removal of the solvent under reduced pressure to yield a cream solid which was oven-dried at 70 °C for 24 hr (5.70 g).

NMR (400 MHz, D_2O) δ_H (ppm): 1.14 – 1.31 (m, 10H), 1.64 – 1.73 (m, 4H), 1.90 (brs, 3H), 2.02 – 2.08 (m, 1H), 2.22 (m, 5H), 2.85 – 2.91 (m, 3H), 4.79 (HOD, NH and OH rapidly exchanging in D_2O). (101 MHz, D_2O) δ_C (ppm): 22.94, 32.11, 36.86, 44.66, 55.72. (128 MHz, D_2O) δ_B (ppm): not obtained.

2.7.11 Attempted synthesis of 4,4'-trimethylene*bis*(*N*-methylpiperidine) triborate, $[C_{15}H_{32}N_2][B_3O_3(OH)_5]$

4,4'-Trimethylene*bis*(*N*-methylpiperidine) (4.77 g, 20.0 mmol) and $B(OH)_3$ (2.47 g, 40.0 mmol) were dissolved in a 1:1 MeOH:H_2O mixture (100 mL) with gentle warming. The solution was allowed to stir for 1 hr before removal of the solvent under reduced pressure to yield a dark cream solid which was oven dried at 70 °C for 24 hr (6.34 g).

NMR (400 MHz, D_2O) δ_H (ppm): 1.25 – 1.42 (m, 12H), 1.83 (d, 4H, J = 16.0 Hz), 2.50 (m, 10H), 3.11 (d, 4H, J = 12.0 Hz), 4.79 (HOD, NH and OH rapidly exchanging in D_2O). (101 MHz, D_2O) δ_C (ppm): 22.71, 30.25, 33.07, 35.20, 43.82, 54.73. (128 MHz, D_2O) δ_B (ppm): 3.5.

Recrystallization of the crude material from H_2O led to the formation of colourless needle-like crystals of **22**, which is fully characterized in Section 2.5.22.

2.7.12 Attempted synthesis of tribenzylammonium pentaborate, $[C_{21}H_{22}N][B_5O_6(OH)_4]$

Tribenzylamine (5.75 g, 20.0 mmol) was dissolved in MeOH (90 mL) with heating. $B(OH)_3$ (6.18 g, 100.0 mmol) was dissolved in H_2O (10 mL) and was slowly added to the stirred ammonium solution, which almost instantaneously precipitated a glittery-appearance white solid. The solid was filtered off by suction filtration and dried in air (1.42 g) before analysis by NMR showed it to be tribenzylamine.

The remaining filtrate was dried under reduced pressure to yield a white solid, of which NMR analyses showed to be a mixture of starting materials only.

2.7.13 Attempted synthesis of glucosammonium pentaborate, $[C_6H_{14}NO_5][B_5O_6(OH)_4]$

A solution of glucosammonium hydrochloride (2.28 g, 10.6 mmol in 50 mL H_2O) was stirred with excess activated DOWEX anion exchange resin (OH^- form) for 24 hr. The resin was removed by suction filtration and then MeOH (50 mL) and $B(OH)_3$ (3.26 g, 52.8 mmol) was added to the filtrate. Stirring was continued for 1 hr, before removal of the solvent under reduced pressure to yield a light brown solid (3.79 g). NMR analysis showed the solid to be a mixture of starting materials only.

2.7.14 Attempted synthesis of 1,2,3,4-tetrahydroquinoline pentaborate, $[C_9H_{12}N][B_5O_6(OH)_4]$

To a stirred solution of $B(OH)_3$ (5.01 g, 81.0 mmol) in 1:1 MeOH:H_2O (100 mL) was added 1,2,3,4-tetrahydroquinoline (1.07 g, 16.2 mmol). The resulting mixture was stirred for 1 hr at room temperature, before removal of the solvent under reduced pressure, yielding an off-white solid, which was oven-dried at 70 °C overnight. NMR analyses of the resulting solid showed it to be a mixture of starting materials only.

2.8 Preparation of triarylboroxine·amine adducts

The triarylboroxine·amine adducts were all prepared using a general procedure, as detailed in section 2.8.2 for compound **26**.

2.8.1 Preparation of tri(Ar)boroxine {Ar = phenyl (**23**), *p*-chlorophenyl (**24**), pentafluorophenyl (**25**)}

The triarylboroxines were prepared through dehydration of a finely crushed powder of the corresponding boronic acid at 110 °C. The boroxines were stored in sealed vessels under an inert atmosphere.

2.52 g triphenylboroxine, (PB) $[(C_6H_5)_3B_3O_3]$ (**23**) from 3.00 g phenylboronic acid, (98%).

NMR (400 MHz, $CDCl_3$) δ_H (ppm): 7.53 (t, 6H), 7.61 (t, 3H), 8.26 (d, 6H). (101 MHz, $CDCl_3$) δ_C (ppm): 128.13 (CH), 132.84 (CH), 135.80 (CH). (128 MHz, $CDCl_3$) δ_B (ppm): 29.5.

IR (KBr) (ν_{max}/cm^{-1}): 3467 (br), 3077 (m), 3051(m, br), 3024 (m), 1964, 1915, 1829, 1783, 1603 (s), 1494 (m), 1443 (s).1366 (s, br), 1345 (s, br), 1307 (s), 1162 (m), 1086 (m), 1023 (m), 928, 854, 760 (m), 701 (s, br), 578 (s).

p-XRD: d spacing/Å (% rel. int.): 3.44 (100.00), 4.17 (87.69), 4.23 (66.61), 5.74 (50.91), 4.28 (50.78), 6.83 (26.16).

Mp: 218 – 220 °C [lit.[236] 220 – 222 °C]

1.77 g tri-(*p*-chlorophenyl)boroxine (CPB) (**24**) $[(p\text{-}ClC_6H_4)_3B_3O_3]$ from 2.00 g *p*-chlorophenylboronic acid (99%).

NMR (400 MHz, $CDCl_3$) δ_H (ppm): 7.49 (d, 6H), 8.13 (d, 6H). (101 MHz, $CDCl_3$) δ_C (ppm): 128.62 (CH), 137.14 (CH), 139.56 (C-Cl). (128 MHz, $CDCl_3$) δ_B (ppm): 29.1.

IR (KBr) (ν_{max}/cm^{-1}): 3436 (br), 1919, 1595 (s), 1563 (m), 1400 (s, br), 1367 (s, br), 1344 (s, br), 1257 (m, br), 1173 (m), 1086 (s), 1014 (m), 824 (m), 776 (m), 734 (s, br), 679 (s), 480 (m), 455 (s).

p-XRD: d spacing/Å (% rel. int.): 4.69 (100.00), 3.51 (72.69), 3.57 (55.99), 3.17 (54.55), 5.20 (53.75), 5.06 (50.51).

Mp: 306 – 307 °C [lit.[236] 307 – 309 °C]

0.90 g tri-(pentafluorophenyl)boroxine (FPB) (**25**) [$(C_6F_5)_3B_3O_3$] from 1.00 g pentafluorophenylboronic acid (99%).

NMR (376 MHz, $CDCl_3$) δ_F (ppm): -132.8 (m, 2F, *ortho*-F,), -148.2 (t, 1F, *para*-F, $^3J_{FF}$ = 20.3 Hz), -160.6 (m, 2F, *meta*-F) [lit.[225] (CD_3CN): -132.4, -153.7, -163.5]. (128 MHz, $CDCl_3$) δ_B (ppm): 26.9.

IR (KBr) (ν_{max}/cm^{-1}): 3355 (br), 2226, 2169, 2114, 2068, 1651 (s, br), 1526 (s), 1487 (s, br), 1349 (s, br), 1227 (s), 1162 (m), 1091 (m), 981 (s, br), 885 (m), 860 (m), 811, 767 (m), 759 (m), 708 (m), 626 (s), 575 (m), 481 (m).

p-XRD: d spacing/Å (% rel. int.): 3.05 (100.00), 2.11 (7.99), 3.86 (7.91), 3.16 (6.99), 2.03 (5.56), 2.90 (5.22).

Mp: 278 – 280 °C [lit.[237] 282 °C]

2.8.2 Preparation of bis(triphenylboroxine)·4,4'-trimethylenedipiperidine complex $[C_{13}H_{26}N_2]\cdot[PB]_2$ (**26**)

Under an inert atmosphere, 4,4'-trimethylenedipiperidine (0.53 g, 2.5 mmol) was added to a stirred suspension of $[(C_6H_5)_3B_3O_3]$ (1.56 g, 5.0 mmol) in Et_2O. The solid dissolved after approx. 10 minutes, then the solution was filtered and the solvent removed under vacuum. The resulting white solid was recrystallized from CH_3Cl (1.30 g, 99% yield).

NMR (400 MHz, $CDCl_3$) δ_H (ppm): 1.03 – 1.56 (m, 13H), 1.69 – 1.80 (m, 4H), 2.60 – 2.77 (m, 5H), 3.42 (m, 4H), 7.40 (brs, 18H), 8.03 (brs, 12H). (101 MHz, $CDCl_3$) δ_C (ppm): 23.30, 31.69, 34.63, 36.26, 45.23. (128 MHz, $CDCl_3$) δ_B (ppm): not obtained.

IR (KBr) (ν_{max}/cm^{-1}): 3415 (br), 3130, 3068, 3048, 3022, 2991, 2977, 2959, 2936, 2917 (s), 1601, 1453, 1445, 1396, 1347, 1282, 1258, 1122 (s), 1069 (s), 1026 (s), 981 (s), 861 (s), 842 (s), 747 (s), 704 (vs), 680, 575.

Elemental Anal. Calc. (%) for **26**, $C_{31}H_{41}B_3N_2O_3$: C, 70.6; H, 6.8; N, 3.4. Found (%): C, 70.4; H, 6.7; N, 3.3.

p-XRD: d spacing/Å (% rel. int.): 4.03 (100), 5.65 (61.24), 4.84 (58.99), 6.03 (38.93), 3.82 (38.60), 3.52 (38.14).

Mp: 253 – 256 °C.

2.8.3 Preparation of bis(tri(*p*-chlorophenyl)boroxine)·4,4'-trimethylenedipiperidine complex $[C_{13}H_{26}N_2]\cdot[CPB]_2$ (**27**)

1.72 g, 92 % yield.

NMR (400 MHz, $CDCl_3$) δ_H (ppm): 1.06-1.23 (m, 10H), 1.35 (br s, 2H), 1.82 (d, 4H), 2.55 (br s, 4H), 2.75 (br s, 2H), 3.38 (br s, 4H), 7.36 (d, 12H), 7.88 (br s, 12H). (101 MHz, $CDCl_3$) δ_C (ppm): 23.28, 31.56, 34.45, 36.19, 45.14. (128 MHz, $CDCl_3$) δ_B (ppm): not obtained.

IR (KBr) (ν_{max}/cm^{-1}): 3415 (br), 3229, 3072, 3031, 2928, 2856, 1592, 1562, 1486, 1435, 1415, 1380, 1330, 1278, 1247, 1196, 1172, 1120, 1097, 1083, 1044, 1014, 985, 972, 857, 828, 816, 769, 733, 670, 663, 629, 612.

Elemental Anal. Calc. (%) for **27**, $C_{31}H_{38}B_3Cl_3N_2O_3$: C, 56.6; H, 4.8; N, 2.7. Found (%): C, 56.3; H, 4.8; N, 2.6.

p-XRD: d spacing/Å (% rel. int.): amorphous solid.

Mp: 247 – 250 °C.

2.8.4 Preparation of tri(*p*-chlorophenyl)boroxine·cyclohexylamine complex $[C_6H_{13}N]\cdot[CPB]$ (**28**)

0.512 g, 89% yield.

NMR (400 MHz, $CDCl_3$) δ_H (ppm): 1.09-1.26 (m, 5H), 1.59 (d,1H), 1.70 (d, 2H), 1.98 (d, 2H), 2.97 (m, 1H), 3.55 (br s, 2H), 7.38 (d, 2H), 7.90 (d, 2H). (101 MHz, $CDCl_3$) δ_C (ppm): 24.31 ($2CH_2$), 24.91 (CH_2), 33.50 ($2CH_2$), 51.22 (C), 128.04 (6CH), 135.20 (6CH), 136.21 (C-Cl). (128 MHz, $CDCl_3$) δ_B (ppm): 22.2.

IR (KBr) (ν_{max}/cm^{-1}): 3436 (br), 3275 (m), 3233 (m), 3072 (w), 2935 (s, br), 2858 (s), 1592 (s), 1562 (m), 1434 (m), 1408 (s), 1376 (m), 1339 (m), 1327 (m), 1285 (s, br), 1243 (m), 1189 (m), 1120 (m), 1081 (s), 1013 (s), 982 (m), 821 (s), 765 (s, br), 733 (m), 662 (m), 582, 451 (s).

Elemental Anal. Calc. (%) for **28**, $C_{24}H_{25}B_3Cl_3NO_3$: C, 56.1; H, 4.9; N, 2.7. Found (%): C, 54.7; H, 4.8; N, 2.5.

p-XRD: d spacing/Å (% rel. int.): 3.48 (100.00), 4.72 (78.47), 4.12 (54.82), 4.01 (48.31), 4.40 (46.70), 4.89 (43.92).

Mp: 177 – 181 °C.

2.8.5 Preparation of tri(*p*-chlorophenyl)boroxine·morpholine complex [C_4H_9NO]·[CPB] (**29**)

0.55 g, 92% yield.

NMR (400 MHz, $CDCl_3$) δ_H (ppm): 3.05-3.12 (br m, 5H), 3.78 (br s, 4H), 7.37 (d, 6H), 7.90 (d, 6H). (101 MHz, $CDCl_3$) δ_C (ppm): 44.43 ($2CH_2$), 66.09 ($2CH_2$), 128.04 (6CH), 135.44 (6CH). (128 MHz, $CDCl_3$) δ_B (ppm): 21.0.

IR (KBr) (ν_{max}/cm^{-1}): 3437 (br), 3214 (vs), 3070, 3026, 2982, 2854 (m), 1591 (vs), 1484, 1433, 1410 (s), 1374 (m), 1326 (s), 1280 (m), 1248 (m), 1191 (s), 1125 (s), 1088 (s), 1044 (m), 1012 (s), 889 (m), 848 (m), 812 (s), 766 (s), 727 (m), 664 (s), 624, 538, 452 (s).

Elemental Anal. Calc. (%) for **29**, $C_{22}H_{21}B_3Cl_3NO_4$: C, 52.6; H, 4.2; N, 2.8. Found (%): C, 52.4; H, 4.3; N, 2.8.

p-XRD: d spacing/Å (% rel. int.): 5.43 (100), 3.45 (94.66), 3.63 (77.17), 3.82 (68.37), 5.36 (54.12), 5.47 (53.10).

Mp: 217 – 220 °C.

2.8.6 Preparation of tri(*p*-chlorophenyl)boroxine·2-picoline complex [C_6H_7N]·[CPB] (**30**)

0.44 g, 72% yield.

NMR (400 MHz, $CDCl_3$) δ_H (ppm): 2.75 (s, 3H, CH_3), 7.30 (d, 1H), 7.38 (m, 7H), 7.81 (t, 1H), 7.92 (d, 6H), 9.07 (d, 1H). (101 MHz, $CDCl_3$) δ_C (ppm): 23.56 (CH_3), 122.13 (CH), 126.84 (CH), 128.15 (CH), 135.80 (CH), 136.97 (C-Cl), 139.44 (CH), 146.19 (CH), 157.94 (C). (128 MHz, $CDCl_3$) δ_B (ppm): 23.4.

IR (KBr) (ν_{max}/cm^{-1}): 3436 (br), 3071, 3035, 2940, 1620 (m), 1594 (s), 1563 (m), 1485 (m), 1406 (s, br), 1374 (m, br), 1344 (s, br), 1327 (s, br), 1294 (s, br), 1283 (s, br), 1121 (s), 1082 (s, br), 1043 (m, br), 1014 (s), 977 (m), 822 (m), 808 (m), 760 (s, br), 740 (s, br), 694 (m), 613 (s), 457 (s).

Elemental Anal. Calc. (%) for **30**, $C_{24}H_{19}B_3Cl_3NO_3$: C, 56.7; H, 3.8; N, 2.8. Found (%): C, 56.2; H, 3.8; N, 2.2.

p-XRD: d spacing/Å (% rel. int.): 5.47 (100), 3.63 (60.65), 3.49 (53.09), 11.12 (48.70), 3.70 (39.29), 5.27 (34.69).

Mp: 289 – 291 °C.

2.8.7 Preparation of tri(*p*-chlorophenyl)boroxine·4-picoline complex [C_6H_7N]·[CPB] (**31**)

0.59 g, 97% yield.

NMR (400 MHz, $CDCl_3$) δ_H (ppm): 2.50 (s, 3H, CH_3), 7.35 (d, 6H), 7.42 (d, 2H), 7.93 (d, 6H), 8.80 (d, 2H). (101 MHz, $CDCl_3$) δ_C (ppm): 21.72 (CH_3), 126.61 (CH), 127.94 (CH), 135.14 (CH), 143.03 (CH). (128 MHz, $CDCl_3$) δ_B (ppm): 19.9.

IR (KBr) (ν_{max}/cm^{-1}): 3434 (br), 3072, 3029, 1633 (m), 1593 (s, br), 1563 (m), 1485 (m), 1433 (s, br), 1407 (s, br), 1378 (m, br), 1325 (s, br), 1278 (s), 1246 (s), 1206, 1179 (m), 1118 (m), 1081 (s, br), 1043 (m), 1014 (s), 984 (s), 854 (m), 822 (m), 803 (m), 762 (s, br), 743, 732, 696 (m), 660 (m), 636 (m), 508 (m), 453 (s).

Elemental Anal. Calc. (%) for **31**, $C_{24}H_{19}B_3Cl_3NO_3$: C, 56.7; H, 3.8; N, 2.8. Found (%): C, 56.7; H, 3.7; N, 2.7.

p-XRD: d spacing/Å (% rel. int.): 4.62 (100), 5.39 (77.51), 3.46 (55.83), 3.58 (43.66), 4.97 (36.25), 3.25 (26.93).

Mp: 192 – 195 °C.

2.8.8 Preparation of tri(*p*-chlorophenyl)boroxine·benzylamine complex [C_7H_9N]·[CPB] (**32**)

0.61 g, 98% yield.

NMR (400 MHz, $CDCl_3$) δ_H (ppm): 3.72 (s, br, NH_2), 3.93 (s, 2H, CH_2), 7.18 (m, 2H), 7.34 – 7.41 (m, 9H), 7.94 (d, 6H). (101 MHz, $CDCl_3$) δ_C (ppm): 45.11 (CH_2),128.08 (CH), 128.19 (CH), 129.15 (CH), 135.23 (CH), 136.26 (C). (128 MHz, $CDCl_3$) δ_B (ppm): 19.8.

IR (KBr) (ν_{max}/cm^{-1}): 3434 (br), 3274 (s), 3205 (s, br), 3219 (s, br), 3067, 3033, 1920, 1593 (vs, br), 1402 (s), 1376 (s), 1344 (s), 1324 (s), 1289 (s, br), 1243 (s), 1206 (m), 1115 (s), 1083 (s, br), 1050 (m), 1014 (s), 992 (s), 958, 938, 916, 881 (m, br), 822 (s, br), 775 (s), 732 (s), 700 (s), 669 (s), 628, 604, 541 (m), 522 (m), 480 (m), 453 (s).

Elemental Anal. Calc. (%) for **32**, $C_{25}H_{21}B_3Cl_3NO_3$: C, 57.5; H, 4.1; N, 2.7. Found (%): C, 57.1; H, 4.1; N, 2.7.

p-XRD: d spacing/Å (% rel. int.): 3.98 (100.00), 3.38 (91.87), 4.69 (58.18) 2.03 (69.38),
Mp: 155 – 157 °C.

2.8.9 Preparation of tri(*p*-chlorophenyl)boroxine·piperidine complex [$C_5H_{11}N$]·[CPB] (**33**)

0.59 g, 98% yield.

NMR (400 MHz, $CDCl_3$) δ_H (ppm): 1.66 (s, br, 6H), 2.80 (s, br, 5H), 7.37 (d, 6H), 7.91 (d, 6H). (101 MHz, $CDCl_3$) δ_C (ppm): 23.05 (CH_2), 25.37 (CH_2), 127.90 (CH), 135.44 (CH). (128 MHz, $CDCl_3$) δ_B (ppm):24.6.
IR (KBr) (ν_{max}/cm^{-1}): 3520 (br), 3223 (vs), 3069 (m), 3026, 2956 (m, br), 2870 (m), 1912, 1591 (vs), 1484, 1435 (s, br), 1410 (s, br), 1376 (m, br), 1326 (s, br), 1282 (s, br), 1246 (s, br), 1188 (s), 1121 (s), 1085 (s, br), 1044 (m), 1012 (s), 971 (m), 868 (m), 810 (s), 766 (s, br), 728 (m), 662 (s), 614 (m), 512, 477, 450 (s).
Elemental Anal. Calc. (%) for **33**, $C_{23}H_{23}B_3Cl_3NO_3$: C, 55.2; H, 4.6; N, 2.8. Found (%): C, 55.1; H, 4.6; N, 2.8.
p-XRD: d spacing/Å (% rel. int.): 3.54 (100), 3.55 (70.21), 3.67 (39.01), 3.68 (38.59), 3.95 (33.93), 3.18 (30.27).
Mp: 127 – 130 °C.

2.8.10 Preparation of tri(*p*-chlorophenyl)boroxine·TEPO complex [$C_6H_{15}OP$]·[CPB] (**34**)

The CPB·TEPO complex (**34**) was prepared *in situ* through addition of a slight excess of tri(*p*-chlorophenyl)boroxine (**24**) to an NMR sample of triethylphosphine oxide (TEPO) dissolved in $CDCl_3$ (1 mL).

NMR (400 MHz, $CDCl_3$) δ_H (ppm): 1.15 – 1.23 (m, 9H, $3CH_3$), 1.78 – 1.87 (m, 6H, $3CH_2$), 7.35 – 7.47 (m, 6H, 6CH), 7.76 – 8.10 (m, 6H, 6CH). (101 MHz, $CDCl_3$) δ_C (ppm): 5.66 (d, ^2J = 4.7 Hz, CH_3), 18.96 (d, ^1J = 67.6 Hz, CH_2), 128.45 (CH arom.), 136.77 (CH arom.). (128 MHz, $CDCl_3$) δ_B (ppm): 29.1. (162 MHz, $CDCl_3$) δ_P (ppm): 62.0.

2.8.11 Preparation of triphenylboroxine·TEPO complex [$C_6H_{15}OP$]·[PB] (**35**)

The PB·TEPO complex (**35**) was prepared *in situ* through addition of a slight excess of triphenylboroxine (**25**) to an NMR sample of triethylphosphine oxide (TEPO) dissolved in $CDCl_3$ (1 mL).

NMR (400 MHz, $CDCl_3$) δ_H (ppm): 1.09 – 1.17 (m, 9H, CH_3), 1.72 – 1.80 (m, 6H, CH_2), 7.46 (brs, 18H, CH arom.), 8.14 (brs, 12H, CH arom.). (101 MHz, $CDCl_3$) δ_C (ppm): 5.52 (d, ^2J = 5.1 Hz, CH_3), 18.69 (d, ^1J = 66.7 Hz, CH_2), 127.63 (CH arom.), 130.83 (CH arom.), 134.59 (CH arom.). (128 MHz, $CDCl_3$) δ_B (ppm): 25.8. (162 MHz, $CDCl_3$) δ_P (ppm): 61.7.

2.8.12 Preparation of tris(pentafluorophenyl)boroxine·TEPO complex [$C_6H_{15}OP$]·[FPB] (**36**)

The FPB·TEPO complex (**36**) was prepared *in situ* through addition of a slight excess of triphenylboroxine (**26**) to an NMR sample of triethylphosphine oxide (TEPO) dissolved in THF (1 mL).

NMR (400 MHz, THF) δ_H (ppm): 1.56 – 1.63 (m, 9H, $3CH_3$), 3.42 – 3.45 (m, 6H, $3CH_2$). (376 MHz, THF) δ_F (ppm): -133.85 (m, 6F), -156.83 (brs, 3F), -165.50 (m, 6F). (128 MHz, THF) δ_B (ppm): 18.1. (162 MHz, THF) δ_P (ppm): 71.5.

Chapter 3:

Synthesis and characterization of polyborate salts

The work presented within this chapter has been published in the following journal articles:
M.A. Beckett, S.J. Coles, R.A. Davies, P.N. Horton and C.L. Jones, *Dalton Trans.*, 2015, **44**, 7032-7040.
C. L. Jones, M. A. Beckett, S. J. Coles, R. A. Davies and P. N. Horton, *Phosphorus, Sulfur Silicon Relat. Elem.,* 2016, **191**, 628-630

3.1 Introduction

Salts containing polyborate anions have attracted recent attention due to their possible applications as luminescent,[91,108], ferroelectric,[103] flame retardant[238] and second harmonic generation non-linear optical materials.[61,94] Due to their potential as porous materials, polyborate salts have also shown applications as potential hydrogen stores.[123]

Polyborate salts are readily prepared from the reaction of boric acid with either a metal salt or an organic base in aqueous solution,[40,44,66,98] although polyborate salts have also been prepared under solvothermal conditions.[24,53,63,87,239] Many of the polyborate salts contain the pentaborate anion, $[B_5O_6(OH)_4]^-$, however, there have also been reports of rarer anions containing three,[21,54] four,[50,55,83] seven,[23,42,43] eight,[15] nine,[17,44] fourteen[20] and fifteen[38] B atoms. In basic aqueous solution, boric acid forms a dynamic combinatorial library[121] (DCL) of polyborate anions, whose concentrations are pH and boron concentration dependent.[240] Almost all of the naturally-occurring polyborate salts contain metal counter cations; *ammonioborite* is an exception to this and contains not only an organic (non-metal) cation, but also the elusive pentadecaborate anion, $[B_{15}O_{20}(OH)_8]^{3-}$, which has only been observed in this solid-state structure. Larger anion types are rare, and have been observed in solid-state structures which contain organic (non-metal) cations.

3.2 Aims of chapter

The aim of the work presented in this chapter was to synthesise and investigate the solid-state structures and thermal properties of novel polyborate salts containing organic (non-metal) cations; the use of organic (non-metal) cations may lead to previously unobserved structures.

The first part of the synthetic work comprises polyborate salts containing smaller, discrete cations and the latter part of the work incorporated larger cations in to the solid-state structures to observe their structure-directing effect. All of the synthesized compounds were fully characterized, and *ca*. 20 new polyborate salt structures are reported within this chapter.

3.3 Results and discussion

3.3.1 Substituted pyrrolidinium pentaborate salts

3.3.1.1 Synthesis and characterization of substituted pyrrolidinium pentaborate salts

The pyrrolidinium pentaborate salts were all prepared in high yields in methanol/deionised water solution from the reaction of the free base (for salts containing **1**, **2**, **4** – **6**) or the quaternary amine hydroxide salt (for salts containing **3**) with boric acid in a 1:5 molar ratio (Equations 3.1 – 3.6). The structures of the organic cations and the pentaborate anions found in salts containing **1**-**6** are shown in Figure 3.1.

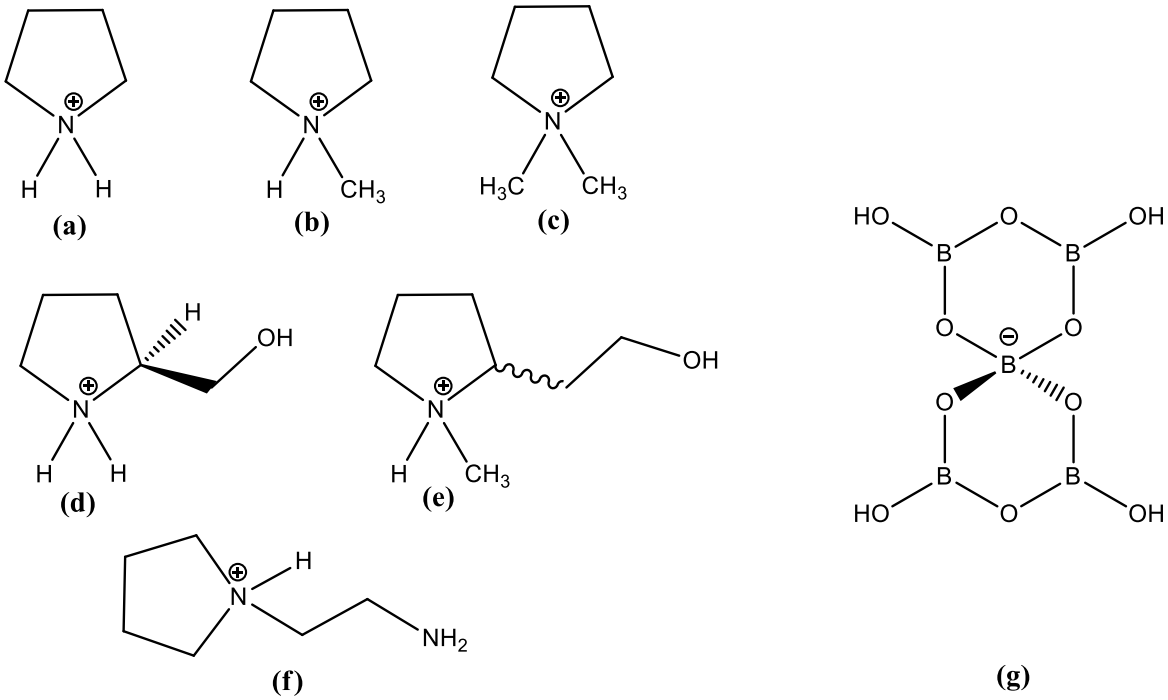

Figure 3.1: The pyrrolidinium cations and (g) pentaborate anion, $[B_5O_6(OH)_4]^-$, as found in (a) $[C_4H_8NH_2][B_5O_6(OH)_4]$ (1), (b) $[C_4H_8NMeH][B_5O_6(OH)_4]\cdot 1.5H_2O$ (2$\cdot 1.5H_2O$) and $[C_4H_8NMeH][B_5O_6(OH)_4]\cdot ½CH_3COCH_3$ (2$\cdot ½CH_3COCH_3$); (c) $[C_4H_8NMe_2][B_5O_6(OH)_4]\cdot ½H_2O$ (3$\cdot ½H_2O$) and $[C_4H_8NMe_2][B_5O_6(OH)_4]$ (3), (d) $[(2\text{-}CH_2OH)\text{-}C_4H_7NH_2][B_5O_6(OH)_4]\cdot ½H_2O$ (4$\cdot ½H_2O$), (e) $[(2\text{-}CH_2CH_2OH)C_4H_7NMeH][B_5O_6(OH)_4]\cdot 0.3H_2O$ (5$\cdot 0.3H_2O$) and (f) $[C_6H_{15}N_2][B_5O_6(OH)_4]$ (6).

$$\textit{cyclo}\text{-}C_4H_8NH + 5B(OH)_3$$

$$\rightarrow [\textit{cyclo}\text{-}C_4H_8NH_2][B_5O_6(OH)_4]\ (\mathbf{1}) + 5H_2O \qquad (3.1)$$

cyclo-$C_4H_8NMe + 5B(OH)_3$

$\rightarrow$ [*cyclo*-$C_4H_8NMeH][B_5O_6(OH)_4]\cdot 1.5H_2O$ (**2**$\cdot 1.5H_2O$) + $3.5H_2O$ (3.2)

[*cyclo*-$C_4H_8NMe_2][OH] + 5B(OH)_3$

$\rightarrow$ [*cyclo*-$C_4H_8NMe_2][B_5O_6(OH)_4]$ (**3**) + $5H_2O$ (3.3)

2-$HOCH_2$-*cyclo*-$C_4H_7NH + 5B(OH)_3$

$\rightarrow$ [2-$HOCH_2$-*cyclo*-$C_4H_7NH_2][B_5O_6(OH)_4].½H_2O$ (**4**$\cdot ½H_2O$) + $4½H_2O$ (3.4)

2-CH_2CH_2OH-*cyclo*-$C_4H_7NMe + 5B(OH)_3$

$\rightarrow$ [2-CH_2CH_2OH-*cyclo*-$C_4H_7NMeH][B_5O_6(OH)_4]\cdot 0.3H_2O$ (**5**$\cdot 0.3H_2O$) + $4.7H_2O$ (3.5)

cyclo-C_4H_8N-($CH_2CH_2NH_2$)- + $5B(OH)_3$

$\rightarrow$ [*cyclo*-C_4H_8NH-($CH_2CH_2NH_2$)][$B_5O_6(OH)_4$] (**6**) + $5H_2O$ (3.6)

Pentaborate salts **1** – **6** were characterized by elemental analysis, NMR and IR spectroscopy, X-ray diffraction and thermal analysis. The solid-state structures of pentaborate salts containing **1 – 5** were confirmed by single-crystal XRD studies and are discussed in more detail later in this chapter. Elemental analysis data were in good agreement with theoretical values, with the crude materials of compounds **2** – **5** found to contain additional interstitial water molecules within the salts' compositions.

Spectroscopic measurements of salts containing **1** – **6**were in agreement with previously reported non-metal cation pentaborate salts. ^{11}B NMR spectra of moderately concentrated aqueous solutions (obtained in D_2O) displayed the three

characteristic signals at ~18, 13 and 1 ppm, which are assigned to the $B(OH)_3/[B(OH)_4]^-$, $[B_3O_3(OH)_4]^-$ and the 4-coordinate centre of $[B_5O_6(OH)_4]^-$, respectively.[8] These species are observed due to the complex borate equilibria present in aqueous solution.[16,240] The $[B_3O_3(OH)_4]^-$ ion undergoes a rapid exchange to equalise all three boron sites[241] which results in the broad signal observed. The average boron environment within the triborate anion is 67% trigonal, and likewise the chemical shift is approximately one-third of the distance from $B(OH)_3$ (19.5 ppm) to $[B(OH)_4]^-$ (2.5 ppm). The pentaborate anion, at ~1 ppm, has a narrower line width and is only ~1 ppm upfield of $[B(OH)_4]^-$. From these observations, Salentine concluded that the pentaborate anion does not undergo a rapid exchange of all five boron atoms on the NMR time scale.[16]

^{11}B NMR spectra obtained in very dilute concentrations can also give some diagnostic information of the species present in aqueous solution. Under these dilute conditions, the formation of polyborate species is suppressed and instead a single peak is observed due to the equilibrium of the monoborate species, $B(OH)_3/[B(OH)_4]^-$; the observed chemical shift is dependent upon the relative proportions of trigonal (B_{trig}) and tetrahedral (B_{tet}) boron present in solution[13] and can be determined using Equation 3.7, where $\delta(B(OH)_3)$ and $\delta[B(OH)_4]^-$ are +19.5 and +2.5 ppm, respectively. In addition to this, the total boron/charge ratio (B/1) can be determined using Equation 3.8, which may be useful in helping to formulate polyborate products of unknown composition.

$$\delta_{calc} = \delta[B(OH)_4]^- + \{[B_{trig}]/[B_{tet}+B_{trig}]\} \times (\delta B(OH)_3 - \delta[B(OH)_4]^-) \quad (3.7)$$

$$B/1 = -17.0/(\delta_{obs} - 19.5) \quad (3.8)$$

Utilising Equations 3.7 and 3.8, a pentaborate salt in very dilute aqueous solution would therefore exhibit a single peak at +16.1 ppm, which was found to be the case for salts containing **1** – **6**, and gives a B/1 ratio of 5.0/1.

^1H and ^{13}C spectra (obtained in D_2O) were fully consistent with those expected for the pyrrolidinium cations, with the NH (**1**, **2**·1.5H_2O, **2**·½CH_3COCH_3,

4·½H_2O, **5**·0.3H_2O and **6**), OH (**4**·½H_2O, **5**·0.3H_2O) and BOH protons overlapping as represented by a broad singlet at ~4.8 ppm due to rapid exchange.

IR spectra of salts containing **1** – **6** were obtained as KBr disks and all clearly show the diagnostic band of pentaborate salts at ~925 cm^{-1}.[67,242] The symmetric and asymmetric stretching of the three coordinate ($B_{(3)}$–O) and four coordinate ($B_{(4)}$–O) bonds are summarised in Table 3.1, and are consistent with observed $B_{(3)}$-O and $B_{(4)}$-O bonds found in other pentaborate salts.[242] The symmetric and asymmetric stretching of the $B_{(3)}$–O and $B_{(4)}$–O bonds observed in the synthesised polyborates were assigned based on the observations made by Li *et al.*[242] who investigated a number of polyborate salts using infrared and Raman spectroscopic methods. Broad peaks were observed (3400 – 3050 cm^{-1}) in all pyrrolidinium pentaborate salts which arise from the OH and NH groups.

Table 3.1: The observed symmetric and asymmetric stretches of the $B_{(3)}$-O and $B_{(4)}$-O bonds found in pentaborate salts 1-6.

Compound	ν_{as} $B_{(3)}$-O	ν_{as} $B_{(4)}$-O	ν_{s} $B_{(3)}$-O	ν_{s} $B_{(4)}$-O
1	1425, 1320	1120, 1017	923	777
2·1.5H_2O **2**·½CH_3COCH_3	1394, 1311	1140, 1018	921	775
3·½H_2O **3**	1415, 1309	1148, 1018	913	772
4·½H_2O	1423, 1313	1149, 1027	923	774
5·0.3H_2O	1432, 1315	1137, 1027	923	776
6	1397, 1314	1147, 1031	925	774

Powder XRD analysis of salts containing **1** – **6** indicated that all of these salts were crystalline materials. The recrystallization of **2**·1.5H_2O from acetone/deionised water yielded a solvated species **2**.½CH_3COCH_3 (confirmed by single-crystal XRD studies – see Sections 3.3.1.3 – 3.3.1.7) with consistent analytical and spectroscopic data. Recrystallization of **3**.½H_2O from acetone/deionised water yielded the salt **3** without any interstitial solvent molecules, which was again

confirmed by single-crystal XRD studies. Recrystallization of **4**·½H_2O and **5**·0.3H_2O from ethanol/deionised water yielded the solvated salts containing ½H_2O and 0.3H_2O, respectively. Single crystals of **6** were not obtained, even after prolonged periods of slow evaporation of solvent.

Compound **4**·½H_2O crystallizes in a non-centrosymmetric space group (see below) and it was of interest to determine whether it displayed non-linear optical (NLO) properties. Its second harmonic generation (SHG) properties were determined by the powder method by Prof. Das' group in Bangalore who reported a value of *ca*. 20% of the standard KH_2PO_4. Thus **4**·½H_2O does show weak SHG properties.

The pentaborate salts **1, 2**·1.5H_2O and **3**·½H_2O were also prepared under solvothermal conditions, in varying $B(OH)_3$:amine ratios, but each time yielded the pentaborate salts as described above. The solvothermal method yielded crystals suitable for single-crystal XRD studies in greater quantities than obtained through slow evaporation of the solvent.

The synthesis of two further substituted pyrrolidinium pentaborate salts was attempted, using 1-pyrrolidinocyclopentene and 1-pyrrolidinoyclohexene as the bases. The reactions were performed at room temperature in 1:1 methanol/deionised water in a 1:5 molar ratio with $B(OH)_3$. The resulting solids were analysed using IR and NMR and were found to be identical to the spectroscopic data found for **1**. It is believed that the enamines were fully hydrolysed to give the pyrrolidinium pentaborate salts and the remaining cyclic ketone by-products were consequently removed, along with the reaction solvents, under vacuum.

3.3.1.2 Thermal properties of substituted pyrrolidinium salts

The thermal properties of the non-metal pentaborate salts containing **1** – **6** were investigated, in air, by thermogravimetric analysis (TGA) and differential scanning calorimetry (DSC) analysis. Studies of other non-metal pentaborates in the literature have shown that they usually dehydrate *via* an endothermic process at temperatures up to 250°C, resulting in anhydrous non-metal cation pentaborate salts.[49,65,243] At higher temperatures the cation is oxidised *via* exothermic processes, followed by

the presence of an intumesced material which upon further oxidation leaves a glassy residue of solid B_2O_3.[66] B_2O_3 is also observed as the residual product if the TGA/DSC is conducted under an inert atmosphere (N_2/Ar).[24,25] The pyrrolidinium pentaborate salts containing **1** – **6** all followed this decomposition pattern, illustrated for **1** in Figure 3.2, with observed dehydration and residual masses of B_2O_3 being consistent with calculated values (see Chapter 2).

For those compounds containing interstitial solvent molecules (**2**·1.5H_2O, **3**·½H_2O, **4**·½H_2O, **5**·0.3H_2O) an additional dehydration step was observed ~100°C, where the loss of these molecules occurs. TGA-DSC analysis was not performed on **2**·½CH_3COCH_3 due to insufficient sample quantity. The step at ~200-250°C occurs from the condensation of the polyborate anions, which forms B-O-B crosslinks.[66] The decomposition of the pentaborates in air can be defined by Equations 3.9 and 3.10.

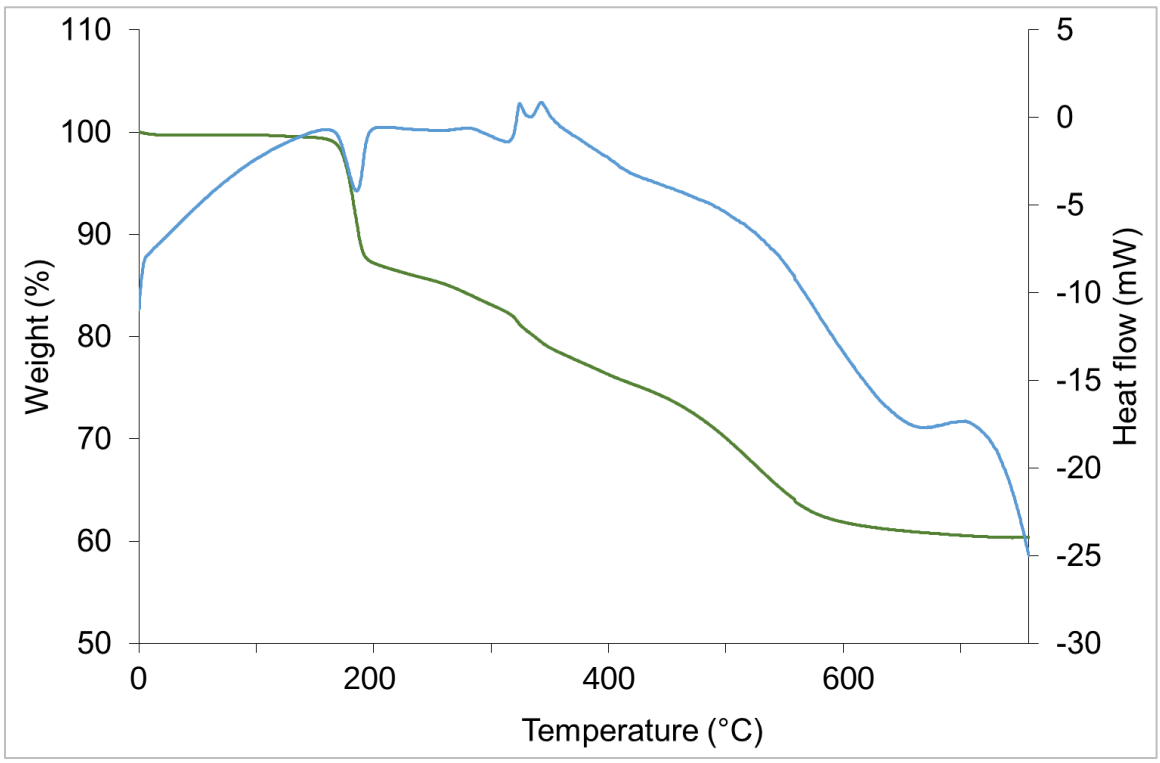

Figure 3.2: TGA (green) and DSC (blue) curve of pyrrolidinium pentaborate (1) showing the dehydration step at ~200°C, followed by oxidation of the cation to leave residual B_2O_3 >700°C.

$$[NMC][B_5O_6(OH)_4] \rightarrow [NMC][B_5O_8] + 2H_2O \quad (3.9)$$

$$[NMC][B_5O_8] + \text{excess } O_2 \rightarrow 2.5B_2O_3 + \text{volatile oxidation products} \quad (3.10)$$

The porosity of compounds **1** and **3**·½H_2O were determined using Brunauer-Emmett-Teller theory to measure their specific surface areas. The samples were each prepared separately, by calcining in air at 250°C, 500°C and 750°C for 24 hours, in order to obtain significant quantities of the anhydrous, intumesced and residual materials. The analysis was conducted by Dr Simon Curling, who is gratefully acknowledged for his assistance. The results of the BET analysis of the 6 calcined materials showed that they were all non-porous, with specific surface areas of <1.0 $m^2\ g^{-1}$, which is similar to BET analysis of other NMC pentaborates.[66]

3.3.1.3 Crystallographic studies of substituted pyrrolidinium pentaborate salts.

The crystal structures of pyrrolidinium pentaborate (**1**), *N*-methylpyrrolidinium pentaborate·½ acetone (**2**·½CH_3COCH_3), *N*,*N*-dimethylpyrrolidinium pentaborate (**3**), 2-hydroxymethylpyrrolidinium pentaborate hemihydrate (**4**·½H_2O), (2-hydroxyethyl)-*N*-methylpyrrolidinium pentaborate·0.3 hydrate (**5**·0.3H_2O) are reported in this section. The spectroscopic and analytical data for the recrystallized products are given in Chapter 2, Sections 2.5.1 – 2.5.5. The crystal structure data were obtained and solved by the National Crystallographic Service at Southampton and the full crystallographic data is available in the appendices with NCS numbers 2012NCS0162 (**1**), 2012NCS0960 (**2**·½CH_3COCH_3), 2013NCS0027 (**3**), 2014NCS0729 (**4**·½H_2O) and 2014NCS0787 (**5**·0.3H_2O).

The structures of **1**, **2**·½CH_3COCH_3, **3** and **4**·½H_2O are free from disorder and are characterized by having discrete (substituted) pyrrolidinium cations and pentaborate anions. The structure of **5**·0.3H_2O was found to have a disordered cation; this was disordered over multiple sites with three significant positions of occupancy identified (4:3:3 ratio), one of which also included a solvated water molecule. All of the cationic pyrrolidinium rings adopt an envelope conformation, including all disordered versions found in **5**·0.3H_2O. Diagrams of the cations and anions present, along with their associated numbering schemes are shown in Figures 3.3, 3.4, 3.5, 3.6 and 3.7 for **1**, **2**·½CH_3COCH_3, **3**, **4**·½H_2O and **5**·0.3H_2O, respectively.

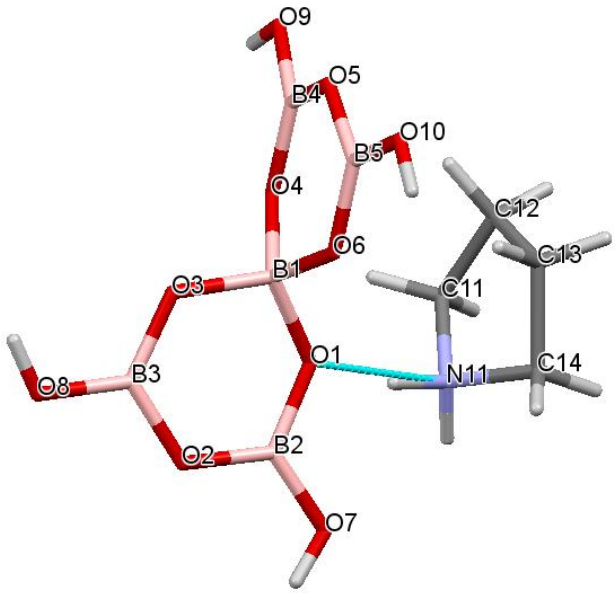

Figure 3.3: The molecular structure of pyrrolidinium pentaborate (1), illustrating the atomic numbering scheme. Hydrogen bonding between the anion and cation is shown in blue.

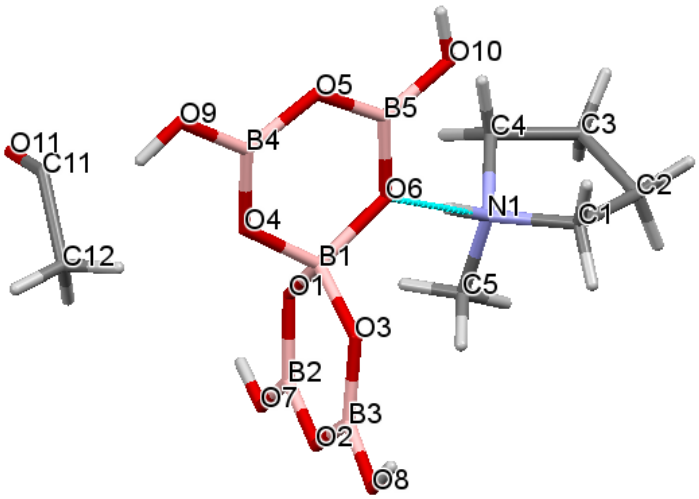

Figure 3.4: The molecular structure of *N*-methylpyrrolidinium pentaborate·½ acetone (2·½CH_3COCH_3), illustrating the atomic numbering scheme. Hydrogen bonding between the anion and cation is shown in blue.

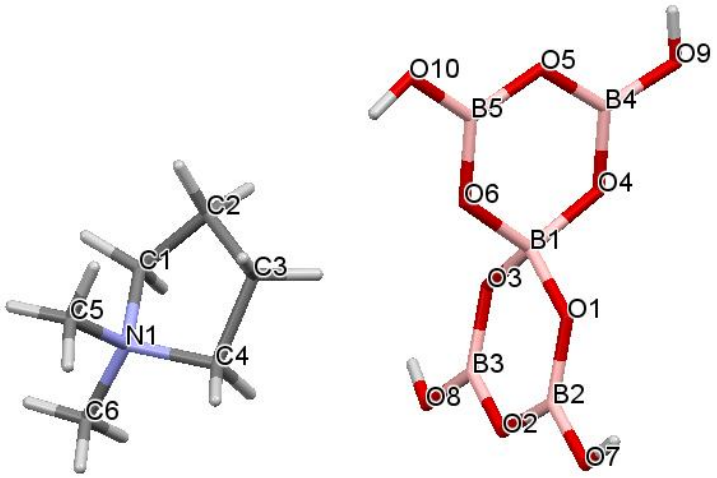

Figure 3.5: The molecular structure of *N*,*N*-methylpyrrolidinium pentaborate (3), illustrating the atomic numbering scheme. There is no H-bonding between the anion and cation in this molecule.

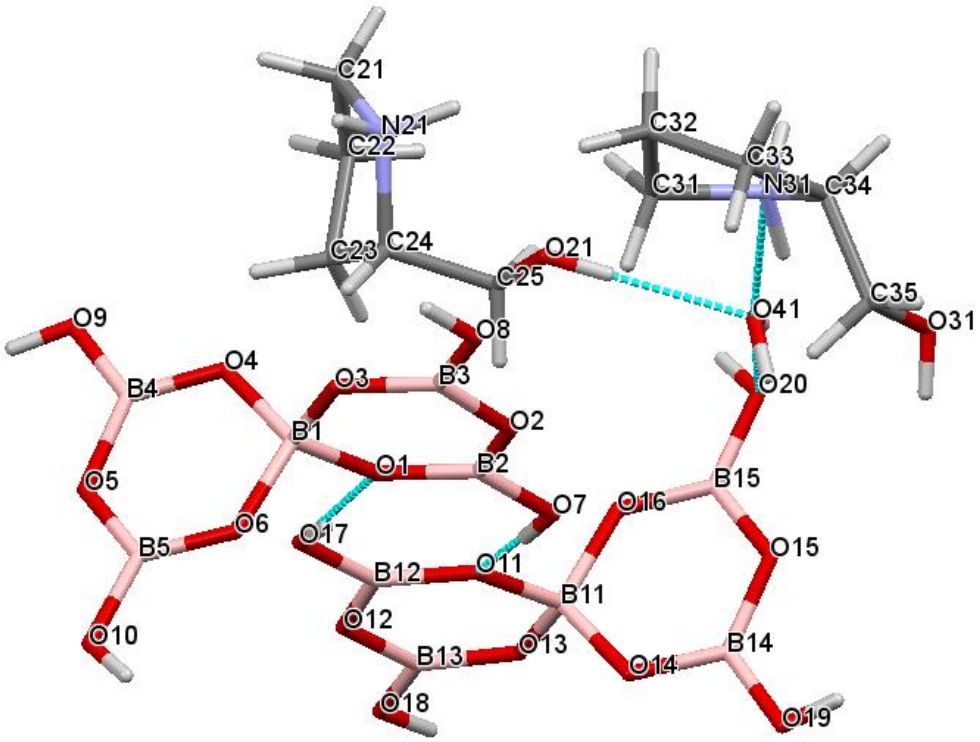

Figure 3.6: The molecular structure of 2-hydroxymethylpyrrolidinium pentaborate hemihydrate (4·½H_2O), illustrating the atomic numbering scheme. Intermolecular H-bonding is shown in blue.

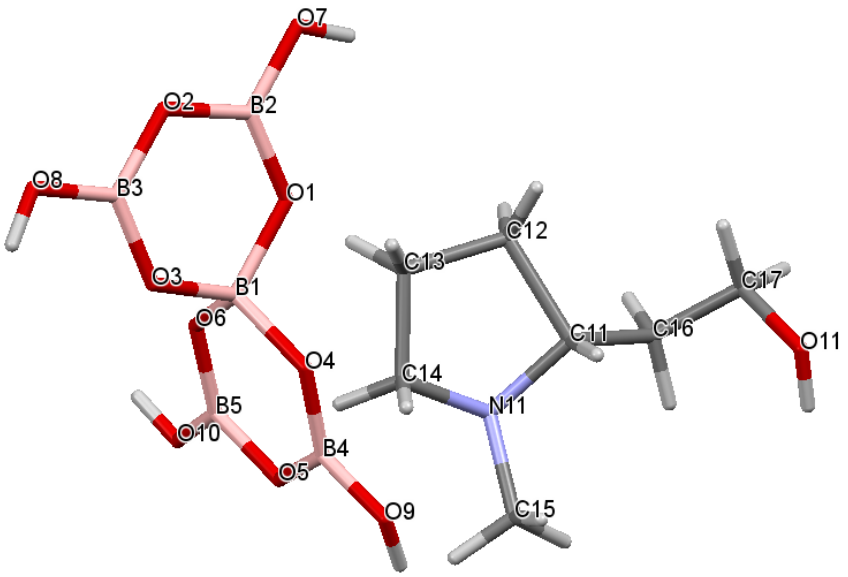

Figure 3.7: The molecular structure of (2-hydroxyethyl)-*N*-methylpyrrolidinium pentaborate, as found in 5·0.3H_2O, illustrating the atomic numbering scheme. For simplicity, the cation's disorder is not shown in this diagram.

Compounds **1**, **3** and **5**·0.3H_2O contain only one cation and one anion per asymmetric unit, with no interstitial solvent molecules present. Compound **2**·½CH_3COCH_3 was found to contain ½ a molecule of acetone per asymmetric unit, which has does not H-bond to either cation or anion. In contrast to this, compound **4**·½H_2O contains two independent cations and anions per unit cell, as well as a water molecule which plays a role in H-bonding. The bond lengths and internuclear angles observed within the pentaborate anions' boroxole (B_3O_3) rings of compounds **1**, **2**·½CH_3COCH_3, **3**, **4**·½H_2O and **5**·0.3H_2O are within the ranges observed for previously reported non-metal cation pentaborate structures;[12,65,66,94,243] the observed bond lengths and internuclear angles are given in Table 3.2. These bond lengths and internuclear angles are also within ranges found in related boroxole (B_3O_3) structures which also contain both 4- and 3-coordinate boron centres bound to oxygen,[244-246] including the crystal structures of the triorganoboroxine complexes reported in Chapter 5.

Table 3.2: The B-O bond lengths (Å) and internuclear angles (°) for pentaborate anions found in compounds containing 1-5.

Compound	B_{tet} bond lengths (Å)	B_{tet} internuclear angles (°)	B_{trig} bond lengths (Å)	B_{trig} internuclear angles (°)
1	1.456(2) – 1.481(2)	107.86(13) – 109.50(13)	1.347(2) – 1.390(2)	116.95(15) – 122.69(16)
2·½CH_3COCH_3	1.4666(12) – 1.4755(12)	107.53(7) – 111.25(8)	1.3556(12) – 1.3862(13)	117.29(9) – 121.84(9)
3	1.452(2) – 1.4889(19)	108.14(13) – 111.94(13)	1.359(2) – 1.388(2)	116.34(13) – 122.66(14)
4·½H_2O[a]	1.459(3) – 1.480(3), 1.453(3) – 1.480(3)	108.14(18) – 110.72(18), 108.08(18) – 111.13(19)	1.352(3) – 1.386(3), 1.353(3) – 1.386(3)	116.5(2) – 122.8(2), 116.9(2) – 123.4(2)
5·0.3H_2O	1.462(3) – 1.472(3)	108.50(17) – 111.11(17)	1.349(3) – 1.389(3)	116.5(2) – 123.5(2)

[a]Compound **4** contains two independent pentaborate anions within its unit cell.

The solid-state structures of salts containing **1** - **5** all possess giant anionic lattices held together by H-bonds, with cations and any co-crystallized species situated within the 'cavities' of the lattice. The structures of **1** and **3** both crystallize in the same space group, with triclinic unit cells and have very similar supramolecular structures (Figures 3.8 and 3.9). The unsubstituted pyrrolidinium cation in **1** is small (formula unit volume = 328.54 $Å^3$) and able to partake in H-bonding interactions, whereas the dimethylated cation in **3** is larger and unable to partake in H-bonding. In order to accommodate the larger cation in **3**, the unit cell is expanded by 13.3% (formula unit volume = 372.35 $Å^3$). The anion-anion H-bond interactions observed in both of these structures may be described[15,66,107] as 'brickwall', with each pentaborate part of a (β-acceptor site) C(8) chain and 3 reciprocal pair (α acceptor site) $R_2^2(8)$ interactions.

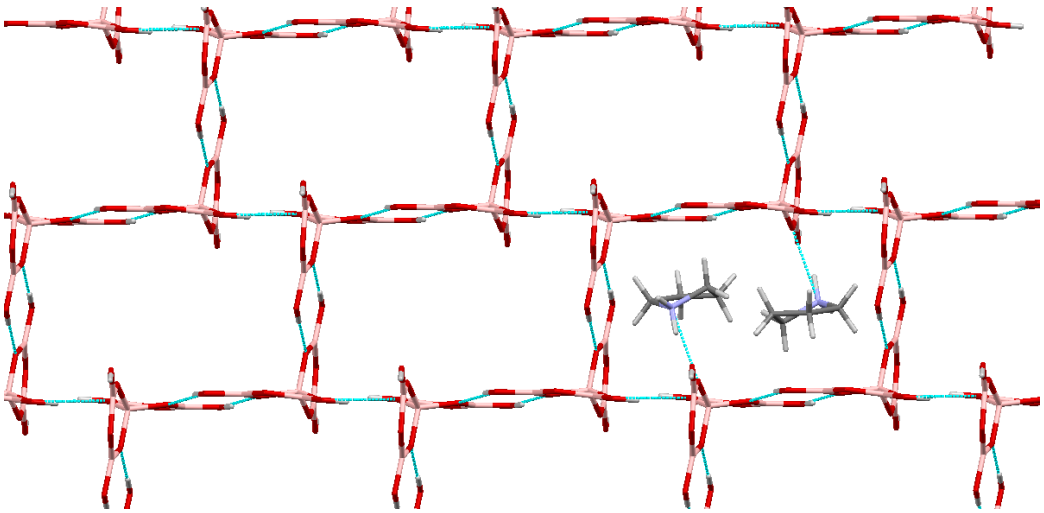

Figure 3.8: The H-bonded anionic lattice of 1. The cations are H-bonded to the anionic lattice and sit within the 'cavities' of the lattice. H-bonds are shown in blue.

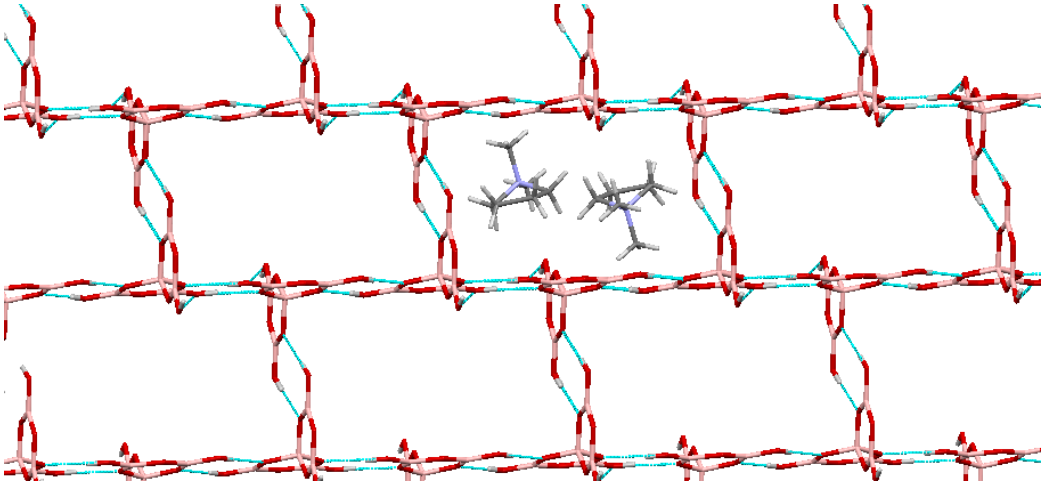

Figure 3.9: The H-bonded anionic lattice of 3; note its similarity to 1. The cations do not partake in H-bonding and simply sit within the 'cavities' of the lattice. Anion-anion H-bond interactions are shown in blue.

The unsubstituted pyrrolidinium cation in **1** partakes in H-bonding to both an α (O1) and a β (O8) acceptor site on the pentaborate anions. Details of the H-bond interactions found within the solid-state structures of all of the (substituted) pyrrolidinium pentaborate salts are shown in Table 3.3.

Table 3.3: The H-bonding interactions found within the solid-state structures of the (substituted) pyrrolidinium pentaborate salts containing 1-5.

Compound	*D*-H···A	*d*(H···A) (Å)	*d*(D···A) (Å)	∠DHA (°)
1	O7–H7···O9	1.93	2.7708(17)	173.7
	O8-H8···O3	1.86	2.6940(17)	176.5
	O9-H9···O4	1.85	2.6753(17)	168.5
	O10-H10···O6	1.88	2.7081(17)	171.0
	N11-H11C···O8	2.11	2.925(2)	146.9
	N11-H11D···O1	1.91	2.8016(19)	162.7
2.½CH_3COCH_3	O7-H7···O3	1.88	2.7200(10)	173.4
	O8-H8···O1	1.95	2.7912(10)	174.4
	O9-H9···O4	1.96	2.7974(11)	172.6
	O10-H10···O8	2.04	2.8274(11)	155.7
	N1-H1···O6	1.88	2.7974(11)	170.7
3	O7-H7···O1	1.86	2.6933(18)	172.5
	O8-H8···O3	1.87	2.702(2)	171.4
	O9-H9···O8	1.94	2.746(2)	159.6
	O10-H10···O6	1.93	2.763(2)	170.7
	C1-H1B···O4	2.60	3.495(2)	149.6
4·½H_2O	O7-H7···O11	1.86	2.688(2)	171.1
	O8-H8···O13	1.88	2.712(2)	169.2
	O9-H9···O7	1.91	2.701(2)	156.4
	O10-H10···O16	1.88	2.717(2)	175.0
	O17-H17···O1	1.84	2.680(2)	172.2
	O18-H18···O3	1.86	2.698(2)	175.0
	O19-H19···O17	1.96	2.736(2)	153.4
	O20-H20···O6	1.91	2.750(2)	174.1
	N21-H21A···O31	1.93	2.853(3)	154.7
	N21-H21B···O12	2.11	3.018(3)	152.3
	O21-H21···O41	1.97	2.807(3)	179.5
	N31-H31C···O14	1.83	2.791(3)	162.7
	N31-H31D···O41	2.18	3.018(3)	140.8
	O31-H31···O4	1.87	2.704(2)	170.0
	O41-H41A···O9	1.92	2.748(2)	159.0
	O41-H41B···O20	2.11	2.940(3)	158.8

Compound	*D*-H···A	*d*(H···A) (Å)	*d*(D···A) (Å)	∠DHA (°)
5·0.3H_2O	O7-H7···O3	1.84	2.678(2)	173.3
	O8-H8···O1	1.86	2.703(2)	177.5
	O9-H9···O5	1.93	2.764(2)	171.2
	O10-H10···O6	1.87	2.709(2)	175.5
	N11-H11A···O4	2.00	2.960(6)	160.6
	N11-H11A···O9	2.31	3.080(6)	133.0
	O11-H11B···O8	2.12	2.904(6)	155.6
	N21-H21A···O4	2.03	2.959(11)	153.9
	N21-H21A···O9	2.26	2.996(11)	128.9
	O21-H21B···O7	1.95	2.771(8)	164.3
	N31-H31A···O41	2.13	3.09(3)	161.3
	O41-H41B···O5	2.34	2.834(9)	117.3

N-H and O-H bond lengths were fixed at 0.99 Å and 0.84 Å, respectively.

Compound **2**·½CH_3COCH_3 also has a 'brickwall' structure from the α,α,α.β pentaborate acceptor site configuration. The repetitive motifs found within this structure are the $R_2^2(8)$ and C(8) chain H-bond interactions. In order to visualise these interactions clearly, they are illustrated in Figure 3.10; the three $R_2^2(8)$ α-acceptor sites are interactions within the plane of the lattice, whereas the β-acceptor site C(8) chain comes out of the plane. Unlike **1** and **3**, the anionic planes which are joined together by the C(8) chains are not superimposed, resulting in a 'staggered' brickwall structure (Figure 3.11). In addition to the anion-anion H-bond interactions observed in **2**·½CH_3COCH_3, there is also a cation-anion H-bond interaction (NH···O) to an α-acceptor site (O6); the co-crystallized acetone molecule simply fills the space within the 'cavity' of the anionic lattice and is not involved in any H-bond interactions. When taking in to account the different *Z* numbers, the volume of **2**·½CH_3COCH_3 is only 1.3% smaller than **3**, at 367.81 $Å^3$.

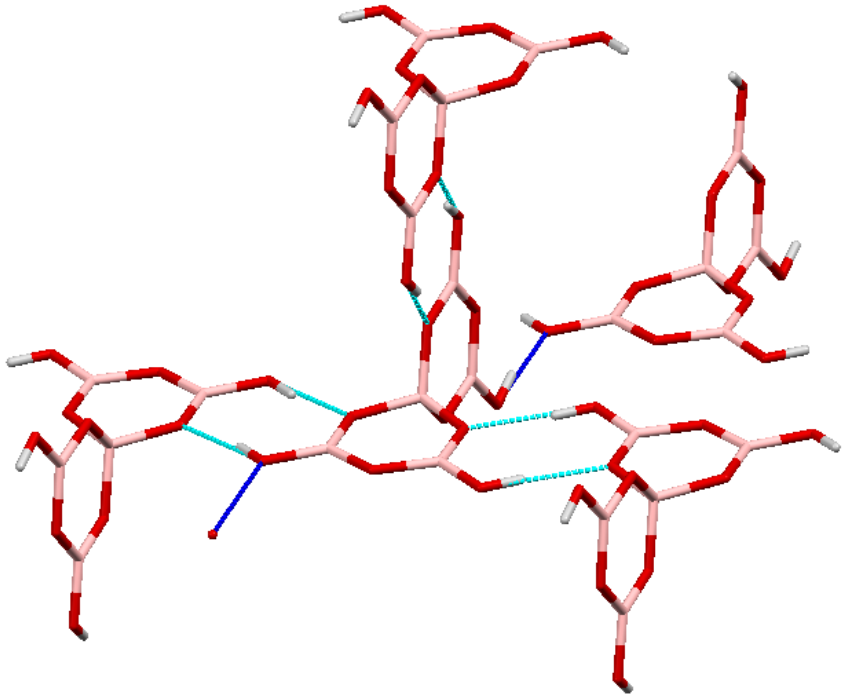

Figure 3.10: Illustration of the α,α,α,β configuration observed in the pentaborate anionic lattices: the three $R_2^2(8)$ α-acceptor H-bond interactions (light blue) between anions are in the plane; the C(8) β-chain is H-bonded out of the plane (dark blue).

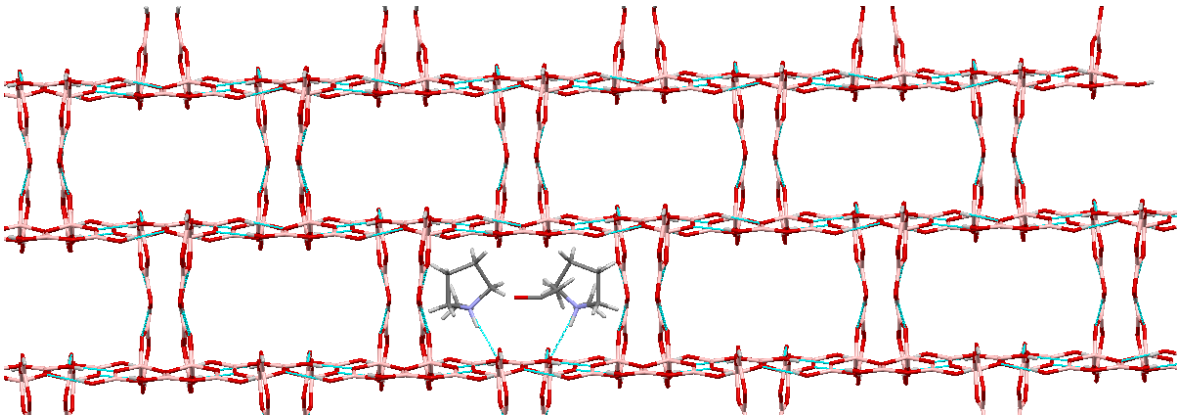

Figure 3.11: The H-bonded anionic lattice of 2·½CH_3COCH_3; the cations partake in H-bonding and simply sit within the 'cavities' of the lattice along with the ½ acetone molecule. H-bond interactions are shown in blue. Unlike compounds 1 and 3, the C(8) chains are slightly off-set, causing a 'staggered' brickwall effect instead of superimposing each plane of anions.

The solid-state structure of **4**·½H_2O is closely related to the 'brickwall' structure in that each pentaborate forms 3 reciprocal pair $R_2^2(8)$ (α-acceptor sites) and one C(8) chain (β-acceptor site) interactions (Figure 3.12). The two independent cations each interact *via* $R_2^2(8)$ H-bonds to a β-O atom (O9) on one pentaborate anion, or to a γ-O (O12) on the other independent pentaborate anion. The co-crystallized H_2O molecule also partakes in H-bonding to β-O acceptor sites of two pentaborates (O9 and O20), as well as accepting a H-bond from the hydroxyl group of one of the cations (O21H) and from the NH group of the other cation (N31H). The volume of the formula unit is 3% smaller (362.41 $Å^3$) than that of **3**.

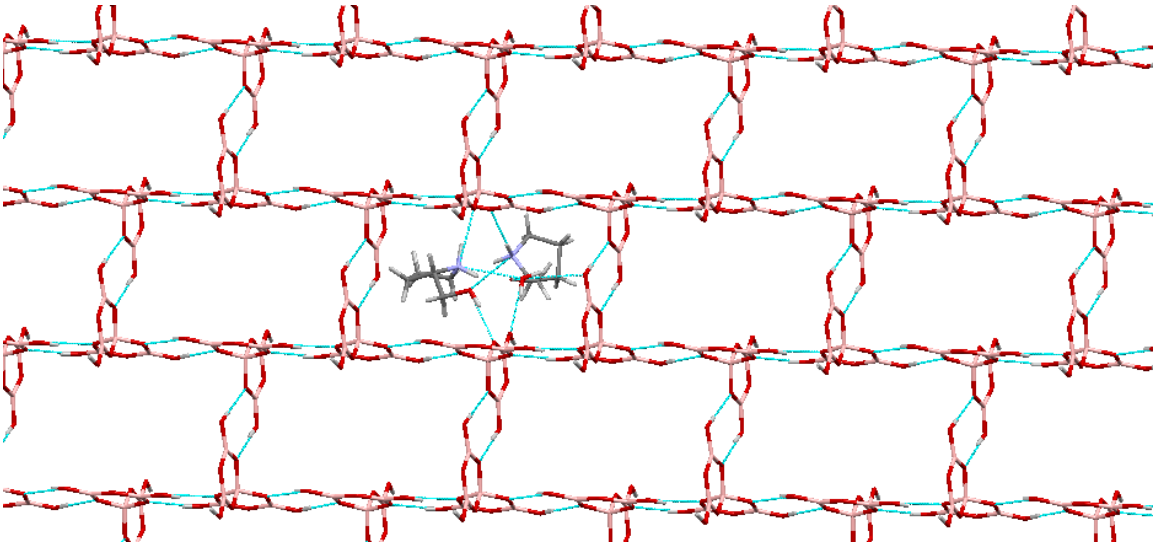

Figure 3.12: The H-bonded anionic lattice of 4·½H_2O; the cations partake in H-bonding and sit within the 'cavities' of the lattice along with the H_2O molecule, which also partakes in H-bonding between the cations and anions. H-bond interactions are shown in blue.

Compound **5**·0.3H_2O also possesses a giant anionic lattice which is held together by H-bonds, with the substituted pyrrolidinium cations and H_2O molecule sitting within the 'cavities' of the lattice. As with structures **1**, **2**·½CH_3COCH_3, **3** and **4**·½H_2O, the anions are arranged in a series of 'planes' which are H-bonded together *via* $R_2^2(8)$ reciprocal pair interactions to α,α,γ acceptor sites (Figure 3.13); the planes are further linked together not by a C(8) β-acceptor, but *via* a further $R_2^2(8)$ α-reciprocal interaction. This different arrangement of the anion-anion interactions

causes the lattice of **5**·0.3H_2O to not have the familiar 'brickwall' structure seen in **1**, **2**·½CH_3COCH_3, **3** and **4**·½H_2O.

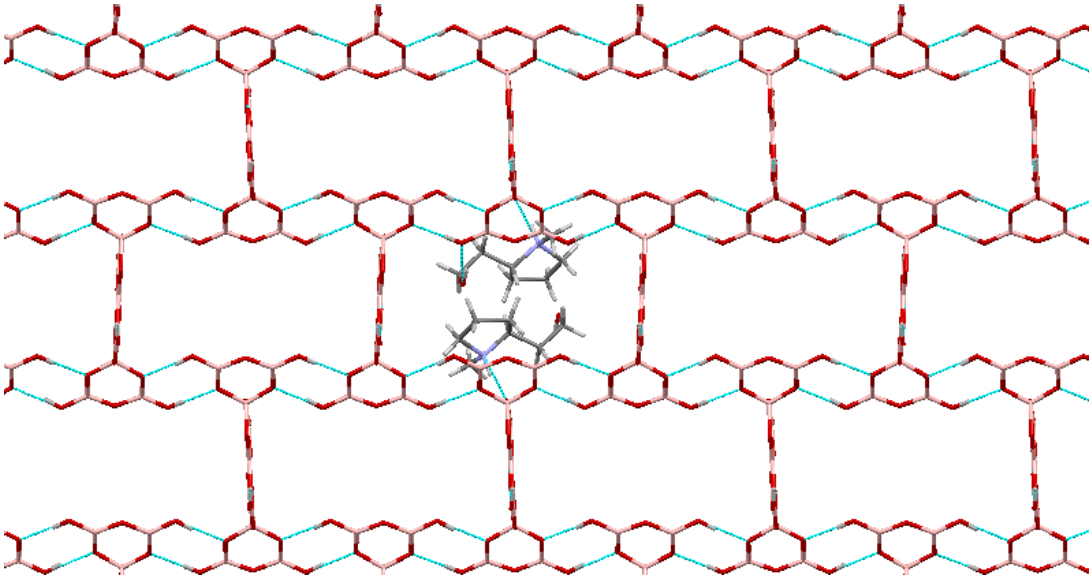

Figure 3.13: The H-bonded lattice of 5·0.3H_2O**. The larger cation results in a different configuration of H-bond interactions than in compounds 1, 2**·½CH_3COCH_3**, 3 and 4**·½H_2O **which does not take the form of the previously observed 'brickwall' structure. For simplicity, the disorder of the cation is omitted in this diagram. H-bond interactions are shown in blue.**

It is of interest to compare the structure of **5**.0.3H_2O with those of compounds **1** and **3**. The α,α,α,β configuration that leads to the 'brickwall' structure is flexible enough to accommodate cations of variable sizes up to a certain limit; for example, the *N,N*-dimethylated pyrrolidinium cation in **3** has a formula unit volume that is 13.3% larger than the unsubstituted cation in **1**, yet both of these lattices take the form of the 'brickwall' structure. The formula unit volume of **5**.0.3H_2O is increased by a further 10.3% (to 410.65 $Å^3$) compared with **3** due to the larger substituted cation; this additional increase is likely to be beyond the limit of the 'brickwall' structure and so the anions adopt a different configuration to account for the larger cation size in the form of the α,α,α,γ arrangement. In addition to the H-bonding between anionic units, there are also cation-anion H-bond interactions which may further stabilize the self-assembled crystal structure from the N11H11···O4, N11H11···O9 and O11H11B···O8.

3.3.2 Aminobenzylammonium pentaborate salts

3.3.2.1 Synthesis and characterization of aminobenzylammonium pentaborate salts

The aminobenzylammonium pentaborate salts **7** - **9** were all prepared in high yields from the reaction of $B(OH)_3$ with the free base in a 5:1 molar ratio in methanol/deionised water. The structures of the organic cations found in compounds **7** - **9** are shown in Figure 3.14.

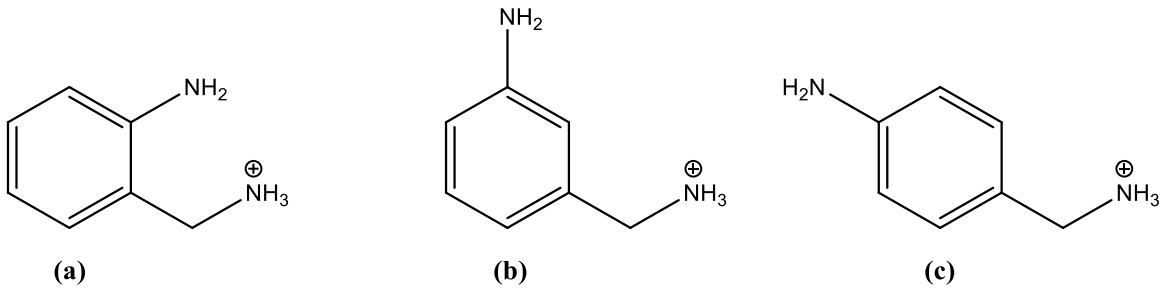

Figure 3.14: The aminobenzylammonium cations as found in (a) 2-aminobenzylammonium pentaborate, $[C_7H_{11}N][B_5O_6(OH)_4]$ (7); (b) 3-aminobenzylammonium pentaborate, $[C_7H_{11}N][B_5O_6(OH)_4]$ (8), and (c) 4-aminobenzylammonium pentaborate, $[C_7H_{11}N][B_5O_6(OH)_4]$ (9).

The pentaborate salts **7** - **9** were characterized by elemental analysis, NMR and IR spectroscopy, and thermal analysis. Powder X-ray diffraction studies indicated that pentaborates **7** and **8** were amorphous solids, however, **9** was found to be a crystalline material and a small number of single crystals of a hemihydrated salt (**9**·½H_2O) suitable for XRD studies were obtained by recrystallization of the crude product from deionised water. The elemental analyses of these compounds (**7** - **9**) were in good agreement with theoretical values, with the product from the recrystallization of **9** containing ½ a molecule of H_2O (**9**.½H_2O). This additional interstitial water molecule was confirmed by single-crystal XRD studies.

Spectroscopic measurements of **7** - **9** were, again, in agreement with previously reported non-metal cation pentaborate salts, with ^{11}B NMR spectra (obtained in D_2O) displaying the three characteristic signals at ~17, 13 and 1 ppm. The ^{1}H and ^{13}C NMR spectra (again obtained in D_2O) were fully consistent with

those expected for aminobenzylammonium cations, with the NH and BOH protons overlapping as represented by a broad singlet at ~4.8 ppm due to rapid exchange.

IR spectra of **7** - **9** were obtained as KBr disks and, as with salts **1** - **6**, clearly show the diagnostic band of pentaborate salts at ~925 cm^{-1}.[242] The symmetric and asymmetric stretching of the 3- and 4-coordinate B-O bonds are summarised in Table 3.4. Broad peaks were observed for the NH and OH bonds in the region of 3171 – 3487 cm^{-1}, as well as the peaks showing the different substituted aromatic rings in the cations (~700-800 cm^{-1}).

Table 3.4: The observed symmetric and asymmetric stretches of the $B_{(3)}$-O and $B_{(4)}$-O bonds found in pentaborates 7 - 9.

Compound	ν_{as} $B_{(3)}$-O	ν_{as} $B_{(4)}$-O	ν_{s} $B_{(3)}$-O	ν_{s} $B_{(4)}$-O
7	1432, 1362	1099, 1025	924	781
8	1421, 1312	1111, 1010	917	773
9[a]	1428, 1327	1190, 1029	919	775

[a]The IR of the recrystallized compound, **9**·½H_2O, showed identical spectroscopic properties.

Compound **9**·½H_2O crystallizes in a non-centrosymmetric space group (Section 3.3.2.3) and it was of interest to determine whether it displayed NLO properties. Its SHG properties were determined by the powder method by Prof. Das' group in Bangalore who reported a value of *ca*. 7% of the standard KH_2PO_4. Thus **9**·½H_2O does show weak SHG properties.

3.3.2.2 Thermal properties of aminobenzylammonium pentaborate salts

The thermal properties of **7** - **9** were investigated by TGA-DSC, in air, between 25 - 800°C. The analyses of the crude materials of **7** - **9** were consistent with previously observed thermal properties of non-metal cation pentaborate salts.[54] The three aminobenzylammonium pentaborate salts followed a two-step decomposition; the first step at ~200°C is the dehydration of the pentaborate anion which is shown by the DSC trace to be an endothermic process, followed by (exothermic) oxidation of the cation to leave behind residual B_2O_3 >750°C. The thermal analysis of the

recrystallized **9**·½H_2O showed an additional endothermic dehydration step at ~110°C; this percentage weight loss equated to ½ of a molecule of water, whose presence was confirmed by the elemental analysis and the single-crystal XRD studies.

3.3.2.3 Crystallographic study of 4-aminobenzylammonium pentaborate hemihydrate, **9**·½H_2O

The crystal structure of 4-aminobenzylammonium pentaborate hemihydrate (**9**·½H_2O) is reported in this section. The spectroscopic and analytical data are given in Chapter 2, Section 2.5.9. The crystal structure data was obtained and solved by the National Crystallographic Service at Southampton and the full crystallographic data is available in the appendices (NCS number 2014NCS0055).

The structure of **9**·½H_2O is free from disorder and is characterized by having a discrete aminobenzylammonium cation and a pentaborate anion, as shown in Figure 3.15.

Compound **9**·½H_2O contains two independent cations and anions per unit cell, as well as a water molecule which also plays a role in H-bonding within this monoclinic structure. The two pentaborate anions are structurally similar to each other and are not notably different from other systems containing isolated $[B_5O_6(OH)_4]^-$ anions,[8,39,55,247] with B-O distances to the 4-coordinate tetrahedral B1 and B11 centres significantly longer than those involving trigonal B centres; the observed bond lengths and internuclear angles are shown in Table 3.5. B-O bonds involving trigonal B atoms and terminal OH groups are at the shorter end of the range (av. 1.366 Å), whereas B-O bonds involving O atoms distal to the tetrahedral B1 and B11 centres (O2, O5 and O12, O15, respectively) are at the longer end of the range (av. 1.383 Å). Internuclear angles within the pentaborate anion range from 107.12(16)° to 110.32(16)° at the B1, 106.57(15)° to 110.67(16)° at the B11 and angles at the other ring B atoms range from 115.72(18)° to 122.96(19)°, which are consistent with sp^3 and sp^2 hybridization, respectively. The angles at the O ring centres range from 117.60(17)° to 124.11(17)°.

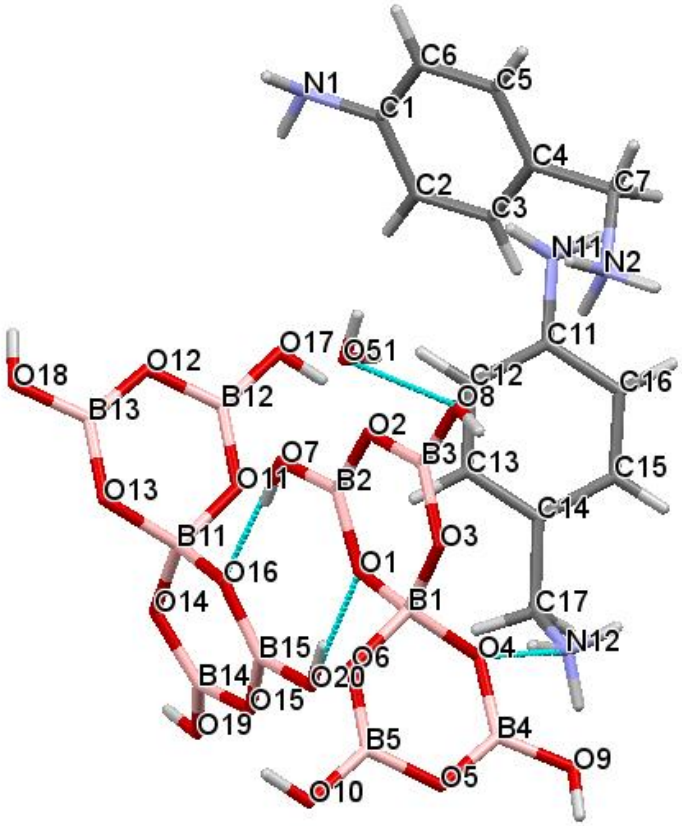

Figure 3.15: The molecular structure of 4-aminobenzylammonium pentaborate hemihydrate (9·½H_2O), illustrating the atomic numbering scheme. Intermolecular H-bonding are shown in blue.

Table 3.5: The B-O bond lengths (Å) and internuclear angles (°) for the two independent pentaborate anions found in compound 9·½H_2O.

B_{tet} bond lengths (Å)	B_{tet} internuclear angles (°)	B_{trig} bond lengths (Å)	B_{trig} internuclear angles (°)
1.452(3) – 1.481(3)	107.12(16) – 110.32(16)	1.349(3) – 1.390(3)	116.36(18) – 122.22(18)
1.462(3) – 1.488(3)	106.57(15) – 110.67(16)	1.358(3) – 1.391(3)	115.72(18) – 122.96(19)

There are numerous H-bond interactions within this compound, which are shown in Table 3.6. The two independent pentaborate anions in the asymmetric unit are H-bonded together at α-O atoms (O1 and O16), forming a $R_2^2(8)$ 8-membered ring. One of the pentaborate anions accepts an H-bond donor from a H_2O molecule at a β acceptor site (O8); the other donor from the H_2O molecule forms an H-bond

to the α-O atom within another unit cell (O14). In addition to this, the H_2O molecule accepts an H-bond from the ammonium N12-H12C of one of the cations within the unit cell, as well as from the N11-H11A amino group from another unit cell. The three NH of each ammonium group all partake in H-bonding; from one cation, the N2-H2A donor forms an H-bond to the O13 α-O acceptor site within another unit cell, the N2-H2B donor has a bifurcated H-bond to the O19 β-O acceptor site within another unit cell and to the O8 β-O acceptor site within the same unit cell, and finally the N2-H2C forms an H-bond to the O10 β-O acceptor site of another unit cell. The ammonium group of the second 4-aminobenzylammonium cation forms an H-bond from the N12-H12A to the O4 α-O acceptor site, N12-H12B to the O17 β-O acceptor site of a pentaborate anion in another unit cell, and finally the N12-H12C (as previously mentioned) forms an H-bond to the O51 atom of the H_2O molecule.

The amino groups of each cation also partake in H-bonding, with the N1-H1A and N1-H1B forms H-bonds with α-O acceptor sites (O3 and O4) of a pentaborate in another unit cell, and the N11-H11A and N11-H11B forms H-bonds with a H_2O molecule (O51) and a β-O acceptor site (O18) of a pentaborate anion within another unit cell.

A giant H-bonded anionic lattice is observed for **9**·½H_2O; each pentaborate anion forms two α-reciprocal $R_2^2(8)$ 8-membered rings (O1, O16 and O6, O11), A C(8) chain at a β-O position (O7, O20) and accepts a H-bond from a water molecule either at a β-O acceptor site (O8) or at an α-O acceptor site (O14). The volume of each formula unit within **9**·½H_2O (376.88 Å^3) is greater than that of the smaller pyrrolidinium pentaborate salts found in **1**, **2**·½CH_3COCH_3, **3** and **4**·½H_2O (328.54 – 372.35 Å^3), which exhibited the α,α,α,β 'brickwall' configuration, but is smaller than the volume of compound **5**·0.3H_2O (410.65 Å^3), which exhibited the α,α,α,γ configuration. The large cations and complex H-bonding observed within **9**·½H_2O lead to a different anionic framework arrangement which can be described as zig-zagged ribbons of H-bonded pentaborate anions that are linked together by H_2O molecules, as shown in Figure 3.16. The 4-aminobenzylammonium cations occupy the 'cavity' that is formed between the linked anionic zig-zagged ribbons.

Table 3.6: The H-bonding interactions found within the solid-state structure of 4-aminobenzylammonium pentaborate hemihydrate (9·½H_2O).

D-H···A	*d*(H···A) (Å)	*d*(D···A) (Å)	∠DHA (°)
O7–H7···O16	1.88	2.7206(19)	173.1
O8–H8···N11^{i}	2.01	2.820(3)	161.7
O9–H9···O7^{ii}	1.87	2.707(2)	173.4
O10–H10···O11^{i}	1.87	2.696(2)	169.3
O17–H17···O6^{iii}	1.85	2.686(2)	171.9
O18–H18···O20^{iv}	1.89	2.720(2)	171.7
O19–H19···N1^{v}	1.93	2.769(3)	176.0
O20–H20···O1	1.79	2.626(2)	172.1
N1–H1A···O3^{iv}	2.37(3)	2.924(2)	122(3)
N1–H1B···O4^{iv}	2.32(2)	3.094(2)	145(2)
N2–H2A···O13^{vi}	2.058(16)	2.901(2)	158(2)
N2–H2B···O8	2.62(2)	3.211(2)	124.1(19)
N2–H2B···O19^{vii}	2.249(18)	2.988(2)	139.8(19)
N2–H2C···O10^{viii}	2.072(17)	2.886(2)	151(2)
N11–H11A···O51^{iii}	2.49(2)	3.171(3)	135(2)
N11–H11B···O18^{ix}	2.33(2)	3.069(2)	141(3)
N12–H12A···O4	2.014(15)	2.870(2)	163(2)
N12–H12B···O17^{ii}	2.001(15)	2.868(2)	163(3)
N12–H12C···O51^{x}	1.910(14)	2.806(2)	171(2)
O51–H51A···O8	2.003(16)	2.801(2)	154(2)
O51–H51B···O14^{vi}	1.945(15)	2.801(2)	170(3)

Symmetry transformations used to generate equivalent atoms: (i) x–1,y,z; (ii) x–1,y,z–1; (iii) x+1,y,z; (iv) x+1,y,z+1; (v) –x+2,y+1/2,–z+1; (vi) –x+1,y–1/2,–z+1; (vii) –x+1,y–1/2,–z; (viii) –x,y–1/2,–z; (xi) –x+2,y–1/2,–z+1; (x) x,y,z–1.

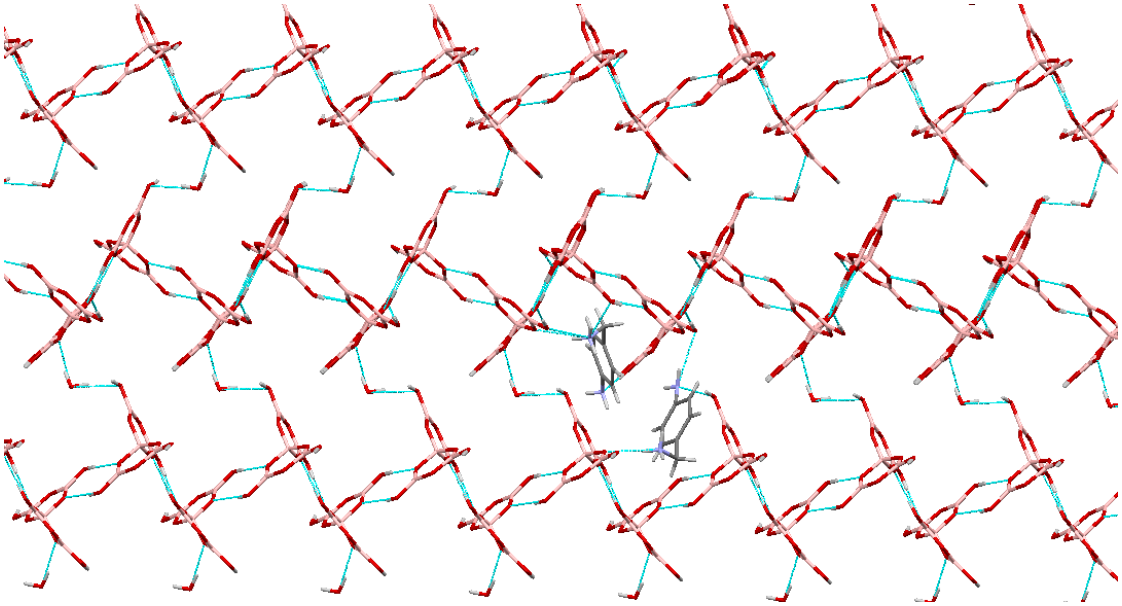

Figure 3.16: The H-bonded anionic lattice of 4-aminobenzylammonium pentaborate hemihydrate (9·½H_2O). The pentaborate anions are arranged as zig-zagged ribbons, held together by H_2O molecules. The 4-aminobenzylammonium cations occupy the 'cavities' formed between the anionic layers.

3.3.3 Bicyclic ammonium pentaborate salts

3.3.3.1 Synthesis and characterization of bicyclic pentaborate salts

The bicyclic pentaborate salts were all prepared in high yields in methanol/deionised water solution from the reaction of the free base with boric acid in a 1:5 molar ratio. The structure of the organic cations found in 2-(3-indolyl)ethylammonium pentaborate hemihydrate (**10**·½H_2O), 1,2,3,4-tetrahydroisoquinoline pentaborate (**11**), 1,2,3,4-tetrahydroisoquinoline pentaborate·1.5 boric acid monohydrate (**11**·1.5$B(OH)_3$·H_2O), and 1,2,3,4-tetrahydronaphthylammonium pentaborate hemihydrate (**12**·½H_2O) are shown in Figure 3.17.

The pentaborate salts containing **10** - **12** were characterized by multi-element NMR and IR spectroscopy, elemental analysis, thermal analysis and powder X-ray diffraction. Powder X-ray diffraction studies indicated that 2-(3-indolyl)ethylammonium pentaborate hemihydrate (**10**·½H_2O) was an amorphous solid, whereas compounds **11** and **12**·½H_2O were obtained as crystalline materials. Recrystallization of **11** from H_2O led to a co-crystallized species which contained a molecule of H_2O, along with an additional 1½ molecules of $B(OH)_3$

(**11**·1.5B(OH)$_3$·H$_2$O); the structure has not been determined from single-crystal XRD studies for this compound. Since single-crystals of **10**·½H$_2$O, **11**, **11**·1.5B(OH)$_3$·H$_2$O and **12**·½H$_2$O were unavailable from attempted crystallizations, their compositions have been formulated on the basis of elemental analysis, spectroscopic analyses and thermal analysis.

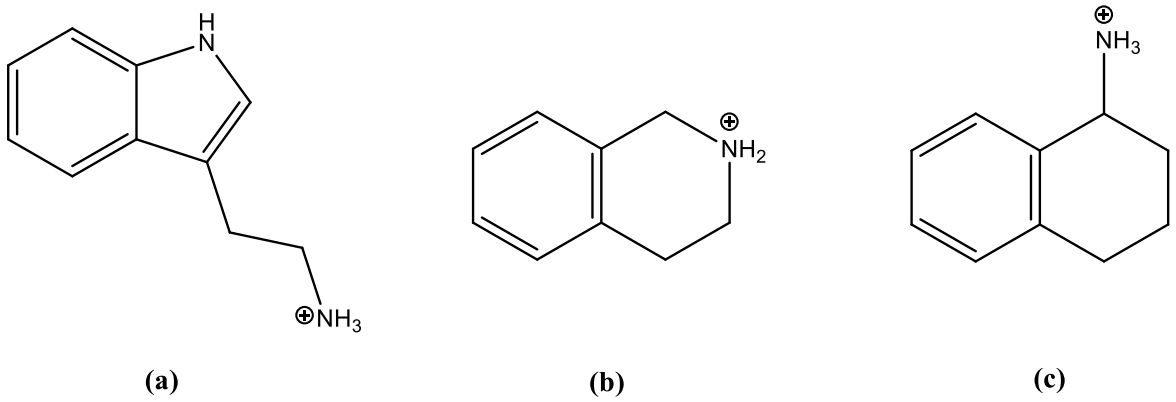

Figure 3.17: The (a) 2-(3-indolyl)ethylammonium; (b) protonated 1,2,3,4-tetrahydroisoquinoline, and (c) 1,2,3,4-tetrahydro-1-naphthylammonium cations as found in pentaborate salts 10·½H$_2$O, 11 (and 11·1.5B(OH)$_3$·H$_2$O), and 12·½H$_2$O, respectively.

Elemental analysis data of compounds **10**·½H$_2$O, **11**, **11**·1.5B(OH)$_3$·H$_2$O and **12**·½H$_2$O were in good agreement with theoretical values. Spectroscopic measurements of the pentaborate salts were, again, in agreement with previously reported non-metal cation pentaborate salts. ^{11}B NMR spectra obtained in D$_2$O showed the 3 characteristic signals at ~17, 13 and 1 ppm, while ^{1}H and ^{13}C NMR spectra were fully consistent with those expected for the bicyclic cations; NH and BOH signals in ^{1}H NMR spectra showed a broad singlet at ~4.8 ppm due to the signals overlapping and rapid exchange with the solvent.

As with the previously reported compounds in this chapter, the IR spectra of **10**·½H$_2$O, **11**, **11**·1.5B(OH)$_3$·H$_2$O and **12**·½H$_2$O were all obtained as KBr disks and all clearly show the diagnostic band of the pentaborate anion at ~925 cm^{-1}. Broad peaks were observed (~3200-3400 cm^{-1}) due to the OH and NH groups. The symmetric and asymmetric signals observed for the 3- and 4-coordinate B-O bonds are given in Table 3.7.

The synthesis of 1,2,3,4-tetrahydroquinoline pentaborate was also attempted (Chapter 2, Section 2.7.14) from the reaction of the free amine (Figure 3.18a) with boric acid in a 1:5 molar ratio in methanol/deionised water. The resulting solid was analysed using multi-element NMR and was found to be only a mixture of starting materials.

Table 3.7: The observed symmetric and asymmetric stretches of the $B_{(3)}$-O and $B_{(4)}$-O bonds found in pentaborate salts containing 10-12.

Compound	ν_{as} $B_{(3)}$-O	ν_{as} $B_{(4)}$-O	ν_{s} $B_{(3)}$-O	ν_{s} $B_{(4)}$-O
10·½H_2O	1421, 1338	1160, 1072	919	781
11, **11**·1.5$B(OH)_3$·H_2O	1427, 1295	1124, 1021	916	774
12·½H_2O	1418, 1300	1089, 1021	919	776

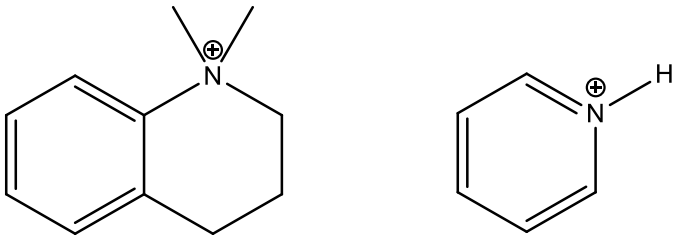

(a) pK_a 5.03 **(b)** pK_a 5.25

Figure 3.18: The structures of (a) protonated 1,2,3,4-tetrahydroquinoline, and (b) protonated pyridine, along with their corresponding pK_a values.

The pK_a value of protonated 1,2,3,4-tetrahydroquinoline (5.03)[248] can be compared with that of protonated pyridine (5.25)[248] which, due to its low basicity and reactivity with boric acid (pK_a = 9.24), is usually used a solvent in the solvothermal synthesis of polyborate salts[62,87]. It can be observed that protonated 1,2,3,4-tetrahydroquinoline has a lower pK_a value than protonated pyridine (Figure 3.18b), which indicates that it is less basic and less likely to form a polyborate salt when reacted with boric acid. In contrast to this, the pK_a value of protonated 1,2,3,4-tetrahydrosioquinoline, which has the amino group positioned further from the aromatic part of the molecule, is 9.53,[249] which is much more basic than pyridine.

3.3.3.2 Thermal properties of bicyclic pentaborate salts

The thermal properties of the bicyclic non-metal pentaborate salts containing **10** – **12** were investigated (in air) by TGA/DSC analysis. The TGA-DSC traces followed a similar trend to the previously reported pentaborate salts.

2-(3-Indolyl)ethylammonium pentaborate hemihydrate (**10**·½H_2O) showed an endothermic dehydration step at ~150°C, which was equal to the loss of 2.5 molecules of water; this indicates an additional ½ molecule of interstitial H_2O, whose presence is confirmed by the elemental analysis data. The cation was oxidized *via* exothermic processes to leave a glassy residue of 2.5B_2O_3 above 750°C.

1,2,3,4-Tetrahydroisoquinoline pentaborate (**11**) showed a two-step process; the first step was an endothermic dehydration step (~180°C) where the pentaborate anions form B-O-B crosslinked polymeric anions, followed by oxidation of the cation to leave a glassy residue of 2.5B_2O_3 >750°C. The recrystallized salt **11**·1.5$B(OH)_3$·H_2O showed an additional dehydration step (~100°C) which was equal to the %weight loss of 2.5H_2O, from both the interstitial H_2O molecule and the dehydration of the interstitial $B(OH)_3$ molecule. The %weight remaining of the residual B_2O_3 found above 750°C was equal to 3.25 moles, which arises from having the additional interstitial $B(OH)_3$ molecule. The presence of these interstitial molecules was confirmed from the results of the elemental analysis.

The final bicyclic pentaborate compound, 1,2,3,4-tetrahydronaphthylammonium pentaborate hemihydrate (**12**·½H_2O), also followed a three step weight loss TGA trace. The first step was an endothermic process which resulted in the loss of ½ of a H_2O molecule (also confirmed by the elemental analysis data), followed by a further dehydration step from the loss of two H_2O molecules from the condensation of the pentaborate anion. The oxidation of the cation again was found to be an exothermic process, leaving behind glassy B_2O_3 above 750°C.

3.3.4 Substituted adamantylammonium pentaborate salts

3.3.4.1 Synthesis and characterization of adamantylammonium pentaborate salts

A series of substituted 1- and 2-adamantylammonium pentaborates were prepared in high yields in methanol/deionised water solution from the reaction of the free base

(for compounds **13**, **14**·1.5H_2O and **16**·2H_2O) or the quaternary amine hydroxide salt (for compounds **15**·3H_2O and **17**·3H_2O) with boric acid in a 1:5 molar ratio. The structures of the organic cations found in compounds containing **13**-**17**·3H_2O are shown in Figure 3.19.

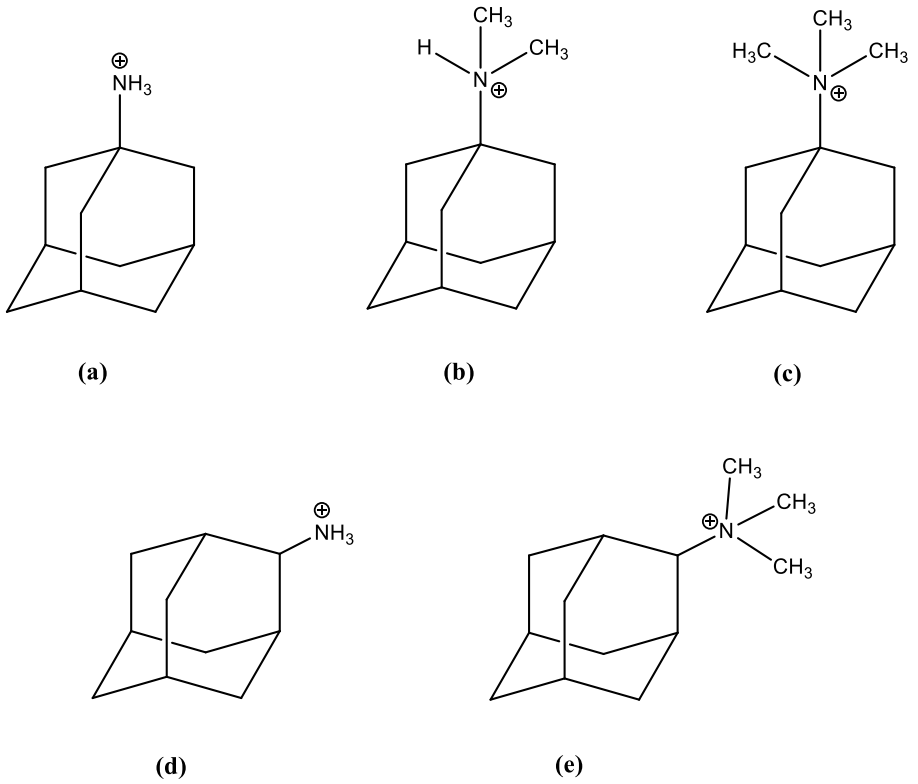

Figure 3.19: The adamantylammonium cations as found in (a) 1-adamantylammonium pentaborate, 13; (b) *N.N,*-dimethyl-1-adamantylammonium pentaborate sesquihydrate, 14·1.5H_2O **and *N.N,*-dimethyl-1-adamantylammonium pentaborate·boric acid monohydrate, 14**·$B(OH)_3$·H_2O**; (c) *N,N,N*-trimethyl-1-adamantylammonium pentaborate trihydrate, 15**·3H_2O**; (d) 2-adamantylammonium pentaborate dihydrate, 16**·2H_2O**; (e) *N,N,N*-trimethyl-2-adamantylammonium pentaborate trihydrate, 17**·3H_2O**.**

1-Adamantylamine was purchased as the free amine; the free amine of 2-adamantylamine was obtained from the neutralisation of the hydrochloride salt with sodium hydroxide. *N*,*N*-Dimethyl-1-adamantylamine was prepared according to the method by Vashkevich[230] which followed the Eschweiler-Clarke reaction. Briefly, the primary amine is methylated using an excess of formic acid and formaldehyde and proceeds to the tertiary amine stage. Quaternary amines are not formed by this

reaction due to the inability of the tertiary amine to form the iminium ion. The mechanism of this procedure is shown in Figure 3.20.

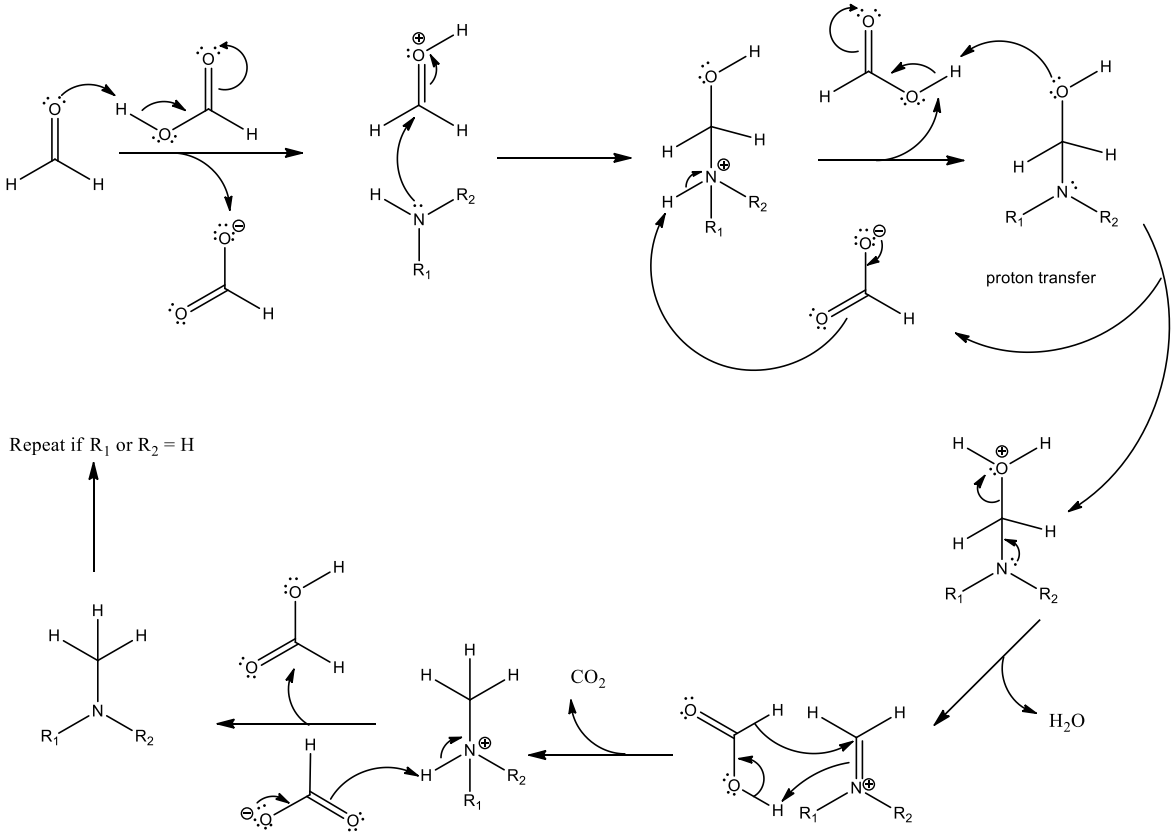

Figure 3.20: The reaction mechanism for the Eschweiler-Clarke reaction used in the synthesis of *N,N*-dimethyl-1-adamantylamine.

The synthesis of *N,N*-dimethyl-2-adamantylamine was attempted by following the same method as above, but the desired product was not obtained. An alternative procedure was identified and was successful in producing *N,N*-dimethyl-2-adamantylamine in moderate yield. The method used was a Borch reductive amination using sodium cyanoborohydride as the reducing agent.[231]

N,N,N-Trimethyl-1-adamantylamine and *N,N,N*-trimethyl-2-adamantylamine were synthesized by following the method by Vashkevich;[230] the resulting iodide salts from the reaction of the dimethylated adamantylamines with methyl iodide were

then converted to their corresponding hydroxide salts before reacting with boric acid to form the pentaborate salts (**15**·3H_2O and **17**·3H_2O).

The pentaborate salts containing **13**-**17** were all characterized by elemental analysis, NMR and IR spectroscopy, thermal analysis and X-ray diffraction. The solid-state structures of compounds **14**·$B(OH)_3$, **15**·3H_2O and **17**·3H_2O were confirmed by single-crystal XRD studies. The elemental analysis data for compounds containing **13**-**17** were in good agreement with the theoretical values, with the crude products of **14**·1.5H_2O and **16**·2H_2O indicating that there were additional (interstitial) water molecules present. The recrystallized product of **14**·$B(OH)_3$·H_2O was found to contain a molecule of $B(OH)_3$ and a molecule of H_2O within its crystal structure, and the recrystallized products from the two trimethylated adamantylammonium pentaborates (**15**·3H_2O and **17**·3H_2O) were each found to contain 3 H_2O molecules within their solid-state structures.

Powder XRD studies were carried out on all of the substituted adamantylammonium pentaborate salts; compounds **13** (1-adamantylammonium pentaborate) and **16**·2H_2O (2-adamantylammonium pentaborate dihydrate) were both found to be amorphous solids. The remaining salts were all crystalline materials.

^{11}B NMR spectra obtained in D_2O of all of the substituted adamantylammonium pentaborate salts all showed the three characteristic signals observed for pentaborate salts, at ~17, 13 and 1 ppm. The ^{1}H and ^{13}C NMR spectra were consistent with those expected for adamantylammonium cations; NH (**13**, **14**·1.5H_2O, **14**·$B(OH)_3$·H_2O, and **16**·2H_2O) and BOH protons were observed as an overlapping broad signal at ~4.8 ppm due to rapid exchange.

IR spectra obtained as KBr disks all showed the characteristic signal for a pentaborate anion, at ~925 cm^{-1}. A summary of the asymmetric and symmetric trigonal and tetrahedral B-O bonds are given in Table 3.8. Signals for the OH and NH groups were observed as broad peaks in the range of 3200-3400 cm^{-1}. Peaks for the substituted adamantylammonium cations were also present in the IR spectra.

Table 3.8: The observed symmetric and asymmetric stretches of the $B_{(3)}$-O and $B_{(4)}$-O bonds found in pentaborate salts containing 13-17.

Compound	ν_{as} $B_{(3)}$-O	ν_{as} $B_{(4)}$-O	ν_{s} $B_{(3)}$-O	ν_{s} $B_{(4)}$-O
13	1422, 1312	1163, 1086	918	781
14·1.5H_2O **14**·$B(OH)_3$·H_2O	1421, 1316	1159, 1075	912	778
15·3H_2O	1422, 1306	1152, 1072	916	771
16·2H_2O	1427, 1361	1101, 1028	923	783
17·3H_2O	1439, 1361	1197, 1026	926	782

The synthesis of *N*,*N*-dimethyl-2-adamantylammonium pentaborate was also attempted (Chapter 2, Section 2.7.8). The ^{1}H and ^{13}C NMR spectra confirmed the presence of the cation, however the ^{11}B NMR spectrum showed only a single peak at +18.2 ppm. This single peak does not correspond to the signal observed for pentaborates in very dilute aqueous solutions (+16.1 ppm), nor does it correspond to the start material, $B(OH)_3$ whose single peak is observed at +19.5 ppm. It is believed that the peak observed for this species arises from an equilibrium mixture of product and unreacted starting materials.

Analysis of the crude material by powder X-ray diffraction showed that the pentaborate was present, but the peaks with the highest intensities were identified as boric acid. There were numerous other peaks present which did not correspond to those from boric acid and are likely to arise from the pentaborate salt.

An IR spectrum of the product was obtained as a KBr disk. A sharp peak was observed at 931 cm^{-1}, which is close to that of the characteristic pentaborate signal observed in IR spectra (at ~925 cm^{-1}). In addition to this, there were peaks present arising from the asymmetric and symmetric B-O bond stretches which were in similar regions to those already reported within this chapter, as well as signals arising from the adamantylammonium cation.

As the material obtained was a mixture, thermal analysis and elemental analysis were not in agreement with theoretical values for a pure pentaborate salt. It is believed that the attempted synthesis of *N*,*N*-dimethyl-2-adamantylammonium pentaborate was successful, but the product was not pure, possibly due to

insufficient reaction time. Attempts at recrystallizing the crude material to isolate the product as pure single crystals proved unsuccessful even after multiple attempts.

3.3.4.2 Thermal analysis of substituted adamantylammonium pentaborates

TGA-DSC was used to analyse the thermal properties of the (substituted) adamantylammonium pentaborate salts containing **13**-**17**. Similar to other non-metal cation pentaborate salts, compounds containing **13**-**17** all dehydrated at temperatures up to ~250 °C, with compounds **14**·1.5H_2O, **15**·3H_2O and **17**·3H_2O having an additional dehydration step at ~100-150 °C due to additional interstitial molecules present. All of the salts' cations oxidised *via* an exothermic process and resulted in a glassy solid of B_2O_3 above 750 °C.

Unlike the unsubstituted 1-adamantylammonium pentaborate (**13**), the thermal analysis data for 2-adamantylammonium pentaborate dihydrate (**16**·2H_2O) indicated the presence of two interstitial H_2O molecules; this was corroborated by the elemental analysis data.

The TGA trace for the recrystallized product of *N*,*N*-dimethyl-1-adamantylammonium pentaborate (**14**·$B(OH)_3$·H_2O) indicated the loss of 2.5 additional H_2O molecules (1.5 from $B(OH)_3$ and 1 from H_2O molecules) at ~110°C, which was confirmed by the elemental analysis data and the refined crystallographic structure. The thermal analyses data for *N,N,N*-trimethyl-1-adamantylammonium pentaborate trihydrate (**15**·3H_2O) and *N,N,N*-trimethyl-2-adamantylammonium pentaborate trihydrate (**17**·3H_2O) indicated the presence of 3 additional H_2O molecules within their structures, which were also confirmed by the elemental analyses data and crystallographic data.

3.3.4.3 Crystallographic studies of substituted adamantylammonium pentaborate salts.

The crystal structures of *N,N*-dimethyl-1-adamantylammonium pentaborate·boric acid monohydrate (**14**·$B(OH)_3$·H_2O), *N,N,N*-trimethyl-1-adamantylammonium pentaborate trihydrate (**15**·3H_2O) and *N,N,N*-trimethyl-2-adamantylammonium pentaborate trihydrate (**17**·3H_2O) are reported in this section. The spectroscopic and

analytical data for the recrystallized products are given in Chapter 2, Sections 2.5.14, 2.5.15 and 2.5.17, respectively. The crystal structure data were obtained and solved by the National Crystallographic Service at Southampton and the full crystallographic data is available in the appendices with NCS numbers 2014NCS0278, 2014NCS0730 and 2015NCS0474 for **14**·$B(OH)_3$·H_2O, **15**·$3H_2O$ and **17**·$3H_2O$, respectively.

The structures of **14**·$B(OH)_3$·H_2O and **15**·$3H_2O$ are free from disorder and are characterized by having discrete (substituted) 1-adamantylammonium cations and pentaborate anions. The structure of showed disorder about the cation and in two of the water molecules. Diagrams of the cations and anions present, along with their associated atomic numbering schemes are shown in Figures 3.21, 3.22 and 3.23 for **14**·$B(OH)_3$·H_2O, **15**·$3H_2O$ and **17**·$3H_2O$, respectively.

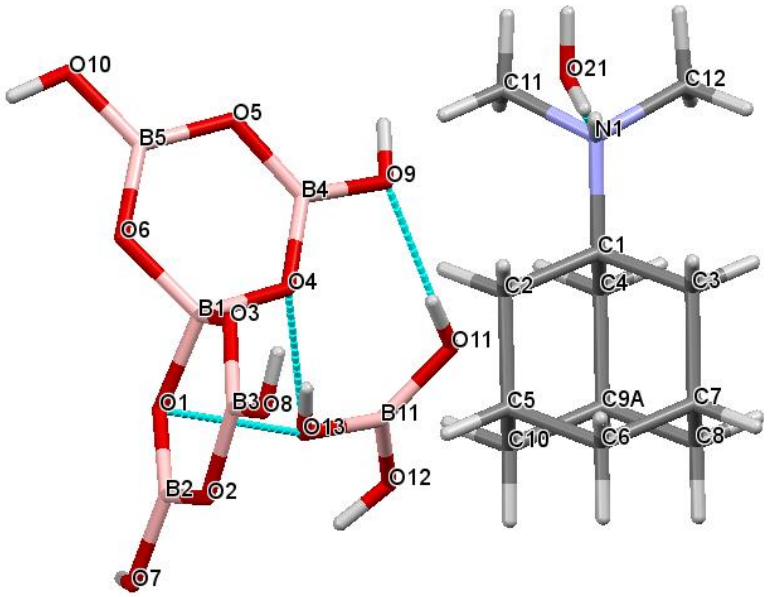

Figure 3.21: The molecular structure of *N,N*-dimethyl-1-adamantylammonium pentaborate as found in 14·$B(OH)_3$·H_2O, illustrating the atomic numbering scheme. Intermolecular H-bonds are shown in blue.

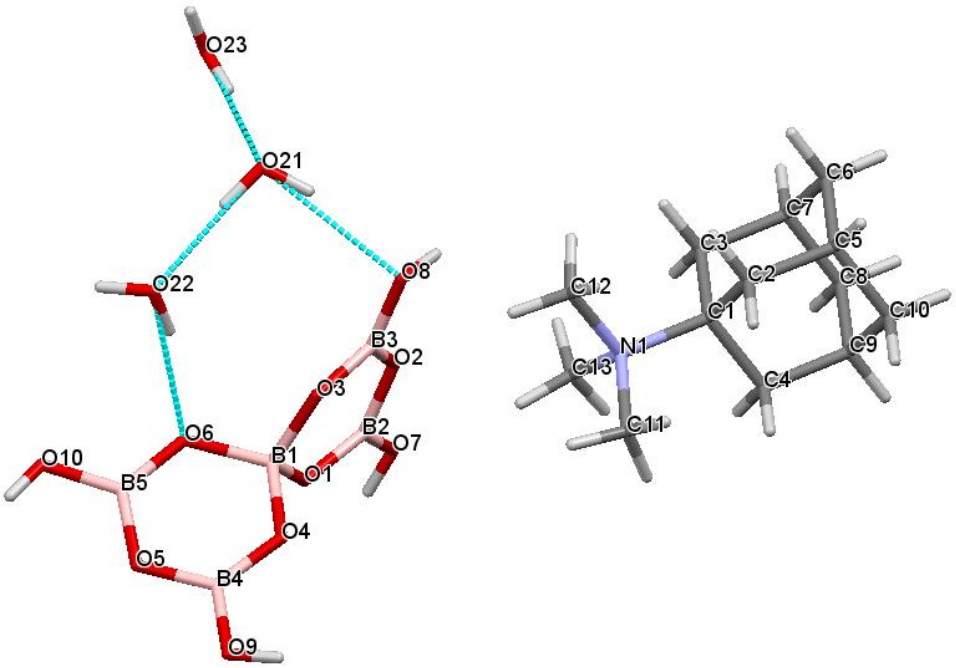

Figure 3.22: The molecular structure of *N,N,N*-trimethyl-1-adamantylammonium pentaborate as found in 15·3H₂O, illustrating the atomic numbering scheme. Intermolecular H-bonds are shown in blue.

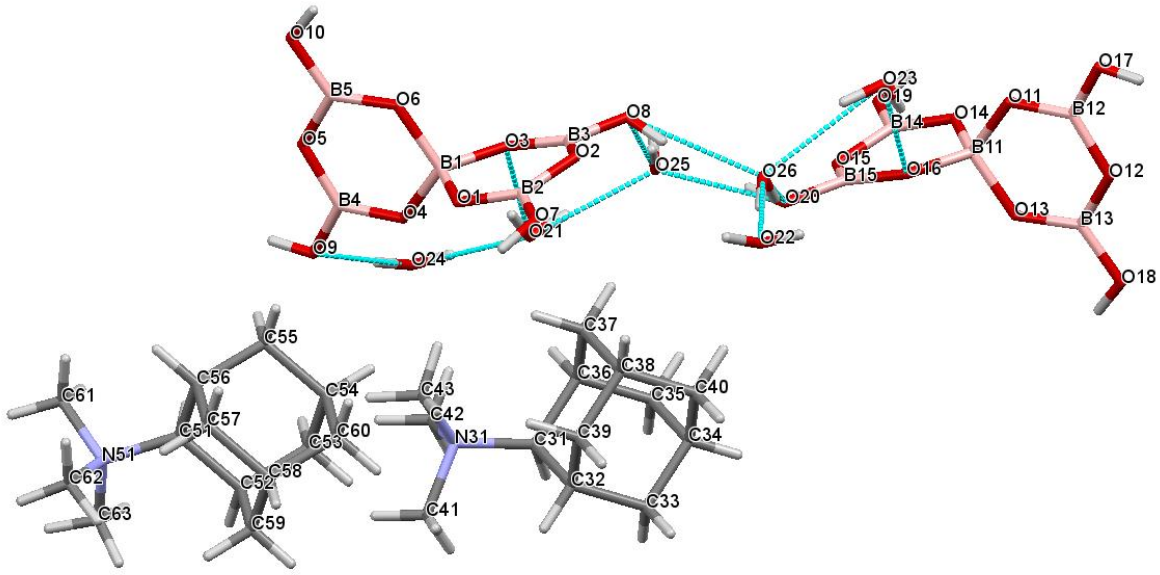

Figure 3.23: The molecular structure of *N,N,N*-trimethyl-2-adamantylammonium pentaborate as found in 17·3H₂O, illustrating the atomic numbering scheme. The disorder of the cation and water molecules are not shown for simplicity. Intermolecular H-bonds are shown in blue.

Compound **14**·$B(OH)_3$·H_2O contains only one pentaborate anion and one dimethyl-1-adamantylammonium cation per asymmetric unit, with one molecule of $B(OH)_3$ and one molecule of H_2O also making up the formula of this structure. Compound **15**·$3H_2O$ also contains only one pentaborate anion and one trimethyl-1-adamantylammonium cation per asymmetric unit, and also contains three co-crystallized molecules of H_2O. In contrast to this, compound **17**·$3H_2O$ contains two independent pentaborate anions and trimethyl-2-adamantylammonium cations per asymmetric unit, as well as six H_2O molecules, two of which are disordered. The three structures all crystallize in the triclinic space group. The bond lengths and internuclear angles observed within the pentaborate anions' B_3O_3 rings of compounds **14**·$B(OH)_3$·H_2O, **15**·$3H_2O$ and **17**·$3H_2O$ are within the ranges observed for the previously reported non-metal cation pentaborate structures; the observed bond lengths and internuclear are given in Table 3.9. These bond lengths and internuclear angles are also within the range observed in other related boroxole ring structures containing both 3- and 4-coordinate boron centres bound to oxygen (see Chapter 5).

Table 3.9: The observed B-O bond lengths (Å) and internuclear angles (°) for pentaborate anions found in compounds 14·$B(OH)_3$·H_2O**, 15**·$3H_2O$ **and 17**·$3H_2O$.

Compound	B_{tet} bond lengths (Å)	B_{tet} internuclear angles (°)	B_{trig} bond lengths (Å)	B_{trig} internuclear angles (°)
14·$B(OH)_3$·H_2O	1.4494(14) – 1.4821(14)	108.70(9) – 111.66(9)	1.3516(15) – 1.3950(15)	115.91(10) – 122.84(10)
15·$3H_2O$	1.4550(12) – 1.4855(12)	107.81(8) – 111.69(8)	1.3531(13) – 1.3900(13)	116.16(9) – 122.69(9)
17·$3H_2O$[a]	1.451(2) – 1.484(2), 1.452(2) – 1.485(2)	108.02(12) – 111.54(13), 108.14(13) – 111.85(13)	1.349(2) – 1.386(2), 1.351(2) – 1.391(2)	115.88(14) – 122.88(15), 115.99(15) – 122.75(15)

[a]Compound **17** contains two independent pentaborate anions per asymmetric unit.

The solid-state structures of compounds **14**·$B(OH)_3$·H_2O, **15**·$3H_2O$ and **17**·$3H_2O$ all possess giant anionic lattices held together by H-bonds, with the cations

sitting within the ‘cavities’ of the lattice. Unlike the previous pentaborate salts reported in this chapter, the co-crystallized species found within compounds **14**·B(OH)$_3$·H$_2$O, **15**·3H$_2$O and **17**·3H$_2$O do not sit within the ‘cavities’ of the anionic lattice and, instead, contribute to the structure of the anionic lattice by acting as ‘spacer’ molecules between anionic units. Details of the H-bonding interactions found within the solid-state structures of all of the (substituted) adamantylammonium pentaborate salts are shown in Table 3.10.

Table 3.10: The H-bonding interactions found within the solid-state structures of the (substituted) adamantylammonium pentaborate salts 14·B(OH)$_3$·H$_2$O**, 15**·3H$_2$O **and 17**·3H$_2$O**.**

Compound	*D*-H···A	*d*(H···A) (Å)	*d*(D···A) (Å)	∠DHA (°)
14·B(OH)$_3$·H$_2$O	O7-H7...O12	1.90	2.7191(12)	165.0
	O8-H8...O3	1.87	2.7054(11)	175.2
	O9-H9...O7	1.82	2.6458(11)	166.7
	O10-H10...O6	1.97	2.7786(12)	162.6
	N1-H1...O21	1.78	2.7584(14)	166.4
	O11-H11...O9	1.94	2.7703(12)	168.8
	O12-H12...O13	1.94	2.7695(12)	171.8
	O13-H13...O4	1.91	2.7441(12)	170.5
	O21-H21A...O10	1.97	2.7962(12)	163.3
	O21-H22B...O5	2.12	2.9384(12)	161.4
15·3H$_2$O	O7-H7A...O1	1.90	2.7340(10)	172.7
	O8-H8...O9	1.93	2.7256(10)	157.5
	O9-H9A...O4	1.84	2.6801(10)	173.8
	O10-H10...O23	1.89	2.7059(19)	162.8
	O21-H21A...O8	2.08	2.9005(11)	163.0
	O21-H21B...O22	1.88	2.727	171.2
	O22-H22A...O6	2.03	2.8627(10)	165.4
	O22-H22B...O23	2.02	2.8504(14)	163.8
	O23-H23A...O10	2.05	2.8451(11)	155.3
	O23-H23B...O21	1.83	2.671	171.3
17·3H$_2$O	O7-H7...O14	1.85	2.6885(14)	174.7
	O8-H8A...O26	2.05	2.8705(14)	163.9
	O8-H8B...O25A	1.87	2.6484(15)	154.3
	O9-H9...O19	1.92	2.7215(15)	158.3
	O10-H10...O13	1.90	2.7311(15)	170.9
	O17-H17...O7	1.92	2.7227(15)	158.3
	O18-H18...O6	1.90	2.7336(15)	171.1
	O19-H19...O1	1.86	2.6930(14)	173.8
	O20-H20...O25	1.84	2.6431(14)	159.0
	O20-H20A...O26A	2.12	2.9117(15)	156.6

Compound	*D*-H···A	*d*(H···A) (Å)	*d*(D···A) (Å)	∠DHA (°)
17·3H_2O (continued)	O21-H21A...O3	2.09	2.9031(13)	159.3
	O21-H21A...O4	2.54	3.2327(12)	139.5
	O21-H21B...O25	1.91	2.732	162.9
	O21-H21B...O25A	2.11	2.922	158.8
	O22-H22A...O17	2.04	2.8733(14)	166.4
	O22-H22B...O23	1.88	2.7217(12)	172.2
	O23-H23A...O11	2.56	3.2353(14)	137.3
	O23-H23A...O16	2.09	2.9029(15)	160.4
	O23-H23B...O26	2.08	2.883	156.5
	O23-H23B...O26A	1.95	2.785	168.3
	O24-H24A...O9	2.04	2.8738(14)	167.8
	O24-H24B...O21	1.88	2.723	172.0
	O25-H25A...O24	1.93	2.7933(12)	171.5
	O25-H25B...O8	2.04	2.8961(15)	168.6
	O25A-H25C...O24	1.85	2.5792(11)	139.8
	O25A-H25D...O20	2.02	2.8828(15)	172.5
	O26-H26A...O22	1.80	2.643	161.6
	O26-H26B...O20	1.81	2.6061(14)	151.8
	O26A-H26C...O22	1.87	2.738	175.1
	O26A-H26D...O8	1.81	2.6454(13)	161.0

The giant H-bonded anionic lattice of *N,N*-dimethyl-1-adamantylammonium pentaborate (**14**·$B(OH)_3$·H_2O) can be described as being based upon the 'brickwall' structures previously observed in the substituted pyrrolidinium pentaborates (**1**, **2**·½CH_3COCH_3, **3** and **4**·½H_2O). Each pentaborate anion forms two $R_2^2(8)$ 8-membered rings to α-O acceptor sites (O3 and O6) and one C(8) chain to a β-acceptor site (O7). A third $R_2^2(8)$ 8-membered ring is observed at α-O acceptor sites (O4 and O9); this interaction is with the co-crystallized $B(OH)_3$ molecule. The co-crystallized H_2O molecule forms an H-bond from the O21-H21A to the β-O acceptor site (O10) of a pentaborate anion in another unit cell, as well as from the O21-H22B to the γ-O acceptor site (O5) of another pentaborate anion in the next unit cell. The H_2O molecule also accepts an H-bond from the N1-H1 of the cation. The H-bonded anionic lattice of **14**·$B(OH)_3$·H_2O is shown in Figure 3.24. The use of these 'spacer' molecules ($B(OH)_3$ and H_2O) allows the 'brickwall' structure to 'expand' in order to accommodate the larger dimethyl-1-adamantylammonium cation (formula unit volume = 559.75 $Å^3$).

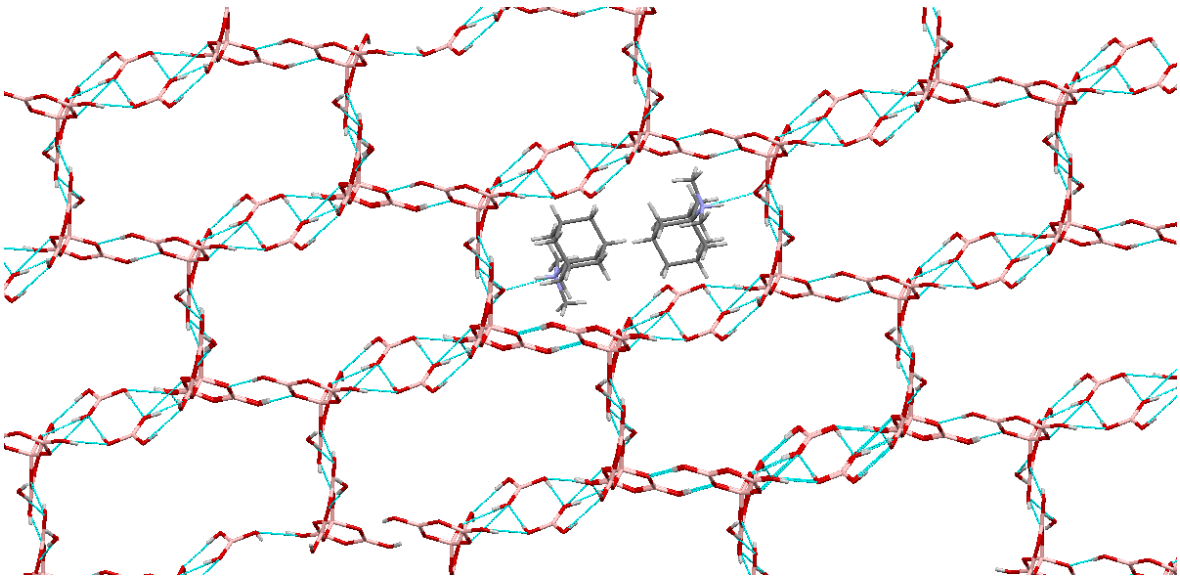

Figure 3.24: The H-bonded anionic lattice of 14·B(OH)$_3$·H$_2$O. The cations are H-bonded to the anionic lattice and sit within the 'cavities' of the lattice. H-bonds are shown in blue.

The giant H-bonded anionic lattice of *N,N,N*-trimethyl-1-adamantylammonium pentaborate trihydrate (**15**·3H$_2$O) also forms a similar arrangement to **14**·B(OH)$_3$·H$_2$O, by forming an 'expanded brickwall' formation through the use of 'spacer' molecules between the pentaborate anions. Each pentaborate anion forms two $R_2^2(8)$ 8-membered rings to α-O acceptor sites (O1 and O4) and one C(8) chain to a β-O acceptor site (O9); the fourth configuration involves another 8-membered ring. In this instance, the 8-membered ring is comprised of three donor sites from two of the water molecules (H22A, H22B and H23A) and three acceptor sites; an α-O and a β-O of the pentaborate anion (O6 and O10, respectively) and two O atoms from the water molecules (O22 and O23). This type of 8-membered ring is called a $R_3^3(8)$. The O10-H10 also forms an H-bond with a H$_2$O molecules (O23) in another unit cell. Interestingly, when two of these asymmetric units are conjoined by H-bonding of the water molecules, they form another repetitive intermolecular H-bond motif, $R_6^6(12)$, in which each water molecule is involved in H-bonding from one donor and one acceptor site (Figure 3.25). This 12-membered ring forms a hexagonal shaped H-bonded ring, which is similar to that observed in the crystal structure of ice.[250]

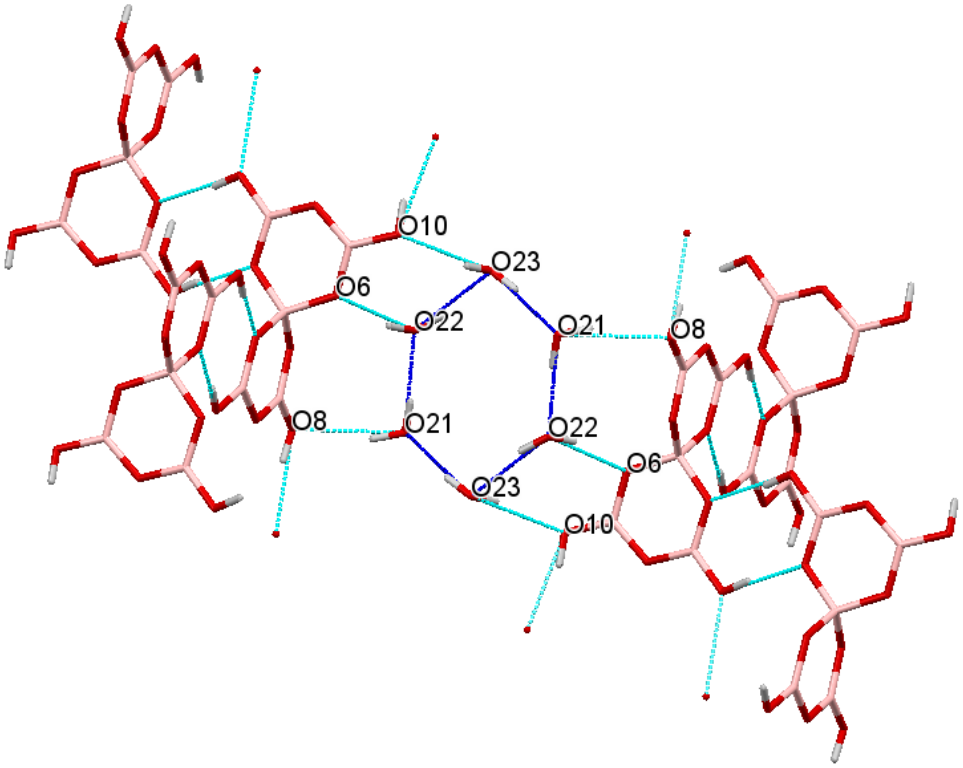

Figure 3.25: Two asymmetric units of 15·3H_2O are joined by H-bond interactions between the co-crystallized water molecules, forming a hexagonal 12-membered ring (shown in dark blue). Other H-bond interactions within this structure are shown in light blue. The atomic numbers are also shown for clarity.

The formation of this hexagonal shaped ring by the water molecules acts as a 'spacer' between the pentaborate anions, which allows the anionic lattice to follow a 'brickwall'-type structure by expanding to accommodate the size of the large cation (formula unit volume = 546.62 $Å^3$). This 'expansion' is similar to that observed in **14**·$B(OH)_3$·H_2O, in which the 'expansion' of that lattice is facilitated by $B(OH)_3$ and H_2O 'spacer' molecules. The giant H-bonded anionic lattice of **15**·3H_2O is shown in Figure 3.26 and shows the cations simply sit within the 'cavities' without partaking in any H-bond interactions.

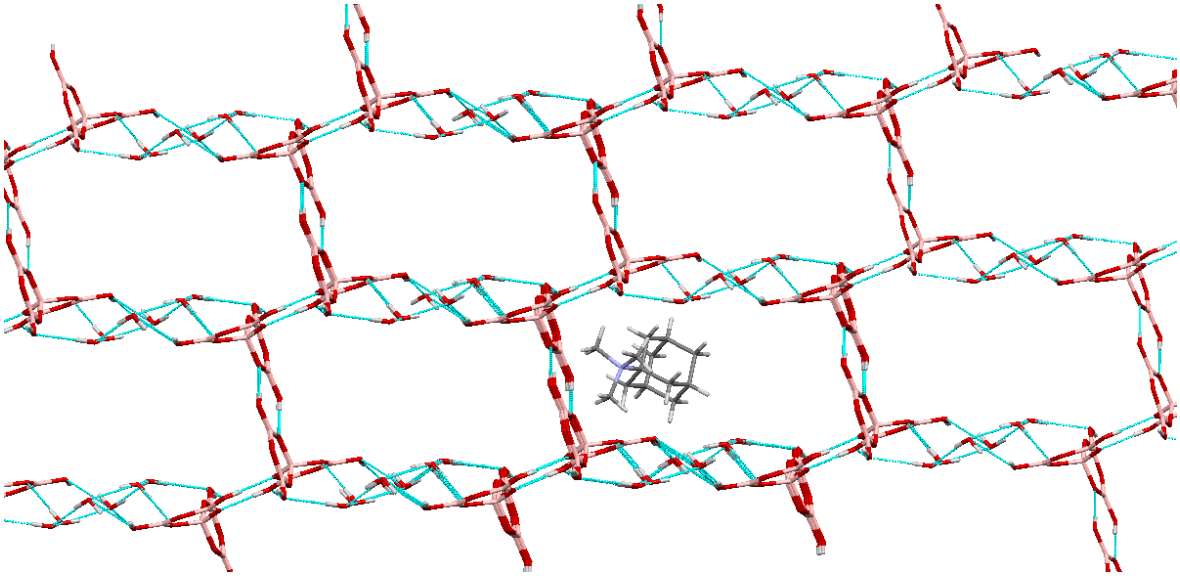

Figure 3.26: The H-bonded anionic lattice of 15·3H_2O, which uses water 'spacer' molecules to 'expand' the 'brickwall' configuration of the anionic lattice. The adamantylammonium cations sit in the 'cavities' of the anionic lattice, without any H-bond interactions. Intermolecular H-bonds are shown in blue.

The giant H-bonded anionic lattice of trimethyl-2-adamantylammonium pentaborate (**17**·3H_2O) forms a similar configuration to that observed in **15**·3H_2O. Both of these structures contain a trimethylated adamantylammonium cation, differing only on the position of the ammonium cation on the hydrocarbon cage, and contain three molecules of H_2O per formula unit. The structure of **17**·3H_2O, however, contains two independent anions and cations per asymmetric unit and contains disordered cations and two (of six) H_2O molecules are also disordered (formula unit volume = 551.65 $Å^3$). Each pentaborate anion within the solid-state structure of **17**·3H_2O forms two $R_2^2(8)$ 8-membered rings to α-O acceptor sites (O1, O14, O6, O13) and once C(8) chain to a β-O acceptor site (O7, O19). The remaining α-O acceptor sites of the pentaborate anions (O3 and O16) form H-bonds with the O21-H21A and O23-H23A of the H_2O molecules, respectively.

The co-crystallized H_2O molecules form numerous H-bonds within the solid-state structure of **17**·3H_2O. The aforementioned H_2O H-bond interactions with the α-O (O3 and O16) acceptor sites of the pentaborate anions are bifurcated and also form weak H-bonds from the O21-H21A to the O4 α-acceptor site and from the O23-H23A to the O11 α-acceptor site, respectively. The O25 and O26 acceptor sites

belong to the two disordered H_2O molecules, which show multiple H-bond formations between other H_2O molecules and to the β-O acceptor sites (O8 and O20). The O22-H22A from a H_2O molecule forms an H-bond with the O17 β-O acceptor site of a pentaborate anion within another unit cell, as well as from the O22-H22B to the O23 acceptor site of a H_2O molecule within another unit cell. The O24-H24A of another H_2O molecule forms an H-bond with a β-O acceptor site on a pentaborate anion and from the O24-H24B to the O21 acceptor site of a H_2O molecule

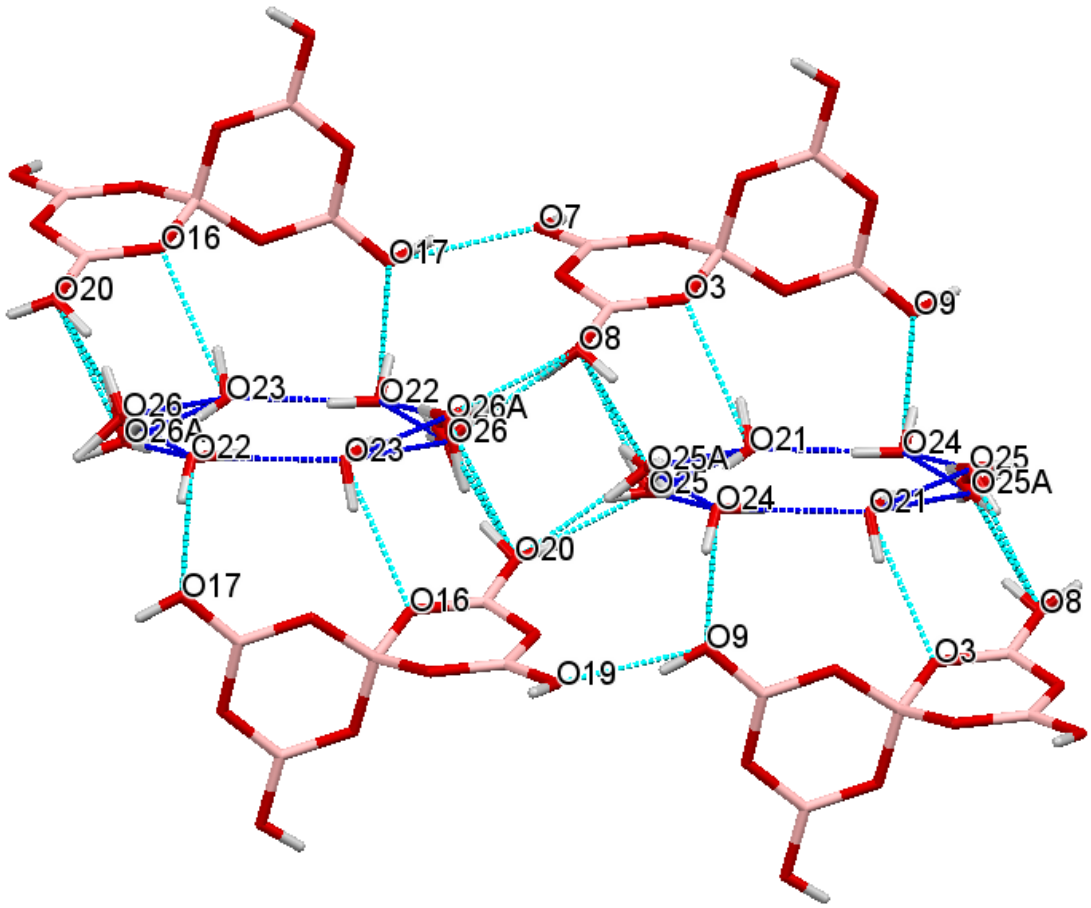

Figure 3.27: Two asymmetric units of 17·3H_2O are joined by H-bond interactions between the co-crystallized water molecules, forming hexagonal 12-membered rings (shown in dark blue). Other H-bond interactions within this structure are shown in light blue. The disorder of the H_2O molecules are shown within this illustration.

. As observed in the solid-state structure of **15**·3H_2O, the H_2O molecules found within the solid-state structure of **17**·3H_2O arrange themselves into hexagonal shaped 12-membered $R_6^6(12)$ rings (Figure 3.27) which, again, act as 'spacer' molecules between the pentaborate anions in order to 'expand' the 'brickwall'-type configuration of the anionic lattice (Figure 3.28). The disordered cations found in **17**·3H_2O again do not take part in any H-bond interactions.

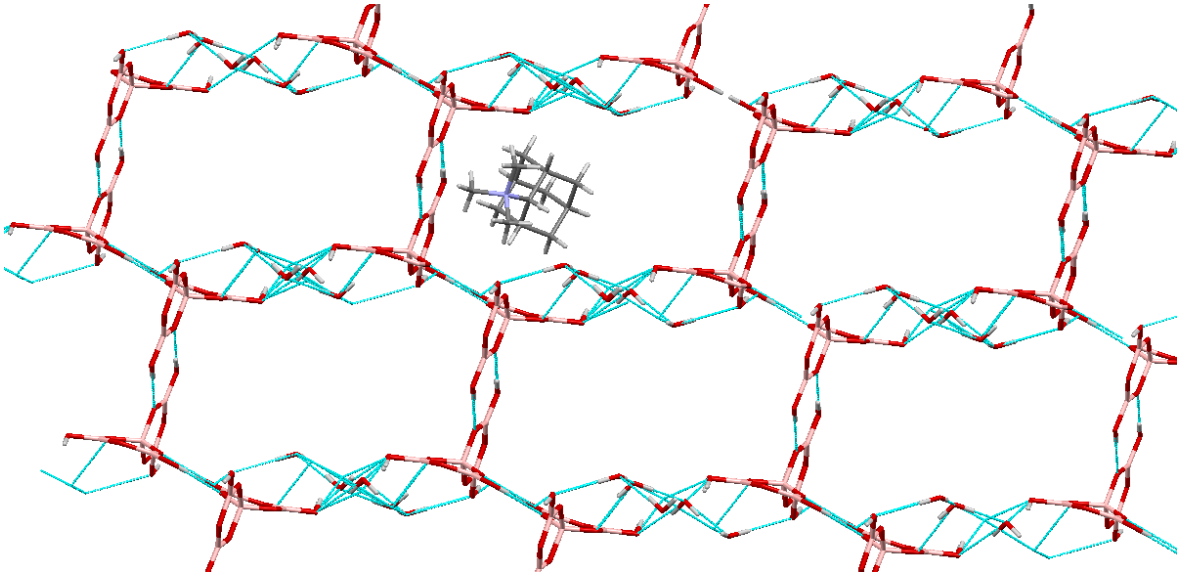

Figure 3.28: The H-bonded anionic lattice of 17·3H_2O is similar to that of 15·3H_2O with the use of water molecules as 'spacer' molecules to expand the 'brickwall' formation. The disordered cations sit within the 'cavities' of the lattice and do not take part in any H-bond interactions, whereas the disordered water molecules form H-bonds between pentaborate anions. Intermolecular H-bonds are shown in blue. The solid-state structure is shown without disorder, for clarity.

3.3.5 Polyborate salts containing larger non-metal cations

3.3.5.1 Synthesis and characterization of Bis(triphenylphosphine)iminium polyborates

Bis(triphenylphosphine)iminium (PPN) chloride was first converted to the hydroxide salt *via* ion exchange, then reacted with boric acid in either a 1:5 (for **18**·1.5H_2O) or 1:3 (for **19**·2.5H_2O) molar ratio in methanol/deionised water solution which gave the products in high yields. The structure of the PPN cation and the polyborate anions

found in PPN pentaborate sesquihydrate (**18**·1.5H_2O) and PPN triborate·2.5 hydrate (**19**·2.5H_2O) are illustrated in Figure 3.29.

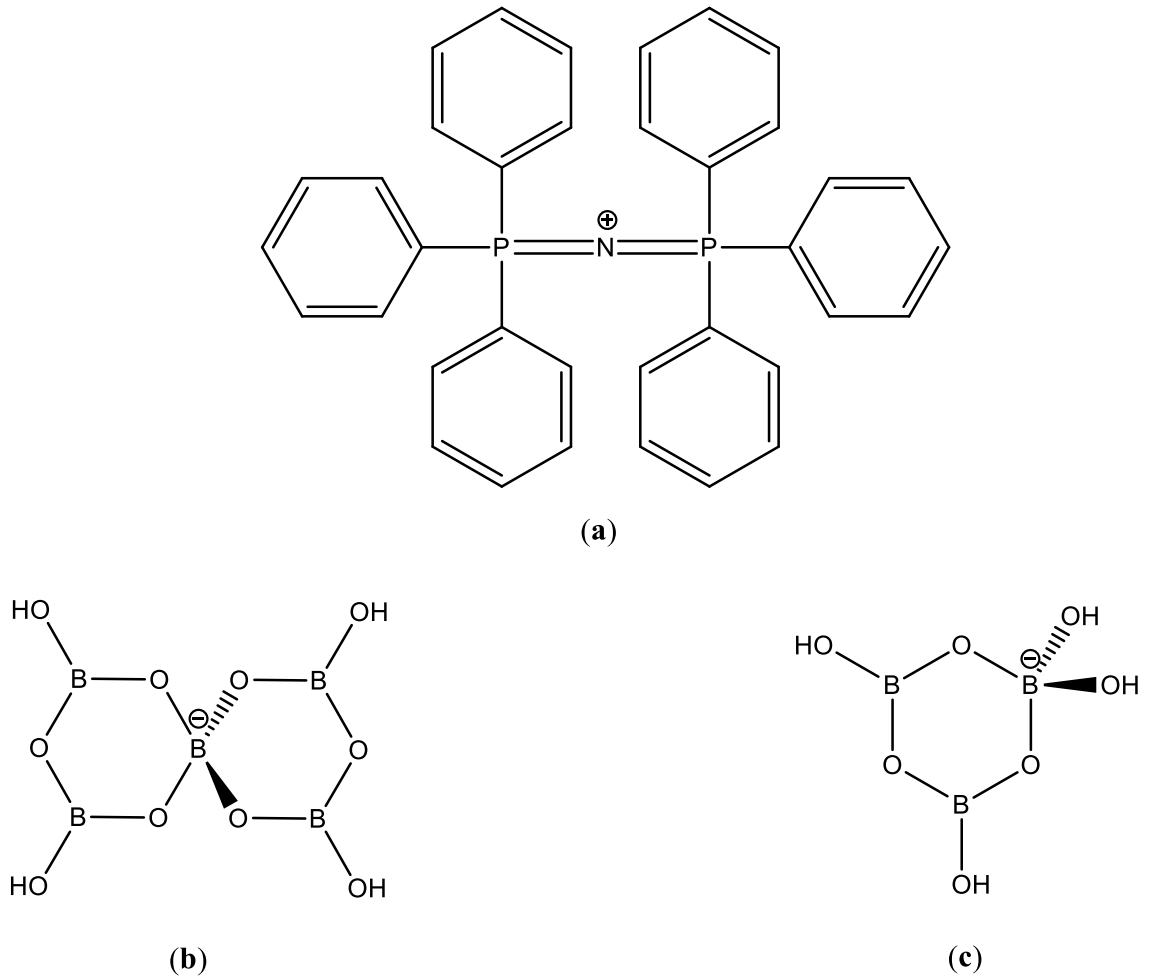

Figure 3.29: The (a) bis(triphenylphosphine)iminium (PPN) cation, (b) the pentaborate anion as found in [$C_{36}H_{30}NP_2$][$B_5O_6(OH)_4$]·1.5H_2O (18·1.5H_2O), and (c) the triborate monoanion as found in [$C_{36}H_{30}NP_2$][$B_3O_3(OH)_4$]·2.5H_2O (19·2.5H_2O).

The polyborate salts **18**·1.5H_2O and **19**·2.5H_2O were characterized by elemental analysis, NMR and IR spectroscopy, thermal analysis and powder X-ray diffraction. The powder X-ray diffraction studies indicated that both materials were crystalline solids, however crystals suitable for single-crystal XRD studies were unavailable for **18**·1.5H_2O. Single crystals of **19**·2.5H_2O were obtained after recrystallization from toluene and, at the time of writing this thesis, are currently under investigation at the National Crystallographic Service in Southampton (NCS

number 2016NCS0211). Since the single-crystal data is unavailable, the compositions of **18**·1.5H_2O and **19**·2.5H_2O have been formulated based on their elemental analysis, spectroscopic analysis and thermal analysis data. Compounds **18**·1.5H_2O and **19**·2.5H_2O were also prepared under solvothermal conditions (Chapter 2, Sections 2.6.12 and 2.6.13, respectively).

Elemental analysis data of compounds **18**·1.5H_2O and **19**·2.5H_2O were in good agreement with theoretical values which suggested the presence of interstitial H_2O molecules in both compounds.

The ^{11}B NMR spectra (obtained in D_2O) showed a single peak at 16.4 ppm and 13.7 ppm for **18**·1.5H_2O and **19**·2.5H_2O, respectively. However, using Equation 3.8, the total boron/charge ratio (B/1) could be determined for these two compounds; B/1 for **18**·1.5H_2O = 5.5, B/1 for **19**·2.5H_2O = 2.93. In addition to this, these polyborate salts are believed to be the first known polyborate salts to be soluble in organic solvents; compounds **18**·1.5H_2O and **19**·2.5H_2O were found to be readily soluble in most organic solvents and ^{11}B NMR spectra obtained in $CDCl_3$ provided some very useful information.

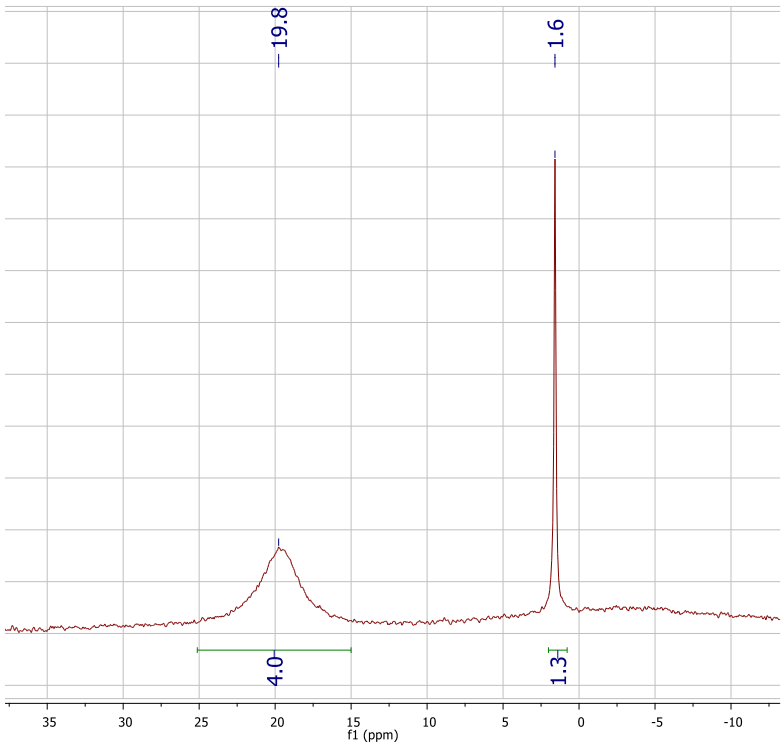

Figure 3.30: The ^{11}B NMR spectrum of 18·1.5H_2O, obtained in $CDCl_3$, showing the presence of two different B environments in a 4:1 ratio.

As can be seen in Figure 3.30, the ^{11}B NMR spectrum obtained in $CDCl_3$ showed the presence of two different boron environments; the first peak at +19.8 ppm is in the region expected for 3-coordinate boron, and the other peak at +1.6 ppm is in the region expected for 4-coordinate boron. The 4:1 ratio of 3-coordinate:4-coordinate boron is as expected for a pentaborate anion, which contains four 3-coordinate boron atoms and one 4-coordinate boron atom. The triborate monoanion observed in **19**·2.5H_2O, contains two 3-coordinate boron atoms and one 4-coordinate boron atom and, based on this, it would be expected that the two environments would have a 2:1 ratio in a ^{11}B NMR spectrum obtained in $CDCl_3$; this was found to be the case, as can be seen in Figure 3.31. The ^{1}H, ^{13}C and ^{31}P NMR spectra obtained in D_2O were fully consistent with those expected for the PPN cation.

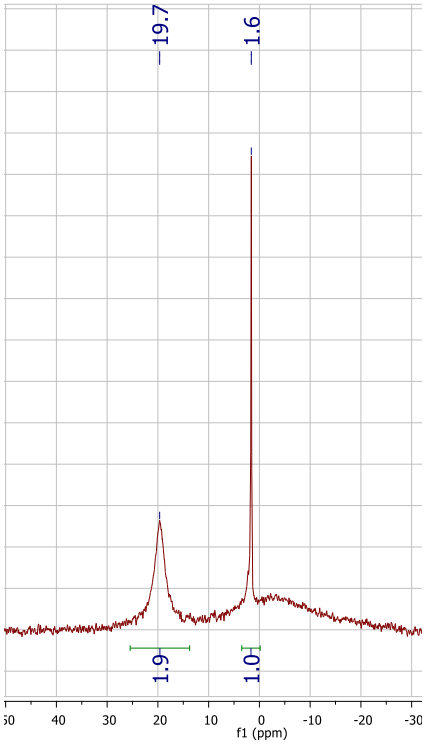

Figure 3.31: The ^{11}B NMR spectrum of 19·2.5H_2O**, obtained in $CDCl_3$, showing the presence of two different B environments in a 2:1 ratio.**

The IR spectrum of **18**·1.5H_2O was obtained as a KBr disk and showed the presence of the characteristic pentaborate peak at ~925 cm^{-1}. The presence of

broad peaks due to the OH groups were observed at ~3220-3370 cm^{-1} and peaks were also observed which were consistent with the cation. The IR spectrum of **19**·2.5H_2O was also obtained as a KBr disk and shows strong/medium peaks at 1437 cm^{-1}, 1296 cm^{-1}, 997 cm^{-1} and 855 cm^{-1} which may be assigned by reference to Jun *et al*.[251] to $\nu_{as}(B_{(3)}\text{-}O)$, $\nu_{as}(B_{(3)}\text{-}O)$, $\nu_{s}(B_{(3)}\text{-}O)$ and $\nu_{s}(B_{(4)}\text{-}O)$, respectively. In addition to this, the broad peaks at ~3200 cm^{-1} were due to the B-OH groups and H_2O present in the compound.

3.3.5.2 Thermal properties of PPN polyborate salts

The thermal properties of PPN pentaborate (**18**·1.5H_2O) and PPN triborate (**19**·2.5H_2O) were investigated in air by TGA/DSC analysis.

The TGA-DSC trace of **18**·1.5H_2O followed a two-step decomposition, with the first step occurring between 120-150 °C. This step was an endothermic process and equated to the %weight loss of 3.5 moles of H_2O; 1.5 moles of interstitial H_2O, and 2 moles of H_2O lost through condensation of the pentaborate anions. The cation oxidised *via* exothermic processes, yielding a glassy residue of B_2O_3 above 650 °C.

The TGA-DSC trace of **19**·2.5H_2O followed a three-step decomposition. The first endothermic process was due to the loss of 2.5 moles of interstitial H_2O at ~100 °C, this was followed by a second endothermic process due to the loss of a further 2 moles of H_2O due to condensation of the triborate anion. As with the pentaborate salts already reported within this chapter, the cation oxides *via* exothermic processes resulting in a glassy solid residue of B_2O_3 above >750 °C; the %weight of B_2O_3 remaining was equal to 1.5 moles, not 2.5 moles as is observed for pentaborate salts.

The presence of the interstitial H_2O molecules indicated by the thermal analyses were confirmed from the results of the elemental analyses.

3.3.5.3 Synthesis and characterization of 4,4'-bipiperidinium heptaborate dihydrate (**20**·2H_2O)

4,4'-Bipiperidine hydrochloride was first converted to the hydroxide salt using activated DOWEX anion exchange resin. The hydroxide salt was then reacted with $B(OH)_3$ in a 1:4 molar ratio in methanol/deionised water solution, which afforded the product 4,4'-bipiperidinium heptaborate dihydrate, $[C_{10}H_{22}N_2][B_7O_9(OH)_5]\cdot 2H_2O$ (**20**·2H_2O). Recrystallization of the crude material from H_2O yielded a few single-crystal XRD quality crystals of **20**·2H_2O, which are discussed in more detail in Section 3.3.5.5. The structures of the organic cation and heptaborate anion found in **20**·2H_2O are shown in Figure 3.32.

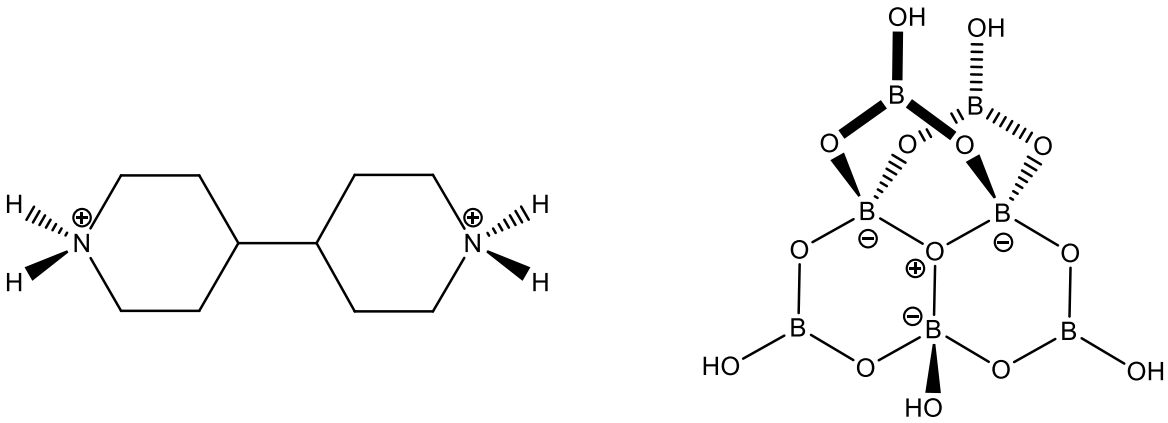

Figure 3.32: The (a) 4,4'-bipiperidinium cation and (b) heptaborate anion, $[B_7O_9(OH)_5]^{2-}$, as found in 20·2H_2O.

The heptaborate salt of **20**·2H_2O was characterized by elemental analysis, NMR and IR spectroscopy and thermal analysis. The elemental analysis of **20**·2H_2O were in good agreement with theoretical values, with the compound also found to contain two additional interstitial molecules of H_2O within its structure; this was confirmed by the thermal analysis and the single-crystal data.

^{1}H and ^{13}C NMR spectra of **20**·2H_2O obtained in D_2O were fully consistent with those expected for the 4,4'-bipiperidinium cation, with the NH, OH and BOH protons represented by a broad signal at ~4.8 ppm due to rapid exchange. The ^{11}B

NMR spectrum obtained in D_2O exhibited a single peak at +14.7 ppm which, using Equation 3.8, gives a B/1 ratio of 3.5 (7:2).

An IR spectrum of **20**·$2H_2O$ was obtained as a KBr disk and shows strong/medium peaks at 1419 cm^{-1}, 1356 cm^{-1}, 1165 cm^{-1}, 1044 cm^{-1}, 986 cm^{-1}, 855 cm^{-1} and 810 cm^{-1} which may be assigned by reference to Jun *et al*.[251] to $\nu_{as}(B_{(3)}\text{-}O)$, $\nu_{as}(B_{(3)}\text{-}O)$, $\nu_{as}(B_{(4)}\text{-}O)$, $\nu_{as}(B_{(4)}\text{-}O)$, $\nu_{s}(B_{(3)}\text{-}O)$, $\nu_{s}(B_{(4)}\text{-}O)$ and $\nu_{s}(B_{(4)}\text{-}O)$, respectively. In addition to this, the peak observed at ~810 cm^{-1} has also been observed in other heptaborate(2^-) salts containing this heptaborate isomer,[42] suggesting its potential to be a diagnostic heptaborate anion ('O^+' isomer) peak. The absence of the characteristic band for the pentaborate anion at ~925 cm^{-1} is also significant. Broad peaks at ~3400 cm^{-1} and ~3250 cm^{-1} were observed for the NH and OH groups, respectively.

3.3.5.4 Thermal properties of 4,4'-bipiperidinium heptaborate dihydrate (**20**·$2H_2O$)

The thermal properties of **20**·$2H_2O$ were investigated (in air) by TGA and DSC analysis. Thermal analyses of other non-metal cation heptaborate salts[42,43] indicate that they follow a similar trend to that observed for non-metal pentaborate salts; first by elimination of any interstitial H_2O molecules, followed by dehydration of the heptaborate anion and then oxidation of the cation to leave a glassy residue of B_2O_3.

The TGA-DSC trace for **20**·$2H_2O$ (Figure 3.33) shows that the loss of H_2O from both the interstitial H_2O molecules and the heptaborate anion occur *via* and endothermic process at ~200 °C; the %weight loss indicates the presence of two interstitial H_2O molecules, which is in agreement with elemental analysis data and single-crystal XRD data. This dehydration step is followed by exothermic oxidation of the cation, leaving the equivalent of 3.5 moles of B_2O_3 above 750 °C.

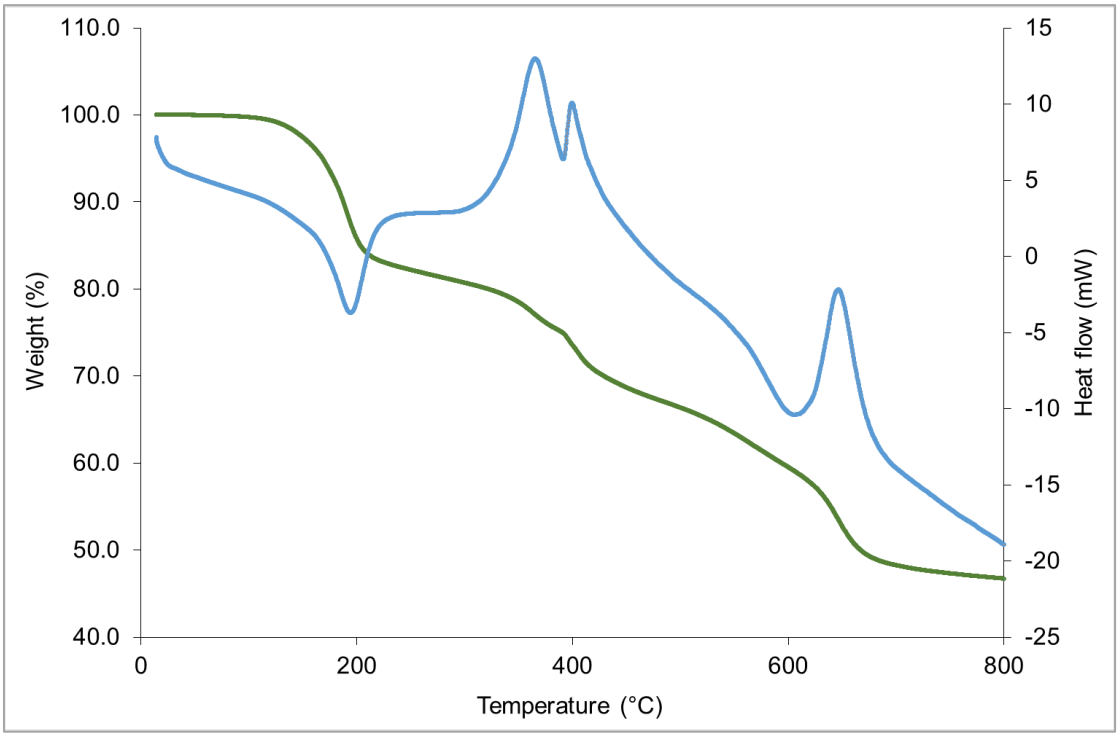

Figure 3.33: TGA (green) and DSC (blue) curve of 4,4'-bipiperidinium heptaborate dihydrate (20·2H_2O) showing the dehydration step at ~200 °C, followed by oxidation of the cation to leave residual B_2O_3 >750 °C.

3.3.5.5 Crystallographic study of 4,4'-bipiperidinium heptaborate dihydrate (**20**·2H_2O)

The crystal structure of 4,4'-bipiperidinium heptaborate dihydrate (**20**·2H_2O) is reported in this section. The spectroscopic and analytical data for the recrystallized product is given in Chapter 2, Section 2.5.20. The crystal structure was obtained and solved by the National Crystallographic Service at Southampton and the full crystallographic data is available in the appendices (NCS number 2015NCS0560).

The structure of **20**·2H_2O is characterized by having one 4,4'-bipiperidinium dication and one heptaborate dianion, as well as containing two interstitial H_2O molecules, one of which is disordered per asymmetric unit. Diagrams of the cation and anion present in **20**·2H_2O, along with the atomic numbering scheme are illustrated in Figure 3.34.

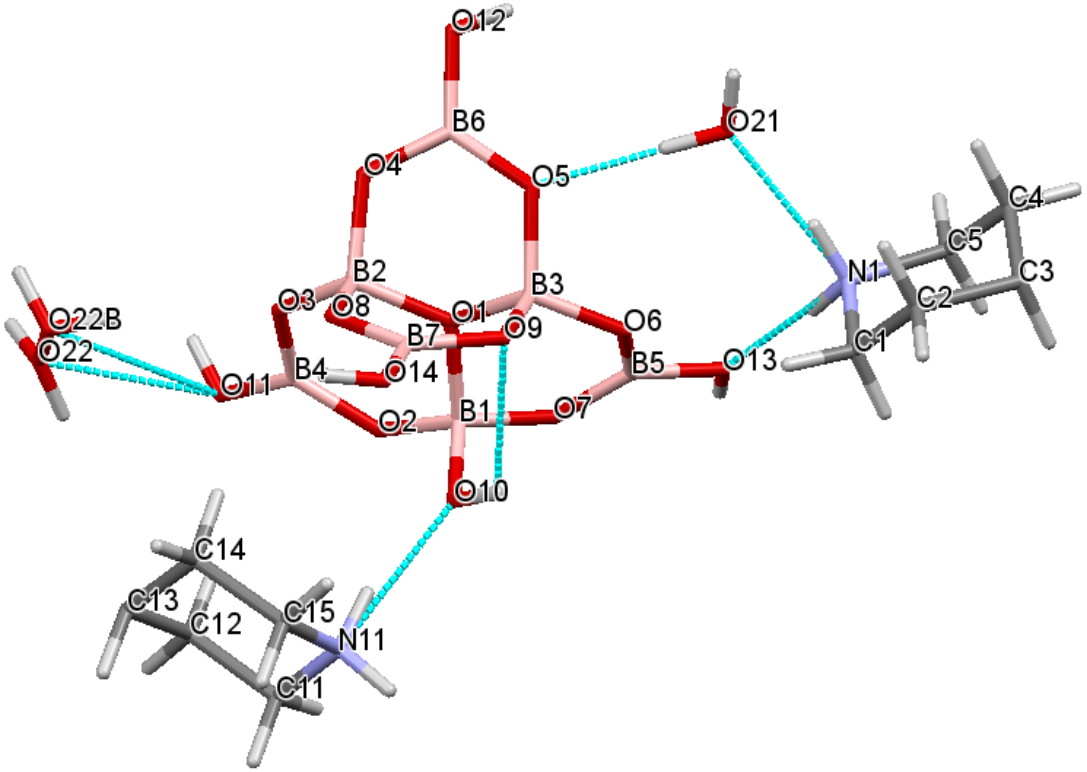

Figure 3.34: The molecular structure of 4,4'-bipiperidinium heptaborate dihydrate (20·2H_2O), illustrating the atomic numbering scheme. H-bonds are shown in blue.

The heptaborate dianion, $[B_7O_9(OH)_2]^{2-}$, observed in the solid-state structure of **20**·2H_2O is the 'O^{+}' isomer, so called due to the presence of the 'O^{+}' atom in the centre of the fused boroxole rings. The observed B-O bond lengths and internuclear angles are given in Table 3.11 and show that the B-O distances to the 4-coordinate boron centres (B1 – B3) are significantly longer than those involving 3-coordinate boron atoms (B4 – B7).

Table 3.11: The observed B-O bond lengths (Å) and internuclear angles (°) for the heptaborate dianion, $[B_7O_9(OH)_5]^{2-}$, found in compound 20·2H_2O.

B_{tet} bond lengths (Å)	B_{tet} internuclear angles (°)	B_{trig} bond lengths (Å)	B_{trig} internuclear angles (°)
1.438(3) – 1.520(2)	104.18(12) – 112.52(18)	1.355(2) – 1.377(4)	115.85(13) – 124.08(18)

Internuclear angles within the heptaborate dianion range from 104.18° – 112.52° at the tetrahedral B atoms, and from 115.85° – 124.08° at the trigonal B atoms, which are consistent with sp^3 and sp^2 hybridization, respectively. The bond lengths and internuclear distances of the B-O bonds found in compound **20**·2H_2O are similar to those observed in other non-metal heptaborate salts containing the 'O^+' isomer.[42,43]

Compound **20**·2H_2O is able to form numerous H-bond interactions which are summarised in Table 3.12. Unlike the pentaborate anions previously reported within this chapter, the heptaborate anion in **20**·2H_2O contains a weak intramolecular H-bond from the O10-H10 to the O9 atom (2.54 Å); this type of intramolecular H-bond interaction has been observed in other non-metal heptaborate salts containing this this heptaborate isomer,[43] and was also observed in computational studies of this isomer which are discussed in Chapter 4, Section 4.3.3.

Table 3.12: The H-bonding interactions found within the solid-state structure of 4,4'-bipiperidinium heptaborate dihydrate (20·2H_2O).

D-H···A	*d*(H···A) (Å)	*d*(D···A) (Å)	∠DHA (°)
O10-H10···O9	2.54	3.0652(18)	121.7
O12-H12···O11^{iii}	2.00	2.756(2)	148.8
O13-H13···O7^{iv}	1.91	2.7479(15)	175.1
O14-H14···O8^{v}	1.89	2.720(2)	171.0
N11-H11A···O4^{vi}	1.84	2.725(3)	162.9
N11-H11B···O10	1.83	2.715(2)	164.0
N1-H1A···O21	1.85	2.7488(18)	169.7
N1-H1B···O13	2.00	2.9026(17)	172.5
O21-H21A···O2^{iii}	1.97	2.8349(16)	177.1
O21-H21B···O5	1.95	2.8058(16)	168.9
O22B-H22A···O3	2.31	3.1739(17)	171.6
O22B-H22A···O11	2.41	2.860(3)	112.6
O22B-H22B···O14^{vii}	2.21	2.688(3)	114.5
O22-H22C···O9^{vii}	2.34	3.117(4)	149.6
O22-H22C···O14^{vii}	1.63	2.362(3)	140.3
O22-H22D···O12^{viii}	2.19	2.983(3)	152.0

Symmetry transformations used to generate equivalent atoms: (i) -x+1/2,-y+3/2,-z+1; (ii) -x+2,y,-z+3/2; (iii) x+1/2,y-1/2,z; (iv) -x+1,y,-z+3/2; (v) -x+1,-y+1,-z+1; (vi) x,y+1,z; (vii) x-1/2,y-1/2,z; (viii) x-1/2,y+1/2,z.

The heptaborate dianion is also able to partake in intermolecular H-bonding with other heptaborate anions and the interstitial H_2O molecules to form a giant three-dimensional anionic lattice, with the 4,4'-bipiperidinium cations sitting in the 'cavities' of the lattice and partaking in H-bond interactions (Figures 3.35 and 3.36). Each heptaborate dianion in **20**·2H_2O forms two $R_2^2(8)$ 8-membered rings with other heptaborate anions at O7 and O8 acceptor sites, and one C(8) chain at an O11 acceptor site. In addition to this, the heptaborate dianion accepts H-bonds from the NH groups of the dication at O10 and O13 acceptor sites. The N11-H11A of the dication also forms an H-bond to an O4 heptaborate acceptor site in the next unit cell, and from the N1-H1A to one of the interstitial H_2O molecules (O21).

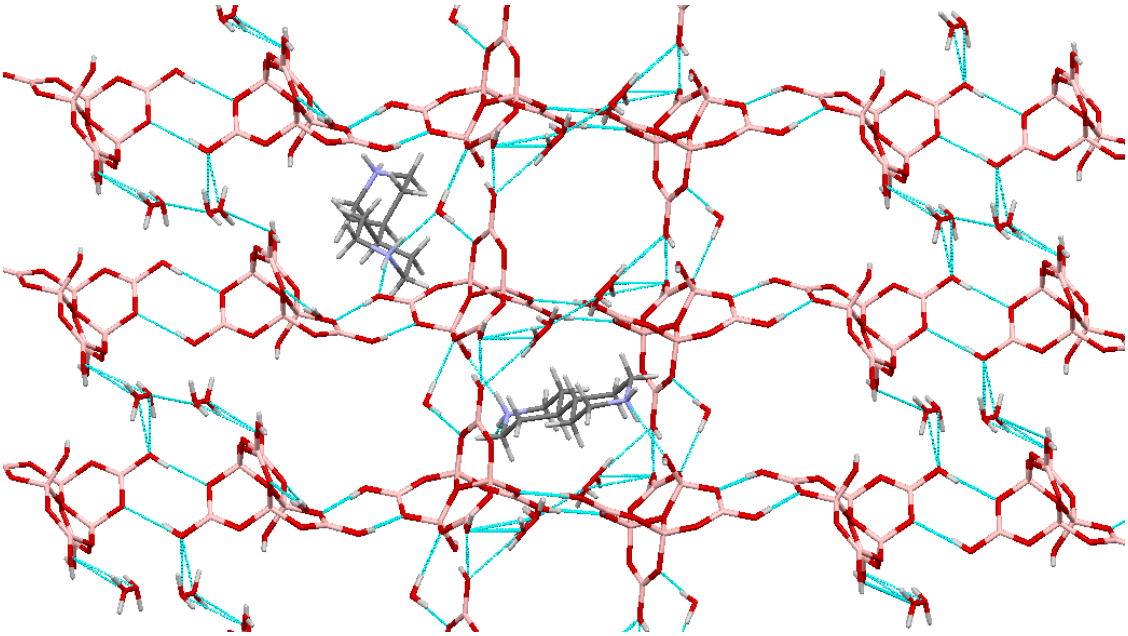

Figure 3.35: The H-bonded anionic lattice of 4,4'-bipiperidinium heptaborate dihydrate (20·2H_2O). The interstitial H_2O molecules facilitate the formation of the anionic lattice, whilst the dications occupy the 'cavities' of the lattice and also partake in H-bonding interactions.

The interstitial H_2O molecules also form numerous H-bonds within compound **20**·2H_2O. The H_2O molecules which is free from disorder forms an H-bond from the N1-H1B with the O5 acceptor site of the heptaborate anion within the same asymmetric unit, and from the N1-H1A to the O2 heptaborate acceptor site in the next asymmetric unit. The disordered H_2O forms multiple H-bonds; the O22-H22C forms a bifurcated H-bond to both the O9 and O14 acceptor sites of a heptaborate

anion in the next asymmetric unit, and from the O22-H22D to the O12 acceptor site in the next asymmetric unit. The O22B-H22A also forms a bifurcated H-bond to the O3 and O11 acceptor sites of the heptaborate within the same asymmetric unit, and from the O22B-H22B to the O14 acceptor site of a heptaborate in the next asymmetric unit.

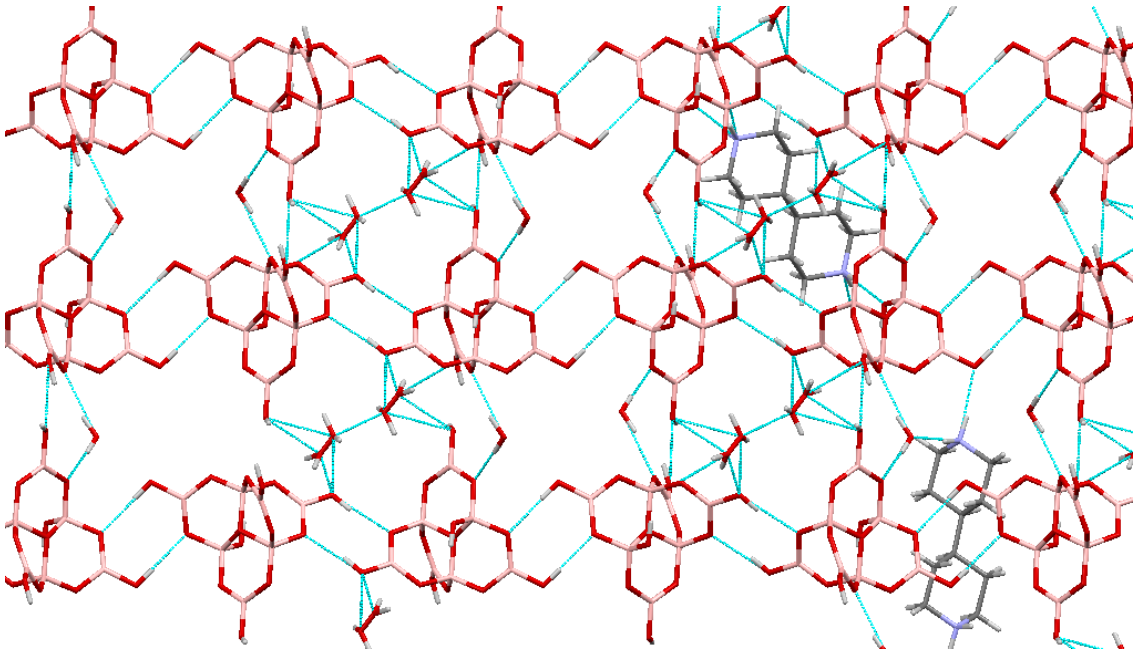

Figure 3.36: The H-bonded anionic lattice of 4,4'-bipiperidinium heptaborate dihydrate (20·2H_2O) as viewed along the b axis. The interstitial H_2O molecules facilitate the formation of the 3D anionic lattice, whilst the dications occupy the 'cavities' of the lattice and also partake in H-bonding interactions.

3.3.5.6 Synthesis and characterization of dibenzylammonium pentaborate (**21**·1.5H_2O)

The synthesis dibenzylammonium pentaborate sesquihydrate (**21**·1.5H_2O) and the attempted synthesis of tribenzylammonium pentaborate (see Chapter 2, Section 2.7.12) was carried out by reacting the free amine with boric acid in a 1:5 molar ratio in methanol/deionised water solution. A pentaborate salt was obtained (**21**·1.5H_2O) in high yield from the reaction of $B(OH)_3$ with dibenzylamine, but the reaction of $B(OH)_3$ with tribenzylamine did not proceed as the tribenzylamine instantaneously

precipitated out of solution upon addition of H_2O to the reaction mixture. The organic amines used in these reactions are shown in Figure 3.37.

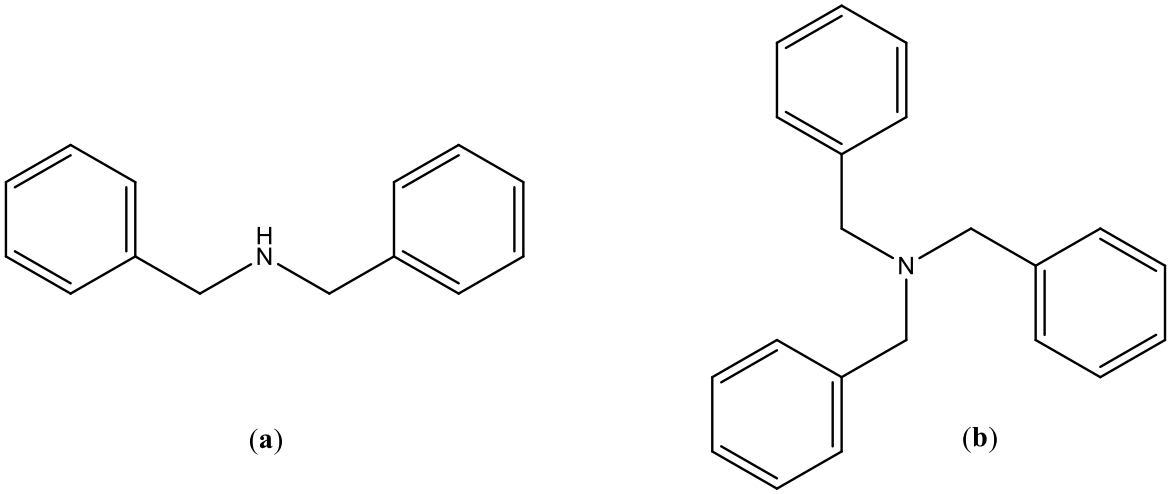

Figure 3.37: The structures of (a) dibenzylamine and (b) tribenzylamine which were used in the synthesis of dibenzylammonium pentaborate sesquihydrate (21·1.5H_2O) and the attempted synthesis of tribenzylammonium pentaborate, respectively.

The sesquihydrated dibenzylammonium pentaborate salt (**21**·1.5H_2O) was characterized by elemental analysis, IR and NMR spectroscopy, thermal analysis and powder X-ray diffraction. Elemental analysis of **21**·1.5H_2O indicated the presence of 1.5 interstitial molecules of H_2O present within the crude material.

Powder X-ray diffraction studies indicated that the crude pentaborate salt (**21**·1.5H_2O) was a crystalline material and recrystallization of the crude material led to a few crystals of non-hydrated **21** which were suitable for single-crystal XRD analysis. Single-crystal XRD analysis has not been carried out and so the composition of **21** has been formulated on the basis of the elemental analysis, spectroscopic analysis and thermal analysis.

NMR spectroscopic analysis of **21**·1.5H_2O and **21** were in agreement with previously reported non-metal cation pentaborate salts, with ^{11}B NMR spectra (obtained in D_2O) showing the three characteristic signals observed for a pentaborate salt at ~19, 13 and 1 ppm, which arise from the $B(OH)_3$/$[B(OH)_4]^-$,

$[B_3O_3(OH)_4]^-$ and 4-coordinate boron centre of the $[B_5O_6(OH)_4]^-$ species, respectively.[8]

IR spectra of **21**·1.5H_2O and **21** (obtained as a KBr disks) showed the presence of the strong characteristic pentaborate peak at ~925 cm^{-1}. In addition to this, the asymmetric and symmetric stretching of the 3- and 4-coordinate B-O bonds are given in Table 3.13.

Table 3.13: The observed symmetric and asymmetric stretches of the $B_{(3)}$-O and $B_{(4)}$-O bonds found in the non-hydrated dibenzylammonium pentaborate (21) and dibenzylammonium pentaborate sesquihydrate (21·1.5H_2O**).**

ν_{as} $B_{(3)}$-O	ν_{as} $B_{(4)}$-O	ν_{s} $B_{(3)}$-O	ν_{s} $B_{(4)}$-O
1423, 1305	1093, 1024	916	781

Peaks consistent with the NH and OH groups were observed as broad peaks in the regions of ~3200 cm^{-1} and ~3000 cm^{-1}, respectively.

3.3.5.7 Thermal properties of dibenzylammonium pentaborate

The thermal analysis of the crude and recrystallized dibenzylammonium pentaborate salts were investigated using TGA-DSC analysis (in air). The crude and recrystallized materials (**21**·1.5H_2O and **21**, respectively) showed a dehydration step equal to the loss of two H_2O molecules which occurs from dehydration of the pentaborate anion at ~220 °C, followed by oxidation of the cation to leave a glassy residue of B_2O_3 above 750 °C. The crude material (**21**·1.5H_2O) showed an additional dehydration step at ~150 °C which corresponded to the loss of the 1.5 additional molecules of H_2O. The presence of this additional dehydration step complemented the results of the elemental analysis, which suggested the interstitial H_2O was present.

3.3.6 Attempted syntheses of polyborate salts

3.3.6.1 Attempted synthesis of (substituted) 4,4'-trimethylenedipiperidinium triborates

The synthesis of 4,4'-trimethylenedipiperidinium triborate and 4,4'-trimethylene*bis*(*N*-methylpiperidinium) triborate were attempted by reacting the free amines with $B(OH)_3$ in a 1:2 molar ratio in methanol/deionised water solution.

^{1}H and ^{13}C NMR analysis of the resulting solid from the reaction of 4,4'-trimethylenedipiperidine with $B(OH)_3$ confirmed the presence of the amine, but no peak was observed in the ^{11}B NMR spectrum (obtained in D_2O). No further characterization was performed on this solid material due to the absence of any boron present in the isolated 'product'.

^{1}H and ^{13}C NMR analysis of the resulting solid from the reaction of 4,4'-trimethylene*bis*(*N*-methylpiperidine) with $B(OH)_3$ again confirmed the presence of the cation, with a broad singlet observed at ~4.8 ppm due to rapid exchange and overlapping of the OH and suspected NH protons. A single peak was observed in the ^{11}B NMR spectrum (obtained in D_2O) at +3.5 ppm. This chemical shift did not correspond to a triborate anion, which would be expected to be at ~13 ppm. It was assumed a polyborate salt had been prepared and, using Equation 3.8, the B/1 ratio was calculated as 1.1.

The unidentified crude solid was recrystallized from H_2O to give needle-like crystals of the unexpected product, 4,4'-trimethylene*bis*(*N*-methylpiperidine)·$B(OH)_3$, **22**. The recrystallized material was characterized by elemental analysis, spectroscopic analysis, thermal analysis and powder X-ray diffraction. The solid-state structure of **22** was confirmed by single-crystal XRD studies and are discussed in Section 3.3.6.3.

The elemental analysis data of **22** was in good agreement with theoretical values, which were consistent with the co-crystallization of one $B(OH)_3$ molecule with one molecule of 4,4'-trimethylene*bis*(*N*-methylpiperidine). The %B composition within the product was determined using a gravimetric method (Chapter 2, Section 2.2) and were also in good agreement with theoretical values.

The ^{11}B NMR spectrum (obtained in D_2O) showed a strong peak at +4.7 ppm and ^{1}H and ^{13}C NMR spectra were consistent with those expected for 4,4'-trimethylene*bis*(*N*-methylpiperidine).

The IR spectrum (obtained as KBr disks) of **22** showed the peaks consistent with the organic amine and showed a broad peak at 3271 cm^{-1} which was consistent with the OH stretching in the $B(OH)_3$ molecule and a peak at 1423 cm^{-1} which corresponds to the asymmetric stretching of the $B_{(3)}$-O bond.[251] The IR spectrum did not show any other characteristic peaks for $B(OH)_3$, for which significant peaks at ~ 1193 cm^{-1} and ~883 cm^{-1} corresponding to the asymmetric and symmetric $B_{(3)}$-O bonds, respectively, would be expected.[251]

3.3.6.2 Thermal properties of 4,4'-trimethylene*bis*(*N*-methylpiperidine)·$B(OH)_3$ (**22**)

The thermal properties of the co-crystallized 4,4'-trimethylene*bis*(*N*-methylpiperidine)·$B(OH)_3$ compound (**22**) were investigated using TGA-DSC analysis (in air). The thermal decomposition proceeded *via* a two-step weight loss; the first corresponded to the endothermic dehydration of the $B(OH)_3$ molecule at ~60 °C which is consistent with the temperature at which $B(OH)_3$ dehydrates. The amine then underwent oxidation *via* exothermic processes, leaving a glassy residue of B_2O_3 above 600 °C.

3.3.6.3 Crystallographic studies of the co-crystallized species 4,4'-trimethylene*bis*(*N*-methylpiperidine·$B(OH)_3$ (**22**)

The crystal structure of **22** is reported in this section, with spectroscopic and analytical data given in Chapter 2, Section 2.5.22. The crystal structure was obtained and solved by the National Crystallographic Service at Southampton and the full crystallographic data is available in the appendices (NCS number 2014NCS0908).

The solid-state structure of **22** is free from disorder and comprises of one molecule of $B(OH)_3$ and one molecule of 4,4'-trimethylene*bis*(*N*-methylpiperidine) per asymmetric unit (Figure 3.38).

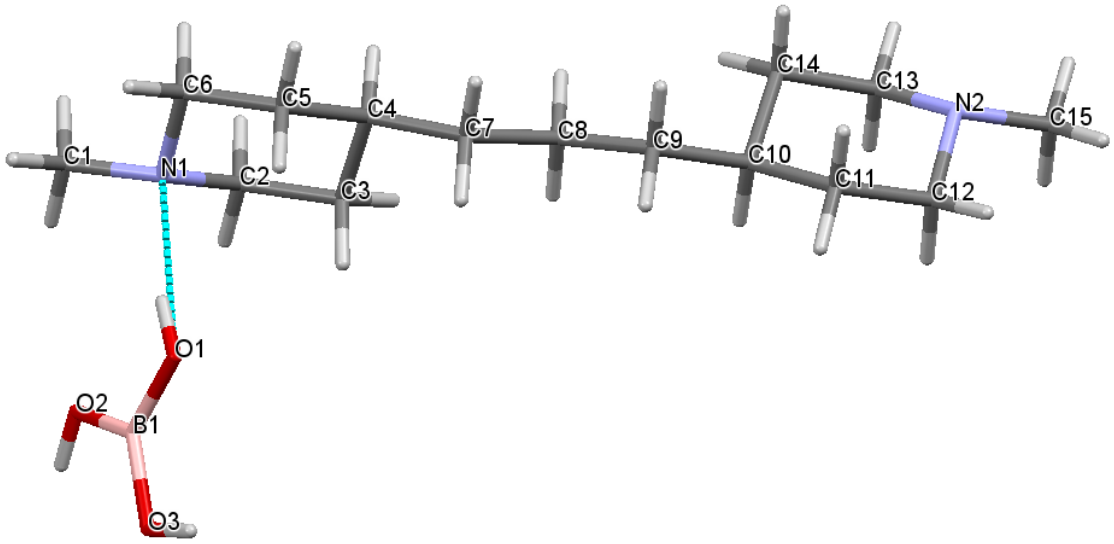

Figure 3.38: The molecular structure of 4'-trimethylene*bis*(*N*-methylpiperidine·B(OH)$_3$ (22), illustrating the atomic numbering scheme.

The average B-O bond lengths observed in **22** is 1.368 Å, which is similar to the 3-coordinate B-O bond lengths observed in all of the polyborate salts reported within this Chapter. In addition to this, the average B-O internuclear angles (120.00°) were consistent with sp^2 hybridization.

The $B(OH)_3$ molecule partakes in H-bonding; the O1-H1 forms an H-bond with the N1 atom of the organic amine. The N2 atom of the amine forms an H-bond with the O2-H2 from a $B(OH)_3$ molecule from another unit cell. The O3-H3 from the $B(OH)_3$ molecule forms an H-bond with the O1 atom of another $B(OH)_3$ molecule in another unit cell; these two $B(OH)_3$ molecules H-bond together and form a $R_2^2(8)$ 8-membered ring (Figure 3.39). The amines and $B(OH)_3$ molecules H-bond together, forming a 2D infinite sheet which arranges itself in a 'step'-like manner (Figure 3.40).

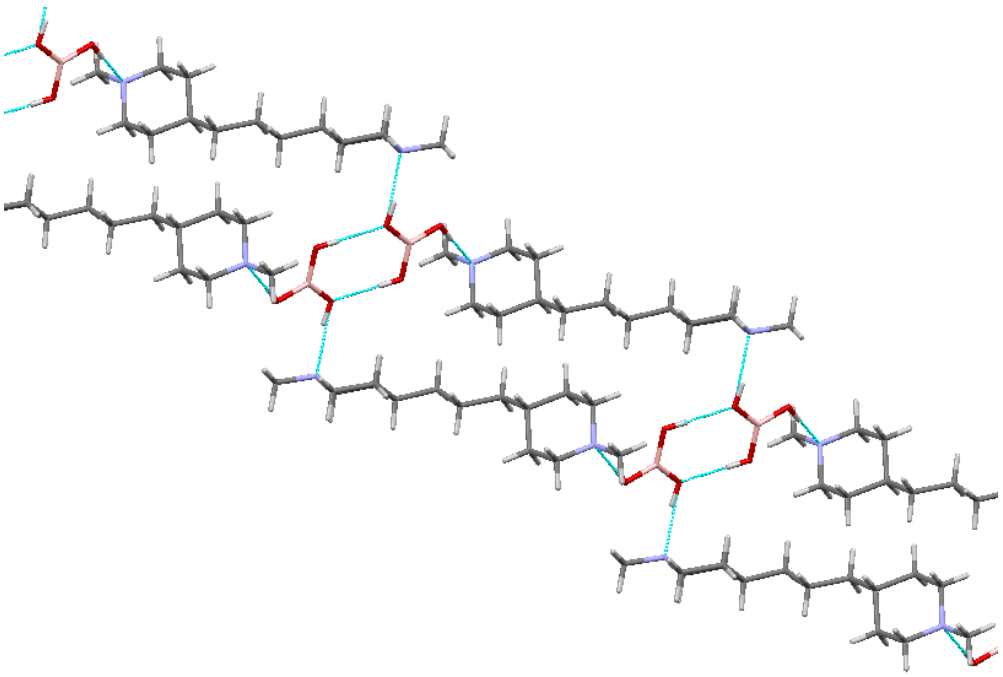

Figure 3.39: The H-bonding interactions observed in 22, looking down on to the $R_2^2(8)$ rings formed between $B(OH)_3$ molecules.

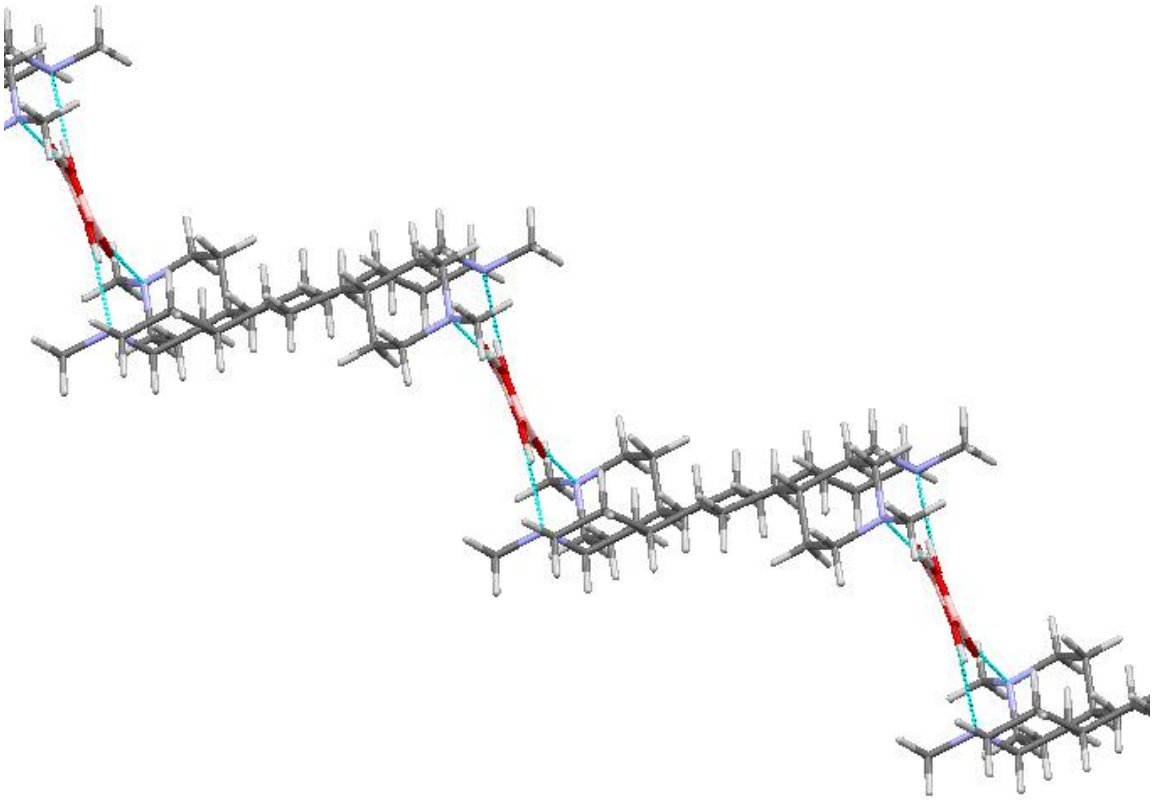

Figure 3.40: The molecular structure of 22, which forms a 'step'-like structure comprised of the organic amine and $B(OH)_3$ molecules H-bonded together.

3.3.6.4 Carboranyl-(substituted)-ammonium pentaborate salts

The syntheses of polyborate salts containing amino-*o*-carboranes as the counter cations were attempted. The amino-*o*-carboranes synthesized for use in the attempted syntheses of polyborate salts are shown in Figure 3.41.

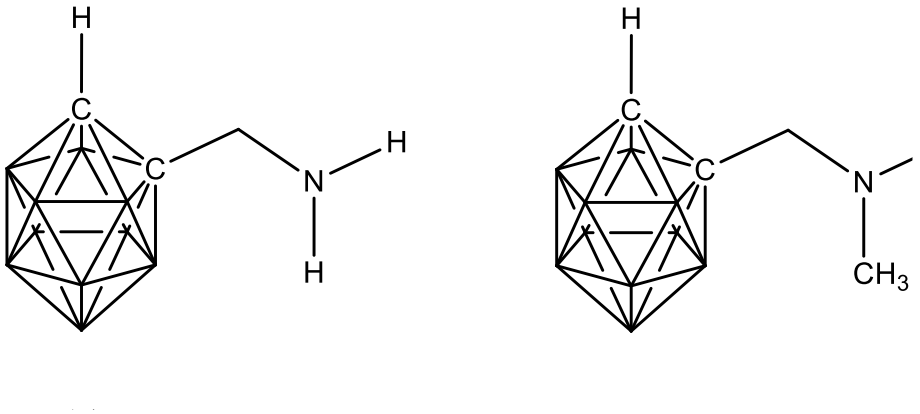

Figure 3.41: The structures of (a) aminomethyl-*o*-carborane and (b) *N*,*N*-dimethylaminomethyl-*o*-carborane, which were synthesized to be used as potential counter cations in the formation of polyborate salts. Unmarked polyhedral vertices are boron atoms with associated *exo* hydrogen atoms.

The hydrochloride salt of aminomethyl-o-carborane was prepared from a four step synthesis. Removal of the chloride ion proved difficult; the use of DOWEX anion exchange resin destroyed the carborane cluster, the use of silver(I) oxide also failed to exchange the chloride ion and neutralisation was difficult as the use of strong bases was already known to degrade the cluster.[252] The free amine was eventually obtained by a slow neutralisation using a very dilute solution of NaOH and recovering the free amine in ether. The free amine was then reacted with 5 molar equivalents of $B(OH)_3$, in a methanol/deionised water solution. NMR analysis of the product showed it to be a mixture of starting materials. The reaction was repeated under solvothermal conditions to help promote the reaction under high pressure and temperature, but again resulted in a mixture of starting materials. It was then assumed that the electron withdrawing nature of the boron cluster and the acidity of

the methylene group between the amino group and the carborane rendered the amino group to be non-basic.

Methylation of the amino group may increase its basicity and a method by Heying *et al*.[235] was used to synthesise *N,N*-dimethylaminomethyl-*o*-carborane. Reaction of the dimethylated carborane with $B(OH)_3$, using the same methods as for aminomethyl-*o*-carborane, again yielded a mixture of starting materials, indicating that methylation of the amine was not enough to increase its basicity for a reaction with $B(OH)_3$ to occur.

3.3.6.5 Larger miscellaneous NMC polyborate salts

This section discusses the attempted syntheses of polyborate salts not covered elsewhere within this chapter.

The synthesis of polyborates salts from the reaction of $B(OH)_3$ with the following amine and ammonium hydroxides was attempted: choline hydroxide, glucosamine hydroxide and hexadecylamine. All three of these amines are basic, with pK_a values of the protonated bases in the range of 10.63 – 13.9, and their structures are given in Figure 3.42.

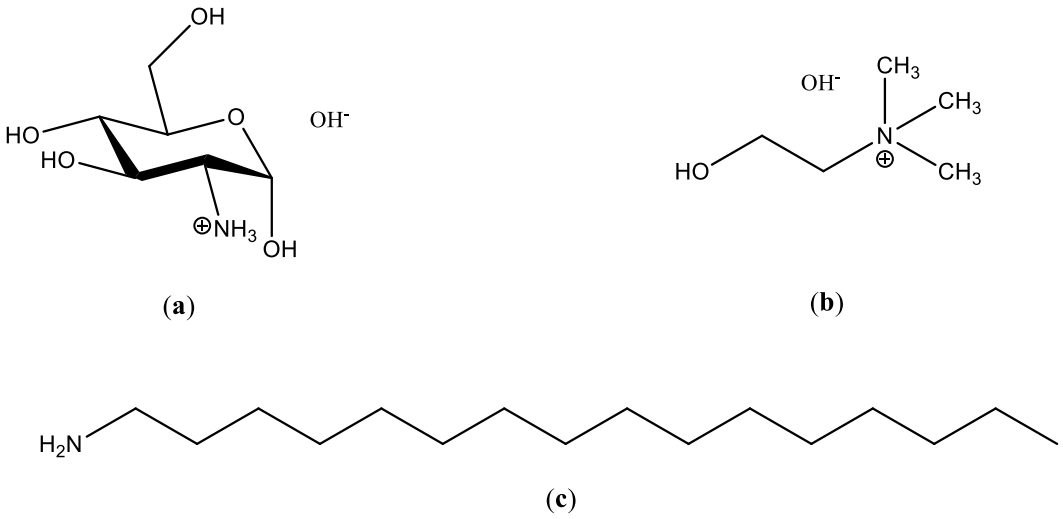

Figure 3.42: The structures of (a) glucosamine hydroxide, (b) choline hydroxide and (c) hexadecylamine.

A pentaborate salt containing choline as the counter cation has already been reported in the literature;[8] the synthesis of a triborate salt from the reaction of choline hydroxide with $B(OH)_3$ was attempted using solvothermal methods. Multiple attempts (including an attempt to obtain the reported pentaborate salt) yielded a charred insoluble solid; the inference from this is that the choline hydroxide is degraded under these solvothermal conditions and this method cannot be used to prepare polyborate salts containing choline.

The reaction of $B(OH)_3$ with hexadecylamine was attempted in a 5:1 molar ratio *via* the solvothermal method, using a mixture of pyridine and deionised water as the solvent, with the aim of obtaining a pentaborate salt; pyridine was used in order to aid the solubility of the hydrophobic amine. The resulting solid was found to be a mixture of starting materials. This reaction was also attempted using the room temperature methanol/deionised water solution but also resulted in a mixture of start materials. Whilst this amine is basic enough to react with $B(OH)_3$ (pK_a = 10.63), it is the solubilities of the reagents that is believed to be the cause of no product formation; $B(OH)_3$ is soluble in aqueous solutions, whereas hexadecylamine is soluble in organic solvents, therefore the two reagents are unlikely to be dissolved in the same solvent to promote an interaction between them.

Glucosamine was chosen as a potential cation as its structure contains multiple OH and NH bonds which could form interesting H-bond interactions within a polyborate salt. Glucosamine was purchased as glucosamine hydrochloride and was first converted to the hydroxide salt using activated DOWEX anion exchange resin. The hydroxide salt was reacted with $B(OH)_3$ in a 1:5 molar ratio with the resulting solid found to be a mixture of starting materials only. The pK_a value of protonated glucosamine is 13.9, indicating that this is a basic material, and is readily soluble in aqueous solutions. It is unknown why the amino-sugar did not react with $B(OH)_3$ to form a polyborate salt; it is possible that the hydrochloride salt was not fully converted to the hydroxide salt before reacting with $B(OH)_3$, which would prevent the reaction from occurring.

3.4 Summary

Twenty-one new polyborate salts have been prepared in high yields and characterized using spectroscopic (NMR, IR) and analytical (elemental analysis, melting point, X-ray diffraction, TGA-DSC analysis) techniques. The crystal structures of the following pentaborate salts are reported within this chapter: pyrrolidinium pentaborate (**1**), *N*-methylpyrrolidinium pentaborate·½ acetone (**2**·½CH_3COCH_3), *N,N*-dimethylpyrrolidinium pentaborate (**3**), 2-hydroxymethylpyrrolidinium pentaborate hemihydrate (**4**·½H_2O), (2-hydroxyethyl)-*N*-methylpyrrolidinium pentaborate·0.3 hydrate (**5**·0.3H_2O), 4-aminobenzylammonium pentaborate hemihydrate (**9**·½H_2O), *N,N*-dimethyl-1-adamantylammonium pentaborate·boric acid monohydrate (**14**·$B(OH)_3$·H_2O), *N,N,N*-trimethyl-1-adamantylammonium pentaborate trihydrate (**15**·3H_2O), and *N,N,N*-trimethyl-2-adamantylammonium pentaborate trihydrate (**17**·3H_2O).

All of these pentaborate salts show extensive H-bonding within their supramolecular structures and form giant H-bonded anionic lattices. The configuration of the pentaborate lattice depends on the size of the cation which needs to fill the 'cavity' of the lattice and many pentaborates form a 'brickwall' type structure through α,α,α,β anion-anion interactions; this 'brickwall' structure can accommodate cations of varying sizes and may even 'expand' by using co-crystallized 'spacer' molecules. Many of the H-bond interactions were observed as repetitive motifs, which are computationally modelled in Chapter 4.

The crystal structure of a heptaborate salt, 4,4'-bipiperidinium heptaborate dihydrate (**20**·2H_2O) is also reported within this chapter. As with the pentaborate salts, the heptaborate anions form a 3D anionic lattice, held together *via* extensive H-bond interactions. In addition to intermolecular H-bonding, the heptaborate anion observed in **20**·2H_2O also contained a weak intramolecular H-bond; this type of H-bonding is also observed within the computational studies undertaken in Chapter 4.

In addition to the synthesis and characterization of the twenty-one polyborate salts, a co-crystallized species containing $B(OH)_3$ and 4,4'-trimethylene*bis*(*N*-methylpiperidine) (**22**) has also been synthesized and its crystal structure reported.

Chapter 4:

Computational studies of polyborate anions

The work presented within this chapter has been published in the following journal articles:
M.A. Beckett, S.J. Coles, R.A. Davies, P.N. Horton and C.L. Jones, *Dalton Trans.*, 2015, **44**, 7032-7040.
R.A. Davies, M.A. Beckett and C.L. Jones, *Phosphorus, Sulfur Silicon Relat. Elem.* 2016, **191**, 4, 633-637.

4.1 Introduction

Polyborate salts containing organic (non-metal) cations are easily prepared in aqueous solution. Many of these salts contain the pentaborate anion, $[B_5O_6(OH)_4]^-$, although there have also been reports of rarer anions containing three,[21, 54] four,[50, 55,83] seven,[23,42,43] eight,[15] nine,[17,44] fourteen[20] and fifteen[38] B atoms. The reason for the different anion types occurring is due to the fact that $B(OH)_3$ in basic aqueous solution forms a dynamic combinatorial library[121] (DCL) of polyborate anions whose concentrations are pH and boron concentration dependent.[240] However, in mildly basic solutions it is estimated that <5% of the total boron is in the form of the pentaborate anion, $[B_5O_6(OH)_4]^-$, with the triborate monoanion, $[B_3O_3(OH)_4]^-$, and the tetraborate dianion, $[B_4O_5(OH)_6]^{2-}$, the dominant species.[122,253,254] Beckett *et al*.[255] recently performed density functional theory (DFT) studies on the relative stabilities of the different isolated polyborate anion types and concluded that the order of stability follows the monoborate, $[B(OH)_4]^-$, > triborate monoanion, $[B_3O_3(OH)_4]^-$, > pentaborate anion, $[B_5O_6(OH)_4]^-$, > triborate dianion, $[B_3O_3(OH)_5]^{2-}$, > tetraborate dianion, $[B_4O_5(OH)_4]^-$. Contrary to this, however, it is the pentaborate anion, $[B_5O_6(OH)_4]^-$, which is the most commonly observed polyborate anion type to crystallize from aqueous solution. The structure-directing cations within the salts can influence the polyborate salt structures by size, charge, and their ability to form strong H-bond interactions;[69] H-bonds are ranked high for intermolecular interaction energies in crystal engineering.[256] H-bond interactions between polyborate anions are ubiquitous[247] in polyborate salts, although cation-anion interactions also play a significant role in the solid-state energetics.[69]

Isolated pentaborate anions, $[B_5O_6(OH)_4]^-$, can associate *via* H-bonding, forming intermolecular rings and continuous chains. As discussed in Chapter 1, the intermolecular H-bonding patterns conform to a systematic nomenclature devised by Etter.[107] Briefly, H-bond intermolecular association of the anions resulting in ring formations are denoted ‘R’, and intermolecular association resulting in continuous H-bonded chains are denoted ‘C’. The number of atoms partaking in the H-bond motif is given in parenthesis, whilst for ring motifs the number of H-bond donor and acceptor sites are represented in the subscript and superscript values immediately after the motif letter: *e.g*. $\mathrm{R}_2^2(8)$.

In addition to the Etter nomenclature, Schubert *et al*.[15] describe the position of the H-bond acceptor sites within the pentaborate anions as being α, β or γ, relative to the tetrahedral boron centre (Figure 4.1).

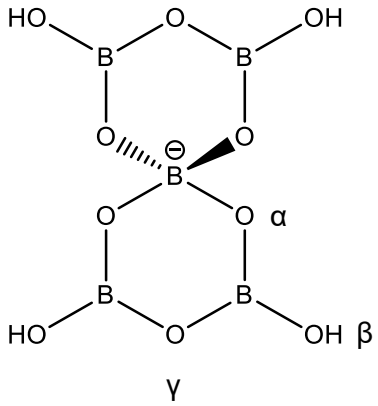

Figure 4.1: The pentaborate anion, $[B_5O_6(OH)_4]^-$, illustrating the labelling scheme used by Schubert *et al*.[15] to show H-bond acceptor sites.

There are four possible H-bond donor interactions per pentaborate anion unit and ten potential H-bond acceptor sites. The most commonly observed interactions are the 8-membered rings, $R_2^2(8)$, although $R_2^2(12)$ 12-membered rings are also observed. Continuous C(8) chains are also observed within pentaborate H-bonded anionic frameworks; these contain only one H-bond interaction between the pentaborate anions. The H-bonding between pentaborate anions can occur in a number of varying configurations; some configurations occur frequently and some configurations are unique to particular structures.[9] The α,α,α,β acceptor-site configuration is particularly common, with both the 'herringbone'[37,87] and 'brick wall'[66,108] variants reported, both of which contain a C(8) chain as the H-bond interaction at the β acceptor site.[49,66,243]

Density functional theory (DFT) investigations of polyborate anions are rare, with only two papers previously reported in the literature. Zhou *et al*.[257] investigated the different optimized geometries, energies and vibrational frequencies of smaller polyborate anions in both the solvated and gaseous phases; measurements were carried out on polyborates containing up to five boron atoms. Beckett *et al*.[255] investigated the isolated polyborate anions in the gas phase, and expanded on

Zhou's study to include polyborates containing up to seven boron atoms, including both heptaborate isomers found in solid-state structures. Both of these DFT studies used the Becke-3-Lee-Yang-Parr (B3LYP) functional, but differed on the basis sets used. Computational studies on other boron-oxygen compounds can also be found in the literature, including investigations in to the infrared vibrational spectra of boric acid,[258,259] and the hydration, acidity and NMR shifts of boric acid;[260,261] H-bonding in boronic acid dimers,[262-264] and investigation into the structures of boroxines.[265,266]

Quantum theory of atoms in molecules (QTAIM) was devised by Bader in 1990[267] and can be used to give an indication of the relative strength of an interaction between two nuclei by comparing the electron density at the bond critical point (BCP), ρ_b.[268] Weak interactions are indicated by smaller electron density values, bond and ring critical point (RCP) coalescence or the lack of a BCP between two nuclear critical points (NCP). The Laplacian of the electron density, $\nabla^2\rho_b$, is calculated by summing the eigenvalues (λ_1, λ_2 and λ_3) of the Hessian matrix (Equation 4.1), with a negative value indicating a concentration of electron density (*i.e*. a covalent interaction). A positive Laplacian value would indicate a depletion of electron density (*i.e*. a closed-shell electrostatic interaction such as an H-bond).

$$\nabla^2(\rho_b) = \lambda_1 + \lambda_2 + \lambda_3 \qquad (4.1)$$

The bond ellipticity, ε, (defined by Equation 4.2) measures the extent at which density is preferentially accumulated in a given plane containing the bond path:

$$\varepsilon = \frac{\lambda_1}{\lambda_2} - 1 \quad \text{(where } |\lambda_1| \geq |\lambda_2|) \qquad (4.2)$$

When the ellipticity, ε, is zero, this is indicative of cylindrically symmetrical bonds such those found in idealised single or triple bonds. In contrast to this, if the ellipticity is significantly greater than zero, this indicates double bond character.

Critical points can be classified according to rank (ω) and signature (σ). The rank is the number of non-zero curvatures of ρ at the critical point; for most molecular systems, ρ = 3. The signature is the sum of the signs of the curvatures. There are four stable types of critical points:

- (3, -3) nuclear critical point (NCP, 0-D, magenta dot)
- (3, -1) bond critical point (BCP, 1-D, red dot)
- (3, +1) ring critical point (RCP, 2-D, yellow dot)
- (3, +3) cage critical point (CCP, 3-D, green dot)

All QTAIM bond paths within this chapter obey the Poincaré-Hopf relationship for molecular systems (Equation 4.3).

$$n_{NCP} - n_{BCP} + n_{RCP} - n_{CCP} = 1 \quad (4.3)$$

A ring critical point will always be found in the interior of a ring of chemically bonded atoms; a cage critical point arises when several rings are connected and enclose an interstitial space.

4.2 Aims of the chapter

The aims of the chapter were threefold. Firstly, to use DFT and QTAIM to model the pentaborate anions and investigate the binding energies of the H-bonds found in the C(8), $R_2^2(8)$ and $R_2^2(12)$ motifs which occur when the pentaborate anions interact with one another.

Secondly, only one form of the hexaborate anion, $[B_6O_7(OH)_6]^{2-}$, is known to exist in the solid-state, with this being the 'O^+' isomer found in the metal cation hexaborate salt: [1-cyanopiperazinium][Co{$B_6O_7(OH)_6$)}$_2$].[111] DFT and QTAIM analysis was used to model the hexaborate 'O^+' isomer's relative conformational stability and intramolecular hydrogen bonding (IHB) present in the gas phase.

Thirdly, the rotamers of the 'O^+' heptaborate anions were investigated in the gas phase, using DFT and QTAIM. Beckett *et al*.[255] had previously modelled the

heptaborate anions in the gas phase and discovered that the 'chain' isomer was more energetically stable than the 'O^{+}' isomer by ~10 kJ mol^{-1}. Ten unique rotamers were modelled and reported for the heptaborate 'chain' isomer and yet only two out of a possible thirty-two rotamers for the 'O^{+}' isomer were modelled. For completeness, these two, along with the remaining 'O^{+}' heptaborate anion isomers were investigated and are reported within this chapter.

B3LYP/6-311++G(*d*,*p*) DFT Calculations were performed using Gaussian09 and analysed using GaussView 5.0 and WebMO visualization packages.[269] Implicit water (ε = 78.3553) solvation was performed using the Polarizable Continuum Model (PCM) Self Consistent Reaction Field (SCRF) approach.[270-273] QTAIM (Quantum Theory of Atoms in Molecules) analyses were performed using AIM2000.[274] All DFT calculations were performed in the gas phase unless otherwise stated.

4.3 Results and discussion

4.3.1 Pentaborate anions

Initially, DFT geometry optimizations were performed on the pentaborate anion monomer structures prior to calculations of the dimers. The monomeric units contain four planar OH groups which can give rise to a maximum of sixteen different rotamers (2^4). Some of the rotamers were degenerate in both structure and energy and therefore the number of different unique rotamers was reduced to six, as shown in Table 4.1 and Figure 4.2. In order to differentiate between different OH orientations; *i* and *o* were used to denote configurations where the proton points inwards towards and outwards away from the tetrahedral boron centre, respectively (Figure 4.2). Harmonic vibrational frequency analyses confirmed that all rotamers were not only stationary points (zero RMS gradient) but also minima (all positive frequencies / eigenvalues of the Hessian matrix).

Table 4.1: Summary of the data obtained for the six unique rotamers of the pentaborate monomer calculated in the gas phase. Relative energy (kJ mol^{-1}) is calculated as: (absolute energy – lowest absolute energy) x 2625.5.

Configuration	Point group	Absolute Energy (Ha)	Relative Energy (kJ mol^{-1})	Lowest vibrational frequency ν_1 (cm^{-1})
iiii	D_{2d}	-880.106381268	0	37
iiio	C_s	-880.104865663	4	35
oiio	C_2	-880.103337087	8	35
ooii	C_{2v}	-880.102151838	11	33
oooi	C_s	-880.100605661	15	33
oooo	D_{2d}	-880.097856310	22	33

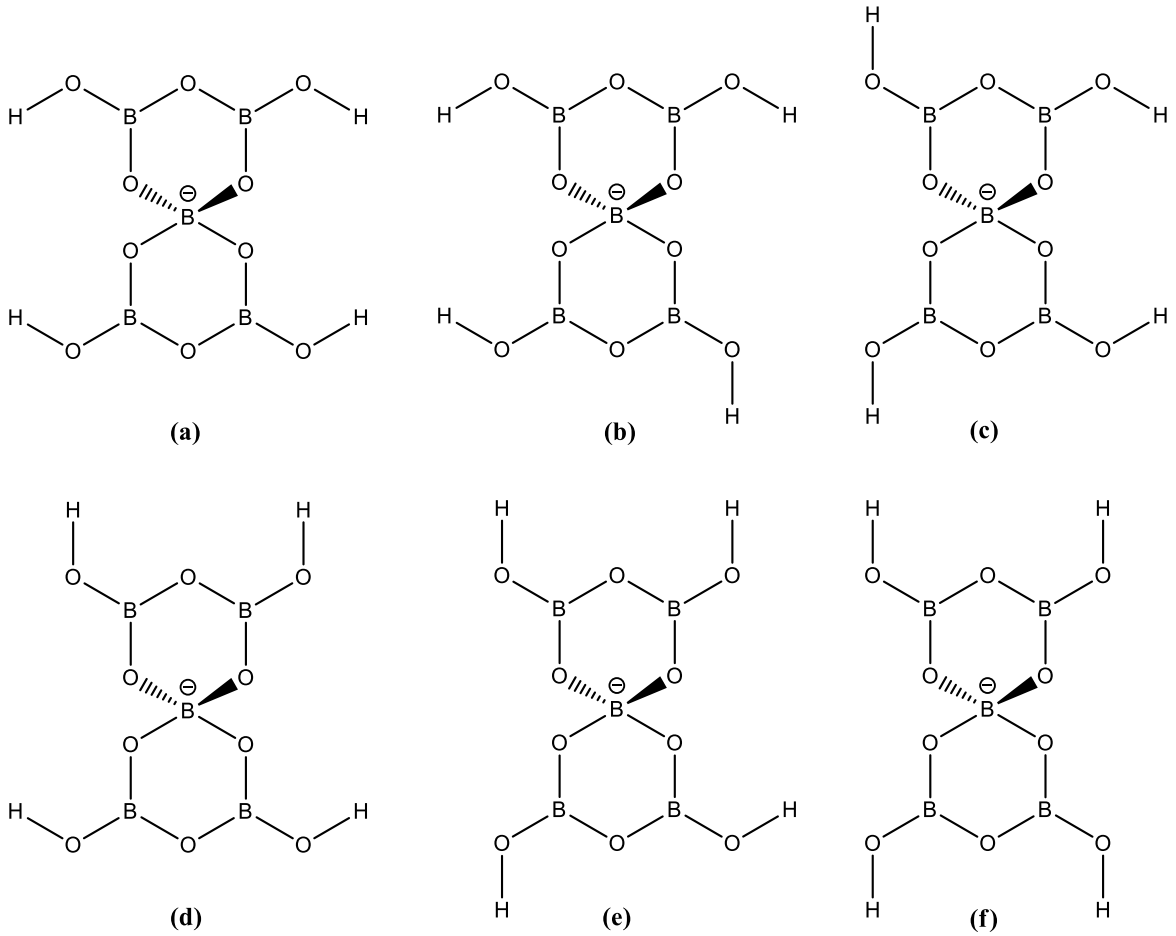

Figure 4.2: The different configurations of the pentaborate anions; (a) *iiii;* (b) *iiio*; (c) *oiio*; (d) *ooii*; (e) *oooi*; and (f) *oooo*; where *i* refers to the hydroxyl hydrogen atom pointing in towards the tetrahedral boron centre, and *o* is outwards away from the tetrahedral boron centre.

The OH groups in the minimized structures were all found to be in the plane of the boroxole ring, which agrees with work previously carried out by Beckett *et al*.[255] The lowest energy rotamer was found to have its four OH groups all pointing in towards the tetrahedral boron centre (*iiii*); this anion type has only been observed in one structure in the solid-state: [1,2,3-$Me_3C_3N_2H_2$][$B_5O_6(OH)_4$], which has significantly non-planar boroxole rings.[73] The most commonly observed rotamer in solid-state structures is the one in which one OH group points away from, and three OH groups point in towards the tetrahedral boron centre (*iiio*). This rotamer is only 4 kJ mol^{-1} higher in energy (when calculated in the gas phase) and has been observed in many of the pentaborate structures reported in Chapter 3.

Dimerization of the pentaborate monomers can form ring or continuous chain structures which contain both proton acceptors and donors. The intermolecular rings

formed when two pentaborate anions are joined together by H-bonding at α- and γ-reciprocal positions are the 8-membered $R_2^2(8)$ rings, each formed with two proton donors and two proton acceptors. The H-bonded intermolecular ring formed in the dimerization of the pentaborate anions at the β reciprocal position is the 12-membered $R_2^2(12)$ ring; this again has two proton donors and two proton acceptors within the ring. Finally, an 8-membered continuous chain formed through dimerization at a β-position is called the C(8) chain; this dimer contains only one H-bond from one proton donor and one acceptor.

The binding energies (kJ mol^{-1}) of these dimer formations (Figure 4.3) were investigated using an approach used previously for networks of neutral boric acid polymers (unpublished results) in which the binding energy was calculated as the difference between the energies of the dimer and the sum of the energies of the monomeric units.

The gas-phase *iiio* rotamer was used as the starting geometry for DFT calculations involving anionic dimers in the geometries shown in Figure 4.3. Initial attempts to pair the anions resulted in endothermic (*ca*. +150 kJ mol^{-1}), rather than exothermic, interactions, which were presumably a result of unfavourable Coulombic forces. This issue was initially overcome by protonating the pentaborate anions on γ-O atoms on the boroxole rings which were not involved in H-bonding, as shown in Figure 4.4, to obtain a neutral species and thus eliminate the anion-anion charge repulsion.

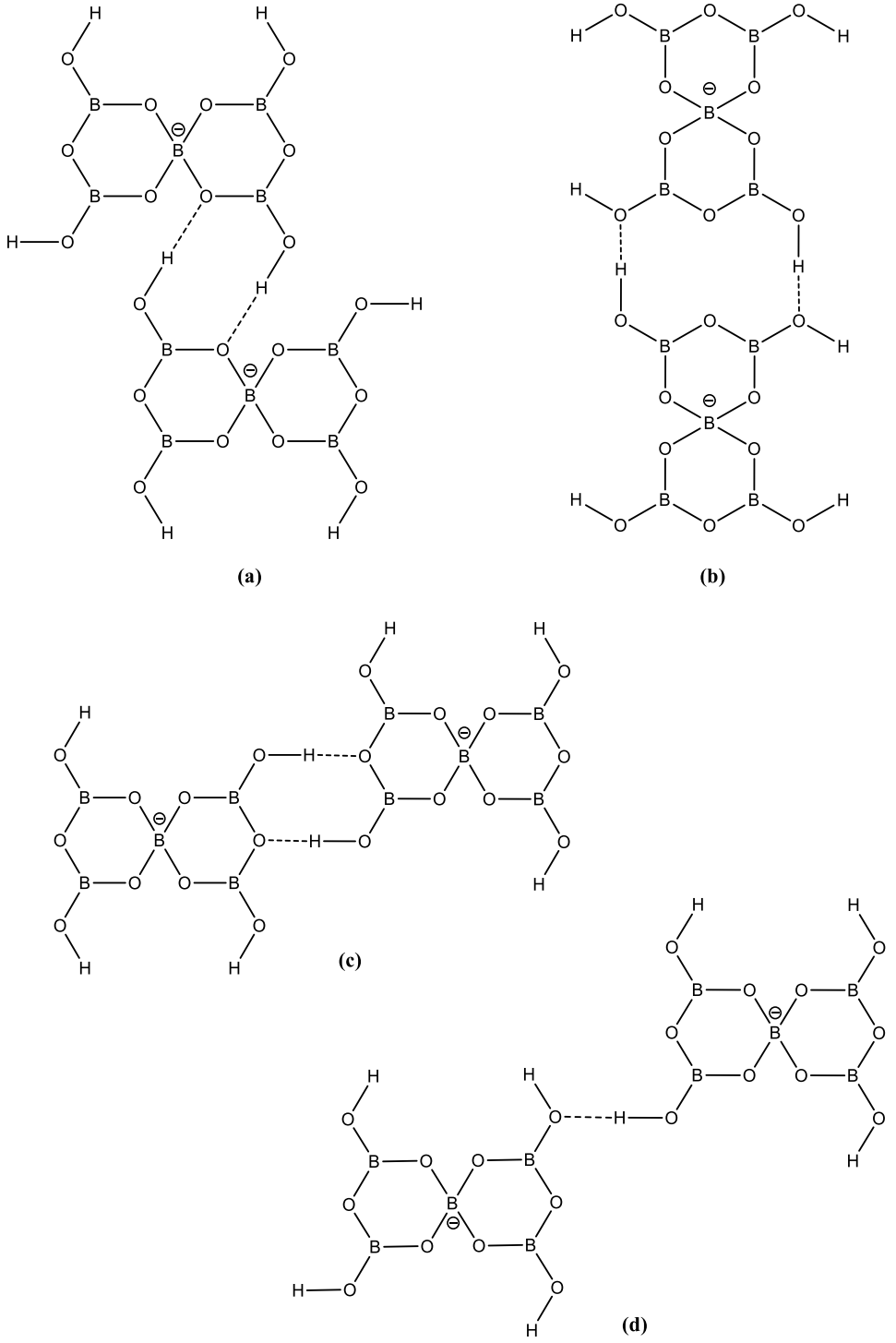

Figure 4.3: The four pentaborate dimers which were modelled using DFT: (a) the α-reciprocal $R_2^2(8)$ dimer; (b) the β-reciprocal $R_2^2(12)$ dimer; (c) the γ-reciprocal $R_2^2(8)$ dimer; and (d) the C(8) β-chain.

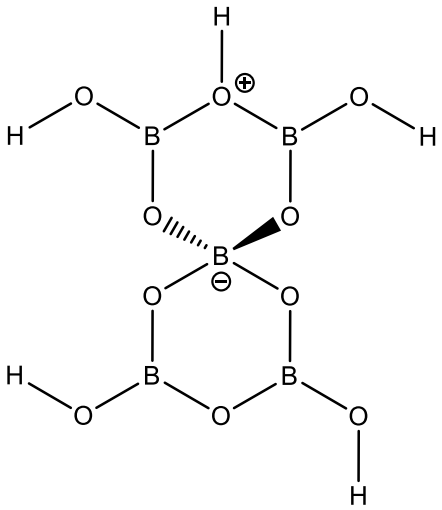

Figure 4.4: The *iiio* rotamer which was protonated at a γ-O atom of the boroxole ring not involved in H-bond interactions when forming dimers.

This method appeared to work and interactions became exothermic, however, minimised structures were distorted away from their idealised planar conformations, as shown for the γ-reciprocal $R_2^2(8)$ dimer in Figure 4.5, and were therefore considered to be unrepresentative of the dimers observed in solid-state structures.

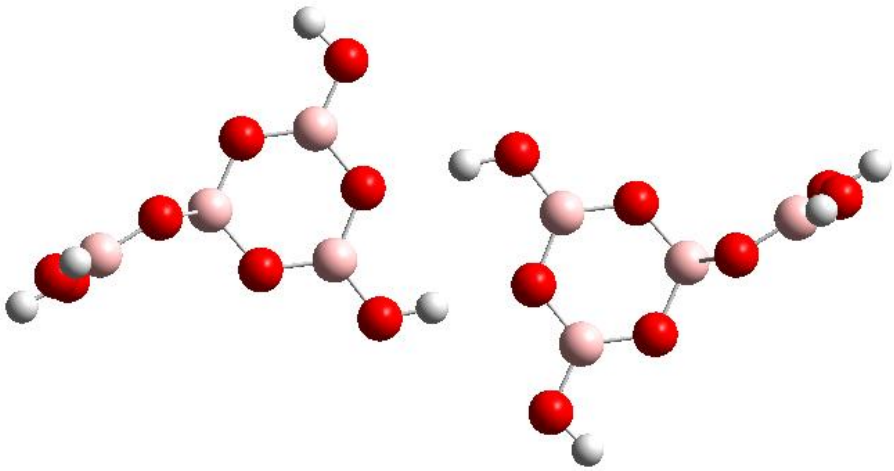

Figure 4.5: The *iiio-iiio* pair of pentaborate rotamers positioned as the γ-reciprocal $R_2^2(8)$ dimer; the boroxole rings not involved in the H-bond interactions are distorted and non-planar.

An alternative approach was applied, which involved using 'solvated' rather than 'gas phase' DFT energies in the dimer calculations. The solvent chosen in this method was water; not only is this a polar solvent which can reduce the anion-anion repulsion found in the gas phase calculations, but it is also a solvent in which the solid-state structures are soluble in. The monomer units were recalculated using the solvated approach and the results of these are given in Table 4.2. Zhou *et al*.[257] recently calculated solvated energies of the *iiio* pentaborate anion at a lower computational level and gives a similar result to that shown in Table 4.2, although they cannot be directly compared since different basis sets were used.

Table 4.2: Summary of the data obtained for the six unique rotamers of the pentaborate monomer calculated in the solvated phase. Relative energy is calculated as: (absolute energy – lowest absolute energy) x 2625.5.

Configuration	Point group	Absolute Energy (Ha)	Relative Energy (kJ mol^{-1})	Lowest vibrational frequency v_1 (cm^{-1})
iiii	D_{2d}	-880.192001237	0	33
iiio	C_s	-880.191584124	1	32
oiio	C_2	-880.191232128	2	33
ooii	C_{2v}	-880.191100343	2	32
oooi	C_s	-880.190674755	3	31
oooo	D_{2d}	-880.190184174	5	31

As can be seen in Table 4.2, the energies of the rotamers in the solvated phase did not significantly differ from one another, however the *iiio* was again chosen as the rotamer in the dimer calculations as this is the one most commonly observed in solid-state structures. The harmonic vibrational frequencies also show that the conformers are all minima and not transition state structures. The solvated rotamers were dimerized as shown previously in Figure 4.3 and exothermic energies were computed, without any boroxole distortions. The data for these interactions are given in Table 4.3.

Table 4.3: DFT calculated energies (solvated phase) of H-bond interactions found in solid-state structures containing pentaborate anions, $[B_5O_6(OH)_4]^-$. Relative energy is calculated as the energy of the dimer – (2 x energy of *iiio* monomer).

Species	Point group	Absolute Energy (Ha)	Relative Energy (kJ mol^{-1})	H-bond energy (kJ mol^{-1})	Lowest vibrational frequency v_1 (cm^{-1})
$[B_5O_6(OH)_4]^-$ *iiio*	C_s	-880.191584124	0	n/a	32
$R_2^2(8)$ α-reciprocal	C_i	-1760.39907124	-42	-21	11
$R_2^2(12)$ β-reciprocal	C_2	-1760.39049058	-19	-10	8
$R_2^2(8)$ γ-reciprocal	C_{2h}	-1760.39517215	-32	-16	7
C(8) β-chain	C_1	-1760.38916054	-16	-16	4

As shown in Table 4.3, all of the energies of the H-bonds formed within the anion-anion interactions are exothermic, indicating that these H-bond interactions are stabilising the structures. The $R_2^2(8)$ α-reciprocal dimer shows the strongest binding energy (-42 kJ mol^{-1}), and the presence of H-bonds is confirmed by the changes in O-H bond lengths and vibrational frequencies; calculated vibrational frequencies showed there to be a red shift (*ca*. 430 cm^{-1}) for the O–H bonds within this dimer, due to the elongation and weakening of the donor O–H bonds (from 0.963 Å to 0.983 Å). The length of the H-bond in the $R_2^2(8)$ α-reciprocal dimer is the shortest of all the calculated interactions at 1.773 Å, which correlates well with it being the strongest H-bond (-21 kJ mol^{-1}).

The $R_2^2(8)$ γ-reciprocal dimer has the second strongest binding energy (-32 kJ mol^{-1}), with H-bond lengths of 1.849 Å. The donor O–H bonds are elongated from 0.963 Å to 0.976 Å and show a red shift of *ca*. 290 cm^{-1} in the calculated vibrational frequencies. The C(8) β-chain gives comparable results to the $R_2^2(8)$ γ-reciprocal dimer; both show energies of -16 kJ mol^{-1} per H-bond. Further investigation in to the H-bond found within the C(8) chain showed it to be very similar in length to the $R_2^2(8)$ γ-reciprocal dimer, having a H-bond length of 1.846 Å. Likewise, the donor O–H bond is elongated from 0.963 Å to 0.975 Å and shows a red shift in the vibrational frequencies of *ca*. 250 cm^{-1}.

Finally, the $R_2^2(12)$ β-reciprocal dimer shows the weakest binding energy (-19 kJ mol^{-1}), along with the longest H-bond length of 1.973 Å. The donor O–H bonds are elongated from 0.963 Å to 0.974 Å and show a red shift of *ca*. 200 kJ mol^{-1} in the vibrational frequency data. The bond lengths and vibrational frequencies of each H-bond and O–H bond are summarised in Table 4.4.

Table 4.4: Summary of bond lengths and vibrational frequencies of the OH and H-bonds found in each computed motif.

H-bonding motif	Bond	Bond length, r_{OH} (Å)	Vibrational frequency, ν_{OH} (cm^{-1})
$R_2^2(8)$ α-reciprocal	H-bond	1.773	n/a
$R_2^2(8)$ α-reciprocal	donor O-H bond	0.983	3422 – 3451
$R_2^2(8)$ α-reciprocal	non-interacting O-H bond	0.963	3852 – 3853
$R_2^2(12)$ β-reciprocal	H-bond	1.973	n/a
$R_2^2(12)$ β-reciprocal	donor O-H bond	0.974	3635 – 3638
$R_2^2(12)$ β-reciprocal	non-interacting O-H bond	0.963	3851 – 3853
$R_2^2(8)$ γ-reciprocal	H-bond	1.849	n/a
$R_2^2(8)$ γ-reciprocal	donor O-H bond	0.976	3563 – 3581
$R_2^2(8)$ γ-reciprocal	non-interacting O-H bond	0.963	3852 – 3853
C(8) β-chain	H-bond	1.846	n/a
C(8) β-chain	donor O-H bond	0.975	3596
C(8) β-chain	non-interacting O-H bond	0.963	3849 – 3853

Examination of a plot of the bond length of the O–H bonds against their vibrational frequencies shows that they are correlated with one another (Figure 4.6). As the bond length is increased, the strength of the bond is weakened and this is observed as a red-shift in the vibrational frequencies.

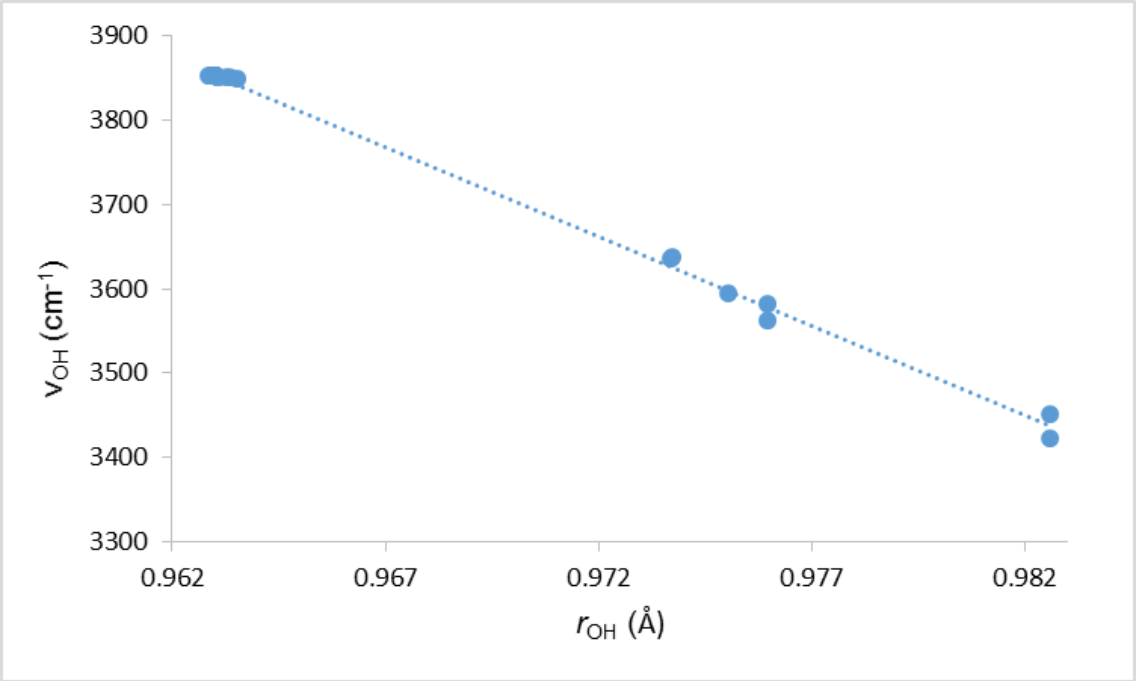

Figure 4.6: Graph of all calculated pentaborate anion O–H bond lengths (r_{OH}) against their corresponding vibrational frequencies (ν_{OH}) [ν_{OH} = 24287 – 21218r_{OH}; n = 30, R^2 = 0.9981, σ = 6 cm^{-1}].

The DFT calculations show that the $R_2^2(8)$ α-reciprocal dimer is considerably more favoured per H-bond (−21 kJ mol^{-1}) than the C(8) β-chain (−16 kJ mol^{-1}). Durka *et al.* have calculated H-bond energies for boronic acid dimers, which also contain a $R_2^2(8)$ ring, and have reported an energy of −23.7 kJ mol^{-1}.[263] The calculated structural data for the $R_2^2(8)$ α-reciprocal system in this project for D···A, angle OHO, H···O and O–H are 2.76 Å, 178.1°, 1.77 Å and 0.98 Å, and these agree well with Durka's values (2.73 Å, 176.8°, 1.73 Å, 0.99 Å) which were computed at a lower level. It is difficult to compare the calculated values with those observed by X-ray crystallography because the O–H distances in the solid-state structures found within Chapter 3 are crystallographically fixed at 0.84 Å. However, the calculated data does agree within the observed ranges for the structural data available for structures published elsewhere.[66] This leads to the conclusion that this approach is valid and that the reciprocal-α H-bonds in these systems are relatively strong, and strongly influence the structure.[69] The H-bond strengths for the $R_2^2(8)$ reciprocal-γ interaction is comparable to that of a C(8) β-chain, and is favoured over that of the $R_2^2(12)$ reciprocal-β interaction.

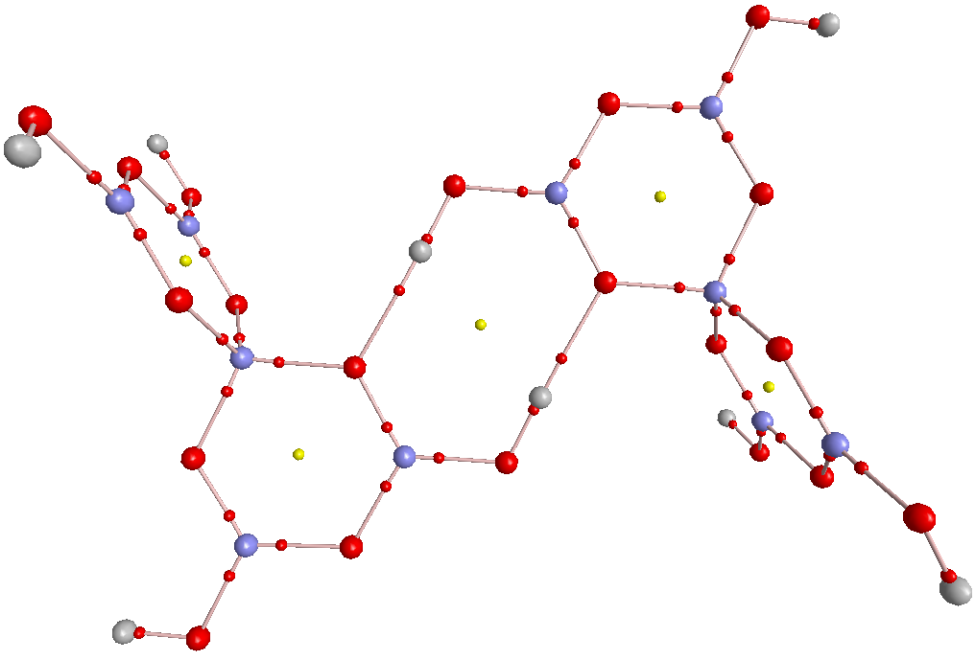

Figure 4.7: QTAIM analysis of the $R_2^2(8)$ α-reciprocal dimer. Bond critical points (BCP) are represented by small red dots, and ring critical points (RCP) are indicated by small yellow dots.

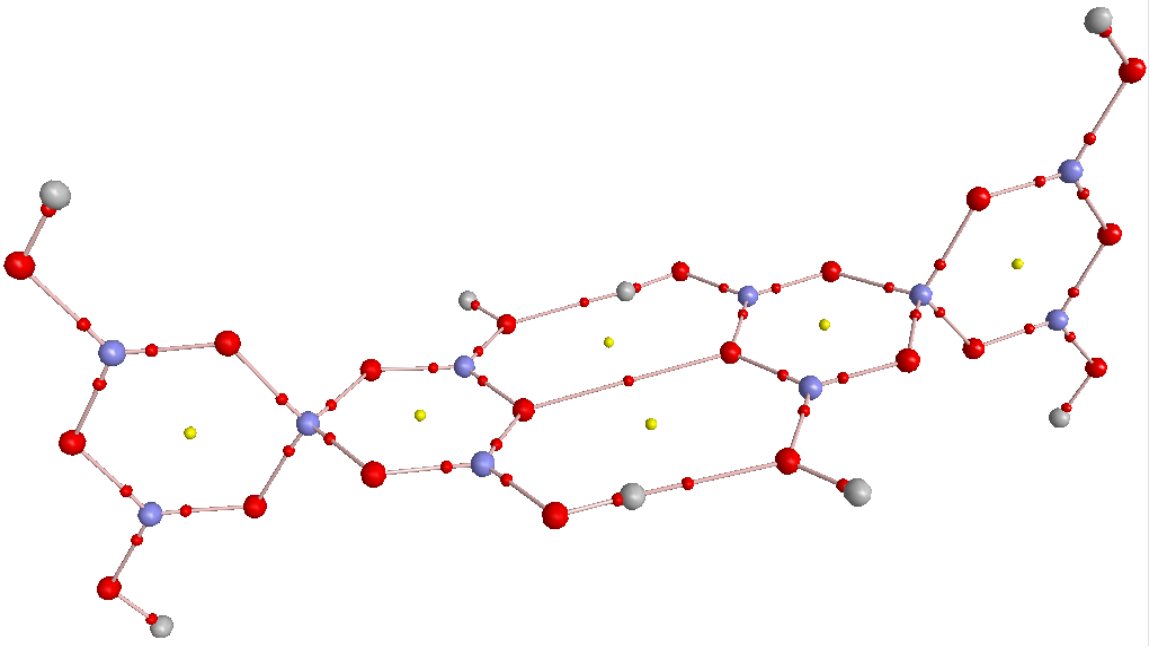

Figure 4.8: QTAIM analysis of $R_2^2(12)$ β-reciprocal dimer. Bond critical points (BCP) are represented by small red dots, and ring critical points (RCP) are indicated by small yellow dots.

QTAIM calculations (Figures 4.7 – 4.10) on all of the H-bonded motifs show that the H-bonds have bond critical points, with the energies of the H-bonds mirroring the electron density (ρ_b) at their bond critical points.

The calculated $R_2^2(12)$ reciprocal-β interaction has a close O···O contact (3.04 Å) which is similar to that observed in [2-^{i}PrN$_2$C$_3$H$_4$][B$_5$O$_6$(OH)$_4$] (2.98 Å).[73] QTAIM analysis indicates that there exists a further bond critical point between these two O atoms, in addition to those of the two H-bonds. ρ_b for these H-bonds are the lowest of the four calculated H-bond interactions and this is in agreement with less favourable H-bond energies.

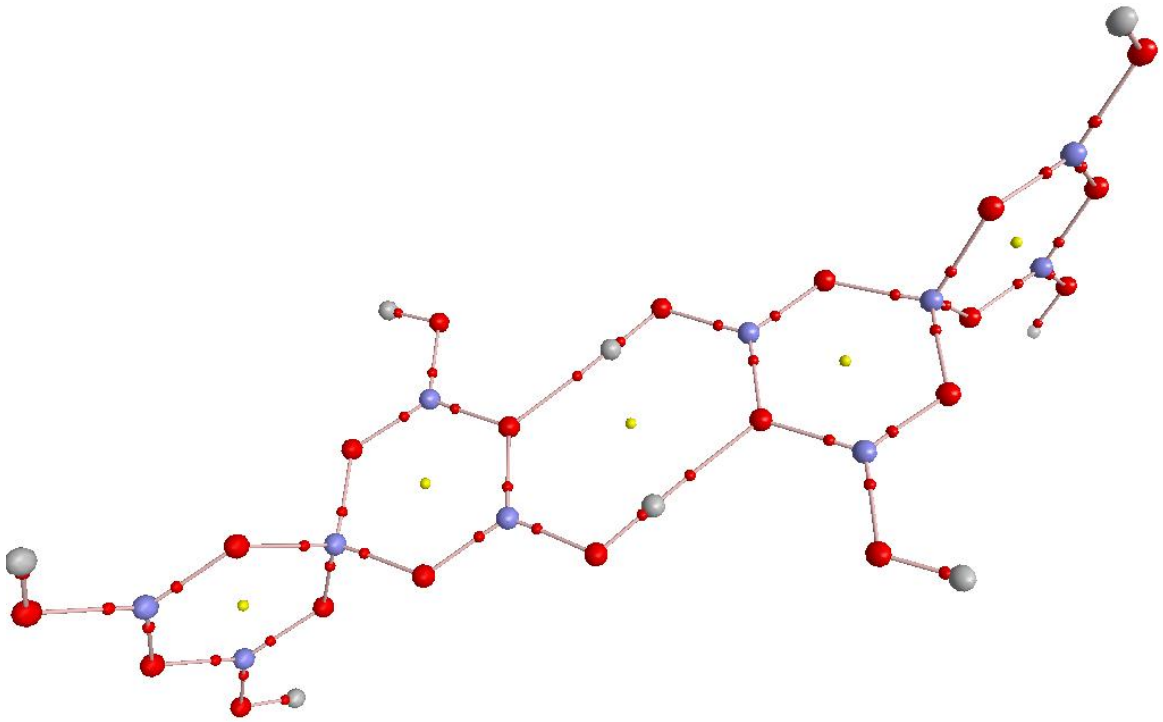

Figure 4.9: QTAIM analysis of $R_2^2(8)$ γ-reciprocal dimer. Bond critical points (BCP) are represented by small red dots, and ring critical points (RCP) are indicated by small yellow dots.

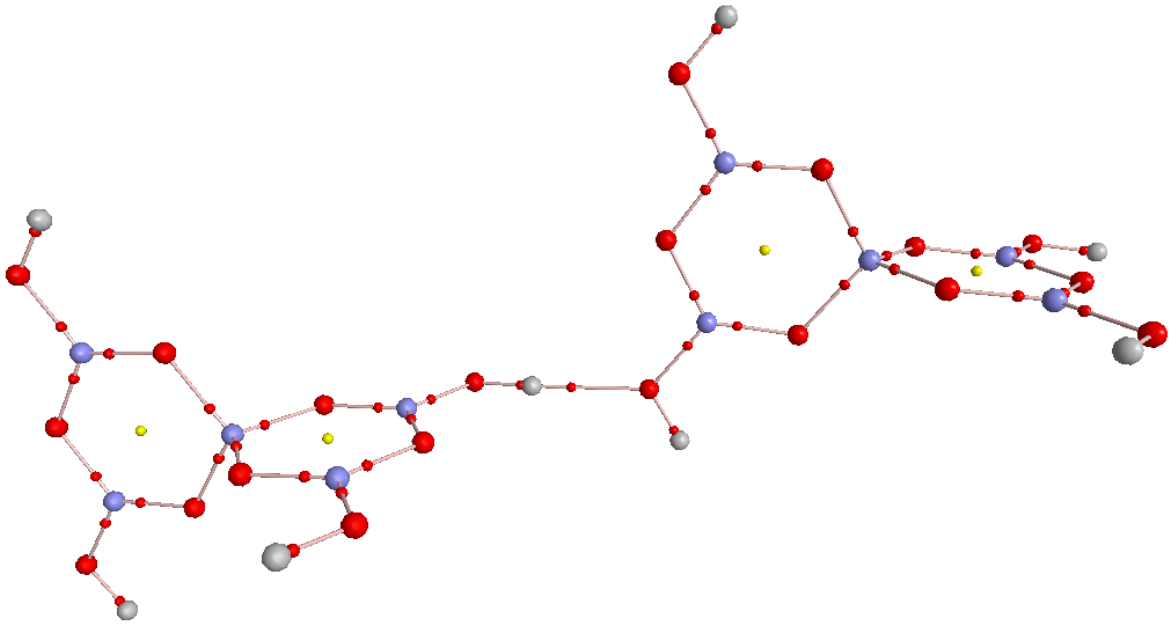

Figure 4.10: QTAIM analysis of the C(8) β-chain. Bond critical points (BCP) are represented by small red dots, and ring critical points (RCP) are indicated by small yellow dots.

A summary of the results obtained from the QTAIM analyses for the four observed pentaborate dimer motifs are given in Tables 4.5-4.7. As expected, the ρ_b values found for the H-bonds are all low (<0.1 a.u.) and indicate the presence of closed shell interactions, and the ρ_b values for the O–H bonds are higher (>0.3 a.u.) which is indicative of covalent bonding.[268] The values for the Laplacian are in agreement with these and show the presence of covalent bonding in the O–H bonds ($\nabla^2(\rho_b) < 0$) and H-bonding ($\nabla^2(\rho_b) > 0$) between the two anionic species. The ellipticity of both the donor O–H bonds and H-bonding suggest the presence of cylindrically symmetrical (single) bonds, rather than any double bonds. The QTAIM analysis data observed for the $R_2^2(12)$ β-reciprocal showed a BCP present between the two γ-O atoms within the 12-membered ring. Analysis of the BCP indicates that a close O···O contact is present, which possesses some π-bond character (ε = 0.142); for comparison, C-C bonds have ellipticity values of 0.23 a.u. in benzene and 0.45 a.u. in ethylene.[275]

Table 4.5: Summary of QTAIM analyses of the H-bonding within the calculated motifs.

Dimerization position	Dimerization ring type	H-bond Energy (kJ mol^{-1})	H-Bond Length (Å)	ρ_b (a.u.)	$\nabla^2(\rho_b)$ (a.u.)	ε
α-reciprocal	$R_2^2(8)$	-21	1.773	0.037	0.121	0.058
γ-reciprocal	$R_2^2(8)$	-16	1.849	0.030	0.106	0.066
β-reciprocal	$R_2^2(12)$	-10	1.973	0.022	0.082	0.085
β-chain	C(8)	-16	1.846	0.030	0.109	0.059

Table 4.6: Summary of QTAIM analyses of the donor O–H bonds within the calculated motifs.

Dimerization position	Dimerization ring type	O-H Bond Length (Å)	ρ_b (a.u.)	$\nabla^2(\rho_b)$ (a.u.)	ε
α-reciprocal	$R_2^2(8)$	0.983	0.336	-2.342	0.006
γ-reciprocal	$R_2^2(8)$	0.976	0.344	-2.413	0.007
β-reciprocal	$R_2^2(12)$	0.974	0.347	-2.439	0.007
β-chain	C(8)	0.975	0.345	-2.425	0.007

Table 4.7: Summary of QTAIM analyses of the O···O close contact within the calculated $R_2^2(12)$ motif.

Dimerization position	O…O Bond Length (Å)	ρ_b (a.u.)	$\nabla^2(\rho_b)$ (a.u.)	ε
β-reciprocal	$R_2^2(12)$	0.008	0.026	0.142

4.3.2 Hexaborate anions

The hexaborate dianion, $[B_6O_7(OH)_6]^{2-}$, is comprised of three 6-membered B_3O_3 boroxole rings which share a common central oxygen atom, and contains both trigonal and tetrahedral boron atoms, as shown in Figure 4.11. It has the descriptors

6:3Δ+3T or 3Δ3□:[Φ]<Δ2□>I<Δ2□>I<Δ2□>I. This is the only isomer of the hexaborate anion known to exist at the time of writing this thesis and is found in the solid-state structure of [1-cyanopiperazinium][Co{$B_6O_7(OH)_6$)}$_2$] where it is coordinated to a Co(II) atom;[111] this isomer may be described as the 'O$^+$' isomer due to the positively-charge oxygen atom found in the centre of the anion.

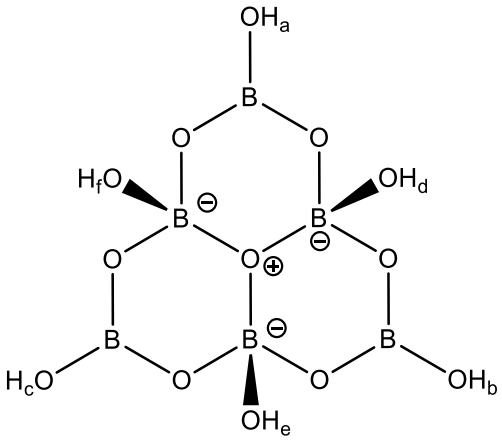

Figure 4.11: The 'O$^+$' isomer of the hexaborate dianion, $[B_6O_7(OH)_6]^{2-}$.

No other isomer of the hexaborate dianion is known to exist to date, yet the heptaborate dianion, $[B_7O_9(OH)_5]^{2-}$, which is structurally similar to the hexaborate dianion with an additional $B(OH)_3$ unit condensed on to the 'O$^+$' isomer, exists in two different isomers: the 'O$^+$' isomer as described, and the 'chain' isomer (Section 4.3.3, Figure 4.17a and b, respectively). The 'chain' isomer of the heptaborate can be considered as being an extended pentaborate structure and is given the descriptor of 7:5 Δ+2T or 5Δ2□:<2Δ□>-<Δ2□>-<2Δ□>, whereas the 'O$^+$' isomer is given the descriptor 6:(3Δ+3T)+Δ or 4Δ3□:[Φ]<Δ2□>I<Δ2□>I<Δ2□>I=<Δ2□>.[9,27,31,79] The different possible rotamers of the known 'O$^+$' isomer were investigated for their conformational stability and any intramolecular H-bonding (IHB) present in the gas phase, using B3LYP/6-311++G(*d*,*p*) DFT calculations.

The OH groups attached to the trigonal and tetrahedral boron atoms were labelled in a clockwise manner, based upon the O$^+$ atom being the centre of an imaginary clock face. Specific hydrogen atoms are labelled as being clockwise (C) or anticlockwise (A) relative to the boron atom (Figure 4.12). An additional mid (M)

orientation in which the hydroxyl hydrogen atom is *antiperiplanar* to the B^{-}–O^{+} bond is found for the tetrahedral boron OH groups.

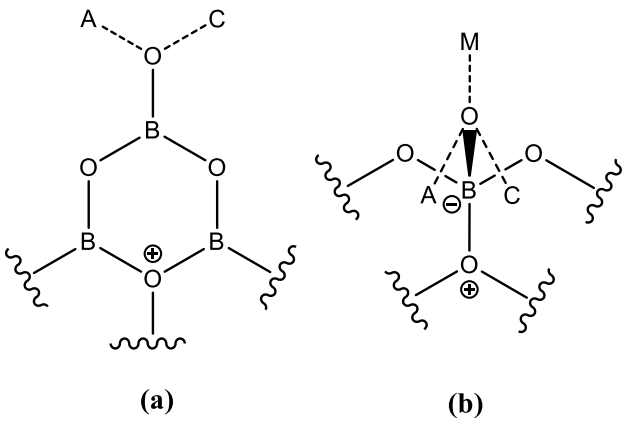

Figure 4.12: The rotamer orientations – A (anticlockwise), C (clockwise) and M (mid) in (a) trigonal and (b) tetrahedral B atoms.

Out of a possible sixty-four (2^6) different configurations based on C/A configurations of OH bonds, the optimized geometries of twelve unique rotamers were obtained and these are summarised in Table 4.8. The results of the harmonic vibrational frequencies show that all twelve unique rotamers of the hexaborate anion are minima and not transition states. The most stable of these 'O^{+}' isomers are the structures which possess an unbroken, quasi-triangular cyclic network of cooperative intramolecular H-bonds (as shown in Figure 4.13); these structures possess the maximum number (three) of stabilizing IHBs. The rotation of any of the tetrahedral BO bonds affects the position of the hydrogen atom of the OH group, thus breaking the IHB network.

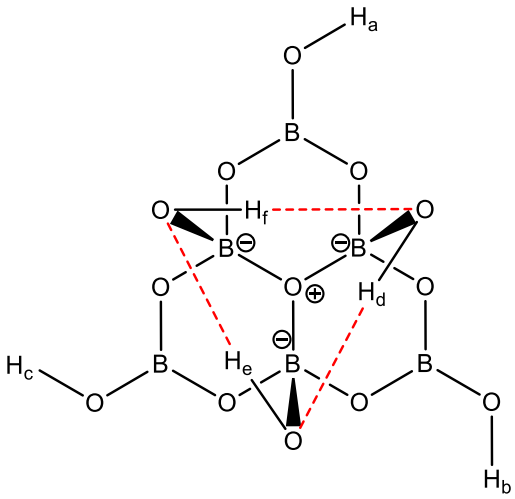

Figure 4.13: The 'O^{+}' isomer of the hexaborate anion, $[B_6O_7(OH)_6]^{2-}$, shown in the CCCCCC configuration; IHBs are shown as red dashed lines.

Table 4.8: Relative energies (to the nearest kJ mol^{-1}) of the 'O^{+}' isomer of the hexaborate anion, $[B_6O_7(OH)_6]^{2-}$, obtained in the gas phase.

Outer (trigonal) OH groups			Inner (tetrahedral) OH groups			Relative energy (kJ mol^{-1})	Number of IHBs[a]	Lowest vibrational frequency ν_1 (cm^{-1})
a	b	c	d	e	f			
C	C	C	A	A	A	0	3	62
C	C	C	C	C	C	0	3	61
C	C	A	A	A	A	1	3	61
C	C	A	C	C	C	1	3	61
C	C	A	A	A	C (M)	14	2	54
C	C	A	C	C	A (M)	14	2	53
C	C	C	C (M)	A	A	15	2	53
C	C	C	C	C	A (M)	16	2	53
C	C	A	C (M)	A	A	16	2	52
C	C	A	A (M)	C	C	17	2	53
C	C	A	A	C (M)	A	18	2	53
C	C	A	C	A (M)	C	19	2	52

[a] Confirmed by QTAIM analyses conducted after geometry optimization.

Should the hydrogen atom of the OH group in the IHB be orientated in an opposite position to the other two (e.g. CCA, rather than CCC) then an unstable hydrogen-hydrogen interaction is found between the two neighbouring OH groups. This interaction can be considered as an anti-hydrogen bond as a blue shift is observed in the harmonic vibrational frequency, which correlates with a shorter O–H bond length;[276] this instability is in contrast to the stable hydrogen-hydrogen interaction between CH groups in phenanthrene.[277] During geometry optimization, the tetrahedral B–O bond undergoes further rotation to achieve the stable minimum structures which show the hydrogen atom of the OH group to be *antiperiplanar* to the B^{-}–O^{+} bond; this rotation also eliminates any destabilizing hydrogen-hydrogen interactions and creates an additional stabilizing H-bond (Figure 4.14).

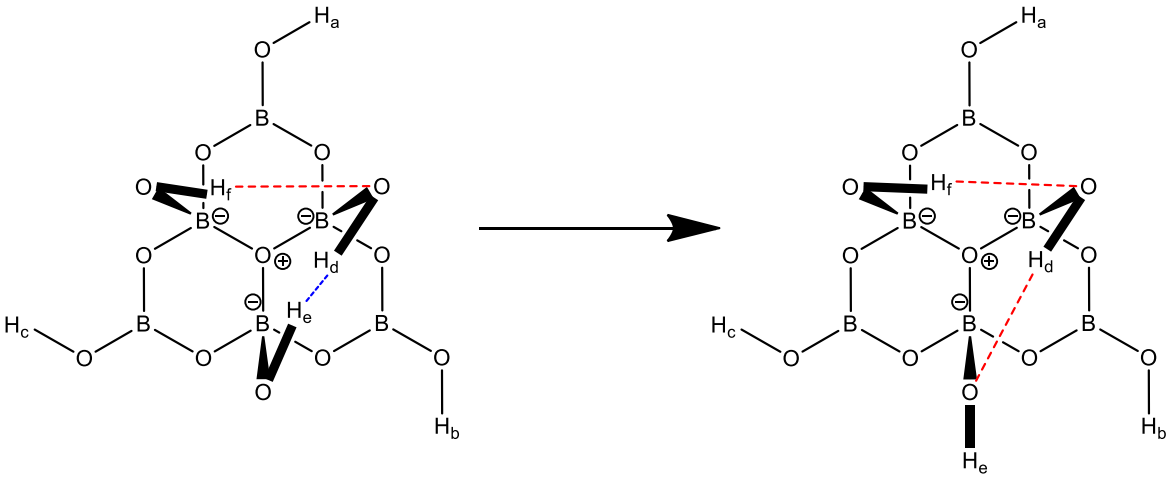

Figure 4.14: The conversion of a destabilizing hydrogen-hydrogen interaction (blue dashed line) into an additional stable H-bond (red dashed line) observed during geometry optimization; the example shown here is the CCCCCA rotamer.

When comparing these tetrahedral B–O rotations to those of the trigonal B–O bonds it can be noted that rotation of any of the trigonal B–O bonds has very little effect on the overall energy of the molecule, due to the absence of any IHBs. This is confirmed by QTAIM analysis, which shows no bond nor ring critical points for the hypothetical 4-membered ring).

The energy of the intramolecular H-bond may be estimated by comparing the average energies of the rotamers containing three and two IHBs, respectively; the

estimated energy is *ca*. 15 kJ mol^{-1}, which is consistent with H-bond energies reported elsewhere.[255,257]

A summary of the H-bond and O-H bond lengths and vibrational frequencies found within the hexaborate anion are given in Table 4.9. QTAIM analyses of the 'O^{+}' hexaborate isomer are summarised in Table 4.10 and illustrated in Figure 4.15. Briefly, the data confirms the presence of covalent O–H bonds from the presence of large ρ_b and negative Laplacian $\nabla^2(\rho_b)$ values. In contrast to this, the analyses of the IHB BCPs indicate that these are weaker, closed-shell interactions, which is shown by their smaller ρ_b and $\nabla^2(\rho_b)$ values. A *ca.* 0.007 a.u. reduction in ρ_b, a *ca.* 0.005 Å elongation in the O–H bond length and a red shift (*ca.* 100 cm^{-1}) in the harmonic vibrational frequency of the O–H bond length (ν_{OH}) are observed for *exo* tetrahedral B-OH *vs.* trigonal planar B-OH groups, reflecting the loss in electron density that occurs during hydrogen bond formation.

Table 4.9: Summary of bond lengths and vibrational frequencies within the 'O^{+}' isomer of the hexaborate anion, $[B_6O_7(OH)_6]^{2-}$.

Rotamer	Bond type	Bond length (Å)	ρ_b (a.u.)	ν_{OH}
CCCAAA	H-bond	2.252	0.016	n/a
	B_{tet}–OH	0.967	0.360	3749 – 3764
	B_{trig}–OH	0.962	0.367	3861
CCCCCC	H-bond	2.253	0.016	n/a
	B_{tet}–OH	0.967	0.360	3751 – 3765
	B_{trig}–OH	0.962	0.367	3860
CCAAAA	H-bond	2.230 – 2.279	0.015 – 0.016	n/a
	B_{tet}–OH	0.967	0.359 – 0.360	3747 – 3770
	B_{trig}–OH	0.961 – 0.962	0.367	3861 – 3862
CCACCC	H-bond	2.229 – 2.273	0.015 – 0.016	n/a
	B_{tet}–OH	0.967	0.359 –0.360	3747 – 3768
	B_{trig}–OH	0.961 – 0.962	0.367	3860 – 3862

Rotamer	Bond type	Bond length (Å)	ρ_b (a.u.)	ν_{OH}
CCAAAC	H-bond	2.140 – 2.238	0.015 – 0.018	n/a
	B_{tet}–OH	0.966 – 0.968 (0.960)	0.358 – 0.360 (0.367)	3744 – 3774 (3872)
	B_{trig}–OH	0.961 – 0.962	0.367	3858 – 3862
CCACCA	H-bond	2.131 – 2.250	0.015 – 0.018	n/a
	B_{tet}–OH	0.966 – 0.968 (0.960)	0.358 – 0.360 (0.367)	3742 -3781 (3872)
	B_{trig}–OH	0.962	0.367	3859 - 3861
CCCCAA	H-bond	2.133 – 2.263	0.015 – 0.018	n/a
	B_{tet}–OH	0.966 – 0.968 (0.960)	0.358 – 0.360 (0.367)	3741 – 3781 (3873)
	B_{trig}–OH	0.961 – 0.962	0.367	3858 – 3863
CCCCCA	H-bond	2.143 – 2.249	0.015 – 0.017	n/a
	B_{tet}–OH	0.966 – 0.968 (0.960)	0.359 – 0.360 (0.367)	3750 – 3779 (3873)
	B_{trig}–OH	0.961 – 0.962	0.367	3860 – 3861
CCACAA	H-bond	2.121 – 2.273	0.014 – 0.019	n/a
	B_{tet}–OH	0.965 – 0.968 (0.960)	0.358 – 0.360 (0.367)	3739 – 3786 (3873)
	B_{trig}–OH	0.961 – 0.962	0.367	3859 – 3863
CCAACC	H-bond	2.153 – 2.242	0.015 – 0.017	n/a
	B_{tet}–OH	0.966 – 0.968 (0.960)	0.359 (0.367)	3752 – 3775 (3873)
	B_{trig}–OH	0.961 – 0.962	0.367	3861 – 3862
CCAACA	H-bond	2.143 – 2.262	0.015 – 0.018	n/a
	B_{tet}–OH	0.966 – 0.968 (0.960)	0.359 – 0.360 (0.367)	3749 – 3780 (3874)
	B_{trig}–OH	0.961 – 0.962	0.367 – 0.368	3861 – 3864
CCACAC	H-bond	2.133 – 2.270	0.014 – 0.018	n/a
	B_{tet}–OH	0.965 – 0.968 (0.960)	0.358 – 0.360 (0.370)	3747 – 3784 (3874)
	B_{trig}–OH	0.961 – 0.962	0.367 – 0.368	3860 - 3864

Figures shown in parenthesis are the mid orientated B_{tet}-OH acceptor sites only; there are no hydrogen atom donors from this OH group.

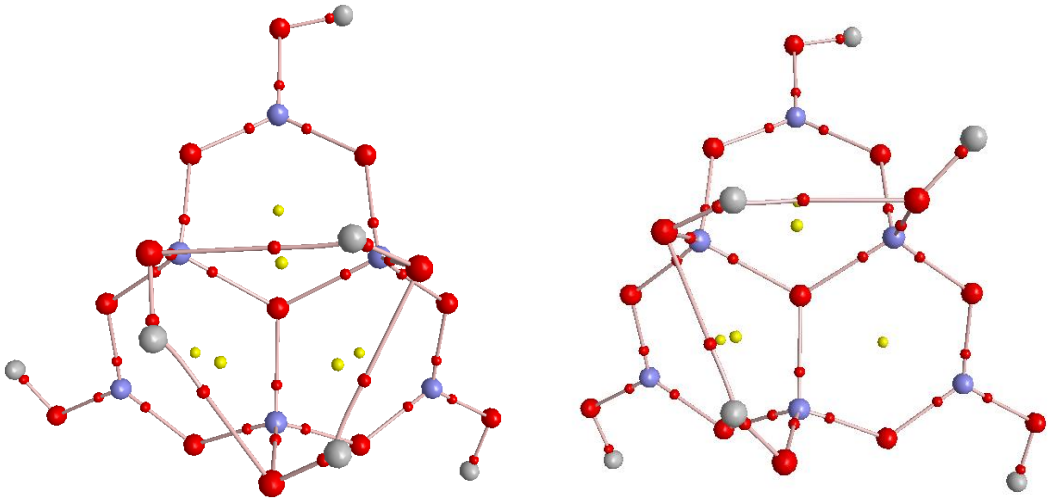

(a) (b)

Figure 4.15: QTAIM analyses of the 'O^{+}' isomer hexaborate anion, $\{B_6O_7(OH)_6]^{2-}$: (a) CCCAAA rotamer and (b) CCAA(M)CC rotamer. BCP and RCP are shown as small red and yellow dots, respectively.

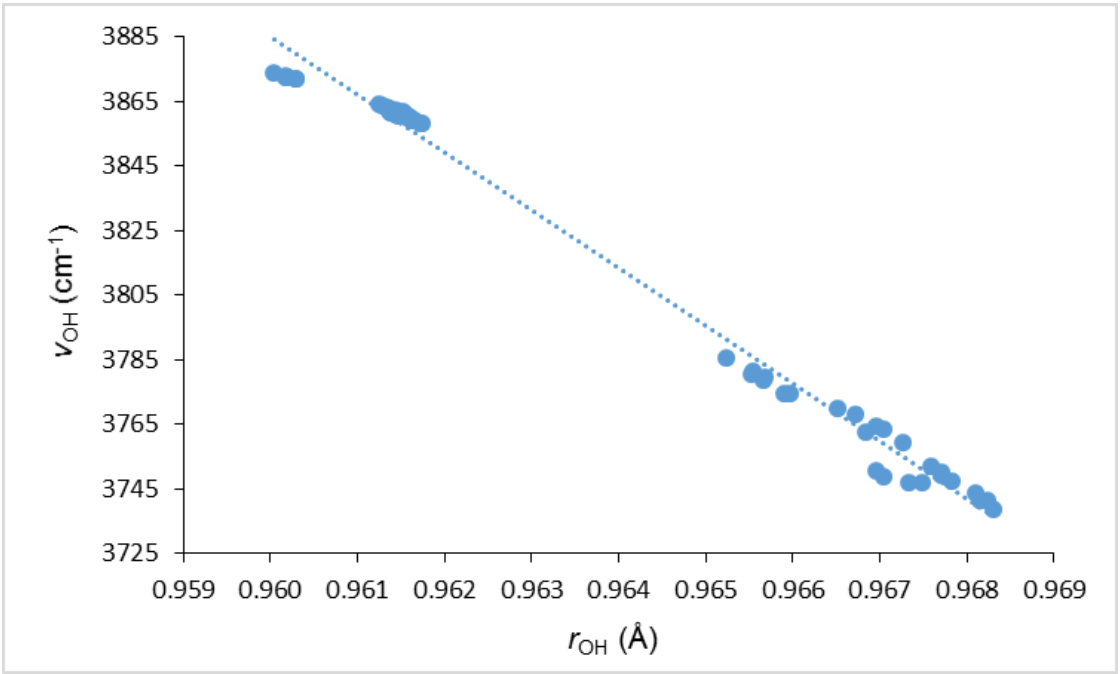

Figure 4.16: Graph of the calculated hexaborate anion O–H bond lengths (r_{OH}) against their corresponding vibrational frequencies (ν_{OH}) [ν_{OH} = 21075 – 17906r_{OH}; n = 64, R^2 = 0.9916, σ = 5 cm^{-1}].

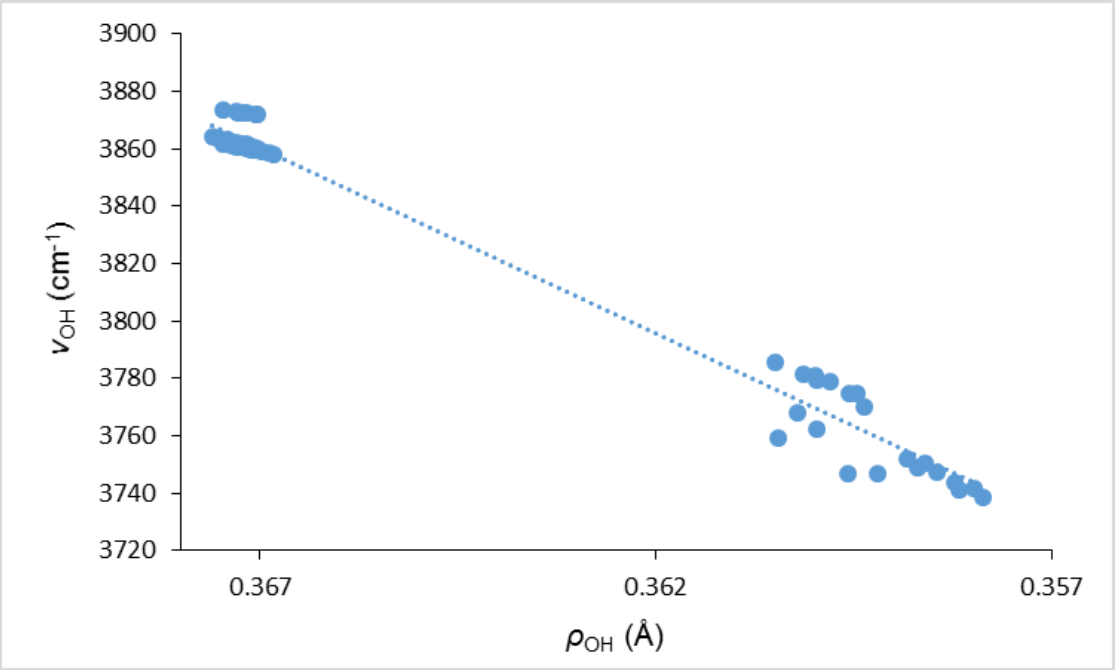

Figure 4.17: Graph of the calculated hexaborate anion O–H bond density (ρ_{OH}) against their corresponding vibrational frequencies (ν_{OH}) [ν_{OH} = -895 + 12957r_{OH}; n = 58, R^2 = 0.9825, σ = 7 cm^{-1}].

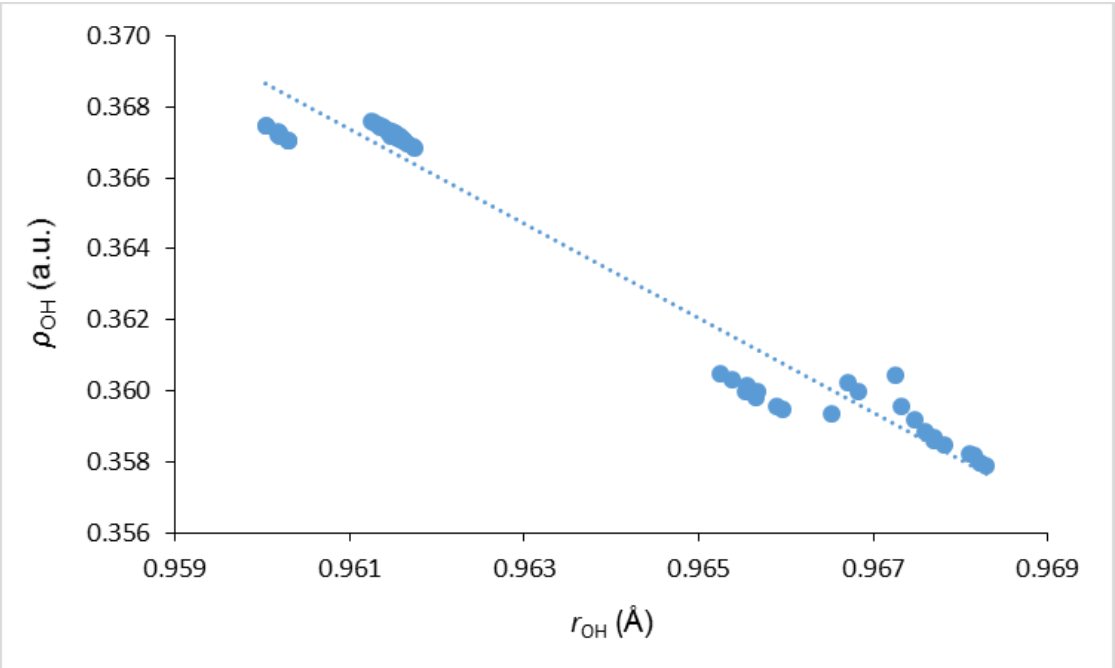

Figure 4.18: Graph of the calculated hexaborate anion O–H bond lengths (r_{OH}) against their corresponding bond density (ρ_{OH}) [ρ_{OH} = 1.65 – 1.34r_{OH}; n = 60, R^2 = 0.9584, σ = 0 cm^{-1}].

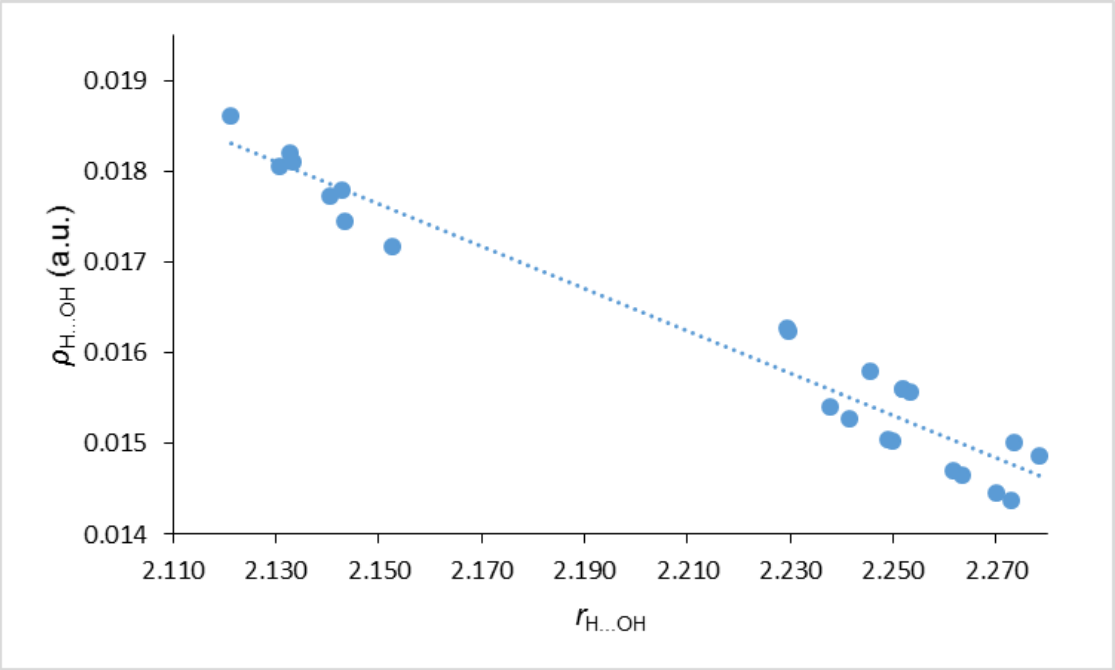

Figure 4.19: Graph of the calculated hexaborate anion H-bond lengths ($r_{H...OH}$) against their corresponding bond density ($\rho_{H...OH}$) [$\rho_{H...OH} = 0.07 - 0.02r_{H...OH}$; n = 24, $R^2 = 0.9478$, $\sigma = 0$ cm^{-1}].

Figure 4.16 shows a good correlation between the O-H bond length and its corresponding vibrational frequency. We can conclude that an elongation in bond length results in a red shift in the vibrational frequency. In addition to this, the density at the O-H bond critical point decreases with this observed red shift (Figure 4.17). Figure 4.18 confirms the relationship between the O-H bond length and the density at the O-H bond critical point; as the bond length increases, the density at the bond critical point decreases as the electron density is shifted due to the formation of a H-bond.

Figure 4.19 shows a correlation between the density at the H-bond critical point and its corresponding bond length. A longer bond length corresponds to having a lower value for ρ_b, whereas a shorter bond length has a greater ρ_b value; we can also conclude from this that the shorter bond lengths correspond to a stronger H-bond formation.

Table 4.10: QTAIM analysis data for the 'O^{+}' isomer hexaborate anion, $[B_7O_9(OH)_5]^{2-}$.

Rotamer	Bond type	$\nabla^2(\rho_b)$ (a.u.)	ε
CCCAAA	H-bond	0.048	0.106
	B_{tet}–OH	-2.405	0.012
	B_{trig}–OH	-2.451	0.011
CCCCCC	H-bond	0.048	0.108
	B_{tet}–OH	-2.406	0.012
	B_{trig}–OH	-2.450	0.011
CCAAAA	H-bond	0.046 – 0.050	0.099 – 0.117
	B_{tet}–OH	-2.405 – -2.407	0.012
	B_{trig}–OH	-2.448 – -2.451	0.011
CCACCC	H-bond	0.046 – 0.050	0.099 – 0.115
	B_{tet}–OH	-2.405 – -2.407	0.012
	B_{trig}–OH	-2.448 – -2.449	0.011
CCAAAC	H-bond	0.048 – 0.062	0.054 – 0.140
	B_{tet}–OH	-2.416 – -2.449 (-2.422)	0.011 – 0.014 (0.015)
	B_{trig}–OH	-2.448 – -2.449	0.011
CCACCA	H-bond	0.047 – 0.063	0.053 – 0.152
	B_{tet}–OH	-2.416 – -2.424 (-2.393)	0.011 – 0.014 (0.015)
	B_{trig}–OH	-2.447 – -2.450	0.011
CCCCAA	H-bond	0.046 – 0.063	0.062 – 0.150
	B_{tet}–OH	-2.415 –-2.423 (-2.396)	0.011 – 0.014 (0.015)
	B_{trig}–OH	-2.449 – -2.450	0.011
CCCCCA	H-bond	0.047 – 0.061	0.049 – 0.149
	B_{tet}–OH	-2.419 – -2.423 (-2.387)	0.012 – 0.014 (0.014)
	B_{trig}–OH	-2.445 – -2.450	0.011
CCACAA	H-bond	0.045 – 0.064	0.061 – 0.163
	B_{tet}–OH	-2.416 – -2.423 (-2.395)	0.011 – 0.014 (0.015)
	B_{trig}–OH	-2.447 – -2.449	0.011
CCAACC	H-bond	0.048 – 0.060	0.050 – 0.138
	B_{tet}–OH	-2.418 – -2.422 (-2.387)	0.011 – 0.014 (0.014)
	B_{trig}–OH	-2.445 – -2.449	0.011
CCAACA	H-bond	0.046 – 0.061	0.061 – 0.146
	B_{tet}–OH	-2.418 – -2.422 (-2.390)	0.012 – 0.014 (0.015)
	B_{trig}–OH	-2.444 – -2.449	0.011

Rotamer	Bond type	$\nabla^2(\rho_b)$ (a.u.)	ε
CCACAC	H-bond	0.045 – 0.063	0.060 – 0.159
	B_{tet}–OH	-2.418 – -2.423 (-2.390)	0.012 – 0.014 (0.015)
	B_{trig}–OH	-2.444 – -2.448	0.011

Figures shown in parenthesis are the mid orientated B_{tet}-OH acceptor sites only; there are no hydrogen atom donors from this OH group.

4.3.3 Heptaborate anions

As mentioned briefly in Section 4.3.2, the 'O$^+$' isomer of the heptaborate anion, $[B_7O_9(OH)_5]^{2-}$, is closely related to the observed hexaborate anion, $[B_6O_7(OH)_6]^{2-}$, as it contains the three conjoined 6-membered rings. The difference with the heptaborate anion is that it contains a fourth conjoined 6-membered ring which is formed through condensation of a $B(OH)_3$ molecule with two *exo* OH groups of a hexaborate anion.

Previous computational analyses of the two heptaborate anion isomers (the 'O$^+$' and 'chain' isomers – see Figure 4.20a and b, respectively) concluded that the 'chain' isomer was a more stable configuration by *ca*. 10 kJ mol^{-1}, despite the 'O$^+$' isomer displaying intramolecular H-bonding.[255] However, only two rotamers out of a possible thirty-two (2^5) were investigated for the 'O$^+$' isomer, whereas the 'chain' isomer was investigated fully. Both the 'O$^+$' isomers of the heptaborate and hexaborate anions display evidence of intramolecular H-bonding. To be confident that the 'chain' isomer of the heptaborate anion is the more stable rotamer, the remaining possible rotamers of the heptaborate anion ('O$^+$' isomer) were investigated using DFT and QTAIM.

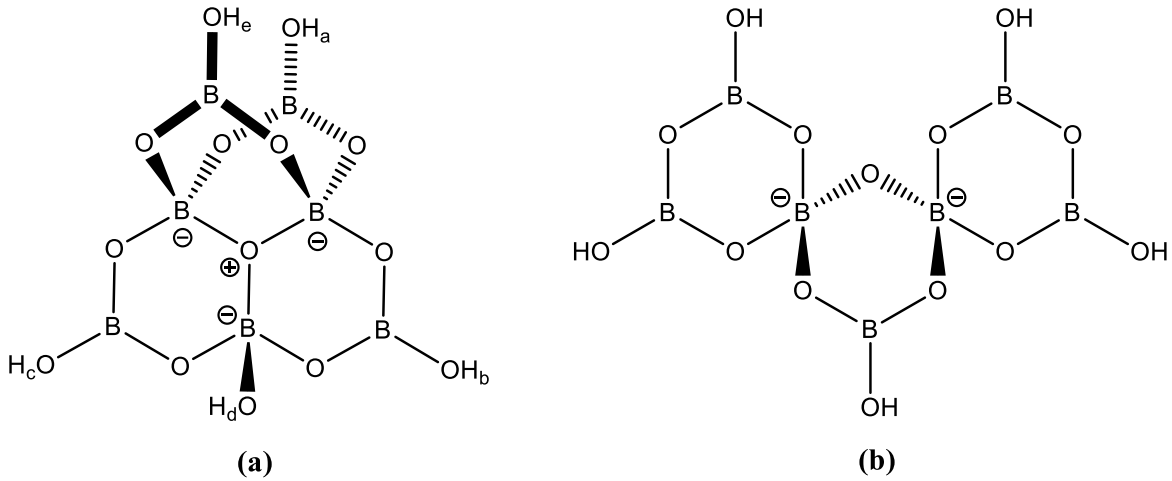

Figure 4.20: The isomers of the heptaborate anion, $[B_7O_9(OH)_5]^{2-}$; (a) the 'O$^+$' isomer, and (b) the 'chain' isomer.

As with the hexaborate anions, the OH groups attached to the trigonal and tetrahedral boron atoms were labelled in a clockwise manner, based upon the O^+ atom being the centre of an imaginary clock face. Specific hydrogen atoms were again labelled as being clockwise (C) or anticlockwise (A) relative to the boron atom (Section 4.3.2, Figure 4.13). Out of a possible thirty-two different rotamers (2^5) based upon C/A rotation of the OH bonds only, 16 unique rotamers were obtained and their relative energies are shown in Table 4.11.

As can be seen from these results, all 16 unique rotamers were minima, which was confirmed by the harmonic vibrational frequency data. As with the hexaborate anion, rotation of any planar trigonal B-OH groups (labelled a-e) have very little effect on the energy of the rotamers, due to the absence of any IHBs. IHBs may form between the *exo*- tetrahedral B-OH group and either oxygen atom on the fourth 6-membered boroxole ring (see Figure 4.21); this was found to be the case in over 60% of the rotamers.

Table 4.11: The relative energies of the heptaborate anion, $[B_7O_9(OH)_5]^{2-}$, modelled in the gas phase at the B3LYP/6-311++G(*d*,*p*) level of DFT theory.

Orientation of OH bond					Relative energy (kJ mol^{-1})	Number of IHBs[a]	Lowest vibrational frequency ν_1 (cm^{-1})
a	b	c	d	e			
C	C	C	C	C	0	1	48
C	C	C	A	A	0	1	50
C	A	A	A	A	1	1	49
C	A	C	A	A	1	1	49
C	C	A	A	A	1	1	50
C	A	C	C	C	1	0	49
C	C	A	C	C	1	1	49
C	A	A	C	C	2	1	49
C	C	C	C	A	2	1	47
C	C	C	A	C	2	0	47
C	A	A	A	C	2	0	46
C	A	C	A	C	2	0	46
C	C	A	A	C	3	0	46
C	A	C	C	A	3	0	47
C	C	A	C	A	3	1	48
C	A	A	C	A	4	1	48

[a] Confirmed by QTAIM analyses conducted after geometry optimization.

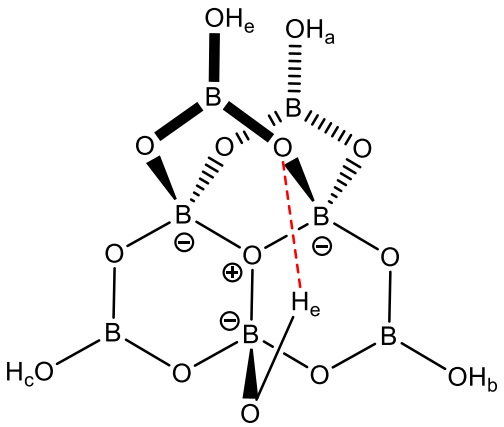

Figure 4.21: The intramolecular H-bond (IHB) between the *exo*-B_{tet}-OH and oxygen atom on the fourth boroxole ring found within the 'O^{+}' isomer of the heptaborate anion; orientation of the remaining OH groups have been omitted for clarity – IBH is shown as a red dashed line.

No trend is observed between the relative conformational energy and the number of heptaborate IHBs (which are confirmed by the presence of a BCP and RCP upon QTAIM analysis). The energies of the 16 rotamers are all found to be the same (within computational error), therefore this confirms that the rotamer used in the previous computational study by Beckett *et al*.[255] was the most stable rotamer for comparison against the 'chain' isomer.

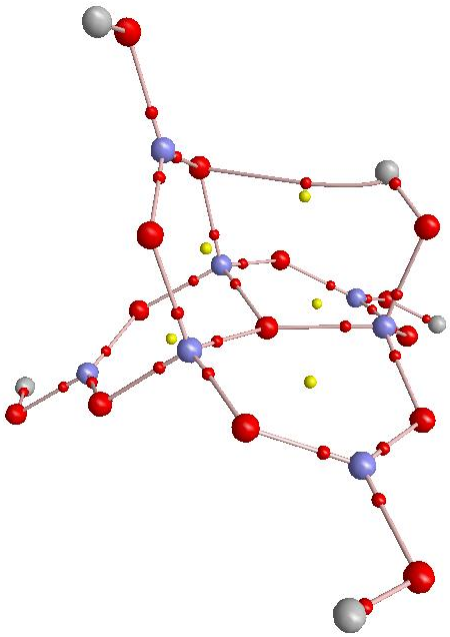

Figure 4.22: QTAIM analysis of the 'O^{+}' isomer of the heptaborate anion, $[B_7O_9(OH)_5]^{2-}$, shown in the CCCAA conformation. BCP and RCP are shown as small red and yellow dots, respectively.

QTAIM analyses of the rotamers (Figure 4.22) confirmed the presence of very weak IHBs within a number of the conformers outlined in Table 4.12. This was observed from low ρ_b values (<0.01 a.u.) and much shorter BCP-RCP distances. In comparison, the RCPs found within ring formations in the pentaborate anions were at a maximum distance, indicating much stronger ring formations. In addition to this, a small reduction in ρ_b, a negligible elongation in r_{OH} and *ca*. 15 cm^{-1} red shift in ν_{OH} are observed for interacting B-OH groups, compared with non-interacting B-OH groups. The bond lengths and vibrational frequencies for the 'O^{+}' isomer of the heptaborate anion are given in Table 4.12. QTAIM results obtained for the 'O^{+}' isomer of the heptaborate anion are summarised in Table 4.13.

Table 4.12: Summary of bond lengths and vibrational frequencies within the 'O^{+}' isomer of the hexaborate anion, $[B_7O_9(OH)_5]^{2-}$.

Rotamer	Bond type	Bond length (Å)	ρ_b (a.u.)	ν_{OH}
CCCCC	H-bond	2.6186	0.008	n/a
	OH_e	0.9619	0.365	3847
	OH_{a-d}	0.9615 – 0.9617	0.367	3860 – 3862
CCCAA	H-bond	2.5904	0.008	n/a
	OH_e	0.9620	0.365	3844
	OH_{a-d}	0.9615 – 0.9616	0.367	3860 – 3862
CAAAA	H-bond	2.5946	0.008	n/a
	OH_e	0.9619	0.365	3846
	OH_{a-d}	0.9615 – 0.9617	0.367	3860 – 3863
CACAA	H-bond	2.6240	0.008	n/a
	OH_e	0.9618	0.365	3848
	OH_{a-d}	0.9615 – 0.9617	0.367	3860 - 3862
CCAAA	H-bond	2.5668	0.009	n/a
	OH_e	0.9621	0.365	3842
	OH_{a-d}	0.9614 – 0.9617	0.367	3859 - 3863
CACCC	H-bond	n/a	n/a	n/a
	OH_e	0.9618	0.365	3848
	OH_{a-d}	0.9614 – 0.9616	0.367	3861 – 3863
CCACC	H-bond	2.5912	0.008	n/a
	OH_e	0.9621	0.365	3843
	OH_{a-d}	0.9615 – 0.9617	0.367	3860 - 3863
CAACC	H-bond	2.6132	0.008	n/a
	OH_e	0.9620	0.365	3844
	OH_{a-d}	0.9614 – 0.9616	0.367	3861 – 3863
CCCCA	H-bond	2.6114	0.008	n/a
	OH_e	0.9616	0.365	3850
	OH_{a-d}	0.9615 – 0.9616	0.367	3861 – 3862
CCCAC	H-bond	n/a	n/a	n/a
	OH_e	0.9615	0.365	3852
	OH_{a-d}	0.9615 – 0.9616	0.367	3861 – 3862
CAAAC	H-bond	n/a	n/a	n/a
	OH_e	0.9616	0.365	3850
	OH_{a-d}	0.9615 – 0.9616	0.367	3861 - 3863

Rotamer	Bond type	Bond length (Å)	ρ_b (a.u.)	ν_{OH}
CACAC	H-bond	n/a	n/a	n/a
	OH_e	0.9614	0.366	3852
	OH_{a-d}	0.9615 – 0.9616	0.367	3861 – 3863
CCAAC	H-bond	n/a	n/a	n/a
	OH_e	0.9617	0.365	3849
	OH_{a-d}	0.9614 – 0.9616	0.367	3861 – 3863
CACCA	H-bond	n/a	n/a	n/a
	OH_e	0.9614	0.366	3852
	OH_{a-d}	0.9614 – 0.9615	0.367	3862
CCACA	H-bond	2.5873	0.008	n/a
	OH_e	0.9617	0.365	3848
	OH_{a-d}	0.9614 – 0.9615	0.367	3861 – 3864
CAACA	H-bond	2.6028	0.008	n/a
	OH_e	0.9615	0.365	3851
	OH_{a-d}	0.9614 – 0.9615	0.367	3862 – 3863

Bond lengths are reported to 4 decimal places in order to show the negligible change.

Table 4.13: QTAIM analysis data for the 'O^{+}' isomer heptaborate anion, $[B_7O_9(OH)_5]^{2-}$.

Rotamer	Bond type	$\nabla^2(\rho_b)$ (a.u.)	ε
CCCCC	H-bond	0.037	2.569
	OH_e	-2.050	0.014
	OH_{a-d}	-2.084 – -2.087	0.011
CCCAA	H-bond	0.038	0.934
	OH_e	-2.051	0.014
	OH_{a-d}	-2.085 – -2.087	0.011
CAAAA	H-bond	0.038	1.129
	OH_e	-2.051	0.014
	OH_{a-d}	-2.084 – -2.087	0.011
CACAA	H-bond	0.037	5.424
	OH_e	-2.049	0.014
	OH_{a-d}	-2.084 – l-2.087	0.011
CCAAA	H-bond	0.039	0.614
	OH_e	-2.053	0.014
	OH_{a-d}	-2.083 – -2.087	0.011

Rotamer	Bond type	$\nabla^2(\rho_b)$ (a.u.)	ε
CACCC	H-bond	n/a	n/a
	OH_e	-2.048	0.014
	$OH_{a\text{-}d}$	-2.083 – -2.087	0.011
CCACC	H-bond	0.038	0.913
	OH_e	-2.052	0.014
	$OH_{a\text{-}d}$	-2.084 – -2.086	0.011
CAACC	H-bond	0.037	1.632
	OH_e	-2.050	0.014
	$OH_{a\text{-}d}$	-2.083 – -2.086	0.011
CCCCA	H-bond	0.037	6.142
	OH_e	-2.048	0.014
	$OH_{a\text{-}d}$	-2.084 – -2.088	0.011
CCCAC	H-bond	n/a	n/a
	OH_e	-2.048	0.014
	$OH_{a\text{-}d}$	-2.083 – -2.086	0.011
CAAAC	H-bond	n/a	n/a
	OH_e	-2.047	0.014
	$OH_{a\text{-}d}$	-2.084 – -2.087	0.011
CACAC	H-bond	n/a	n/a
	OH_e	-2.046	0.014
	$OH_{a\text{-}d}$	-2.084 – -2.087	0.011
CCAAC	H-bond	n/a	n/a
	OH_e	-2.049	0.014
	$OH_{a\text{-}d}$	-2.084 – -2.085	0.011
CACCA	H-bond	n/a	n/a
	OH_e	-2.046	0.014
	$OH_{a\text{-}d}$	-2.083 – -2.088	0.011
CCACA	H-bond	0.038	1.365
	OH_e	-2.050	0.014
	$OH_{a\text{-}d}$	-2.083 – -2.085	0.011
CAACA	H-bond	0.037	2.403
	OH_e	-2.049	0.014
	$OH_{a\text{-}d}$	-2.083 – -2.086	0.011

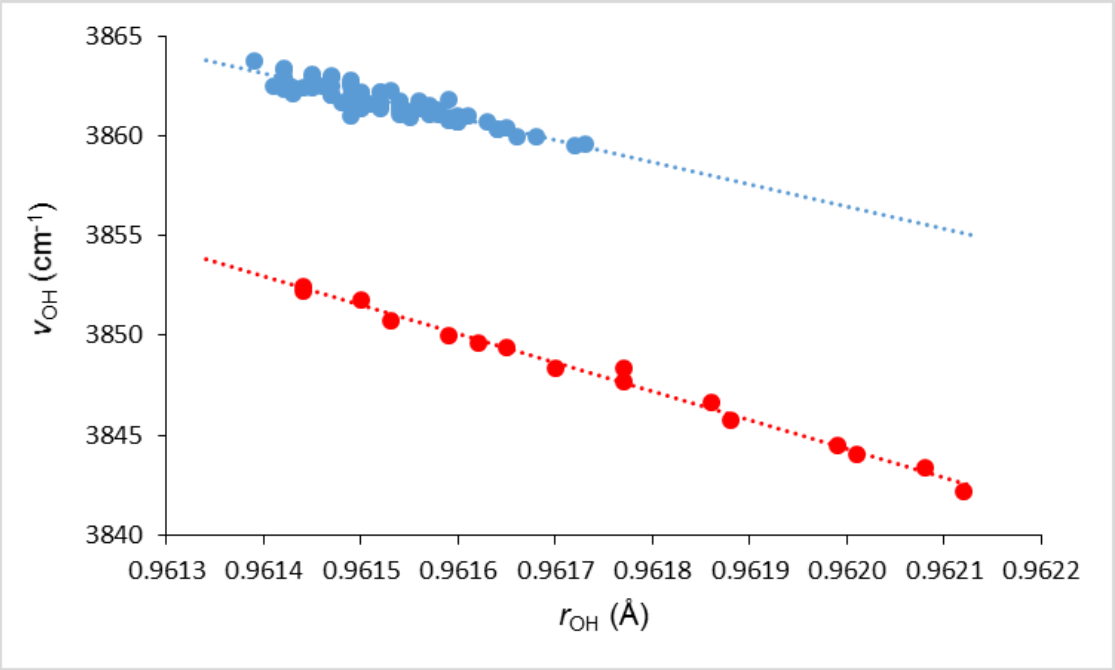

Figure 4.23: Graph of the calculated heptaborate anion O–H bond lengths (r_{OH}) against their corresponding vibrational frequencies (ν_{OH}). Non-interacting O–H bonds are shown in blue, [ν_{OH} = 14471 – 11034r_{OH}; n = 65, R^2 = 0.8274, σ = 1 cm^{-1}]; interacting O–H bonds are shown in red, [ν_{OH} = 17697 – 14400r_{OH}; n = 16, R^2 = 0.9915, σ = 1 cm^{-1}].

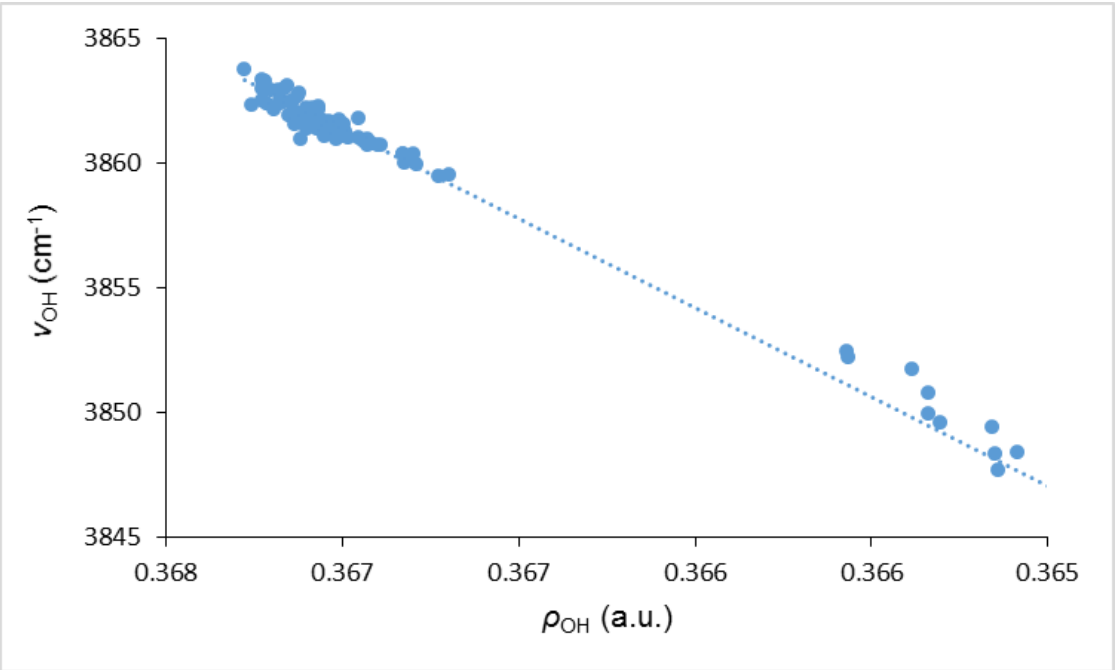

Figure 4.24: Graph of the calculated heptaborate anion O–H bond density (ρ_{OH}) against their corresponding vibrational frequencies (ν_{OH}) [ν_{OH} = 1241 + 7140r_{OH}; n = 81, R^2 = 0.9882, σ = 1 cm^{-1}].

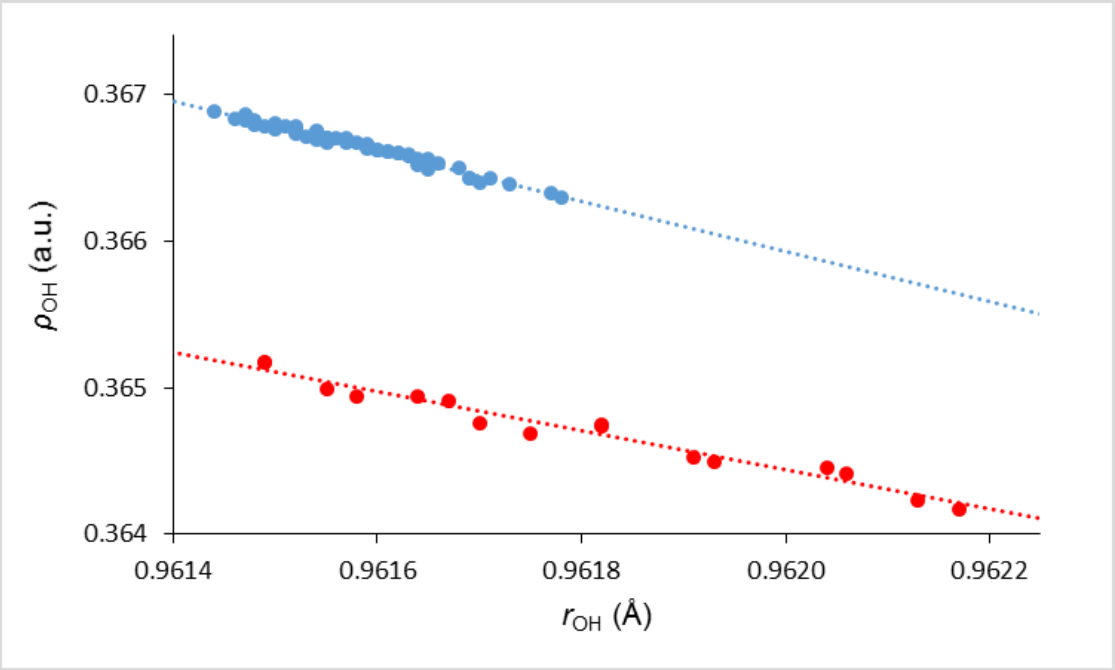

Figure 4.25: Graph of the calculated heptaborate anion O–H bond lengths (r_{OH}) against their corresponding bond density (ρ_{OH}) Non-interacting O–H bonds are shown in blue, [ρ_{OH} = 2.01 – 1.71r_{OH}; n = 65, R^2 = 0.9784, σ = 0 cm^{-1}]; interacting O–H bonds are shown in red, [ρ_{OH} = 1.65 – 1.33r_{OH}; n = 16, R^2 = 0.9656, σ = 0 cm^{-1}].

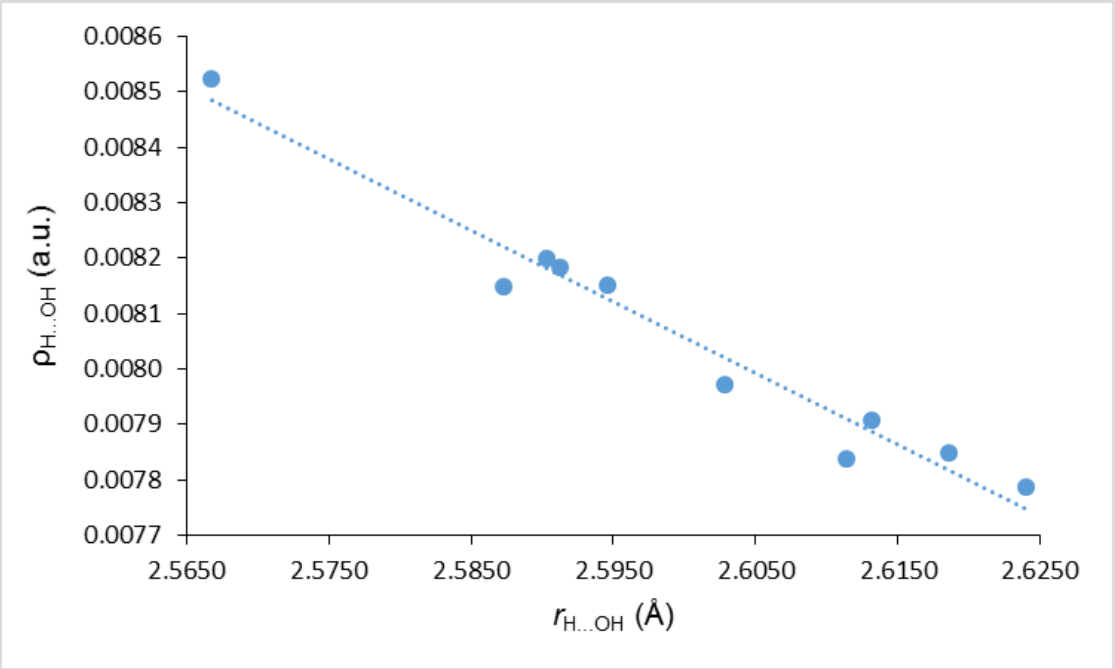

Figure 4.26: Graph of the calculated heptaborate anion H-bond lengths ($r_{H...OH}$) against their corresponding bond density ($\rho_{H...OH}$) [$\rho_{H...OH}$ = 0.042 – 0.013$r_{H...OH}$; n = 10, R^2 = 0.9600, σ = 0 cm^{-1}].

Figure 4.23 shows a good correlation between the non-interacting O–H bond lengths (blue) and its corresponding vibrational frequency; the same can be observed for the interacting O–H bond lengths (red). A negligible elongation in bond length results in a small red shift in the vibrational frequency (*ca*. 15 cm^{-1}). The density at the O-H bond critical point also decreases slightly with this observed red shift (Figure 4.24), which complements these findings. Combining these findings and plotting the O–H bond length against the density (Figure 4.25) confirms there is a direct correlation between the O–H bond lengths and the density; as the bond length increases, the density at the bond critical point decreases due to the formation of an H-bond.

Plotting a graph of the H-bond length against the density (Figure 4.26) shows a good correlation. Longer bond lengths have a lower value for ρ_b, whereas shorter bond lengths have a greater ρ_b value.

4.4 Summary

In solid-state structures, the pentaborate anion, $[B_5O_6(OH)_4]^-$, forms a 3D supramolecular framework in the form of anion-anion interactions, formed *via* H-bonding at different proton acceptor sites (α, β, γ, relative to the tetrahedral boron centre). These interactions can form H-bonded 8- or 12-membered rings, which contain two proton donor and two proton acceptor sites, and are given the Etter notation of $R_2^2(8)$ and $R_2^2(12)$, respectively.[107] An additional interaction may occur at a (β-O) proton donor acceptor site, in the form of an 8-membered continuous chain which has the Etter notation of C(8).[107] These H-bond interactions have been successfully examined and modelled using solvated DFT calculations and show that the strength of these H-bonds are relatively strong. The two types of $R_2^2(8)$ H-bond interactions (α: -21 kJ mol^{-1} and γ: -16 kJ mol^{-1}) are energetically favoured over $R_2^2(12)$ interactions (β: -10 kJ mol^{-1}). The strength of the H-bond which is found in the C(8) β-chain was found to be comparable with that of the γ- $R_2^2(8)$ H-bond (-16 kJ mol^{-1}). The results of these H-bond strengths coincide with the occurrence of these motifs within solid-state structures, with the α,α,α,β configuration being the most frequently observed.

The rarer hexaborate and heptaborate dianions, $[B_6O_7(OH)_6]^{2-}$ and $[B_7O_9(OH)_5]^{2-}$, respectively, have both been observed in solid-state structures as an 'O^+' isomer.[111] Beckett *et al*. modelled the alternative, 'chain' isomer of the heptaborate dianion, $[B_7O_9(OH)_5]^{2-}$, and found it to be *ca*. 10 kJ mol^{-1} more stable than the 'O^+' isomer;[255] the complete set of 'chain' isomer conformers were investigated, whereas only two possible conformers of the 'O^+' isomer were investigated. For completeness of this work, the relative conformational stability and intramolecular hydrogen bonding found within 'O^+' isomers of the heptaborate anion, along with the conformers of the structurally related hexaborate anion were investigated in the gas phase using DFT calculations. The results of these calculations show that the most energetically stable conformers of the hexaborate anion contain an unbroken, quasi-triangular cyclic network of IHBs, which were each found to have an estimated energy of 15 kJ mol^{-1}. In contrast to this, the conformers of the '$O^{+\prime}$ isomer of the heptaborate anion showed very weak or no IHBs, which resulted in similar energies. This confirms that the 'chain' isomer of the heptaborate anion is indeed more stable than the heptaborate anion's 'O^+' isomer, as previously calculated by Beckett *et al*.[255]

Chapter 5:

Lewis base adducts of triorganoboroxines

5.1 Introduction

1:1 and 2:1 adducts of triarylboroxines with *N*-donor ligands have been well documented since the middle of the 20th century, when Burg and co-workers reported the syntheses of 1:1 adducts using ammonia and trimethylamine as ligands in 1940.[278] In 1958, Snyder *et al.* proposed that the structure of the adducts involved the coordination of the *N* atom in the ligand to one of the boron atoms in the boroxine rings[209] and since then, several groups have reported 1:1 adducts of triarylboroxines with *N*-donor ligands,[209,245,279-283] with some having also investigated other stoichiometric ratios including 2:1 *N*-donor ligand to boroxine[278] and 1:2 ratios using diamine ligands which form adducts with two triarylboroxine units;[280] Figure 5.1 shows the 1:1 stoichiometry for triorganoboroxine:amine complexes.

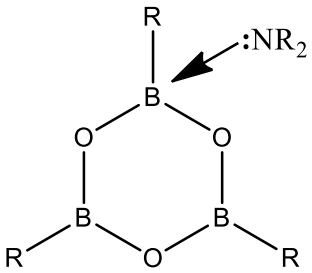

Figure 5.1: Diagram showing the 1:1 triorganoboroxine·amine adducts which are studied within this chapter.

The triarylboroxines and their adducts have been the focus of structural characterisation since 1938 when Snyder *et al*. proposed[284] that the boroxine rings possess some aromatic character through delocalisation of the lone pair of electrons on each oxygen atom on to the empty orbitals of the boron atoms. It has been deduced more recently this is not actually the case, and that the stability of the boroxine ring is due to ring strain and not due to any aromaticity.[266,285,286]

Triarylboroxine adducts have been studied through ^{1}H NMR spectroscopy solution, and in 1968 Ritchey[280] concluded that at room temperature the three boron centres were equivalent. In 1983, Yalpani and Boese reinvestigated Ritchey's adducts using low temperature ^{1}H NMR and indicated that in solution there is a temperature dependent fluctuation of the amine between the three borons of the

boroxine ring.[287] Low temperature ^{1}H NMR studies of the adducts is of great use as the Gibbs free energy of activation ($\Delta G^{\ddagger}$) can be determined when the ligand exchange process is slowed. Low temperature ^{1}H NMR solution studies previously done by Beckett *et al.* have concluded that neither steric congestion nor electronic effects of the aryl rings of the boroxines affect the $\Delta G^{\ddagger}$ for ligand exchange in solution.[245,283]

The Lewis acidity of the boron atoms partaking in the Lewis adduct formation with the *N*-donor ligands can also be calculated. The method was first derived by Gutmann[288] and Mayer *et al*.[289] and is based upon a quantitative parameter, known as an acceptor number (AN). The ANs are derived from changes in $^{31}P\{^{1}H\}$ NMR chemical shifts of triethylphosphine oxide (TEPO) produced in electrophilic solvents. The phosphorus atom in TEPO is deshielded through inductive effects from the nearby oxygen atom donating electron density to the surrounding solvent. The AN can be compared against a range of AN values – known as the Gutmann scale; this scale has fixed points, with the weak Lewis acid hexane at zero, and the strong Lewis acid antimony pentachloride at 100. The Gutmann method of measuring AN values was adapted by Beckett *et al*. and is now used to describe the Lewis acidity of boron centres[290] through measurement of the change in the $^{31}P\{^{1}H\}$ NMR chemical shift of TEPO dissolved in the boron containing species, using Equation 5.1.

$$AN = 100 \text{ X } (\delta\ ^{31}P_{(sample)} - 41.0) / (86.1 - 41.0) \qquad (5.1)$$

The numbers 86.1 and 41.0 are the chemical shifts of TEPO in antimony pentachloride and hexane, respectively.

5.2 Aims of chapter

The aims of this chapter were to synthesise and investigate the structures of the Lewis base adducts of triphenylboroxine (PB) (**24**), tri(4-chlorophenyl)boroxine (CPB) (**25**), and tris(pentafluorophenyl)boroxine (FPB) (**26**). Previous work done by

Beckett *et al*.[245, 283] has already shown that the activation energy for the ligand exchange behaviour in other triarylboroxine·amine complexes were independent of electronic and steric effects associated with the ligand and the triarylboroxine. The triorganoboroxines named above were chosen in order to further explore whether electronic effects relating to the aryl rings attached to the boroxine system have any effect on the free energy for ligand exchange in solution.

5.3 Results and discussion

5.3.1 Preparation and characterisation of the triarylboroxines

Finely crushed powders of the arylboronic acids phenylboronic acid, 4-chlorophenylboronic acid and pentafluorophenylboronic acid were dehydrated at 110°C to give the corresponding boroxines **24** – **26**. To prevent hydrolysis back to the arylboronic acids, the boroxines were stored in a sealed vessel under an inert atmosphere. The analytical data for the three triarylboroxines can be found in Chapter 2, Section 2.8.1.

The melting points obtained for **24** – **26** correspond favourably with those previously reported in the literature (Chapter 2, Section 2.8.1). The ^{1}H NMR spectrum for **24** showed three signals in the aromatic region; these comprised of a doublet and two triplets, of intensities 2:1:2. The doublet corresponds to the protons *ortho* to the boron atom, and is found furthest downfield. The protons at the *meta* position to the boron atom are found as the triplet furthest upfield and, finally, the signal arising from the proton which is found *para* to the boron atom is situated between the *ortho* and *meta* proton signals.

The ^{1}H NMR spectrum for **25** showed two AB doublets in the aromatic region and, as with the spectrum for **24**, the doublet furthest downfield corresponds to the protons *ortho* to the boron atom. The ^{19}F NMR data for **26** showed three signals of intensity 2:1:2 and correspond with those reported in the literature by H-J. Frohn *et al*.[291] The ^{11}B{^{1}H} NMR spectra for all three triarylboroxines obtained in $CDCl_3$ showed a broad singlet at approx. +30 ppm, which did not significantly differ from the singlet observed in the spectra of the corresponding boronic acids.

The triarylboroxines **24** and **25** dissolved sufficiently in $CDCl_3$ in order to obtain $^{13}C\{^1H\}$ NMR spectra. The spectrum for **24** shows three signals in the aromatic region, with the chemical shifts not significantly differing from those of phenylboronic acid. There was no visible peak observed for the *ipso* C atom. The $^{13}C\{^1H\}$ NMR spectrum for **25** also showed three signals in the aromatic region which did not differ significantly in terms of chemical shift compared to 4-chlorophenylboronic acid. As was the case with **24**, there was no visible peak observed for the *ipso* C atom in the $^{13}C\{^1H\}$ NMR spectrum of **25**. The low solubility of **26** in $CDCl_3$ inhibited the acquisition of a $^{13}C\{^1H\}$ NMR spectrum.

The IR spectra obtained for **24** – **26** all showed strong bands due to the B-O ring stretches at 1345 (br, s), 1344 (br, s) and 1349 cm^{-1} (br, s), respectively. These B-O ring stretching bands are similar to those observed in other triarylboroxines reported elsewhere in the literature.[292]

5.3.2 Formation of amine complexes

Six 1:1 triarylboroxine:amine complexes **29** – **34** were prepared from the reaction of **25** with the amines *cyclo*-hexylamine, morpholine, 2-picoline, 4-picoline, benzylamine and piperidine, in Et_2O. The triarylboroxine was insoluble in the reaction solvent, but upon addition of the corresponding amine, it almost instantaneously dissolved, resulting in a pale yellow solution. The syntheses of the 1:1 complexes proceeded according to Equation 5.2.

$$L + Ar_3B_3O_3 \rightarrow L{\cdot}Ar_3B_3O_3$$

(Ar = 4-ClC_6H_4, CPB (**25**)) (5.2)

The triarylboroxines **24** and **25** were also independently reacted with 4,4'-trimethylenedipiperidine (shown in Figure 5.2) in a 2:1 stoichiometric ratio, also in Et_2O. As with the 1:1 adduct formations, the triarylboroxine alone was insoluble in the reaction solvent but, upon addition of the amine, the white solid dissolved to form

a pale yellow solution. This was indicative that the 2:1 triarylboroxine:amine adducts (**27**-**28**) had been formed, and occurred almost instantaneously.

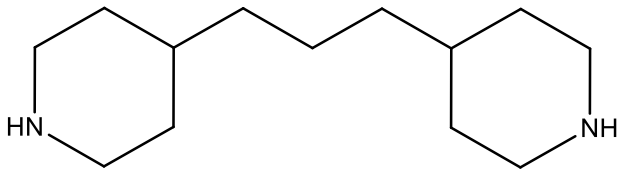

Figure 5.2: The *N* donor ligand 4,4'-trimethylenedipiperidine, which was reacted with two equivalents of triarylboroxines (24 and 25) to form adducts 27 and 28.

Yields were generally near quantitative and all compounds gave satisfactory elemental analyses. The compounds were air-stable, white solids with clearly defined melting points (see Chapter 2, Sections 2.8.2 – 9), and were readily soluble in chlorinated solvents, but less soluble in Et_2O and petroleum ether.

NMR spectra of the triarylboroxine·amine adducts, obtained at room temperature, all exhibited similar characteristics as exemplified by 4-picoline·CPB (**32**). Upon adduct formation, the chemical shift of the protons *ortho* to the B atom shifted upfield by ~2 ppm; this is as expected due to the increased shielding from addition of electron density to the B atom by the amino group. Likewise, the protons at the *meta* position also had an upfield chemical shift of ~1 ppm compared with those of the uncomplexed triarylboroxine. The ^{1}H NMR spectra of the ligand also showed a change in chemical shift; a downfield shift of ~4 ppm was observed for the protons closest to the N atom upon adduct formation, with a smaller change in chemical shift (~3 ppm) observed for the protons *meta* to the N atom. This observation is due to the reduction in electron density across the aryl ring of the ligand, causing deshielding of the nuclei closest to the N atom. The changes in chemical shift observed for both the triarylboroxine and the ligand upon adduct formation were typical for each adduct formed (**27**-**34**).

A similar pattern was observed when comparing the $^{13}C\{^{1}H\}$ NMR spectra of the adducts obtained at room temperature with the $^{13}C\{^{1}H\}$ NMR spectra of the triarylboroxines. Again, using **32** as an example, the chemical shift of the C atoms *ortho* to the B atoms in the adduct were found to be ~2 ppm further upfield of those

of the same C atoms in the triarylboroxine; the C atoms at the *meta* positions in the adducts were also found to be shifted upfield by ~1 ppm. This change in chemical shift to an upfield position confirms that addition of electron density to the B atom increases the shielding around the nuclei of the atoms closest to the B atoms within the aryl rings.

The signals from the room temperature solution $^{11}B\{^{1}H\}$ NMR spectra were not unequivocally obtained due to poor solubility which led to a low signal to noise ratio; however, weakly observable signals were found to be in the range of 20-23 ppm for the 1:1 adducts (**28**-**34**), which appear to be a weighted average in between the chemical shifts expected for a three coordinate boron signal (*ca*. 30 ppm) and a four coordinate boron signal (*ca*. 4 ppm).[293]

The ^{1}H and $^{13}C\{^{1}H\}$ NMR spectra of the triarylboroxine·amine adducts all showed that the aryl groups are equivalent on the NMR timescale at room temperature, which would indicate that each aryl ring would be coordinated to a ligand or fluctional processes are occurring. However, the relative intensities of the ^{1}H NMR signals and the elemental analysis results indicate that only one amine is coordinated to each triarylboroxine. Variable temperature NMR studies in related triarylboroxine·amine adducts carried out by Beckett *et al.*[245,283,294,295] have shown that this behaviour is down to the process of ligand dissociation-recombination, which is effectively a rapid movement of the ligand on and off the triarylboroxine and that an average signal is observed on the NMR timescale at room temperature.

Due to time constraints, adducts with *N* donor ligands were unfortunately not obtained using **26**. However, due to the strongly electron withdrawing C_6F_5 group, it is anticipated that this would have a large effect on the Lewis acidity of the B atom, lowering the electron density at the B atom and increasing the Lewis acid strength which would then, in turn, readily form adducts with *N* donor ligands. A further explanation on the measurement of the Lewis acidity of the B atoms is given further in this Chapter (Section 5.3.4).

5.3.3 Variable temperature ^{1}H NMR spectroscopy of triorganoboroxine·amine complexes

The triorganoboroxine·amine adducts all exhibited temperature dependent ^{1}H NMR spectra, which were investigated in more detail; those studied were **28**, **30**, **31**, **32** and **34**. The ^{1}H NMR spectra were recorded at 500 MHz over the temperature range of +35 to -35 °C, generally in 5 °C intervals. Due to the solubility of the adducts in this solvent, the spectra were all recorded in deuterated chloroform. Although $CDCl_3$ has a low melting point (-64 °C), spectra were not recorded lower than -35 °C (nor below -10 °C for **28**) due to issues with the stability of the shim coils within the NMR machine below this temperature. Figure 5.3 shows the variable temperature ^{1}H NMR signals obtained for the bis(tri(*p*-chlorophenyl)boroxine)·4,4'-trimethylenedipiperidine adduct (**28**).

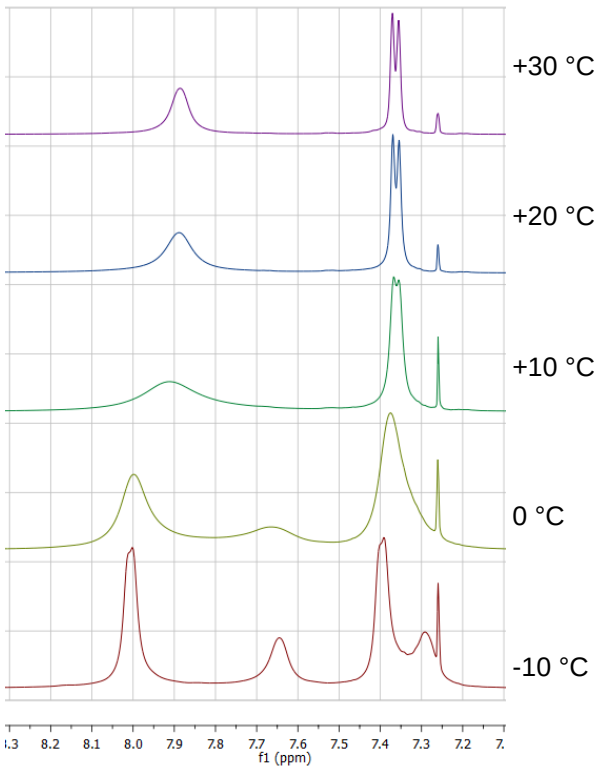

Figure 5.3: Variable temperature ^{1}H NMR signals of the aryl substituents on tri(*p*-chlorophenyl)boroxine, as found in adduct (28), showing that as the temperature decreases, the ligand dissociation-recombination process slows until they are no longer seen as equivalent protons on the NMR timescale.

The variable temperature ^{1}H NMR data for **28** can be discussed in detail; at -10 °C it can be seen that the protons on the aryl rings appear as 4 separate signals at 7.29, 7.39, 7.65 and 8.00 ppm, with the relative intensities 8:4:8:4. The reason for the appearance of the four signals is because the ligand exchange process is slow at this temperature relative to the NMR timescale and as a consequence the protons on the aryl group attached to the coordinated boron atom are no longer equivalent to the aryl groups attached to the uncoordinated boron atoms. Upon warming, the signals for the protons which are at the *meta* positions to the boron atoms broaden and coalesce at -5 °C, then with continued warming sharpen into a doublet. Likewise, the signals for the protons which are at the *ortho* positions to the boron atoms broaden and coalesce at +5 °C, then sharpen into a broad singlet. With continued heating, this signal would also sharpen in to a single doublet peak, however the temperature at which this would be observed is beyond the temperature limit of the solvent and cannot be seen in this example. The chemical shift of the two different proton signals appear as weighted averages of the four signals observed at -10 °C (intensity 12:12).

Variable temperature ^{11}B{^{1}H} NMR spectra were not recorded due to the low signal:noise ratios observed in the spectra obtained at room temperature (25 °C) because of the low solubility of the boroxine adducts.

Beckett *et al*. determined the nature of the exchange process occurring at room temperature in analogous triarylboroxine·amine complexes.[283,295] The Gibbs free energy of activation ($\Delta G^{\ddagger}$) for the ligand exchange process taking place can be calculated using the Eyring equation, which uses values obtained from the ligand-exchange rate (k) at coalescence temperature (T_c) and the low temperature peak separation at slow-exchange (δ_v); the calculated $\Delta G^{\ddagger}$ data can be found in Table 5.1. For CPB complex **31**, slow exchange was not observed in the ^{1}H NMR spectra, even at -35 °C. The $\Delta G^{\ddagger}$ values obtained for the CPB·amine complexes lie in the range of 49-58 kJmol^{-1}, which are similar in magnitude to those in the literature of the related (*p*-$BrC_6H_4)_3B_3O_3$·amine complexes.[245] Upon reviewing this information, it can be deduced that the values are independent of steric effects which might be associated with the amine ligand of the adduct and triarylboroxine. This has also been found to be the case for the amine adducts of (2-$MeC_6H_4)_3B_3O_3$ (OTB), (3,5-

$MeC_6H_4)_3B_3O_3$ MXB, $(4\text{-}MeC_6H_4)_3B_3O_3$ (PTB), $(4\text{-}BrC_6H_4)_3B_3O_3$ (PBB) and $(3\text{-}NO_2C_6H_4)_3B_3O_3$ (MNB), which are reported in the literature.[245,283,295]

Table 5.1: Variable temperature ^{1}H NMR data.

No	Complex	T_c (K)	δ_v (Hz)	k (s^{-1})[a]	$\Delta G^{\ddagger}$ ($kJmol^{-1}$)[b]
28[c]	4,4'trimethylenedipiperidine·$[CPB]_2$	268	50	111	54.9
28[d]		278	175	389	54.1
30[c]	morpholine·CPB	255	50	111	53.8
30[d]		260	160	355	50.7
32[c]	4-picoline·CPB	258	95	211	51.4
32[d]		253	225	500	48.5
34[c]	piperidine·CPB	283	55	122	57.9
34[d]		293	175	389	57.2

[a] $k=2^{-1/2}\pi\delta_v$

[b] $\Delta G^{\ddagger}=-RT\ln(khk_B^{-1}T^{-1})$

[c] from upfield aromatic doublet of $(p\text{-}ClC_6H_4)_3B_3O_3$·L

[d] from downfield aromatic doublet of $(p\text{-}ClC_6H_4)_3B_3O_3$·L

5.3.4 Measurement of Lewis acidity at boron centre

Table 5.2 contains the AN values obtained for the triarylboroxines **24** – **26**. The Lewis acidity of the triarylboroxines decreases in the order FPB>CPB>PB, which is as expected due to the substituents attached to the aryl rings of the boroxine. Triphenylboroxine (**24**) has H substituents attached to the aryl rings and has the lowest AN. Tri(*p*-chlorophenyl)boroxine (**25**) has one electronegative atom attached at the *para* position; the electron withdrawing property of the chlorine atom has a minor effect on the Lewis acidity, increasing the AN only by 0.6. Both PB and CPB are moderate Lewis acids, with AN similar those reported for other triarylboroxines.[292]

Table 5.2: The $^{31}P\{^{1}H\}$ chemical shift (δ) and acceptor numbers for TEPO with triarylboroxines 24-26.

Compound number	δ ($^{31}P\{^{1}H\}$)	Acceptor number (AN)
24	61.7[a]	45.8
25	62.0[a]	46.4
26	71.5[b]	67.5

[a] Obtained in $CDCl_3$

[b] Obtained in THF

Interestingly, tris(pentafluorophenyl)boroxine (**26**) has an AN which is 21 higher than tri(*p*-chlorophenyl)boroxine, which means FPB is a much stronger Lewis acid. This is likely due to the fact that FPB has multi electron-withdrawing F atom substituents on the aryl rings, which causes a greater increase in electron density withdrawal from the boron atoms.

5.3.5 Crystal Structures of morpholine·CPB (**30**) and benzylamine·CPB (**33**)

The crystal structures of morpholine·tri(*p*-chlorophenyl)boroxine (**30**) and benzylamine·tri(*p*-chlorophenyl)boroxine (**33**) are reported in this section. Crystals suitable for single-crystal X-ray diffraction studies were obtained through recrystallization of the crude products from chloroform. The spectroscopic and analytical data for the recrystallized products are given in Chapter 2, Sections 2.8.5 and 2.8.8. The crystal structure data were obtained and solved by the National Crystallographic Service at Southampton and the full crystallographic data is available in appendices (NCS numbers 2015NCS0475 and 2013NCS0216, respectively).

The crystallographic structure of **30** is shown in Figure 5.4 and selected bond lengths and angles are given in Table 5.3. Consisting of two identical molecules within the unit cell (*Z*=2), the triclinic molecular structure of **30** comprises of a six-membered alternating B_3O_3 (boroxole) ring, which is similar to that found in the CPB (**25**) starting material, with an additional coordination from the nitrogen atom (N1) of the morpholine to one of the three ring boron atoms (B1), resulting in the B1 atom having a distorted tetrahedral geometry with bond angles in the range of 103.42(9) – 114.67(10)°. The two remaining boron atoms are three-coordinate and trigonal

planar, with bond angles in the range of 117.16(11) – 121.44(11)°, whilst the three ring oxygen atoms are two-coordinate with bond angles in the range of 119.32(10) – 122.16(10)°. The coordinated morpholine ligand is found to be in a chair conformation; the C-N-B angles are 114.53(9)° and 115.34(9)°, whilst the C-N-C angle is 108.98(9)°. There is also H-bonding taking place from the N1-H1 atom of the morpholine ligand to a Cl2 atom of an identical molecule within the unit cell (2.516(17) Å).

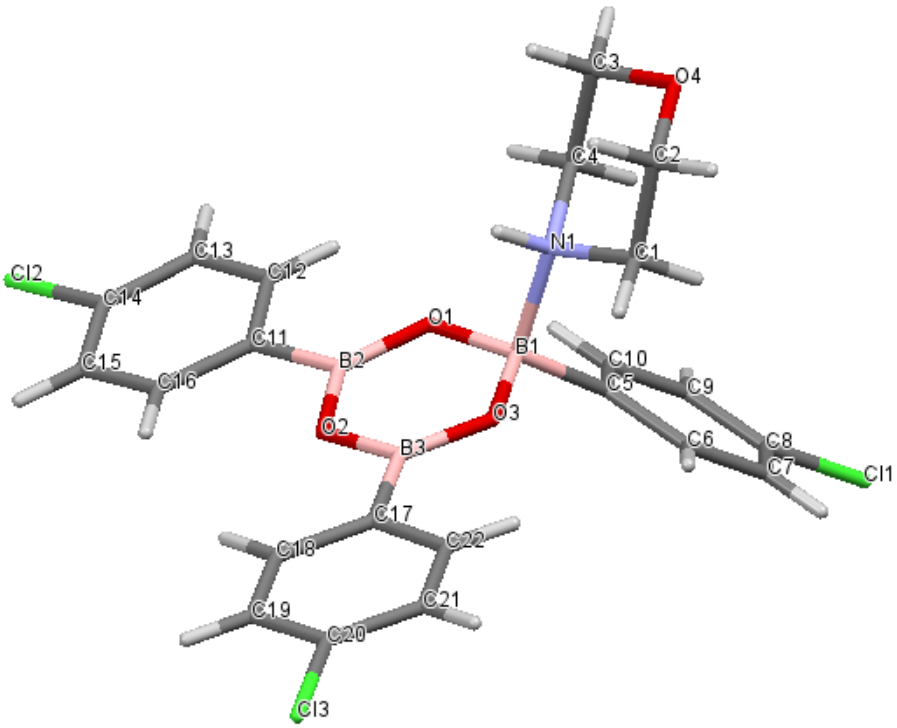

Figure 5.4: Molecular structure of morpholine·tris(*p*-chlorophenyl)boroxine (30) showing the atomic numbering scheme.

The aryl C-C-C bond angles at the carbon atoms linked to boron (C5, C11 and C17) are found to be in the range of 116.72(11) – 118.16(11)° and are smaller than the ideal 120° value expected due to their linkage to the boron atoms (B1, B2 and B3, respectively). The C-Cl bond lengths were found to be in the range of 1.7451(13) – 1.7587(12) Å. The B-O and B-N distances will be discussed further later in this section.

Table 5.3: Selected bond lengths (Å) and angles (°) for morpholine·tri(*p*-chlorophenyl)boroxine (30).

Bond lengths (Å)			
B1-O1	1.4583(16)	B1-C5	1.6090(18)
B1-O3	1.4623(16)	B2-C11	1.5675(18)
B2-O1	1.3477(16)	B3-C17	1.5690(18)
B2-O2	1.3846(17)	C8-Cl1	1.7451(13)
B3-O3	1.3542(16)	C14-Cl2	1.7587(12)
B3-O2	1.3873(16)	C20-Cl3	1.7479(13)
B1-N1	1.6551(17)		
Bond angles (°)			
O1-B1-O3	113.44(10)	C1-N1-B1	114.53(9)
O1–B1–C5	111.79(10)	B2–O1–B1	122.16(10)
O3–B1–C5	114.67(10)	B2–O2–B3	119.32(10)
O1–B1–N1	103.57(9)	B3–O3–B1	121.78(10)
O3–B1–N1	103.42(9)	C6-C5-C10	116.72(11)
C5–B1–N1	108.87(9)	C16-C11-C12	118.16(11)
O1–B2–O2	121.18(11)	C22-C17-C18	117.91(11)
O1–B2–C11	119.74(11)	C6–C5–B1	122.86(11)
O2–B2–C11	119.08(11)	C10–C5–B1	120.40(11)
O3–B3–O2	121.39(11)	C16–C11–B2	122.30(11)
O3–B3–C17	121.44(11)	C12–C11–B2	119.52(11)
O2–B3–C17	117.16(11)	C22–C17–B3	121.49(11)
C4–N1–C1	108.98(9)	C18–C17–B3	120.60(11)
C4–N1–B1	115.34(9)		

The molecular structure of benzylamine·tri(*p*-chlorophenyl)boroxine (**33**) was also crystallized in a triclinic crystal system, with two independent molecules per unit cell (*Z*=4). The solved molecular structure of (**33**) is shown in Figure 5.5, with selected bond lengths and angles given in Tables 5.4 and 5.5, respectively.

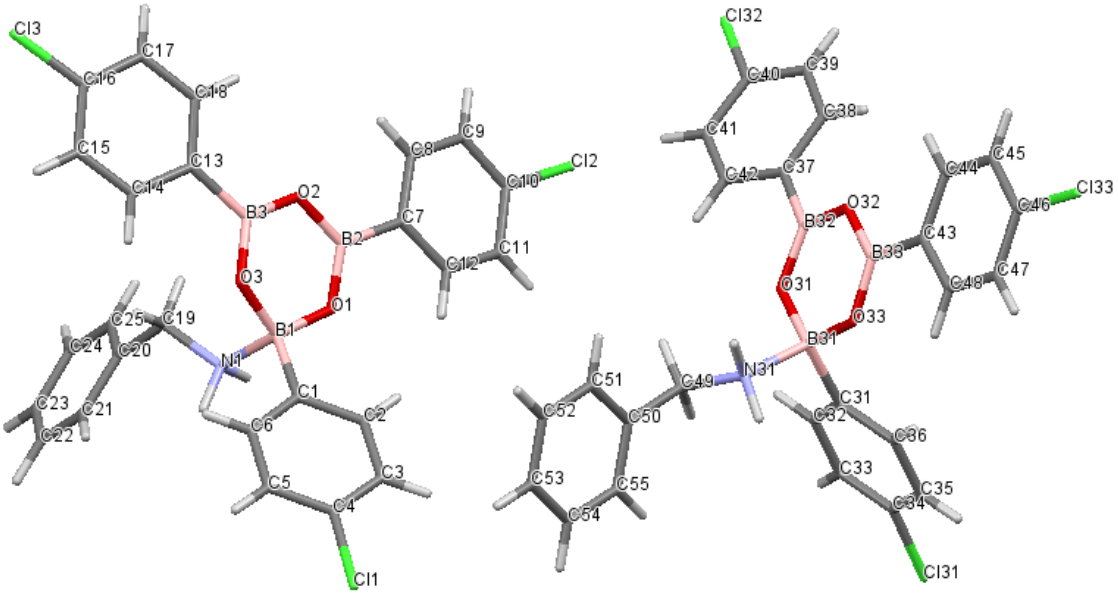

Figure 5.5: Molecular structure of benzylamine·tris(*p*-chlorophenyl)boroxine (33) showing the atomic numbering scheme.

The molecular structure of **33** comprises of two independent molecules per asymmetric unit, which each consist of a six-membered boroxole ring, again similar to that of the starting material CPB (**25**), with additional coordination from the nitrogen donor atoms (N1 and N31) of the benzylamine ligands to one of the three ring boron atoms (B1 and B31, respectively), giving these boron atoms a distorted tetrahedral geometry with bond angles in the range of 104.85(16) – 113.87(17)° and 103.42(16) – 113.15(18)°, respectively. The two remaining boron atoms on each molecule are both three-coordinate and trigonal planar, with bond angles in the range of 118.15(19) – 120.61(19)° and 119.0(2) – 121.3(2)°, whilst the three ring oxygen atoms are two-coordinate with bond angles in the range of 119.36(17) – 122.92(17)° and 118.99(17) – 122.73(17)°. C-N-B bond angles are 118.72(17)° and 116.92(16)°, respectively, and the aryl rings of the ligands sit almost perpendicularly to the boroxole rings (83.15° and 87.59°). The C-C-C bond angles at the carbon atoms linked to boron (C1, C7, C13, and C31, C37 and C43) are found to be in the ranges 117.1(2) – 117.66(19)° and 116.7(2) – 117.5(2)°, respectively; as with (**30**), these are all found to be smaller than the idealised 120° bond angle due to their linkages with boron. The C-Cl bond lengths were found to be similar those found in complex **30**, and are in the range 1.734(2) – 1.743(2) Å.

Table 5.4: Selected bond lengths (Å) for benzylamine·tri(*p*-chlorophenyl)boroxine (33).

Bond lengths (Å)			
B1-O1	1.444(3)	B31-O31	1.452(3)
B1-O3	1.450(3)	B31-O33	1.461(2)
B2-O1	1.346(3)	B32-O31	1.345(3)
B2-O2	1.384(3)	B32-O32	1.387(2)
B3-O3	1.358(3)	B33-O33	1.336(3)
B3-O2	1.387(3)	B33-O32	1.385(3)
B1-N1	1.679(3)	B31-N31	1.638(3)
B1-C1	1.605(3)	B31-C31	1.606(3)
B2-C7	1.563(3)	B32-C37	1.558(3)
B3-C13	1.557(3)	B3-C13	1.557(3)
C4-Cl1	1.734(2)	C34-Cl31	1.743(2)
C10-Cl2	1.734(2)	C40-Cl32	1.738(2)
C16-Cl3	1.737(2)	C46-Cl33	1.738(2)

Table 5.5: Selected bond angles (°) for benzylamine·tri(*p*-chlorophenyl)boroxine (33).

Bond angles (°)			
O1-B1-O3	113.18(17)	O31-B31-O33	113.05(17)
O1–B1–C1	113.12(17)	O31–B31–C31	113.15(18)
O3–B1–C1	113.87(17)	O33–B31–C31	112.06(17)
O1–B1–N1	104.85(16)	O31–B31–N31	106.31(16)
O3–B1–N1	104.89(16)	O33–B31–N31	103.42(16)
C1–B1–N1	105.82(16)	C31–B31–N31	108.08(16)
O1–B2–O2	120.50(19)	O31–B32–O32	121.3(2)
O1–B2–C7	118.91(18)	O31–B32–C37	119.60(18)
O2–B2–C7	120.53(19)	O32–B32–C37	119.05(18)
O3–B3–O2	121.05(19)	O33–B33–O32	121.21(18)
O3–B3–C13	118.15(19)	O33–B33–C43	119.0(2)
O2–B3–C13	120.61(19)	O32–B33–C43	119.78(19)
C19–N1–B1	118.72(17)	C49–N31–B31	116.92(16)
B2–O1–B1	122.92(17)	B32–O31–B31	121.99(16)
B2–O2–B3	119.36(17)	B32–O32–B33	118.99(17)
B3–O3–B1	121.01(17)	B33–O33–B31	122.73(17)
C6-C1-C2	117.1(2)	C36-C31-C32	116.7(2)
C12-C7-C8	117.48(19)	C42-C37-C38	117.5(2)
C18-C13-C14	117.66(19)	C48-C43-C44	117.45(19)
C6–C1–B1	121.75(18)	C36–C31–B31	120.88(19)
C2–C1–B1	121.08(18)	C32–C31–B31	122.42(19)
C12–C7–B2	119.85(18)	C42–C37–B32	120.70(18)
C8–C7–B2	122.62(18)	C38–C37–B32	121.75(18)
C18–C13–B3	123.79(19)	C48–C43–B33	119.79(19)
C14–C13–B3	118.25(18)	C44–C43–B33	122.7(2)

The B-O and B-N bond distances in the morpholine·CPB (**30**) and benzylamine·CPB (**33**) adducts can be compared with distances reported elsewhere for analogous adducts. The average B-O and B-N bond lengths are summarised in Table 5.6, with Figure 5.6 indicating the numbering scheme used.

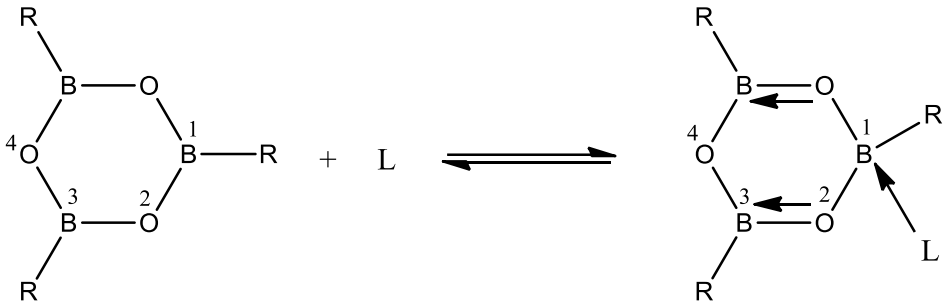

Figure 5.6: Schematic of electronic effects of a triorganoboroxine·amine adduct, including atomic labelling scheme as used in Table 5.6.

Table 5.6: Average B-O, B-N and B-L distances found in triorganoboroxines and triorganoboroxine·amine complexes.

Compound name	Average bond lengths (Å)			
	B^1-O^2	B^3-O^2	B^3-O^4	B-L distance
morpholine·CPB (**30**)	1.460	1.350	1.386	1.655
benzylamine.CPB (**33**)	1.452	1.346	1.384	1.659
4-picoline·PTB[283]	1.467	1.350	1.400	1.648
PTB[283]	1.384	1.384	1.384	n/a
Boroxine, $H_3B_3O_3$[296]	1.375	1.375	1.375	n/a

The average B^1-O^2 distances in the triorganoboroxine·amine complexes are considerably longer (1.435 – 1.467 Å) than those of the uncoordinated triorganoboroxine (1.384 Å) and boroxine (1.375 Å). The longer B-O distances observed at the four-coordinate B^1 atom is due to loss of π-bonding with the adjacent O^2 atom upon coordination of the *N* donor amine ligand; the π-electron density is forced over from the O^2 atom towards the B^3 atom which then shortens the bond (by *ca*. 0.01 – 0.04 Å relative to the uncoordinated triorganoboroxine) and results in a stronger π-bond interaction. The B^3-O^4 bond distances found in the triorganoboroxine·amine adducts do not differ significantly from those of the uncoordinated triorganoboroxines. This is due to the fact that they are at the opposite end of the coordination point on the boroxole ring and are at a great enough distance away to not feel the effects from the addition of electron density at the B^1

atom. The B-N bond distances found in all of the triorganoboroxine·amine adducts are all very similar in length and no trends are observed.

5.4 Summary

Eight new triarylboroxine·amine adducts have been prepared in high yields and characterized using spectroscopic (NMR, IR) and analytical (melting point, elemental analysis) techniques. Variable temperature ^{1}H NMR studies were carried out on a select few of the adducts and were found to have calculated Gibbs free energies of activation ($\Delta G^{\ddagger}$) in the range ~51-58 kJ mol^{-1}. These are not significantly different to those reported elsewhere in the literature, where studies carried out by Beckett *et al*. have found boroxine adducts to have $\Delta G^{\ddagger}$ values between 39-54 kJ mol^{-1}.[245,283,295] From this, we can deduce that the electronic effects associated with the substituents attached to the aryl rings of CPB (**25**) play no part in the barrier to ligand exchange in these triorganoboroxine·amine adducts. The crystal structures of tri(4-chlorophenyl)boroxine·morpholine (**30**) and tri(4-chlorophenyl)boroxine·benzylamine (**33**) have been obtained and are discussed in detail within the chapter.

The Lewis acidity of the triorganoboroxines PB (**24**), CPB (**25**) and FPB (**26**) were investigated; PB (**24**) and CPB (**25**) exhibit moderate Lewis acidity, with acceptor numbers of 45.8 and 46.4, respectively. The strongly electron-withdrawing pentafluorophenyl substituents on **26** has shown to greatly increase the Lewis acidity of the boron atoms, resulting in FPB having a higher acceptor number (67.5).

Chapter 6:

Summary

6.1 Summary

The synthesis and characterization of non-metal cation polyborate salts is described in Chapter 3. A total of twenty-one new polyborate salts are reported within this chapter; nineteen of these are salts containing the pentaborate anion, $[B_5O_6(OH)_4]^-$; one contains the triborate monoanion, $[B_3O_3(OH)_4]^-$; and one contains the heptaborate dianion, $[B_7O_9(OH)_5]^{2-}$. An additional amine-boric acid co-crystallized species is also reported within this chapter. All of the synthesized compounds were characterized using spectroscopic (IR, multi-element NMR) and analytical (melting point, elemental analysis, thermal analysis, powder X-ray diffraction) techniques.

The thermal properties of the non-metal cation polyborate salts were investigated using TGA-DSC analysis (in air) and all showed a similar thermal TGA curve; the polyborate anions are dehydrated *via* an endothermic process at temperatures up to 250 °C, followed by thermal decomposition of the non-metal (organic) cation *via* exothermic processes. At higher temperatures (above 700 °C) a glassy solid of residual B_2O_3 was observed. Polyborate salts with additional interstitial molecules showed an additional dehydration step <200°C due to the loss of these interstitial molecules. Non-metal (organic) cation polyborate salts may be considered as thermal precursor to porous B_2O_3, which meets the US Department of Energy's requirements as a hydrogen store. The porosities of pyrrolidinium pentaborate (**1**) and *N,N*-dimethylpyrrolidinium pentaborate sesquihydrate (**3**·1.5H_2O) were investigated using BET analyses of bulk samples obtained by thermal decomposition. Samples of their corresponding 'anhydrous', 'intumesced' and 'residual' materials were obtained by thermal decomposition at 250 °C, 500 °C and 750 °C, respectively. The results from the BET analysis indicated that all six analysed samples were non-porous, each with specific surface areas <1 $m^2\ g^{-1}$.

The crystal structures of ten polyborate salts are reported and discussed within this chapter: pyrrolidinium pentaborate (**1**), *N*-methylpyrrolidinium pentaborate·½ acetone (**2**·½CH_3COCH_3), *N,N*-dimethylpyrrolidinium pentaborate (**3**), 2-hydroxymethylpyrrolidinium pentaborate hemihydrate (**4**·½H_2O), (2-hydroxyethyl)-*N*-methylpyrrolidinium pentaborate·0.3 hydrate (**5**·0.3H_2O), 4-aminobenzylammonium pentaborate hemihydrate (**9**·½H_2O), *N,N*-dimethyl-1-

adamantylammonium pentaborate sesquihydrate (**14**·1.5H_2O), *N,N,N*-trimethyl-1-adamantylammonium pentaborate trihydrate (**15**·3H_2O), *N,N,N*-trimethyl-2-adamantylammonium pentaborate trihydrate (**17**·3H_2O) and 4,4'-bipiperidinium heptaborate dihydrate (**20**·2H_2O). The crystal structure of the co-crystallized boric acid·4,4'-trimethylene*bis*(*N*-methylpiperidine) (**22**) is also reported.

The solid-state structures of pentaborate salts containing **1**-**5**, **9**, **14**, **15** and **17** all showed giant anionic lattices held together by extensive H-bonding, with the cations (and co-crystallized species) occupying the 'cavities' of the lattice. The 'brickwall' structure, which is made up of anion-anion H-bond interactions at α,α,α,β acceptor sites, was observed in compounds containing **1**-**4**. Comparison of the structures of **1** and **3** shows that the unsubstituted cation (in **1**) is smaller and partakes in H-bonding interactions, whereas the larger dimethylated cation (in **3**) is unable to partake in H-bonding interactions. Despite these differences, **1** and **3** both crystallize in the same space group and have very similar supramolecular structures, with the unit cell of **3** expanded by 13.3% to accommodate the larger cation, indicating that anion-anion H-bond interactions dominate the energetics. The supramolecular framework of **5** contains the largest substituted pyrrolidinium cation in the series, which has a further 10.3% expansion in its unit cell to accommodate this cation. As a consequence of this, the anion-anion H-bond interactions adopt an α,α,α,γ configuration, which is different from the supramolecular structures of **1**-**4**.

The giant anionic lattices observed in pentaborate salts **14**, **15** and **17** form similar-shaped structures to that of the 'brickwall'. The structures are observed as 'expanded' 'brickwall' structures due to the additional molecules behaving as 'spacer' molecules by H-bonding between the anionic units in the lattice, rather than occupying the lattice 'cavities' as observed with the smaller cations. This 'expanded brickwall'-shaped structure arises in order to accommodate the much larger (substituted) adamantylammonium cations, which have unit cells ~70% larger than the dimethylated pyrrolidinium cation found in **3**.

The solid-state structure of the heptaborate(2-) salt observed in **20** contains the larger (and rarer) heptaborate dianion ('O^{+}' isomer), $[B_7O_9(OH)_5]^{2-}$ as well as a larger cation and charge (+2) and is able to form numerous H-bonds within its solid-state structure; in addition to intermolecular H-bond interactions, there is one intramolecular H-bond within the heptaborate anion. The numerous H-bond

interactions present allow the salt to form a giant anionic lattice, with the dications situated within the 'cavities' of the lattice. The H-bond interactions observed in the salt of **20** form repetitive motifs that are also observed within the supramolecular structures of the pentaborate salts. The strength of these repetitive H-bond interactions are discussed in Chapter 4.

Based on the observations of the anionic lattice arrangements, it can be concluded that the 'brickwall' pentaborate supramolecular structure, which arises from the α,α,α,β configuration, is sufficiently flexible to accommodate larger cations (within limits). When these limits are approached, they may be stretched further to accommodate the size of the cations by using 'spacer' molecules to increase the size of the lattice. It is only once the lattice cannot be stretched any further and/or when there are sufficient cation-anion interactions to dominate the energetics that polyborates other than pentaborates may be observed. Computational studies of polyborate anions are described in Chapter 4. DFT theory was used to model the repetitive H-bond interactions observed within the solid-state structures of pentaborate salts reported in the literature; these included the 8-membered $R_2^2(8)$ (observed at α- and γ-reciprocal acceptor sites) and the 12-membered $R_2^2(12)$ (β-reciprocal acceptor site) ring motifs, along with the C(8) β-chain. These motifs were modelled in pentaborate anion dimers (in the solvated phase), with the $R_2^2(8)$ α-reciprocal H-bond interaction found to be particularly strong (-21 kJ mol^{-1} per H-bond). The energetically favoured $R_2^2(8)$ α-reciprocal H-bond interaction is the most frequently observed interaction within the solid-state structures of pentaborate salts.

The relative conformational stabilities of the rarer hexaborate and heptaborate dianions, $[B_6O_7(OH)_6]^{2-}$ and $[B_7O_9(OH)_5]^{2-}$, respectively were also computed using DFT theory (in the gas phase). The results indicated that the most energetically stable conformers of the hexaborate dianion contain an unbroken, quasi-triangular cyclic network of intramolecular H-bonds (estimated H-bond energy = 15 kJ mol^{-1}). In contrast to this, the conformers of the related heptaborate(2-) 'O$^+$' isomer showed very weak or no intramolecular H-bonds, and all had similar energies.

The synthesis and characterization of Lewis base adducts of triorganoboroxines is reported in Chapter 5. Eight new adducts are reported in this

chapter. All of triorganoboroxine·amine adducts were prepared in high yields, and characterized using spectroscopic (IR and multi-element NMR) and analytical (melting point, elemental analysis) techniques. Variable temperature ^{1}H NMR studies were performed on a select few of the synthesized adducts and were found to have calculated Gibbs free energies of activation ($\Delta G^{\ddagger}$) in the range ~51-58 kJ mol^{-1}, which are not significantly different from those reported in the literature for related compounds.

The crystal structures of the triorganoboroxine·amine adducts of tri(4-chlorophenyl)boroxine·morpholine (**30**) and tri(4-chlorophenyl)boroxine·benzylamine (**33**) are also reported within this chapter. The B-O bond lengths and internuclear angles found within the boroxole (B_3O_3) rings of these structures are not significantly different from other compounds containing B_3O_3 rings, including those described in Chapter 3.

The Lewis acidity of the triorganoboroxines triphenylboroxine (**24**), tri(4-chlorophenyl)boroxine (**25**) and tris(pentafluorophenyl)boroxine (**26**) were also investigated. **24** and **25** exhibit moderate Lewis acidity, with acceptor numbers of 45.8 and 46.4, respectively. The strongly electron-withdrawing pentafluorophenyl substituents on **26** greatly increase the Lewis acidity of the B atoms, resulting in **26** having a higher acceptor number (67.5).

It would be of interest in future work to synthesise polyborate salts containing larger cations, in order to investigate their structural properties. It was interesting to observe that a larger cation such as the bis(triphenylphosphine)minium cation (as seen in polyborates **18**·1.5H_2O and **19**·2.5H_2O) allowed the polyborate salt to become soluble in organic solvents, which has not been observed previously with polyborate salts. It could be of interest to investigate the cation size at which the polyborate salt is able to dissolve in organic solvents, as well as investigating whether or not the larger cations may aid the formation of polyborate salts containing previously unobserved polyborate anion types. The crystallographic data for all of the structures reported in this thesis, along with the Cartesian coordinates of the computed conformers and dimers reported in Chapter 4 can be found in the appendices, which are supplied as an electronic disk.

References

1. P. W. Atkins, T. Overton, J. P. Rourke, M. Weller and F. A. Armstrong, *Inorganic chemistry*, Oxford University Press, Oxford,, 2006.

2. N. N. Greenwood and A. Earnshaw, *Chemistry of the Elements*, Elsevier Science, Burlington, 2012.

3. A. W. Laubengayer, D. T. Hurd, A. E. Newkirk and J. L. Hoard, *J. Am. Chem. Soc.,* 1943, **65**, 1924-1931.

4. K. S. Cook and B. D. Bosley, US Pat., 20,160,019,989, 2016.

5. B. Pastina, J. Isabey and B. Hickel, *J. Nucl. Mater.,* 1999, **264**, 309-318.

6. R. F. Barth, A. H. Soloway, R. G. Fairchild and R. M. Brugger, *Cancer,* 1992, **70**, 2995-3007.

7. M. F. Hawthorne, *Angew. Chem. Int. Ed. Eng.,* 1993, **32**, 950-984.

8. M. A. Beckett, C. C. Bland, P. N. Horton, M. B. Hursthouse and K. S. Varma, *J. Organomet. Chem.,* 2007, **692**, 2832-2838.

9. M. A. Beckett, *Coord. Chem. Rev.,* 2016, **323**, 2-14.

10. J. B. Holbrook, B. C. Smith, C. E. Housecroft and K. Wade, *Polyhedron,* 1982, **1**, 701-706.

11. Q. I. Li, F. Xue and T. C. W. Mak, *Inorg. Chem.,* 1999, **38**, 4142-4145.

12. C. C. Freyhardt and M. Wiebcke, *J. Chem. Soc. , Chem. Commun.,* 1994, **0**, 1675-1676.

13. H. D. Smith and R. J. Wiersema, *Inorg. Chem.,* 1972, **11**, 1152-1154.

14. H. Behm and C. Baerlocher, *Acta Crystallogr. Sect. C,* 1985, **41**, 5-7.

15. M. Z. Visi, C. B. Knobler, J. J. Owen, M. I. Khan and D. M. Schubert, *Cryst. Growth Des.,* 2006, **6**, 538-545.

16. C. G. Salentine, *Inorg. Chem.,* 1983, **22**, 3920-3924.

17. D. M. Schubert, R. A. Smith and M. Z. Visi, *Glass Technol.,* 2003, **44**, 63-70.

18. D. M. Schubert, in *Kirk-Othmer Encyclopedia of Chemical Technology* , J. Wiley and Sons, Inc., NY, 2000, p. 1-68.

19. F. H. Nielsenl, *Curr. Top. Plant Biochem. Physiol.,* 1991, **10**, 274-286.

20. Z. H. Liu, L. Q. Li and W. J. Zhang, *Inorg. Chem.,* 2006, **45**, 1430-1432.

21. D. M. Schubert, M. Z. Visi and C. B. Knobler, *Inorg. Chem.,* 2008, **47**, 2017-2023.

22. Z. H. Liu and L. Q. Li, *Cryst. Growth Des.,* 2006, **6**, 1247-1249.

23. C. Y. Pan, G. M. Wang, S. T. Zheng and G. Y. Yang, *Z. Anorg. Allg. Chem.,* 2007, **633**, 336-340.

24. G. M. Wang, Y. Q. Sun and G. Y. Yang, *J. Solid State Chem.,* 2006, **179**, 1545-1553.

25. G. M. Wang, Y. Q. Sun and G. Y. Yang, *J. Solid State Chem.,* 2005, **178**, 729-735.

26. P. Becker, *Z. Kristallogr.,* 2001, **216**, 523-533.

27. J. D. Grice, P. C. Burns and F. C. Hawthorne, *Can. Mineral.,* 1999, **37**, 731-762.

28. ICSD, *http://icsd.cds.rsc.org/*, Accessed 02/09/2016.

29. C. L. Christ, *Am. Mineral.,* 1960, **45**, 334-340.

30. J. R. Clark and C. L. Christ, *Acta Crystallogr. Sect. B,* 1977, **33**, 3272-3273.

31. P. C. Burns, *Can. Mineral.,* 1995, **33**, 1167-1176.

32. P. C. Burns, J. D. Grice and F. C. Hawthorne, *Can. Mineral.,* 1995, **33**, 1131-1151.

33. Z. H. Liu, J. J. Zhang and W. J. Zhang, *Inorg. Chim. Acta,* 2006, **359**, 519-524.

34. H. X. Zhang, S. T. Zheng and G. Y. Yang, *Acta Crystallogr. C,* 2004, **60**, m241-m243.

35. S. L. Wu, H. X. Liu, X. Jiang, Z. D. Shao and Y. X. Liang, *Acta Crystallogr. C,* 2009, **65**, m308-m310.

36. Y. Yang, Y. Wang, J. Sun, M. Cui and C. Meng, *Z. Anorg. Allg. Chem.,* 2011, **637**, 729-734.

37. H. X. Zhang, S. T. Zheng and G. Y. Yang, *Acta Crystallogr. C,* 2004, **60**, o545-o546.

38. S. Merlino and F. Sartori, *Science,* 1971, **171**, 377-379.

39. S. Merlino and F. Sartori, *Acta Crystallogr. Sect. B,* 1969, **25**, 2264-2270.

40. M. A. Altahan, M. A. Beckett, S. J. Coles and P. N. Horton, *Inorg. Chem. Commun.,* 2015, **59**, 95-98.

41. S. Yang, G. Li, S. Tian, F. Liao, M. Xiong and J. Lin, *J. Solid State Chem.,* 2007, **180**, 2225-2232.

42. M. A. Beckett, P. N. Horton, M. B. Hursthouse, J. L. Timmis and K. S. Varma, *Dalton Trans.,* 2012, **41**, 4396-4403.

43. D. M. Schubert, M. Z. Visi, S. Khan and C. B. Knobler, *Inorg. Chem.,* 2008, **47**, 4740-4745.

44. D. M. Schubert, M. Z. Visi and C. B. Knobler, *Inorg. Chem.,* 2000, **39**, 2250-2251.

45. A. Ferrari and A. Magnani, *Gazz. Chim. Ital.,* 1939, **69**, 275-284.

46. R. C. Petersen, M. Finkelstein and S. D. Ross, *J. Am. Chem. Soc.,* 1959, **81**, 3264-3267.

47. B. D. Vineyard and H. C. Godt, *Inorg. Chem.,* 1964, **3**, 1144-1147.

48. G. Heller, *J. Inorg. Nucl. Chem.,* 1968, **30**, 2743-2754.

49. C. C. Freyhardt, M. Wiebcke, J. Felsche and G. Engelhardt, *J. Incl. Phenom. Mol. Rec. Chem.,* 1994, **18**, 161-175.

50. T. J. R. Weakley, *Acta Crystallogr. Sect. C,* 1985, **41**, 377-379.

51. A. Rosenheim and F. Leyser, *Z. Anorg. Allg. Chem.,* 1921, **119**, 1-38.

52. R. Janda, G. Heller and J. Pickardt, *Z. Kristallogr.,* 1981, **154**, 1-9.

53. M. Li, J. Chang, Z. Wang and H. Shi, *J. Solid State Chem.,* 2006, **179**, 3265-3269.

54. M. A. Beckett, P. N. Horton, M. B. Hursthouse and J. L. Timmis, *RSC Adv.,* 2013, **3**, 15185-15191.

55. M. A. Beckett, P. N. Horton, S. J. Coles and D. W. Martin, *Inorg. Chem.,* 2011, **50**, 12215-12218.

56. P. Becker, P. Held and L. Bohaty, *Cryst. Res. Technol.,* 2000, **35**, 1251-1262.

57. Z. H. Liu, W. J. Zhang and J. J. Zhang, *Thermochim. Acta,* 2005, **439**, 151-153.

58. W. J. Zhang and Z. H. Liu, *Z. Kristallogr.,* 2006, **221**, 189-190.

59. R. A. Baber, J. P. H. Charmant, N. C. Norman, A. G. Orpen and J. Rossi, *Acta Crystallogr. Sect. E,* 2004, **60**, o1086-o1088.

60. G. M. Wang, C. Y. Pan, S. T. Zheng and G. Y. Yang, *Acta Crystallogr. Sect. E,* 2007, **63**, o1101-o1103.

61. S. Yang, G. Li, S. Tian, F. Liao and J. Lin, *Cryst. Growth Des.,* 2007, **7**, 1246-1250.

62. G. M. Wang, C. Y. Pan, S. T. Zheng and G. Y. Yang, *Acta Crystallogr. Sect. E,* 2007, **63**, o1104-o1105.

63. C. Y. Pan, G. M. Wang, S. T. Zheng and G. Y. Yang, *Acta Crystallogr. Sect. E,* 2007, **63**, o840-o842.

64. H. X. Yang, W. J. Zhang, X. L. Liu and Z. H. Liu, *Acta Crystallogr. Sect. E,* 2006, **62**, o4877-o4879.

65. M. A. Beckett, P. N. Horton, M. B. Hursthouse, J. L. Timmis and K. S. Varma, *Collect. Czech. Chem. Commun.,* 2010, **75**, 971-980.

66. M. A. Beckett, P. N. Horton, M. B. Hursthouse, D. A. Knox and J. L. Timmis, *Dalton Trans.,* 2010, **39**, 3944-3951.

67. M. A. Beckett, P. N. Horton, S. J. Coles, D. A. Kose and A. M. Kreuziger, *Polyhedron,* 2012, **38**, 157-161.

68. D. A. Kose, M. A. Beckett and N. Colak, *Hacettepe J. Biol. & Chem.,* 2012, **40**, 219-225.

69. M. A. Beckett, S. J. Coles, R. A. Davies, P. N. Horton and C. L. Jones, *Dalton Trans.,* 2015, **44**, 7032-7040.

70. L. J. Csetenyi, F. P. Glasser and R. A. Howie, *Acta Crystallogr. C,* 1993, **49**, 1039-1041.

71. E. Corazza, *Acta Crystallogr. Sect. B,* 1976, **32**, 1329-1333.

72. N. Morimoto, *J. Miner.,* 1956, **2**, 1-18.

73. M. A. Beckett, P. N. Horton, M. B. Hursthouse and J. L. Timmis, *Polyhedron,* 2014, **77**, 96-102.

74. C. G. Salentine, *Inorg. Chem.,* 1987, **26**, 128-132.

75. A. Dal Negro, J. M. M. Pozaz and L. Ungaretti, *Am. Mineral,* 1975, **60**, 897-883.

76. M. A. Altahan, M. A. Beckett, S. J. Coles and P. N. Horton, *Phosphorus, Sulfur Silicon Relat. Elem.,* 2016, **191**, 572-575.

77. E. Corazza, *Acta Crystallogr. Sect. B,* 1974, **30**, 2194-2199.

78. C. L. Christ and J. R. Clark, *Z. Kristallogr.,* 1960, **114**, 321-342.

79. J. R. Clark, D. Appleman and C. Christ, *J. Inorg. Nucl. Chem.,* 1964, **26**, 73-95.

80. J. R. Clark, *Acta Crystallogr.,* 1959, **12**, 162-170.

81. E. N. Kurkutova, I. M. Rumanova and N. V. Belov, *Soviet Phys. Dokl.,* 1966, **10**, 808-810.

82. C. Y. Pan, G. M. Wang, S. T. Zheng and G. Y. Yang, *Acta Crystallogr. Sect. E,* 2007, **63**, o1207-o1209.

83. G. M. Wang, Y. Q. Sun and G. Y. Yang, *J. Solid State Chem.,* 2004, **177**, 4648-4654.

84. D. Lin, X. You and L. Zhu, *Chinese J. Chem.,* 2011, **29**, 463-467.

85. L. Zheng, J. Zhang and Z. Liu, *Chinese J. Chem,* 2009, **27**, 494-500.

86. W. Luo, Y. Wang, T. Wen, H. Zhang, X. Lin, Y. Wang, F. Liao and J. Lin, *J. Mol. Struct.,* 2013, **1048**, 1-5.

87. P. Li, L. Q. Li, H. S. Huang and Z. H. Liu, *J. Clust. Sci.,* 2014, **25**, 893-903.

88. P. Li and Z. Liu, *Chinese J. Chem.,* 2009, **27**, 2183-2189.

89. Y. Liu, H. He, B. F. Yang, Q. Zhang and G. Y. Yang, *J. Clust. Sci.,* 2015, **26**, 1537-1545.

90. C. Y. Pan, L. J. Zhong, J. Lu, D. G. Li, F. H. Zhao and H. M. Yang, *Z. Anorg. Allg. Chem.,* 2014, **640**, 352-356.

91. Y. Yang, D. Fu, G. Li and Y. Zhang, *Z. Anorg. Allg. Chem.,* 2013, **639**, 722-727.

92. V. R. Hathwar, A. K. Paul, S. Natarajan and T. N. G. Row, *J. Phys. Chem. A,* 2011, **115**, 12818-12825.

93. G. Huang, R. Pan, H. He, B. F. Yang and G. Y. Yang, *J. Clust. Sci.,* 2015, **26**, 2023-2032.

94. H. X. Liu, Y. X. Liang and X. Jiang, *J. Solid State Chem.,* 2008, **181**, 3243-3247.

95. C. L. Jones, M. A. Beckett, S. J. Coles, R. A. Davies and P. N. Horton, *Phosphorus, Sulfur Silicon Relat. Elem.,* 2016, **191**, 628-630.

96. Y. Yang, Y. Wang, J. Zhu, R. B. Liu, J. Xu and C. G. Meng, *Z. Anorg. Allg. Chem.,* 2011, **637**, 735-740.

97. L. Zhao, P. Li and B. Cao, *Acta Crystallogr. Sect. E,* 2009, **65**, m368.

98. M. A. Altahan, M. A. Beckett, S. J. Coles and P. N. Horton, *Inorg. Chem.,* 2015, **54**, 412-414.

99. Q. Meng, G. M. Wang, H. He, B. F. Yang and G. Y. Yang, *J. Clust. Sci.,* 2014, **25**, 1295-1305.

100. X. You, L. Zhu and J. Sun, *Chinese J. Chem,* 2010, **28**, 2174-2178.

101. Y. Yang, Y. Wang, J. Zhu, R. B. Liu, J. Xu and C. G. Meng, *Inorg. Chim. Acta,* 2011, **376**, 401-407.

102. Y. Yang, D. Fu, Y. Zhang and C. Meng, *Z. Anorg. Allg. Chem.,* 2014, **640**, 1443-1448.

103. C. Y. Pan, S. Hu, D. G. Li, P. Ouyang, F. H. Zhao and Y. Y. Zheng, *Dalton Trans.,* 2010, **39**, 5772-5773.

104. X. Liu, F. Zhang and X. H. Yin, *Chem. Res. Appl.,* 2010, **22**, 12.

105. N. Penin, L. Seguin, B. Gérand, M. Touboul and G. Nowogrocki, *J. Alloy Compd.,* 2002, **334**, 97-109.

106. W. H. Zachariasen and H. A. Plettinger, *Acta Crystallogr.,* 1963, **16**, 376-379.

107. M. C. Etter, *Acc. Chem. Res.,* 1990, **23**, 120-126.

108. J. Liang, Y. G. Wang, Y. X. Wang, F. H. Liao and J. H. Lin, *J. Solid State Chem.,* 2013, **200**, 99-104.

109. M. A. Beckett, P. N. Horton, M. B. Hursthouse, J. L. Timmis and K. S. Varma, *Inorg. Chim. Acta,* 2012, **383**, 199-203.

110. W. H. Han, L. L. Dang and W. J. Zhang, *Z. Kristallogr.,* 2007, **222**, 403-404.

111. N. Jemai, M. Rzaigui and S. Akriche, *J. Clust. Sci.,* 2015, **26**, 2051-2064.

112. S. Natarajan, W. Klein, M. Panthöfer, L. van Wüllen and M. Jansen, *Z. Anorg. Allg. Chem.,* 2003, **629**, 959-962.

113. S. Yang, G. Li, J. Ju, Z. Yang, F. Liao, Y. Wang and J. Lin, *Inorg. Chim. Acta,* 2008, **361**, 2413-2417.

114. N. Jamai, M. Rzaigui and S. A. Toumi, *Acta Crystallogr. Sect. E,* 2014, **70**, m167-m168.

115. A. Negro, L. Ungaretti and C. Sabelli, *Am. Mineral.,* 1971, **56**, 1553.

116. D. Neiner, Y. V. Sevryugina and D. M. Schubert, *Inorg. Chem.,* 2016, **55**, 8706-8711.

117. G. M. Wang, Y. Q. Sun, S. T. Zheng and G. Y. Yang, *Z. Anorg. Allg. Chem.,* 2006, **632**, 1586-1590.

118. H. X. Zhang, J. Zhang, S. T. Zheng and G. Y. Yang, *Inorg. Chem. Commun.,* 2004, **7**, 781-783.

119. S. Menchetti and C. Sabelli, *Acta Crystallogr. Sect. B,* 1979, **35**, 2488-2493.

120. L. Wei, B. F. Yang, H. He and G. Y. Yang, *J. Clust. Sci.,* 2014, **25**, 617-626.

121. P. T. Corbett, J. Leclaire, L. Vial, K. R. West, J. L. Wietor, J. K. M. Sanders and S. Otto, *Chem. Rev.,* 2006, **106**, 3652-3711.

122. J. L. Anderson, E. M. Eyring and M. P. Whittaker, *J. Phys. Chem.,* 1964, **68**, 1128-1132.

123. Z. E. Lin and G. Y. Yang, *Eur. J. Inorg. Chem.,* 2011, **2011**, 3857-3867.

124. L. Cáceres, A. Soliz and T. Vargas, *J. Electrochem. Soc.,* 2016, **163**, C171-C183.

125. I. Tsuyumoto, Y. Onoda, F. Hashizume and E. Kinpara, *J. Appl. Polym. Sci.,* 2011, **122**, 1707-1711.

126. F. Pitts and M. H. Clubley, US Pat., 3,865,760 A, 1975.

127. N. Bektas, S. Oncel, H. Y. Akbulut and A. Dimoglo, *Environ. Chem. Lett.,* 2004, **2**, 51-54.

128. J. Penninger, M. Sunder, T. Voelkel, B. Kottwitz and W. Pichler, US Pat., 6,228,827 B1, 2001.

129. Q. Liu, X. Zhang, Z. Yang, F. Zhang, L. Liu, J. Han, Z. Li and S. Pan, *Inorg. Chem.,* 2016, **55**, 8744-8749.

130. K. M. Thomas, *Catal. Today,* 2007, **120**, 389-398.

131. A. Züttel, *Mater. Today,* 2003, **6**, 24-33.

132. EERE, *Targets for Onboard Hydrogen Storage Systems for Light-Duty Vehicles*, Accessed 23/11/2012.

133. L. Pan, M. B. Sander, X. Huang, J. Li, M. Smith, E. Bittner, B. Bockrath and J. K. Johnson, *J. Am. Chem. Soc.,* 2004, **126**, 1308-1309.

134. S. H. Jhi, Y. K. Kwon, K. Bradley and J. C. P. Gabriel, *Solid State Commun.,* 2004, **129**, 769-773.

135. S. H. Jhi, Y. K. Kwon, K. Bradley and J. C. P. Gabriel, US Pat., 6,991,773, 2006.

136. P. Becker, *Adv. Mater.,* 1998, **10**, 979-992.

137. P. A. Franken, A. E. Hill, C. W. Peters and G. Weinreich, *Phys. Rev. Lett.,* 1961, **7**, 118-119.

138. A. K. Paul, K. Sachidananda and S. Natarajan, *Cryst. Growth Des.,* 2010, **10**, 456-464.

139. W. G. Woods, *Environ. Health Perspect.,* 1994, **102**, 5-11.

140. N. Hirao and T. Yabuuchi, *J. Pharm. Soc. Japan,* 1954, **74**, 1073-1075.

141. H. C. Brown, E. J. Mead and C. J. Shoaf, *J. Am. Chem. Soc.,* 1956, **78**, 3613-3614.

142. W. Gerrard and M. F. Lappert, *Chem. Rev.,* 1958, **58**, 1081-1111.

143. M. F. Lappert, *Chem. Rev.,* 1956, **56**, 959-1064.

144. E. Wiberg and W. Sutterlin, *Z. Anorg. Allg. Chem.,* 1931, **202**, 1.

145. J. Goubeau and U. Boehm, *Z. Anorg. Allg. Chem.,* 1951, **266**, 161-174.

146. J. Goubeau and E. Ekhoff, *Z. Anorg. Allg. Chem.,* 1952, **268**, 145-158.

147. E. Cherbuliez, J. P. Leber and A. M. Ulrich, *Helv. Chim. Acta,* 1953, **36**, 910-918.

148. H. Schiff, *Ann. Suppl.,* 1867, **5**, 154.

149. W. Gerrard, M. F. Lappert and H. B. Silver, *J. Chem. Soc.,* 1957, 1647-1652.

150. W. Gerrard and M. F. Lappert, *J. Chem. Soc.,* 1951, 2545-2550.

151. A. D. Mcelroy, US Pat., 2,943,916, 1960.

152. W. D. Peterson, US Pat., 2,898,184, 1959.

153. C. Councler, *J. Prakt. Chem.,* 1878, **18**, 371-402.

154. P. A. McCusker and J. H. Bright, *J. Org. Chem.,* 1964, **29**, 2093-2094.

155. N. E. Day and S. J. Groszos, US Pat., 2,957,840, 1960.

156. F. F. Ogden, US Pat., 3,046,136, 1962.

157. E. L. Docks, in *Kirk-Othmer Encyclopedia of Chemical Technology*, J. Wiley and Sons, Inc., 2000.

158. K. H. Klipstein, US Pat., 2,068,415 A, 1937.

159. M. Merlub-Sobel, M. B. Jerome and W. L. Ulmer, US Pat., 2,281,910 A, 1942.

160. H. Schiff and E. Bechi, *Compt. Rend. Acad. Sci.,* 1865, **61**, 697.

161. E. A. M. Maarssen, US Pat., 2,042,952, 1936.

162. A. Finch, J. C. Lockhart and J. Pearn, *J. Org. Chem.,* 1961, **26**, 3250-3253.

163. F. J. Dykstra, US Pat., 2,862,879, 1958.

164. M. F. Lappert, *J. Chem. Soc.,* 1958, 2790-2793.

165. C. S. Chen, B. J. Bulkin and E. M. Pearce, *J. Appl. Polym. Sci.,* 1982, **27**, 1177-1190.

166. S. C. Lin and E. M. Pearce, *J. Appl. Polym. Sci.,* 1979, **23**, 3355-3374.

167. H. A. Cyba, US Pat., 3,598,757, 1971.

168. F. J. Dykstra, US Pat., 3.030.196, 1962.

169. J. P. Doner, A. G. Horodysky and J. A. Keller, US Pat., 4,780,227, 1988.

170. R. H. Black, US Pat., 3,111,413, 1963.

171. S. G. McGriff, US Pat., 3,001,276, 1961.

172. W. Gerrard, *The organic chemistry of boron*, Academic Press, London, New York, 1961.

173. E. Krause and R. Nitsche, *Ber. Dtsch. Chem. Ges.,* 1921, **54**, 2784-2791.

174. W. König and W. Scharrnbeck, *J. Prakt. Chem.,* 1930, **128**, 153-170.

175. F. R. Bean and J. R. Johnson, *J. Am. Chem. Soc.,* 1932, **54**, 4415-4425.

176. E. Khotinsky and M. Melamed, *Ber. Dtsch. Chem. Ges.,* 1909, **42**, 3090-3096.

177. W. P. Cowie, A. H. Jackson and O. C. Musgrave, *Chem. Ind.,* 1959, 1248-1249.

178. H. C. Brown, N. G. Bhat and V. Somayaji, *Organomet.,* 1983, **2**, 1311-1316.

179. H. C. Brown and T. E. Cole, *Organomet.,* 1983, **2**, 1316-1319.

180. D. G. Hall, *Boronic acids: preparation, applications in organic synthesis and medicine*, J. Wiley and Sons, Germany, 2006.

181. A. Michaelis and P. Becker, *Ber. Dtsch. Chem. Ges.,* 1880, **13**, 58-61.

182. A. Michaelis and P. Becker, *Ber. Dtsch. Chem. Ges.,* 1882, **15**, 180-185.

183.. J. E. Burch, W. Gerrard, M. Howarth and E. F. Mooney, *J. Chem. Soc.,* 1960, 4916-4918.

184. A. L. Korich and P. M. Iovine, *Dalton Trans.,* 2010, **39**, 1423-1431.

185. R. T. Hawkins, W. J. Lennarz and H. R. Snyder, *J. Am. Chem. Soc.,* 1960, **82**, 3053-3059.

186. K. Torssell, *Acta Chem. Scand.,* 1954, **8**, 1779-1786.

187. P. C. Condit and J. G. H. Denison, US Pat., 2,346,155, 1944.

188. S. J. Groszos and C. S. Scanley, US Pat., 3,021,206, 1962.

189. J. N. Cambre and B. S. Sumerlin, *Polymer,* 2011, **52**, 4631-4643.

190. N. Miyaura, K. Yamada and A. Suzuki, *Tetrahedron Lett.,* 1979, **20**, 3437-3440.

191. J. Adams, *Cancer Cell,* 2004, **5**, 417-421.

192. Macmillan Cancer Support, http://www.macmillan.org.uk/cancerinformation/cancertreatment/treatmenttypes/biologicaltherapies/cancergrowthinhibitors/bortezomib.aspx, Accessed 06/09/2016.

193. FDA.gov, http://www.fda.gov/AboutFDA/CentersOffices/OfficeofMedicalProductsandTobacco/CDER/ucm094633.htm, Accessed 06/09/2016.

194. P. Bonvini, E. Zorzi, G. Basso and A. Rosolen, *Leukemia,* 2007, **21**, 838-842.

195. P. Wongthai, K. Hagiwara, Y. Miyoshi, P. Wiriyasermkul, L. Wei, R. Ohgaki, I. Kato, K. Hamase, S. Nagamori and Y. Kanai, *Cancer Sci.,* 2015, **106**, 279-286.

196. F. Faiao-Flores, P. Coelho, J. Arruda-Neto and D. Maria, *Appl. Cancer Res. (Online),* 2011, **31**, 52.

197. E. W. Abel, W. Gerrard and M. F. Lappert, *J. Chem. Soc.,* 1957, 112-115.

198. R. L. Letsinger and I. Skoog, *J. Am. Chem. Soc.,* 1954, **76**, 4174-4176.

199. R. L. Letsinger and I. H. Skoog, *J. Am. Chem. Soc.,* 1955, **77**, 5176-5177.

200. W. Gerrard, M. F. Lappert and R. Shafferman, *J. Chem. Soc.,* 1957, 3828-3833.

201. S. Ozaki, A. Z. Suzuki, P. O. Bauer, E. Ebisui and K. Mikoshiba, *Biochem. Biophys. Res. Commun.,* 2013, **441**, 286-290.

202. T. P. Povlock and W. T. Lippincott, *J. Am. Chem. Soc.,* 1958, **80**, 5409-5411.

203. R. L. Letsinger and I. Skoog, *J. Am. Chem. Soc.,* 1955, **77**, 2491-2494.

204. R. Letsinger and J. Nazy, *J. Org. Chem.,* 1958, **23**, 914-915.

205. J. P. Luvisi, US Pat., 3,177,267, 1965.

206. E. H. Goda, H. Steinberg and D. L. Hunter, US Pat., 2,960,819, 1960.

207. J. C. Perrine and R. N. Keller, *J. Am. Chem. Soc.,* 1958, **80**, 1823-1827.

208. K. L. Bhat, G. D. Markham, J. D. Larkin and C. W. Bock, *J. Phys. Chem. A,* 2011, **115**, 7785-7793.

209. H. R. Snyder, M. S. Konecky and W. J. Lennarz, *J. Am. Chem. Soc.,* 1958, **80**, 3611-3615.

210. P. A. McCusker and L. J. Glunz, *J. Am. Chem. Soc.,* 1955, **77**, 4253-4255.

211. P. B. Brindley, W. Gerrard and M. F. Lappert, *J. Chem. Soc.,* 1955, 2956-2958.

212. S. J. Groszos, A. K. Hoffmann and W. M. Thomas, US Pat., 2,950,322, 1960.

213. E. D. Brown Jr., US Pat., 2,830,953, 1958.

214. H. G. Alt, S. J. Palackal, M. B. Welch, D. C. Rohlfing and J. Janzen, US Pat., 5,710,224, 1998.

215. A. P. Côté, A. I. Benin, N. W. Ockwig, M. O'Keeffe, A. J. Matzger and O. M. Yaghi, *Science,* 2005, **310**, 1166-1170.

216. N. L. Campbell, R. Clowes, L. K. Ritchie and A. I. Cooper, *Chem. Mater.,* 2009, **21**, 204-206.

217. D. Cao, J. Lan, W. Wang and B. Smit, *Angew. Chem. Int. Ed. Eng.,* 2009, **48**, 4730-4733.

218. H. M. El-Kaderi, J. R. Hunt, J. L. Mendoza-Cortés, A. P. Côté, R. E. Taylor, M. O'Keeffe and O. M. Yaghi, *Science,* 2007, **316**, 268-272.

219. S. S. Han, H. Furukawa, O. M. Yaghi and W. A. Goddard, *J. Am. Chem. Soc.,* 2008, **130**, 11580-11581.

220. K. E. Maly, *J. Mater. Chem.,* 2009, **19**, 1781-1787.

221. M. Mastalerz, *Angew. Chem. Int. Ed. Eng.,* 2008, **47**, 445-447.

222. R. W. Tilford, W. R. Gemmill, H. C. zur Loye and J. J. Lavigne, *Chem. Mater.,* 2006, **18**, 5296-5301.

223. R. W. Tilford, S. J. Mugavero, P. J. Pellechia and J. J. Lavigne, *Adv. Mater.,* 2008, **20**, 2741-2746.

224. M. A. Mehta, T. Fujinami, S. Inoue, K. Matsushita, T. Miwa and T. Inoue, *Electrochim. Acta,* 2000, **45**, 1175-1180.

225. N. G. Nair, M. Blanco, W. West, F. C. Weise, S. Greenbaum and V. P. Reddy, *J. Phys. Chem. A,* 2009, **113**, 5918-5926.

226. G. Alcaraz, L. Euzenat, O. Mongin, C. Katan, I. Ledoux, J. Zyss, M. Blanchard-Desce and M. Vaultier, *Chem. Commun.,* 2003, , 2766-2767.

227. F. Ibersiene, D. Hammoutène, A. Boucekkine, C. Katan and M. Blanchard-Desce, *J. Mol. Struc. -THEOCHEM,* 2008, **866**, 58-62.

228. R. S. Braman, *Encyclopedia of Industrial Chemical Analysis*, J. Wiley and Sons, Interscience, 1968.

229. D. R. MacFarlane, P. Meakin, J. Sun, N. Amini and M. Forsyth, *J. Phys. Chem. B,* 1999, **103**, 4164-4170.

230. E. V. Vashkevich, N. Y. Yurashevich, N. G. Kozlov, V. I. Potkin and T. N. Potkina, *R. J. Appl. Chem.,* 2001, **74**, 1892-1898.

231. R. Borch F. and A. Hassid I., *J. Org. Chem.,* 1972, **37**, 1673-1674.

232. E. A. Basso, G. F. Gauze and R. J. Abraham, *Magn. Reson. Chem.,* 2007, **45**, 749-757.

233. R. Schaeffer, *J. Am. Chem. Soc.,* 1957, **79**, 1006-1007.

234. J. G. Wilson, A. K. M. Anisuzzaman, F. Alam and A. H. Soloway, *Inorg. Chem.,* 1992, **31**, 1955-1958.

235. T. L. Heying, J. W. Ager, S. L. Clark, D. J. Mangold, H. L. Goldstein, M. Hillman, R. J. Polak and J. W. Szymanski, *Inorg. Chem.,* 1963, **2**, 1089-1092.

236. R. A. Bowie and O. C. Musgrave, *J. Chem. Soc. C,* 1966, 566-571.

237. P. I. Paetzold, W. Scheibit and E. Scholl, *Z. Naturforsch. B,* 1971, **26**, 646-649.

238. D. M. Schubert, F. Alam, M. Z. Visi and C. B. Knobler, *Chem. Mater.,* 2003, **15**, 866-871.

239. H. Li, G. M. Wang, S. Y. Xue and Q. Liang, *Acta Crystallogr. Sect. E,* 2008, **64**, m1269-m1270.

240. J. B. Farmer, *Adv. Inorg. Chem.,* 1982, **25**, 187-237.

241. R. K. Momii and N. H. Nachtrieb, *Inorg. Chem.,* 1967, **6**, 1189-1192.

242. J. Li, S. Xia and S. Gao, *Spectrochim. Acta A,* 1995, **51**, 519-532.

243. M. Wiebcke, C. C. Freyhardt, J. Felsche and G. Engelhardt, *Z. Naturforsch. B,* 1993, **48**, 978-985.

244. M. A. Beckett, C. C. Bland, P. N. Horton, M. B. Hursthouse and K. S. Varma, *Inorg. Chem.,* 2007, **46**, 3801-3803.

245. M. A. Beckett, D. E. Hibbs, M. B. Hursthouse, P. Owen, K. M. A. Malik and K. S. Varma, *Main Group Chem.,* 1998, **2**, 251-258.

246. M. A. Beckett, S. J. Coles, M. E. Light, L. Fischer, B. M. Stiefvater-Thomas and K. S. Varma, *Polyhedron,* 2006, **25**, 1011-1016.

247. G. Heller, *Top. Curr. Chem.,* 1986, **131**, 39-98.

248. P. G. Amateis and L. T. Taylor, *Anal. Chem.,* 1984, **56**, 966-971.

249. G. L. Grunewald, M. R. Seim, J. Lu, M. Makboul and K. R. Criscione, *J. Med. Chem.,* 2006, **49**, 2939-2952.

250. T. L. Malkin, B. J. Murray, C. G. Salzmann, V. Molinero, S. J. Pickering and T. F. Whale, *Phys. Chem. Chem. Phys.,* 2015, **17**, 60-76.

251. L. Jun, X. Shuping and G. Shiyang, *Spectrochim. Acta,* 1995, **51A**, 519-532.

252. H. Ketz, W. Tjarks and D. Gabel, *Tetrahedron Lett.,* 1990, **31**, 4003-4006.

253. J. M. Simon and R. A. Smith, *Glass Technol.,* 2000, **41**, 169-173.

254. D. M. Schubert, *Struct. Bond.,* 2003, **105**, 1-40.

255. M. A. Beckett, R. A. Davies and C. D. Thomas, *Comp. Theor. Chem.,* 2014, **1044**, 74-79.

256. J. D. Dunitz and A. Gavezzotti, *Cryst. Growth Des.,* 2012, **12**, 5873-5877.

257. Y. Zhou, C. Fang, Y. Fang and F. Zhu, *Spectrochim. Acta A,* 2011, **83**, 82-87.

258. D. Stefani, I. Pashalidis and A. V. Nicolaides, *J. Mol. Struc. -THEOCHEM,* 2008, **853**, 33-38.

259. S. X. Tian, K. Z. Xu, M. B. Huang, X. J. Chen, J. L. Yang and C. C. Jia, *J. Mol. Struc. -THEOCHEM,* 1999, **469**, 223-227.

260. J. A. Tossell, *Geochim. Cosmochim. Acta,* 2005, **69**, 5647-5658.

261. J. A. Tossell, *Geochim. Cosmochim. Acta,* 2006, **70**, 5089-5103.

262. Ö Alver and C. Parlak, *Vib. Spectrosc.,* 2010, **54**, 1-9.

263. K. Durka, K. N. Jarzembska, R. Kamiński, S. Luliński, J. Serwatowski and K. Woźniak, *Cryst. Growth Des.,* 2012, **12**, 3720-3734.

264. J. D. Larkin, K. L. Bhat, G. D. Markham, B. R. Brooks, H. F. Schaefer and C. W. Bock, *J. Phys. Chem. A,* 2006, **110**, 10633-10642.

265. J. Kua and P. M. Iovine, *J. Phys. Chem. A,* 2005, **109**, 8938-8943.

266. J. Beckmann, D. Dakternieks, A. Duthie, A. E. K. Lim and E. R. T. Tiekink, *J. Organomet. Chem.,* 2001, **633**, 149-156.

267. R. F. W. Bader, *Atoms in Molecules: A Quantum Theory*, Oxford University Press, Oxford, UK, 1990.

268. A. Becke, C. F. Matta and R. J. Boyd, *The quantum theory of atoms in molecules: from solid state to DNA and drug design*, J. Wiley and Sons, 2007.

269. M. J. Frisch, G. W. Trucks, H. B. Schlegel, G. E. Scuseria, M. A. Robb, J. R. Cheeseman, G. Scalmani, V. Barone, B. Mennucci, G. A. Petersson, H. Nakatsuji, M. Caricato, X. Li, H. P. Hratchian, A. F. Izmaylov, J. Bloino, G. Zheng, J. L. Sonnenberg, M. Hada, M. Ehara, K. Toyota, R. Fukuda, J. Hasegawa, M. Ishida, T. Nakajima, Y. Honda, O. Kitao, H. Nakai, T. Vreven, J. A. Montgomery Jr., J. E. Peralta, F. Ogliaro, M. Bearpark, J. J. Heyd, E. Brothers, K. N. Kudin, V. N. Staroverov, R. Kobayashi, J. Normand, K. Raghavachari, A. Rendell, J. C. Burant, S. S. Iyengar, J. Tomasi, M. Cossi, N. Rega, J. M. Millam, M. Klene, J. E. Knox, J. B. Cross, V. Bakken, C. Adamo, J. Jaramillo, R. Gomperts, R. E. Stratmann, O. Yazyev, A. J. Austin, R. Cammi, C. Pomelli, J. W. Ochterski, R. L. Martin, K. Morokuma, V. G. Zakrzewski, G. A. Voth, P. Salvador, J. J. Dannenberg, S. Dapprich, A. D. Daniels, Ö Farkas, J. B. Foresman, J. V. Ortiz, J. Cioslowski and D. J. Fox, *Gaussian09, Revision C.01*, Gaussian, Inc., Wallingford, CT., 2009.

270. J. Tomasi, B. Mennucci and R. Cammi, *Chem. Rev.,* 2005, **105**, 2999-3094.

271. J. Tomasi, B. Mennucci and E. Cancès, *J. Mol. Struc. -THEOCHEM,* 1999, **464**, 211-226.

272. G. Scalmani and M. J. Frisch, *J. Chem. Phys.,* 2010, **132**, 114110.

273. J. L. Pascual-ahuir, E. Silla and I. Tuñon, *J. Comput. Chem.,* 1994, **15**, 1127-1138.

274. F. Biegler-König and J. Schönbohm, *J. Comput. Chem.,* 2002, **23**, 1489-1494.

275. B. B. Iversen, F. K. Larsen, B. N. Figgis and P. A. Reynolds, *J. Chem. Soc. , Dalton Trans.,* 1997, 2227-2240.

276. E. Cubero, M. Orozco, P. Hobza and F. J. Luque, *J. Phys. Chem. A,* 1999, **103**, 6394-6401.

277. C. F. Matta, J. Hernández-Trujillo, T. H. Tang and R. F. W. Bader, *Chem. Eur. J.,* 2003, **9**, 1940-1951.

278. A. B. Burg, *J. Am. Chem. Soc,* 1940, **62**, 2228-2234.

279. J. F. Mariategui and K. Niedenzu, *J. Organomet. Chem.,* 1989, **369**, 137-145.

280. J. M. Ritchey. PhD Thesis, University of Colorado, 1968.

281. W. Fielder, M. Chamberlain and C. Brown, *J. Org. Chem.,* 1961, **26**, 2154-2155.

282. Q. G. Wu, G. Wu, L. Brancaleon and S. Wang, *Organomet.,* 1999, **18**, 2553-2556.

283. M. A. Beckett, G. C. Strickland, K. S. Varma, D. E. Hibbs, M. B. Hursthouse and K. M. A. Malik, *Polyhedron,* 1995, **14**, 2623-2630.

284. H. R. Snyder, J. A. Kuck and J. R. Johnson, *J. Am. Chem. Soc.,* 1938, **60**, 105-111.

285. P. v. R. Schleyer, H. Jiao, N. J. R. v. E. Hommes, V. G. Malkin and O. L. Malkina, *J. Am. Chem. Soc.,* 1997, **119**, 12669-12670.

286. P. W. Fowler and E. Steiner, *J. Phys. Chem. A,* 1997, **101**, 1409-1413.

287. M. Yalpani and R. Boese, *Chem. Ber.,* 1983, **116**, 3347-3358.

288. V. Gutmann, *Coord. Chem. Rev.,* 1976, **18**, 225-255.

289. U. Mayer, V. Gutmann and W. Gerger, *Monatsh. Chem.,* 1975, **106**, 1235-1257.

290. M. A. Beckett, G. C. Strickland, J. R. Holland and K. S. Varma, *Polym. Comm.,* 1996, **37**, 4629-4631.

291. H. J. Frohn, N. Y. Adonin, V. V. Bardin and V. F. Starichenko, *Z. Anorg. Allg. Chem.,* 2002, **628**, 2827-2833.

292. P. Owen. PhD Thesis, University College of North Wales, Bangor, 1998.

293. H. Nöth and B. Wrackmeyer, *NMR spectroscopy of boron compounds*, Springer Berlin Heidelberg, 1978.

294. M. A. Beckett, D. S. Brassington, P. Owen, M. B. Hursthouse, M. E. Light, K. M. A. Malik and K. S. Varma, *J. Organomet. Chem.,* 1999, **585**, 7-11.

295. M. A. Beckett, G. C. Strickland, K. M. S. Varma, D. E. Hibbs, M. B. Hursthouse and K. M. A. Malik, *J. Organomet. Chem.,* 1997, **535**, 33-41.

296. C. H. Chang, R. F. Porter and S. H. Bauer, *Inorg. Chem.,* 1969, **8**, 1689-1693.